

Modulation of Conformational Equilibria of Human H-Ras Protein by Metal-Chelate Derivatives and High Pressure Studied by NMR Spectroscopy

Dissertation

zur Erlangung des Doktorgrades der Naturwissenschaften (Dr. rer. nat.)
der Naturwissenschaftlichen Fakultät III
- Biologie und Vorklinische Medizin -
der Universität Regensburg



vorgelegt von
Ina Rosnizeck
aus Burglengenfeld

Januar 2010

Das Promotionsgesuch wurde eingereicht am: 12.01.2010

Das Promotionskolloquium fand statt am: 11.06.2010

Die Arbeit wurde angeleitet von: Prof. Dr. Dr. Hans Robert Kalbitzer

Prüfungsausschuss: Vorsitzender: Prof. Dr. Thomas Dresselhaus

1. Gutachter: Prof. Dr. Dr. Hans Robert Kalbitzer

2. Gutachter: Prof. Dr. Christian Herrmann

3. Prüfer: Prof. Dr. Reinhard Sterner

CONTENTS

1	INTRODUCTION	1
1.1	The Ras Protein	1
1.1.1	Ras – A Molecular Switch within Signal Transduction	1
1.1.2	Three Dimensional Structure of Ras	3
1.1.3.	The Switch Mechanisms and Conformations	5
1.1.3.1	Structural Differences	5
1.1.3.2	The 'Switch On' Reaction	5
1.1.3.3	The 'Switch Off' Reaction	7
1.1.4	Association of Ras with Effectors	8
1.1.4.1	Structural Principles	8
1.1.4.2	Interaction between Ras and Raf-RBD	9
1.1.4.3	Partial Loss-of-Function Mutants	9
1.1.5	³¹ P NMR Spectroscopy – The Bound Nucleotide as Probe	10
1.1.5.1	³¹ P NMR Spectroscopy	10
1.1.5.2	Conformational Dynamics in Active Ras	11
1.1.5.3	³¹ P High Pressure NMR Spectroscopy on Ras(wt)·Mg ²⁺ ·GppNHp	14
1.1.6	Targeting Ras in Antitumoral Therapy	15
1.1.6.1	Oncogenic Ras Mutants	15
1.1.6.2	General Strategies	16
1.1.6.3	Peptides with Consensus Ras Binding Sequences	18
1.1.6.4	Stabilization of the Weak Effector-Binding Conformation in Active Ras	19
1.2	Identification and Characterization of Ligand Binding by NMR Spectroscopy	21
1.2.1	Integration of NMR in the Drug Development Process	21
1.2.2	Saturation Transfer Difference Spectroscopy	22
1.2.2.1	The Transferred NOE-Effect	22
1.2.2.2	The STD NMR Experiment	22
1.2.2.3	Quantification and Characterization of Ligand Binding	24
1.2.3	Chemical Shift Perturbation Mapping in 2D NMR Spectroscopy	24
1.2.4	Paramagnetic Relaxation Enhancement	25
2	MATERIALS	26
2.1	Chemicals	26
2.2	Enzymes	26
2.3	Frequently Used Buffer Solutions	26
2.4	Plasmids	27
2.5	Bacteria Strains	27

2.6	Media and Antibiotics	27
2.7	Protein Standard	28
2.8	Expendable Materials	28
2.9	Columns	29
2.10	Instruments	29
2.11	Data Analysis and Graphical Software	29
3	METHODS	30
3.1	Molecular Biology	30
3.1.1	Expression and Purification of Unlabeled Ras Proteins	30
3.1.2	Expression and Purification of Uniformly ¹⁵ N-Labeled Ras	30
3.1.3	Expression and Purification of Raf-RBD	31
3.1.4	Nucleotide Exchange	32
3.1.4.1	Nucleotide Exchange against GTP	32
3.1.4.2	Nucleotide Exchange against GppNHp and GTPγS	32
3.2	Biochemical Methods	32
3.2.1	SDS-Polyacrylamide Gel Electrophoresis (SDS-PAGE)	32
3.2.2	Determination of Protein Concentrations	33
3.3	NMR Spectroscopy	33
3.3.1	Saturation Transfer Difference Spectroscopy	33
3.3.1.1	Sample Preparation, Data Collection and Processing	33
3.3.1.2	Quantification of Ligand Binding	34
3.3.2	³¹ P NMR Spectroscopy	34
3.3.3	[¹ H, ¹⁵ N](-TROSY)-HSQC Spectroscopy	35
3.3.3.1	Sample Preparation and Data Collection	35
3.3.3.2	Data Processing and Evaluation	35
3.3.3.3	Determination of Binding Constants	36
3.3.4	High Pressure NMR Spectroscopy	36
3.3.4.1	Sample Preparation and Data Collection	36
3.3.4.2	Data Processing and Evaluation	37
3.3.4.3	Analysis of the Chemical Shifts	37
3.3.4.4	Analysis of the Signal Volumes	39
4	RESULTS	41
4.1	Saturation Transfer Difference Spectroscopy	41
4.1.1	General Considerations	41
4.1.2	Determination of Measurement Parameters	41
4.1.3	STD NMR Spectroscopy with the Known Ras Ligand Zn ²⁺ -Cyclen	45
4.1.4	Identification of Zn ²⁺ -BPA as Ras Ligand	46

4.2	³¹P NMR Spectroscopic Investigations on the Influence of Metal(II)-Cyclen and -BPA on Ras	48
4.2.1	Binding of Metal(II)-Cyclen and -BPA to Mg ²⁺ ·GppNHp	48
4.2.2	Binding of Zn ²⁺ -BPA to Ras(wt)·Mg ²⁺ ·GppNHp	50
4.2.3	Binding of Cu ²⁺ -BPA to Wild Type Ras and Ras(T35A) Complexed to Mg ²⁺ ·GppNHp	51
4.2.4	Binding of Zn ²⁺ -Cyclen and -BPA to Ras(G12V) Complexed to Mg ²⁺ ·GTP and Mg ²⁺ ·GppNHp	53
4.2.5	Binding of Metal(II)-Cyclens to Mg ²⁺ ·GTPγS in Free form and Complexed to Ras	56
4.2.6	Binding of Cyclens and Metal(II)-BPA to Ras·Mg ²⁺ ·GDP	61
4.3	Perturbation of the Ras-Raf-RBD Interaction by Metal(II)-Chelates	64
4.3.1	General Considerations	64
4.3.2	³¹ P NMR Titration of Ras(T35S)·Mg ²⁺ ·GppNHp Complexed to Raf-RBD with Zn ²⁺ -Cyclen and Zn ²⁺ -BPA	64
4.3.3	Competitive ³¹ P NMR Titrations of Ras(T35A)·Mg ²⁺ ·GppNHp with Raf-RBD and Zn ²⁺ -Cyclen	68
4.4	Localization of the Binding Sites of the Metal(II)-Chelates in Ras(T35A)·Mg²⁺·GppNHp	71
4.4.1	General Procedure	71
4.4.2	Backbone Assignment of Ras(T35A)·Mg ²⁺ ·GppNHp at pH 7.5	71
4.4.3	Results Obtained for Metal(II)-Cyclen	72
4.4.4	Results Obtained for Metal(II)-BPA	76
4.5	Development of Bivalent Ras Ligands	80
4.5.1	Linkage of Zn ²⁺ -Cyclen and Zn ²⁺ -BPA to a Peptide with a Consensus Ras Binding Sequence	80
4.5.2	Determination of the Affinity of the Bivalent Ligands by STD NMR	82
4.6	Characterization of the Interaction between Ras and Peptides Derived from Raf-RBD	84
4.6.1	Localization of the Binding Site in Ras(wt)·Mg ²⁺ ·GppNHp and Ras(T35A)·Mg ²⁺ ·GppNHp	84
4.6.2	³¹ P NMR Titration of Ras(wt)·Mg ²⁺ ·GppNHp with CCAVFRL	87
4.7	Comparison of the [¹H, ¹⁵N]-TROSY-HSQC Spectra of the Ras Mutants T35S and T35A Complexed to Mg²⁺·GppNHp	87
4.8	High Pressure NMR Spectroscopic Investigations on Ras(wt)·Mg²⁺·GppNHp	89
4.8.1	Pressure Dependence of the Chemical Shifts	90
4.8.2	Pressure Response of the Chemical Shifts and Related Gibbs Free Energies	95
4.8.3	Pressure Response of the Signal Intensities and Related Gibbs Free Energies	100

5	DISCUSSION	107
5.1	Saturation Transfer Difference Spectroscopy	107
5.2	Modulation of the Conformational Equilibrium in Active Ras by Metal(II)-Chelates	110
5.3	Perturbation of the Ras-Effector Interaction by Zn^{2+}-Cyclen and Zn^{2+}-BPA	117
5.4	Peptide Ligands for Ras·Mg^{2+}·GppNHp Derived from the Primary Sequence of Raf-RBD	119
5.5	High Pressure NMR Spectroscopy on Wild Type Ras Complexed to Mg^{2+}·GppNHp	121
6	SUMMARY	125
7	REFERENCES	128
8	APPENDIX	143
8.1	List of Abbreviations	143
8.2	Experimental Data	144
8.3	Contributions to Conferences and Publications	161
8.4	Curriculum Vitae	163
8.5	Acknowledgement	165

1 INTRODUCTION

1.1 The Ras Protein

1.1.1 Ras - A Molecular Switch within Signal Transduction

Three different *ras* genes are found in mammals encoding the four highly homologous proteins H-Ras, N-Ras, K-Ras4A and K-Ras4B. These 21 kDa proteins consist of 188-189 amino acids and play a vital role in cell signalling events. Except the so-called hyper variable region (HVR), which comprises the 25 carboxy terminal amino acids, the Ras proteins show high sequence homology. In order to be biologically active they are posttranslational modified at the cysteine residue of the so-called CAAX-box (C is a cysteine, A is an aliphatic amino acid, X is any amino acid) by the attachment of lipophilic groups and thereupon membrane-anchored (Williamson et al. 1984).

Altering between an inactive GDP- and an active GTP-bound conformation Ras and the members of the superfamily act as molecular switches (Figure 1.1), whereby two classes of regulatory proteins determine the lifetime of these two states: guanine nucleotide exchange factors (GEFs) and GTPase activating proteins (GAPs).

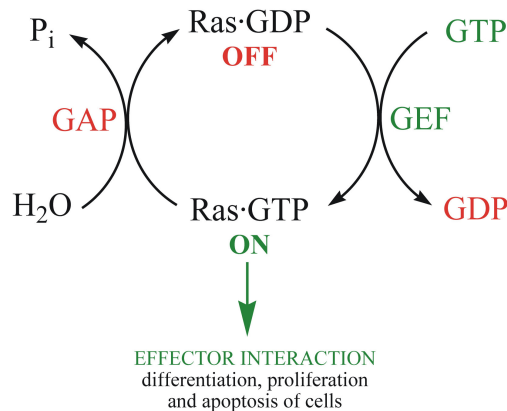


Figure 1.1: The molecular switch of Ras. Bound to GDP Ras is in its inactive form. Upon the stimulated exchange of GDP against GTP Ras becomes activated and is now able to interact with its effectors. The signal is terminated by the hydrolysis of the bound GTP. Ras turns back into its GDP-bound state and can no longer interact with effectors.

The resting GDP-bound state of Ras becomes activated by the stimulated exchange of GDP against GTP. This reaction is intrinsically very slow and can be accelerated by several orders of magnitude. GDP dissociates in less than one second from the protein in complex with its GEF. Subsequently GTP, the most abundant nucleotide in the cell enters the binding pocket followed by the release of the exchange factor. In its active state Ras is now able to interact with effector molecules activating the corresponding cellular response (see e.g. Herrmann 2003). Signalling can be switched off by the hydrolysis of the bound

GTP at the γ -phosphate. Ras itself exhibits intrinsic GTPase activity for this reaction, which is very slow with 0.028 min^{-1} at 37°C and can be accelerated by a factor of 10^5 in the presence of GTPase activating proteins (Scheffzek et al. 1997 1996). Upon the release of inorganic phosphate Ras is in its inactive state again and can no longer interact with effector molecules.

Ras is the founding member of the superfamily of Ras-related guanine nucleotide binding (GNB) proteins, which can be subdivided into the five major subfamilies Ras, Rho, Rab, Ran and Arf (Wennerberg et al. 2005). They have the common ability to bind GDP and GTP with high selectivity and high affinity, which is in the order 10 pM for Ras strongly dependent on the presence of Mg^{2+} -ions (John et al. 1990, Neal et al. 1990, Schmidt et al. 1996). About 100-150 different GNB proteins are present in a single cell and regulate a multitude of signal transduction and transport processes (Wennerberg et al. 2005). The different subfamilies and their specific function within the cell are summarized in Table 1.1.

Table 1.1: Subfamilies of the Ras-related GNB proteins, their members and cellular function.

Subfamily		Members	Cellular Function
Ras	<u>R</u> at <u>s</u> arcoma	Ras, Rap, Rit, Rem, TC21, Rad, Gem, Rheb, Ral, Rerg	proliferation, differentiation, apoptosis
Rho	<u>R</u> as <u>h</u> omologous	Rho, Rnd, Rif, Rac, Cdc42, TC10, TCL, Wrch	cytoskeleton, proliferation, gene expression
Rab	<u>R</u> as-like proteins in <u>b</u> rain	Rab	vesicular transport
Ran	<u>R</u> as-like <u>n</u> uclear protein	Ran	nuclear transport
Arf	<u>A</u> DP- <u>r</u> ibosylation <u>f</u> actor	Arf, Sar, Arl, Ard	vesicular transport

Ras initiates different signal cascades, which control cell differentiation, proliferation or apoptosis by transducing extracellular ligand-mediated stimuli to the nucleus. The most prominent and best understood Ras-mediated pathway is the mitogen-activated protein kinase (MAPK) cascade, which receives stimuli from growth factors and hormones, which are transmitted to the cell by tyrosine kinase receptors (Burgering and Bos 1995). Binding of the external ligand to its receptor tyrosine kinase (RTK) leads to the phosphorylation and dimerization of the receptor. The activated RTK becomes phosphorylated at specific tyrosine residues in its intracellular domain followed by the binding of the sequence homology 2 (SH2) domains of adaptor proteins like Grb2 (growth-factor-receptor bound protein 2) to the phosphorylated residues. These proteins also contain a SH3 domain

capable of binding proline rich motifs in proteins like SOS (son-of-sevenless), which is a guanine nucleotide exchange factor of Ras. SOS is recruited to the plasma membrane, binds to Ras and catalyzes the exchange of GDP against GTP. Ras, now in its active conformation associates with its downstream effector Raf, a serine/threonine kinase. Upon activation of its kinase activity Raf phosphorylates and activates the MAPK kinase (MAPKK) MEK, which in turn catalyzes the phosphorylation and activation of ERK, another MAPK. Consequently ERK both activates its cytosolic substrates and translocates to the nucleus, where different cellular events such as proliferation, differentiation or apoptosis are stimulated. It has to be noted here that Ras is not only involved in one linear signalling pathway, but rather part of a complex network of signal transduction events (Schubbert et al. 2007). It can be activated by several signals and relays the information to more than one downstream effector as revealed by experiments with effector region mutants of Ras: whereas certain pathways are blocked others are not affected (White et al. 1995, Qui et al. 1995 1997, Koshravi-Far et al. 1995).

1.1.2 Three Dimensional Structure of Ras

The highly flexible C-terminus of Ras impairs crystal packing of the full length protein. Since this region is not essential for the biochemical properties of Ras (John et al. 1989), but only for its biological activity, versions truncated at either position 166 or 172 have been successfully crystallized. Correspondingly, biophysical investigations are mainly carried out with truncated Ras. All members of the Ras superfamily share the same overall structural fold, the so-called G domain, which is responsible for the basic processes such as nucleotide binding and hydrolysis. This core domain consists of a central six-stranded β -sheet and five α -helices located on both sides of the sheet (Vetter and Wittinghofer 2001). It contains six conserved sequence elements involved in either coordinating the guanine base (G motifs) or the magnesium ion and/or the phosphate groups (PM motifs). The PM1 motif $^{10}\text{GxxxxGK(S/T)}^{17}$ encircles the β - and γ -phosphate of the bound nucleotide and is for that reason also called phosphate binding loop or P-loop (Saraste et al. 1990). The invariant lysine¹⁶ adopts a ring-like structure and twines around the β -phosphate. A positively polarized environment is created for the negatively charged phosphate groups by the main chain nitrogens of residues 13–16 pointing towards the phosphates and the side chain of lysine¹⁶. Serine¹⁷ coordinates the magnesium ion via its side chain hydroxyl group and additionally forms a hydrogen bond with the β -phosphate via its main chain NH (Saraste et al. 1990). The totally conserved threonine³⁵ residue represents the PM2 motif. In the triphosphate form its side chain interacts with the magnesium ion and the main chain NH forms a hydrogen bond with the γ -phosphate. This residue is key player within the conformational switch process upon hydrolysis (see section 1.1.3.2) along with glycine⁶⁰ of the PM3 motif $^{57}\text{DxxG(Q/H/T)}^{61}$, which forms a main chain hydrogen bond with the γ -phosphate (Vetter and Wittinghofer 2001). Within the latter motif aspartate⁵⁷ is

connected to the γ -phosphate through a water molecule and glutamine⁶¹ plays a crucial role in the hydrolysis mechanism by the stabilization of the transition state (see section 1.1.3.3). Figure 1.2 shows the ternary and primary structure of Ras.

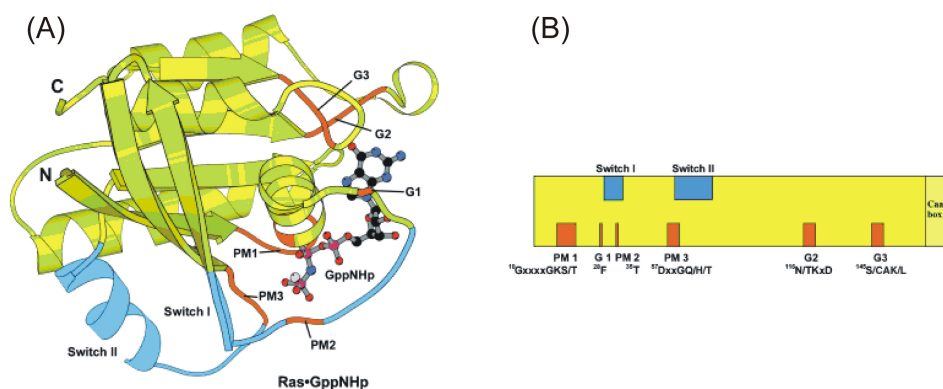


Figure 1.2: Primary and ternary structure of Ras. (A) Ribbon plot of wild type Ras complexed to GppNHp. Conserved sequence elements around the nucleotide are colored orange. The two switch regions are shown in blue. (B) Schematic representation of the location of the conserved sequence elements in the primary structure, color coded analogous to (A) (modified from Wittinghofer and Waldmann 2000).

As mentioned above nucleotide binding is very strong in Ras proteins, which is reflected by the large number of polar interactions between GppNHp and the nucleotide binding site in wild type Ras (Figure 1.3).

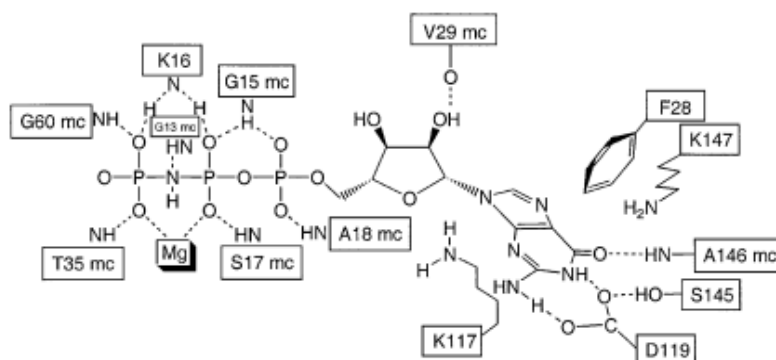


Figure 1.3: Interactions between selected residues in Ras with GppNHp bound (taken from Wittinghofer and Waldmann 2000).

Only members of the Ras superfamily share the G1 motif, which is either tyrosine or phenylalanine (Phe²⁸ in the case of Ras). This residue is orientated orthogonal to the guanine base and forms strong hydrophobic interactions supported by lysine¹¹⁷ from the G2 motif (¹¹⁶(N/T)KxD¹¹⁹). This motif provides additional ionic interactions and hydrogen bonds. The side chains of the G3 motif with only the alanine residue being totally conserved is not involved in any binding of the nucleotide by its side chains. By stabilizing amino acids from other G motifs, e.g. lysine¹⁴⁷ stabilizes the G1 motif, it functions as helper for nucleotide binding. The strong hydrogen bond formed between the main chain

of alanine¹⁴⁶ and O6 of the base is responsible for the specificity for guanine nucleotides (Rensland et al. 1995).

1.1.3 The Switch Mechanisms and Conformations

1.1.3.1 Structural Differences

Switching from the inactive state to the active one and vice versa is accompanied by structural changes within two adjacent regions of the protein, namely switch I (residues 30-40) and switch II (residues 60-76) (Milburn et al. 1990). These residues have been shown to be highly flexible by NMR and EPR studies (Ito et al. 1997, Farrar et al. 1997). The universal switch mechanism involves the invariant Ras residues Thr³⁵ and Gly⁶⁰, which are hydrogen bonded to the γ -phosphate oxygens of the bound nucleotide via their main chain NH-groups. In the so-called 'loaded-spring' mechanism the release of the γ -phosphate upon hydrolysis allows the switch regions to adopt a more relaxed conformation (Vetter and Wittinghofer 2001). The inactive and the active conformation of wild type Ras are shown in Figure 1.4.

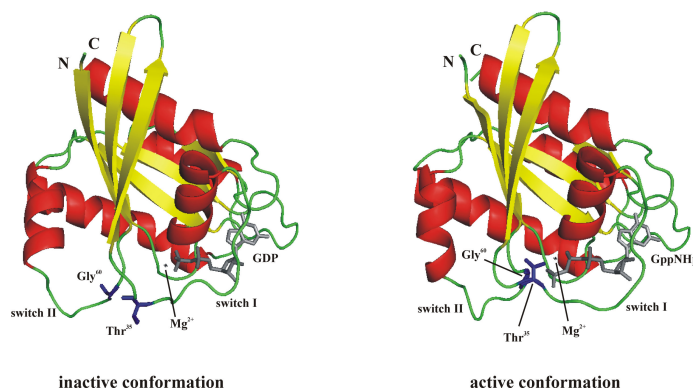


Figure 1.4: Wild type Ras in its inactive and active conformation. Shown are the crystal structures of Ras(wt)·Mg²⁺·GDP (left, pdb 4q21) and Ras(wt)·Mg²⁺·GppNHp (right, pdb 5p21). The invariant residues threonine³⁵ and glycine⁶⁰ are highlighted in blue.

1.1.3.2 The 'Switch On' Reaction

The 'switch on' reaction, the exchange of GDP against GTP is increased by guanine nucleotide exchange factors, which can be subgrouped into two different classes (Downward et al. 1996). The first group comprises RasGEFs, which are activated by second messengers like Ca²⁺, Ca²⁺-calmodulin or diacylglycerol (Shou et al. 1992, Martegani et al. 1992). The second class is represented by SOS (son-of-sevenless), which possesses a proline-rich region for the interaction with the SH3 domain of adapter molecules like Grb2 (Li et al. 1993). Two regions are conserved in all Ras-specific GEFs: the Cdc25-like domain, necessary and sufficient for nucleotide exchange (Lenzen et al.

1998) and the so-called Ras exchange motif (REM), which is located in a variable distance. This domain is mainly responsible for the stability of the catalytic domain (Fam et al. 1997). The GEF stimulated nucleotide exchange reaction is a multistep mechanism involving binary and ternary complexes between the Ras protein, the nucleotide and the exchange factor. In SOS the Ras exchange motif and the Cdc25-like domain are adjacent to each other and built the so-called SOS^{cat} region, comprising about 500 residues. The structure of the complex between SOS^{cat} and nucleotide-free Ras was solved by Boriak-Sjodin et al. (1998) providing more detailed mechanistic insight into the exchange reaction. SOS mainly interacts with the switch regions, the P-loop and helix $\alpha 3$ of Ras. Selected interactions are shown in Figure 1.5 and compared to the structure of wild type Ras·Mg²⁺·GppNHp. The Ras-nucleotide interaction is affected in two ways due to the action of SOS. First of all the affinity for the nucleotide is weakened due to the disruption of crucial interactions with the nucleotide, the magnesium ion and the phosphate group. The tight binding of SOS induces a structural rearrangement in the backbone of switch II.

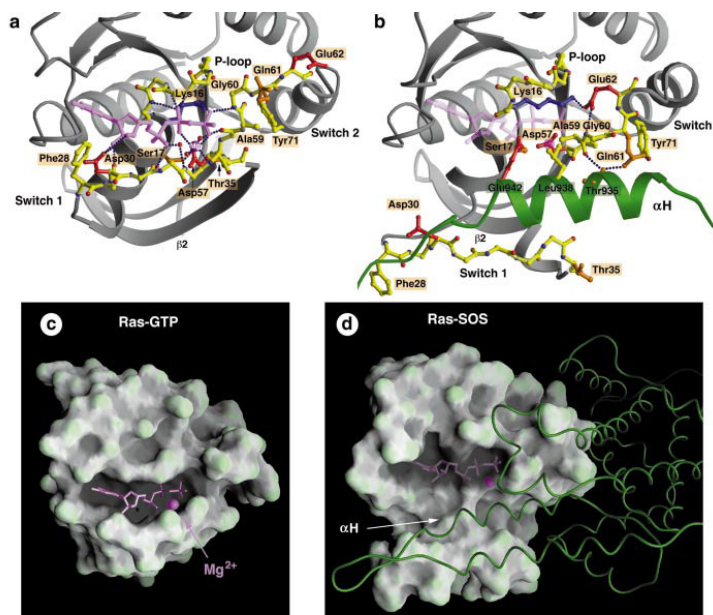


Figure 1.5: Interactions in the nucleotide-binding site compared between active wild type Ras alone and its complex with SOS. (a) Selected interactions between Ras and a GTP analogue (pdb 5p21). (b) Selected interactions between Ras and SOS are shown in the same orientation as in (a). Only helix αH and selected side chains of SOS are shown. (c) The nucleotide-binding site on the surface of Ras in a Ras-GTP analogue (pdb 5p21) is shown. The side chain of Tyr 32 was deleted from the surface calculations for clarity. (d) The surface of Ras in the Ras-SOS complex is shown with the backbone of SOS (N-domain deleted) as a green ribbon. Ras is in a slightly different orientation from that in (c). In (b) and (d) the nucleotide is shown for reference only (taken from Boriak-Sjodin et al. 1998).

As a consequence alanine⁵⁹ occupies the magnesium binding site and the glutamate⁶² side chain interacts with both the NH of glycine⁶⁰ and side chain of lysine¹⁶. Secondly, the release of the bound nucleotide is facilitated. The nucleotide binding site opens up by the insertion of a helical hairpin (helix αH of SOS), which forces switch I to flip out of its position in the GTP-bound conformation. The stabilizing interaction of phenylalanine²⁸

with the nucleotide is now missing. Magnesium and phosphate binding is additionally disturbed by the side chain interaction of leucine⁹³⁸ with serine¹⁷ in Ras and the carboxyl group of glutamate⁹⁴², which is located, where the α -phosphate is found in the nucleotide-bound form. In summary switch I is pushed away from its normal position, whereas switch II is pulled towards the nucleotide binding site. This mode of GEF action has been termed 'push-and-pull mechanism' (Vetter and Wittinghofer 2001). It has to be mentioned that an additional binding site distal to the binding site of nucleotide free Ras in SOS^{cat}, which is specific for Ras-GTP was identified by Maragrit et al. (2003). They solved the crystal structure of the ternary Ras·GppNHp:SOS^{cat}:Ras(nucleotide-free) complex. The interaction of Ras-GTP with SOS resembles the interaction of active Ras with its effectors. Due to its binding the REM motif is oriented differently and the number of interaction sites between nucleotide-free Ras and the active site of SOS is increased.

1.1.3.3 The 'Switch off' Reaction

Since oncogenic activation lacks the intrinsic as well as the GAP accelerated GTPase reaction (see section 1.1.6) the 'switch off' reaction is of high biochemical and medicinal interest. Ras signalling can be terminated by either its intrinsic or its GAP mediated GTPase activity. Both reactions are not understood in detail to date. The main discussion is about the nature of the phosphoryl transfer, which might be associative or dissociative (Wittinghofer 2006). The intrinsic GTPase reaction is proposed to rely on a substrate-assisted mechanism, where the γ -phosphate group itself acts as a base and activates the nucleophilic attack of the water molecule (Schweins et al. 1995). The GAP-mediated hydrolysis reaction has been subject to discussions for a long time. In one assumption the role of GAP was confined to catalyzing a rate-limiting isomerization in the Ras protein. Ras only becomes activated through the action of GAP and is itself an efficient GTPase (Rensland et al. 1991). In a second model GAP is directly involved in the hydrolysis reaction, providing crucial residues and stabilizing the transition state. Figure 1.6 gives a detailed view of the interaction between Ras and RasGAP. The so-called 'arginine-finger hypothesis' with a conserved arginine residue of GAP being such a residue has been supported by several experimental data. It has, for example been shown to be necessary for GAP catalysis, but not for binding of GAP (Ahmadian et al. 1996 1997). Scheffzek et al. (1997) solved the structure of the Ras-GDP-AlF₃-GAP-334 complex mimicking the transition state of the hydrolysis reaction. Indeed, Arg⁷⁸⁹ of GAP represents a key residue in hydrolysis. Its side chain (the 'arginine-finger') points into the active site of Ras and coordinates an oxygen of the γ -phosphate group and the β,γ -bridging oxygen. Its carbonyl oxygen is hydrogen bonded to the side chain NH of Ras Gln⁶¹, which also forms hydrogen bonds to the attacking water molecule along with Thr³⁵ (see Figure 1.6). This mechanism is not common to all Ras-like proteins, e.g. RanGAP and RapGAP do not provide an arginine finger (Seewald et al. 2002, Scrima et al. 2008).

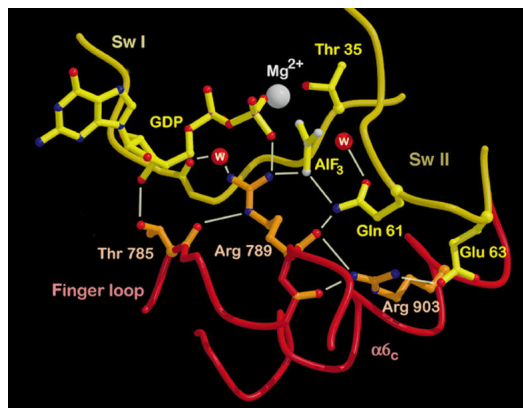


Figure 1.6: Details of the interaction between Ras and RasGAP: structural view on the active site. Critical residues of Ras (yellow) and GAP-334 (red) are shown in ball and stick (taken from Scheffzek et al. 1997).

1.1.4 Association of Ras with Effectors

1.1.4.1 Structural Principles

In spite of the fact that all known Ras effectors differ in their function and show no remarkable sequence homology, they do have a common region of roughly 100 amino acids responsible and sufficient for the interaction with Ras, termed Ras binding domain (RBD) or, in the case of AF6 and RalGDS Ras association (RA) domain (Ponting and Benjamin 1996). NMR and X-ray analyses of the RB or RA domains of the Ras effectors Raf (Emerson et al. 1995), RalGDS (Huang et al. 1997, Kigawa et al. 1998, Geyer et al. 1997, Vetter et al. 1999), AF6 (Steiner et al. 2000) and Byr 2 (Gronwald et al. 2001) revealed that they all share the same topology, the ubiquitin fold ($\beta\beta\alpha\beta\beta\alpha\beta$). They interact in a similar manner with Ras (Nassar et al. 1995 1996, Huang et al. 1998, Walker et al. 1999, Pacold et al. 2000, Scheffzek et al. 2001), forming an intermolecular β -sheet by the antiparallel co-alignment of RBD β 2 and Ras β 2 within the switch I region. Additionally residues flanking the so-called effector region of Ras (residues 32-40) contribute to the interaction. Despite this common interaction pattern in Ras-effector complexes the binding affinities can differ up to 100-fold ranging between 20 nM and 2 μ M (Wohlgemuth et al. 2005), which indicates precise adjustments within the interface for distinct specificities. Recently a different type of Ras-effector interaction involving switch II of Ras has been reported (Stieglitz et al. 2008). In NORE 1 (novel Ras effector) the RA domain is not sufficient for the association of Ras. Additional residues provided by the N-terminal extension of the RA fragment are necessary. Residues cysteine²²⁰ and leucine²²¹ build strong hydrophobic interactions with Ras switch II residues tyrosine⁶⁴ and methionine⁶⁷.

1.1.4.2 Interaction between Ras and Raf-RBD

The structure of Ras and the RBD of Raf has not been solved so far, but the crystal structures of the Ras analogues Rap1A and Raps (Rap(E30D,K31E)) in complex with Raf-RBD (Raf residues 51-131) are available (Nassar et al. 1995 1996). The overall sequence homology between Raps and Ras is 50% and in the interface region 95%. Raps residues 33-41, almost matching switch I are involved in the interaction with Raf-RBD. However, mutations in the switch II region, e.g. D57A and A59T of Ras also impair binding of Raf-RBD (Shirouzo et al. 1994). An additional region in Raf, the so-called cysteine rich domain (CRD) comprising residues 139-154 influences the Ras-Raf interaction (Gosh et al. 1994, Gosh and Bell 1994). It requires an intact switch II region for its binding activity (Drugan et al. 1996). Peptides comprising residues of the Raf-RBD, which do not contribute to the interaction with Raps in the crystal structure have been shown to have an inhibitory effect on Ras-Raf association (Barnard et al. 1995). The Ras-Raf-RBD complex is highly dynamic, exhibiting both fast association and dissociation (Gorman et al. 1996). The association between Ras and Raf-RBD can be described by a minimal model comprising a two-step binding mechanism resulting in a hyperbolic dependence of the observed rate constants on increasing concentrations of Raf-RBD (Sydor et al. 1998, Linnemann et al. 1999). First a loosely bound encounter complex is formed, which subsequently isomerizes into a tight binding complex. A dissociation constant $K_1 = k_{-1}/k_1$ of 12 μM , a k_2 -value of 415 s^{-1} and an overall affinity of 0.05 μM is derived for the association between wild type Ras and Raf-RBD (Spoerner et al. 2001). Studies on the kinetics with 10 different RBDs and Raf demonstrated that the rate constants are conserved during evolution (Kiel et al. 2004). Since the Ras-Raf-RBD interface mainly constitutes of electrostatic interactions (Nassar et al. 1996, Zeng et al. 1999, Wohlgemuth et al. 2005, Kiel et al. 2005, Kiel and Serrano 2006) it is proposed that the formation of the initial low affinity complex is mainly driven by electrostatics and allows Ras to discriminate binding partners very quickly (Goldfinger 2008) before isomerizing to the higher affinity complex. Experimental data of the association between NORE1 and Ras support this assumption. Whereas the on-rate of the association is similar compared to Raf-RBD the off-rate is much lower probably to the additional interaction provided by the N-terminal extension with Ras switch II (Stieglietz et al. 2008).

1.1.4.3 Partial Loss-of-Function Mutants

Certain mutations in the effector region of Ras lead to so-called partial loss-of-function mutants, which only interact with a subset of the known Ras effectors (White et al. 1995, Akasaka et al. 1996). These mutants have intensively been used to investigate the role of Ras in certain signalling pathways (Joneson et al. 1996, Koshravi-Far et al. 1996, Rodriguez-Vicinia et al. 1996 1997, Wolthuis et al. 1996, Vavvas et al. 1998). Threonine³⁵ is a highly conserved residue in the switch I region of Ras. In Ras-effector complexes it is involved in the coordination of the crucial metal ion via its side chain hydroxyl group and of the γ -phosphate of the bound nucleotide via its main chain NH (Nassar et al. 1995 1996,

Vetter et al. 1999). Mutation to serine blocks the association with Byr or RalGDS, whereas the Raf signalling pathway is not affected. Kinetic stopped flow analysis showed that the interaction of Ras(T35S) and Raf-RBD follows a two-step mechanism as described above for wild type Ras, but the affinity for Raf-RBD is diminished by a factor of approximately 60 (Spoerner et al. 2001). In contrary the same experiments with the corresponding alanine mutant indicate a different effector-binding conformation, which does not involve a rate-limiting step. The association kinetic switches into a one step mechanism with linear dependence on the concentration of Raf-RBD (Spoerner et al. 2001). The effector can still be bound by the mutant leading to the weak complex, but the rate limiting step, the isomerization to the high affinity complex is missing (see Figure 1.7).

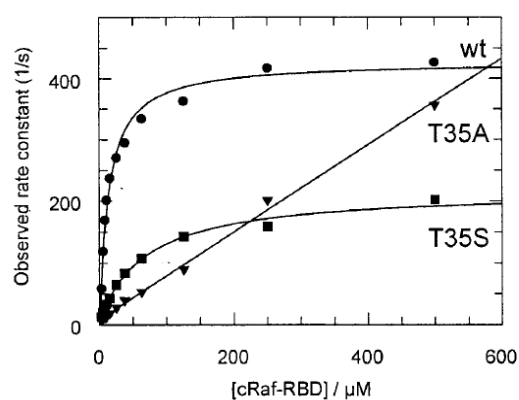


Figure 1.7: Kinetics of the association between wild type and mutant Ras-mantGppNHp and Raf-RBD. Plot of the observed rate constants against the effector concentration (taken from Spoerner et al. 2001).

1.1.5 ^{31}P NMR Spectroscopy - The Bound Nucleotide as Probe

1.1.5.1 ^{31}P NMR Spectroscopy

The ^{31}P isotope is a NMR active nucleus with a spin number of $I = 1/2$ and a natural abundance of 100%. ^{31}P NMR spectroscopy represents a quite attractive method for the study of GNB proteins since the only phosphorus atoms present arise from the bound nucleotide, which is located directly in the active site of Ras. The conformational switch from the inactive to the active state is accompanied by structural changes within regions, which are directly involved in nucleotide binding. These structural differences are directly reflected by changes in the NMR parameters, such as chemical shift values, line widths or relaxation characteristics of the phosphorus atoms in the nucleotide. The ^{31}P chemical shifts of phosphorus compounds can extend over a range of approximately 100 ppm creating spectra with only few overlap. The areas of the observed peaks can be used as a direct measure of relative populations of for example different conformational states. The major drawbacks are the high amount of protein one needs and the quite long acquisition

time due to the low sensitivity of ^{31}P (6.64% of ^1H) and its long relaxation time. The NMR sample commonly consists of 500 μL protein solution with a concentration in the millimolar range. In order to obtain a spectrum with sufficient quality a typical acquisition compromises about 2000 scans and takes about four hours.

1.1.5.2 Conformational Dynamics in Active Ras

As mentioned above the only phosphorus atoms present in the Ras protein are the ones from the bound nucleotide. Consequently one would expect three distinct signals representing the three phosphate groups in active Ras. ^{31}P NMR spectroscopic investigations on Ras bound to its physiological triphosphate nucleotide GTP gives one signal per phosphate group, when recorded at room temperature (Rösch et al. 1986). A different picture is obtained in experiments at lower temperatures with Ras complexed to the GTP-analogues GppCH₂p or GppNHp (see Figure 1.8 (B), (C)), commonly used in biochemical studies due to their reduced rate of hydrolysis.

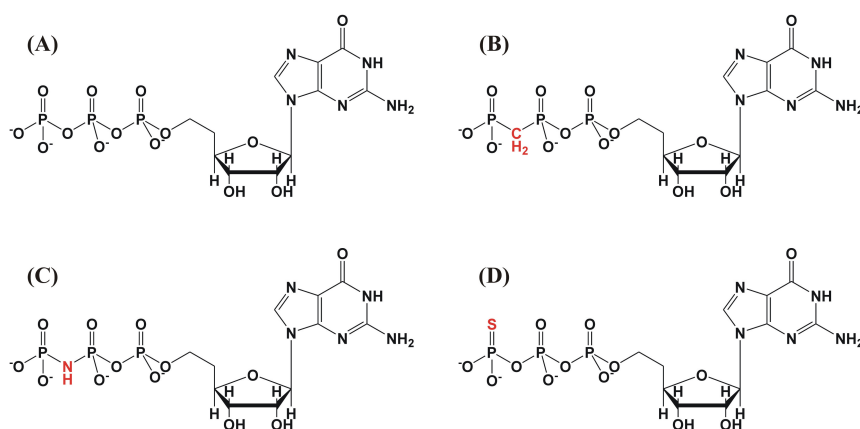


Figure 1.8: GTP (A) and its slowly hydrolyzing analogues GppCH₂p (B), GppNHp (C) and GTPγS (D). These analogues are commonly used in biochemical studies of the active form of Ras due to their reduced rate of hydrolysis. Substitutions compared to the physiological nucleotide are highlighted in red.

At least two distinct conformational states, called state (1) and state (2) represented by different ^{31}P NMR chemical shift values for the α - and γ -phosphate groups can be found in active wild type Ras (see Figure 1.9) with a relative population of state (2) over state (1) of 1.9 at 278 K (Geyer et al. 1996, Spoerner et al. 2001 2005a). These states are in dynamic equilibrium with exchange rates in the millisecond time scale at room temperature. At higher temperatures the exchange between these two conformational states becomes fast and consequently only one peak is observed for each phosphate group with a chemical shift at the population averaged position. The coexistence of both states was also revealed by solid-state ^{31}P NMR- spectroscopic investigations on Ras crystals (Stumber et al. 2002, Iuga et al. 2004) or precipitated Ras (Ader et al. 2007).

As shown in Figure 1.9 state (2) becomes stabilized, when Ras is complexed to the RBDs of its effectors (Geyer et al. 1996 1997, Gronwald et al. 2001, Linnemann et al. 1999, Spoerner et al. 2001 2004 2005a). For that reason state (2) is also known as the effector binding state and is strongly assumed to resemble the structure adopted by Ras in complex with its effectors. In contrast state (1) shows drastically reduced affinity for effector molecules as studied by calorimetric and fluorescence-based methods as well as ^{31}P NMR spectroscopy (Spoerner et al. 2001 2004 2007). The affinity of state (1) to Raf-RBD is smaller by a factor of approximately 20. For that reason state (1) was initially referred as the so-called weak effector-binding state. Recent results demonstrated that conformational state (1) is selectively recognized by the exchange factor SOS (Kalbitzer et al. 2009) as revealed by strong line broadening of the ^{31}P resonances of wild type Ras·Mg $^{2+}$ ·GppNHp upon complex formation with SOS.

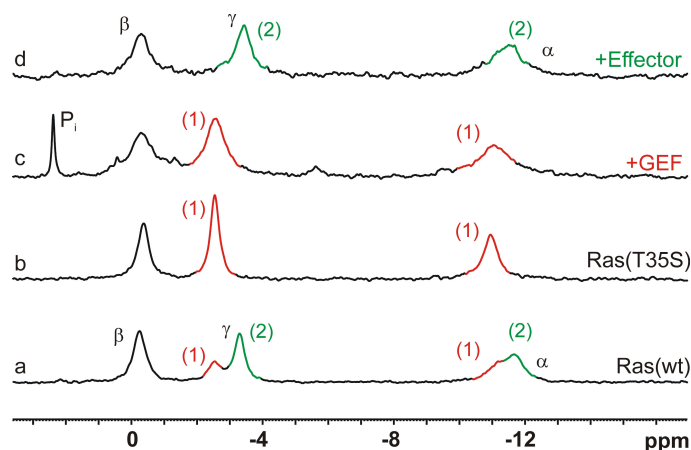


Figure 1.9: Main functional states of Ras·Mg $^{2+}$ ·GppNHp as detected by ^{31}P NMR spectroscopy. ^{31}P NMR spectra of (a) wild type Ras and (b) the partial loss-of-function mutant Ras(T35S) complexed to Mg $^{2+}$ ·GppNHp. Spectra (c) and (d) show Ras(T35S)·Mg $^{2+}$ ·GppNHp in complex with SOS(W729E) and Raf-RBD, respectively (taken from Kalbitzer et al. 2009).

Consequently state (1) is expected to be structurally closer related to the conformation of Ras in complex with GEFs. In the crystal structure of Ras(G60A)·Mg $^{2+}$ ·GppNHp (Ford et al. 2005), which exists in conformational state (1) from the spectroscopic view switch I adopts a position similar to the one found in Ras in the complex with SOS supporting the above suggestion. Threonine³⁵, totally conserved in all members of the Ras superfamily, is involved in the coordination of the Mg $^{2+}$ via its side chain hydroxyl group and contacts the γ -phosphate group with its main chain NH in active wild type Ras. Both interactions are missing in the crystal structure of Ras(G60A)·Mg $^{2+}$ ·GppNHp (Ford et al. 2005). Replacing this threonine residue against serine or alanine gives mutants predominately existing in conformational state (1) (Spoerner et al. 2001). Whereas upon addition of effector-RBDs the dynamic equilibrium shifts towards state (2) in the case of the serine mutant, in the spectra of the alanine mutant solely broadening of the resonance lines can be observed. This difference in effector binding between the two mutants was also revealed by stopped

flow experiments with Ras loaded with a fluorescently labelled nucleotide (see section 1.1.4.3). Figure 1.9 shows the main conformational states of active wild type Ras and the mutant Ras(T35S).

In GTP γ S, another slowly hydrolyzable analogue for GTP the γ -phosphate group is modified by the replacement of an oxygen atom against sulfur (see Figure 1.8 (D)). When bound to wild type Ras only one conformational state corresponding to state (2) in complex with Mg²⁺·GppNHp or Mg²⁺·GppCH₂p is prevalent (Spoerner et al. 2007). In contrast in the ³¹P NMR spectra of the Ras mutants T35A and T35S two sets of resonances are visible for the β - and γ -phosphorus atoms when GTP γ S is bound (see Figure 1.10).

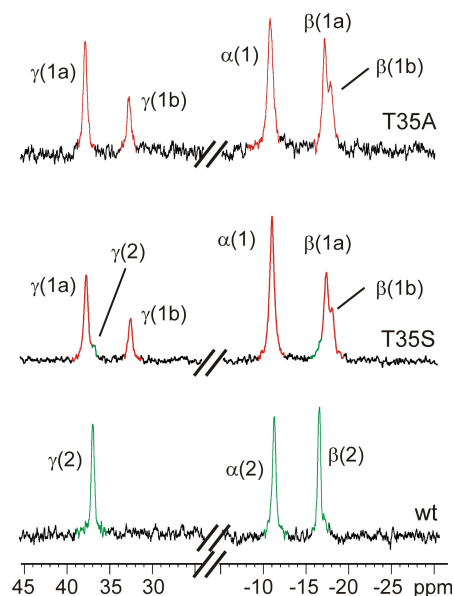


Figure 1.10: ³¹P NMR spectra of wild type and mutant Ras complexed to the GTP analogue GTP γ S (modified from Spoerner et al. 2007).

These states have been identified to represent substates of conformational state (1) interconverting in the millisecond time scale with a free activation energy $\Delta G_{1a1b} = 41 \text{ kJ mol}^{-1}$ and a K_{1a1b} value of 0.5. In the case of the serine mutant a third line corresponding to the one in wild type Ras is visible for the γ -phosphorus. Saturation transfer experiments revealed that state (1b) is also present in wild type Ras but as aforementioned very little populated and thus not visible. In good agreement with previous results obtained with the GppNHp and GppCH₂p complexes only the serine, but not the alanine mutant can be shifted towards conformational state (2) in the presence of different RBDs. As already mentioned the ³¹P NMR spectrum of Ras(wt) complexed to its physiological nucleotide GTP gives one resonance line for each phosphate group (Rösch et al. 1986), representing conformational state (2). ³¹P NMR experiments at higher fields clearly reveal the existence of second set of resonances only little populated for Ras(wt)·Mg²⁺·GTP at 278 K (Spoerner et al., unpublished results). The second

conformational state is identical to the one found in the partial loss-of-function mutants Ras(T35A) and Ras(T35S).

In summary active wild type Ras is in dynamic equilibrium between at least two conformational states with K_{12} values depending on the bound nucleotide. One state becomes stabilized by effector binding, whereas the other one is required for the interaction of GEFs. The coordination of the γ -phosphate group by threonine³⁵ is strongly suggested to be transient in solution indicating a high flexibility of the sidechain and/or the loop containing Thr³⁵ (Bellew et al. 1996, Halkides et al. 1996). Supporting data is derived from the crystal structure of Ras(T35S)·Mg²⁺·GppNHp, where the switch regions are not visible (Spoerner et al. 2001). Additionally it could be shown that both states differ in their GTPase activity with the latter one being faster in conformational state (2) (M. Spoerner, unpublished results). Relaxation measurements on wild type Ras·Mg²⁺·GppNHp indicate that the major part of the catalytic domain of the Ras GTPase is involved in this conformational exchange (O'Connor and Kovrigin 2008).

1.1.5.3 ³¹P High Pressure NMR Spectroscopy on Ras(wt)·Mg²⁺·GppNHp

Conformational dynamics are of high interest when studying the function of proteins. In solution multiple conformational states have to coexist for a given protein allowing the quick response to changes in its environment. In order to obtain a complete picture of the function and dynamics in a protein it is not sufficient to study solely the main conformation, which is usually obtained in crystallography. Different approaches disturbing the environment, such as changing the pH value, the temperature or the addition of chaotropic substances like guanidine hydrochloride are followed in order to force the protein to turn into its structural substates. The main drawback within these methods is the fact that the whole system may be influenced. High pressure NMR represents a novel tool for the characterization of structural subensembles (Kremer 2006, Akasaka 2006). The increased sensitivity of NMR allows for the investigations of the pressure effects in macromolecules at atomic resolution, e.g. the detection of intermediate states (Kachel et al. 2006). Transitions between different conformational states are accompanied by changes in the specific volume (Akasaka and Li 2001). Excited states are generally solvated to higher extend and exhibit a smaller specific volume. Under high pressure structures with smaller specific volumes ΔV_0 are stabilized and consequently low populated excited states can be detected. The structure of the substate of interest is hereby only slightly affected but rather the relative populations between the different conformations allowing for structural characterization. In order to distinguish real structural changes from chemical shift differences induced by pressure the proton chemical shift dependence on pressure was investigated in random coil model peptides giving an amino acid specific pressure coefficient (Arnold et al. 2002). Unfortunately such data are missing for the amide nitrogen chemical shifts to date, but work is currently ongoing at the department.

As described in section 1.1.5.2 active Ras exists in an equilibrium between different conformational states. Increasing pressure on wild type Ras complexed with GppNHp shifts the dynamic equilibrium towards conformational state (1) in a reversible manner as shown by ^{31}P NMR spectroscopy (Kalbitzer et al. 2009). At a pressure of 200 MPa the relative population of conformational state (2) over (1) decreases from 1.9 to 0.44 at 278 K. The difference of the specific volumes between the two conformational states was calculated to be $\Delta V_0 = 17.2 \text{ ml mol}^{-1}$.

1.1.6 Targeting Ras in Antitumoral Therapy

1.1.6.1 Oncogenic Ras Mutants

In many human malignancies Ras is found mutated (Bos 1989) ranging from 95% in pancreas carcinomas (Almoguera et al. 1988), 65% in colon cancer (Burner and Loeb 1989), 46% in endometrial carcinomas (Enomoto et al. 1990) to 16% in carcinomas of the bladder (Visvanathan et al. 1988). The reason therefore is a point mutation at either position 12, 13 or 61 (Seeburg et al. 1984, Karnoub and Weinberg 2008). As a result the protein is locked in its active GTP-bound conformation due to the loss of both, its intrinsic and GAP accelerated GTPase activity, which contributes to uncontrolled cell growth and thus to tumor formation (Bos 1989). The structural basis for the oncogenic potential of a mutation at either position 12, 13 or 61 in Ras is explained in Figure 1.11.

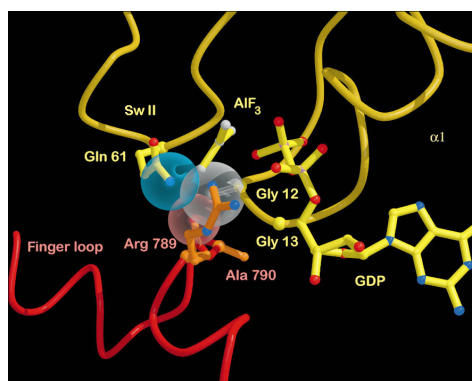


Figure 1.11: Structural basis for the oncogenic potential of Gly¹², Gly¹³ and Gln⁶¹ mutants of Ras. Close approach of the finger loop of GAP-334 to loops L1 (P-loop) and L4 of Ras. In position 12 of Ras, normally glycine, an alanine side chain has been introduced (gray) into the model to show that even small substitutions would be within van der Waals distance (gray sphere) to Gln⁶¹ (NH₂, blue sphere) and Arg⁷⁸⁹ (CO, red sphere), glycine¹³ is more remote from GAP-334 (from Scheffzek et al. 1997).

As described in section 1.1.3.3 Arg⁷⁸⁹ of GAP is coordinated to the side chain of Ras Gln⁶¹ via its carbonyl oxygen explaining the oncogenic potential of mutations at position 61. Glycine¹² mutants bind to GAPs with similar affinity as does the wild type protein. Consequently the mutation can be tolerated in the ground state of the formed complex. A

different picture is obtained in the transition state. The glycine residues of Ras at positions 12 and 13 are in close proximity to the finger loop. Any substitution at these positions, even the smallest possible one against alanine sterically interferes with the interaction between Arg⁷⁸⁹ and Gln⁶¹. The structural basis for the oncogenic potential of a mutation at either position 12, 13 or 61 in Ras is explained in Figure 1.11.

1.1.6.2 General Strategies

In the late 80ies it became more and more apparent that aberrations in signalling pathways contribute to many diseases such as cancer. Consequently a lot of effort has been put into the development of drugs targeting cell signalling events. This type of disease management is termed signal-transduction therapy (Levitzki 1994). In the case of Ras signalling four approaches have been reported for the interruption of aberrant signalling (Figure 1.12) and will briefly be discussed.

Inhibition of Membrane Attachment

As mentioned in section 1.1.1 posttranslational modifications of Ras are necessary in order to obtain biological activity. The first process is catalysed by the enzyme farnesyltransferase, which thioalkylates a cysteine residue within the CAAX (CVLS in Ras) box with a C15 prenyl group followed by C-terminal proteolysis and methylation and the attachment of a C16 palmitoyl group. Inhibition of this posttranslational modification renders the protein inactive due to the impaired membrane attachment (Gelb et al. 2006). The main target of inhibitors in this approach is represented by the enzyme farnesyl transferase (Basso et al. 2006). Tetrapeptides mimicking the CAAX-box represented the first inhibitors (Reiss et al. 1990), followed by peptidomimetics and finally non-peptide inhibitors. An example for the latter is given by BMS-214662 with an IC₅₀-value of 1.35 nM (Hunt et al. 2000, Rose et al. 2001, Cortes et al. 2005). This compound is subject to anticancer clinical trials at the moment.

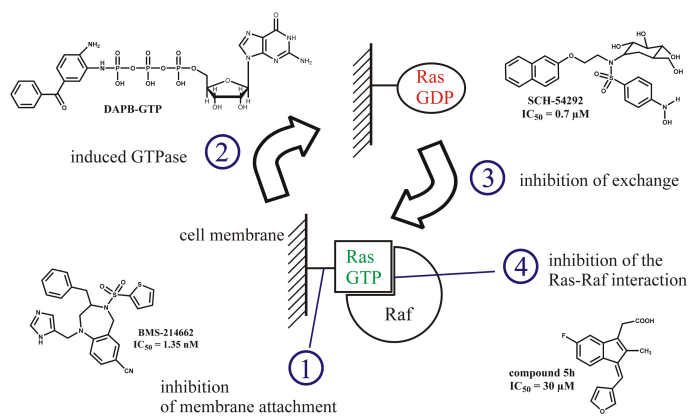


Figure 1.12: General strategies for the inhibition of Ras signalling and selected examples for inhibitors.

Induced GTPase Activity

A key process within the Ras cycle is the 'switch off' reaction, which is missing in the case of oncogenic mutants (Bos et al. 1989). Originally designed as a slowly hydrolyzable GTP-analogue like GppNHp, GppCH₂p or GTP γ S diaminobenzophenonephosphoramidate-GTP (DABP-GTP) was found to be efficiently turned over to the corresponding diphosphate form and DABP-P_i by G_s α (Zor et al. 1997). Similar results have been obtained with active Ras (Ahmadian et al. 1999), where the rate of hydrolysis is even 10-fold higher compared to the physiological nucleotide GTP in wild type Ras. Moreover it was shown, that the rate of hydrolysis in the oncogenic mutants Ras(Q61N) and Ras(G12V) complexed to DABP-GTP can be accelerated up to 220- and 720-fold, respectively (Ahmadian et al. 1999). The crystal structures of Ras(G12V) and Ras(G12P) complexed to DABP-GTP have been solved and can provide tools for the structure-based design of anti-Ras drugs.

Inhibition of the Nucleotide Exchange of GDP against GTP

Since oncogenic mutants of Ras are locked in their active GTP-bound conformation another promising approach contains the inhibition of the GDP-exchange reaction. The Schering-Plough Research Institute has reported on compounds capable of inhibiting the exchange reaction in the low μ M range (Taveras et al. 1997). These compounds form a noncovalent complex with Ras·GDP (Ganguly et al. 1997). The interaction of one of these compounds SCH-54292 with Ras·GDP was investigated in more detail by NMR spectroscopy (Ganguly et al. 1998) revealing the binding site to be close to the switch II region. An important role is adapted by the hydroxylamine group, which is located in close vicinity to both the magnesium ion and the β -phosphate group. Since the sugar moiety of the compound was pointing outside the binding pocket indicating no contribution to the binding, compounds missing the sugar moiety (Colombo et al. 2004, Peri et al. 2005) were designed and tested. However, the detailed modes of binding and inhibition are still under investigation.

Inhibition of the Interaction with Effector Molecules

In order to prevent aberrant signalling in oncogenic Ras the direct inhibition of the interaction with effector molecules represents another interesting approach. The development of inhibitors directly interfering with the Ras-Raf association is quite challenging due to the large surface area covered by the interaction site (Downward 2003). Sulindac, a nonsteroidal anti-inflammatory drug applied in the treatment of many cancers was found to inhibit the growth of tumors containing activated Ras to a higher degree than of those harbouring the wild type *ras* gene (Thompson et al. 1997). Its active metabolite sulindac sulfide has been shown to potently interfere with the Ras-Raf interaction due to its binding activity for active Ras (Herrmann et al. 1998). Ind12, a compound derived from sulindac also interferes with the Ras signalling pathway, but its mode of action remains unclear (Karaguni et al. 2002). The screening of a 189 compound library structurally based on sulindac yielded eight promising hits exhibiting a up to 30 times higher potency in the

cytotoxicity assay than sulindac (Müller et al. 2004). These compounds were further tested concerning their impact on the Ras-Raf interaction and yielded half inhibitory concentrations between 100 μ M to 450 μ M with the exception of compound 5h, which gave an IC_{50} value of 30 μ M (Waldmann et al. 2004). The binding of this compound and sulindac sulfide was further investigated in [1 H, 15 N]-HSQC-NMR titration studies with wild type Ras·Mg $^{2+}$ ·GppNHp. Due to the fact that both switch regions are not visible in the [1 H, 15 N]-HSQC spectrum of wild type Ras·Mg $^{2+}$ ·GppNHp (Ito et al. 1997) the exact binding position remains unknown, but it is strongly suggested that the binding of both compounds takes place in the switch I region.

In conclusion one can say that Ras is an extensively studied target in anticancer therapy. Several research groups and companies work on the development of inhibitors for oncogenic Ras signalling following different approaches. None of them has succeeded yet, but investigations are going on. In the following two paragraphs two additional approaches are presented, which have also been subject to investigations in the present work.

1.1.6.3 Peptides with Consensus Ras Binding Sequences

Using contact epitope scanning and site directed mutagenesis peptides based on the primary sequence of Raf-RBD have been investigated concerning their inhibitory effect on the interaction with Ras·GTP by Barnard et al. (1995). Out of nineteen tested peptides, two containing c-Raf-1 residues 91-105 and 118-143 potentially interfered with Ras association. Further studies revealed that the peptide comprising Raf-residues 91 to 105 could be truncated to seven amino acids without the loss of the inhibitory effect (Barnard et al. 1998). The most potent peptide consisting of Raf residues 95-CCAVFRL-101 is located ~15 Å away from the binding interface in the Ras-Raf-RBD complex (Nassar et al. 1996). Figure 1.13 the calculated complex structure of Ras and Raf-RBD is depicted (Zeng et al. 1999 2001).

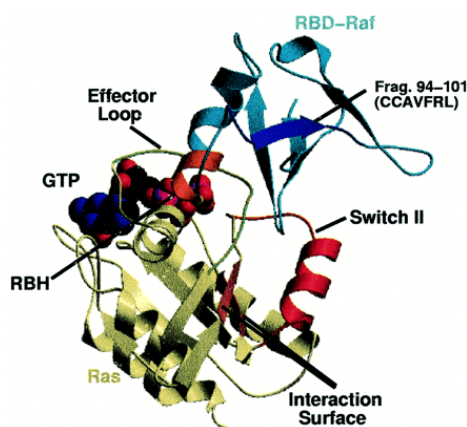


Figure 1.13: Complex structure of Ras-Raf-RBD obtained from a molecular dynamics simulation. The effector loop, the interaction surface and the switch II region in Ras are coloured green, pink and red, respectively. The Ras Binding Helix of Raf is colored brown. The inhibitory peptide CCAVFRL is highlighted blue in the structure (taken from Zeng et al. 2001).

Modifications of single amino acids in the shortened peptide yielded stronger inhibitors for Ras-Raf association *in vitro*. The strongest effect was observed by increasing the hydrophobicity at position 97. Mutations at positions 98, 99 and 100 were tolerated, whereas N-methylation at position 96, 97 or 98 led to a complete loss of the inhibitory effect. This indicates the need of a specific conformation to be fulfilled by the seven amino acid peptide in order to be an active inhibitor. The main question remaining is about the mode of action of the peptide. Since it is also capable of inhibiting the interaction between active Ras and the RBD of RalGDS it is strongly suggested that the peptide binds specifically to the Ras protein (Barnard et al. 1998).

1.1.6.4 Stabilization of the Weak Effector-Binding Conformation in Active Ras

As described in paragraph 1.1.5 ^{31}P NMR spectroscopy reveals the existence of a dynamic equilibrium between at least two distinct conformational states in Ras bound to the GTP analogue GppNHp. One of these states shows drastically reduced affinity for effector molecules. Shifting the equilibrium towards this so-called weak-binding state by its stabilization with suitable ligands thus represents an additional novel approach in antitumoral therapy. Zn^{2+} -cyclen has been reported to selectively recognize state (1) (Spoerner et al. 2005c) and to be capable of shifting the equilibrium completely towards the weak effector-binding state in wild type Ras·GppNHp (Figure 1.14).

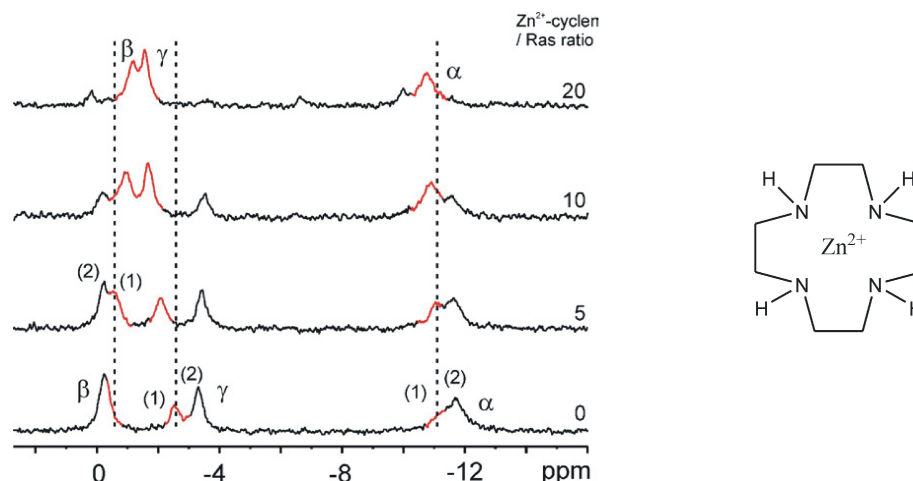


Figure 1.14: Stabilization of the weak effector-binding state in wild type Ras· Mg^{2+} ·GppNHp by the small molecule Zn^{2+} -cyclen (from Spoerner et al. 2005c).

For that reason Zn^{2+} -cyclen serves as a lead compound for the development of a novel class of Ras inhibitors. The binding of this substance in the protein has been investigated in more detail by paramagnetic relaxation enhancement and chemical shift perturbation studies using a paramagnetic and a diamagnetic derivative of cyclen (T. Graf 2006). Three different binding positions have been identified in the partial loss-of-function mutant Ras(T35A)· Mg^{2+} ·GppNHp, whereby one is close to the γ -phosphate group of the bound

nucleotide. The other two binding sites have been found to be located close to histidine²⁷ and phenylalanine²⁸ and at the negatively charged loop comprising amino acids aspartate¹⁰⁵ to methionine¹¹¹. The binding constant for each position was determined yielding millimolar affinity with the one in the active site exhibiting the lowest affinity. Additionally a model of the ligand binding site at the active centre was obtained using the docking programme HADDOCK (T. Graf 2006). In Figure 1.15 the obtained structure is directly compared with the active conformation of wild type Ras·Mg²⁺·GppNHp. Compared to the wild type protein a more opened structure is adopted by Ras(T35A)·Mg²⁺·GppNHp accompanied by changes in both switch regions and the P loop. The amide protons of the cyclen scaffold are in hydrogen bonding contact to glycine¹², aspartate³³, alanine³⁵ and alanine⁵⁹. Tyrosine³² of the effector loop has changed its position considerable as indicated in Figure 1.15.

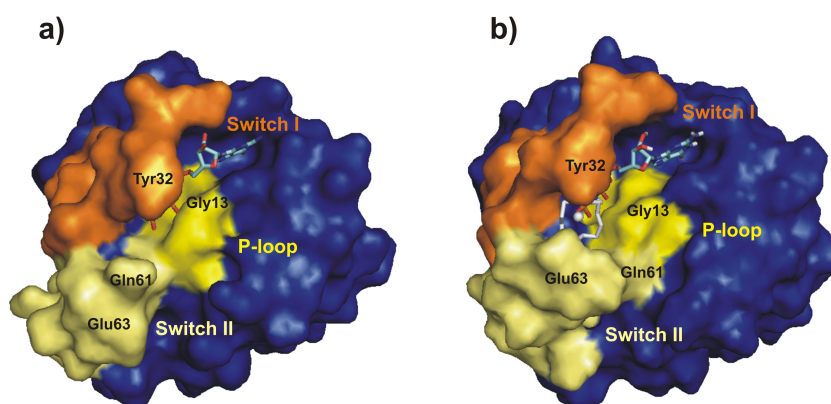


Figure 1.15: Comparison of the crystal structure of a) wild type Ras·Mg²⁺·GppNHp (pdb 5p21) with b) the calculated structure of the complex between Ras(T35A)·Mg²⁺·GppNHp and Cu²⁺-cyclen (T. Graf 2006, Rosnizeck et al., accepted).

Based on the range of the ³¹P NMR chemical shift differences of the γ -phosphorous resonances Geyer et al. (1996) proposed that Tyr³² is extensively involved in the transition between the two active Ras conformations. This is supported by the finding that the mutation of tyrosine³² against arginine shifts the dynamic equilibrium towards the weak-binding state. The residue also differs strongly in its orientation in the crystal structure of wild type Ras complexed to GppNHp and GDP, respectively. Generally Ras(T35A)·Mg²⁺·GppNHp complexed with Cu²⁺-cyclen is structurally closer related to the conformation of inactive Ras(wt)·Mg²⁺·GDP or the mutant Ras(G60A)·Mg²⁺·GppNHp (Ford et al. 2005), which is from the spectroscopic view in conformational state (1) than to wild type Ras·Mg²⁺·GppNHp alone or in its complexes with effector molecules.

1.2 Identification and Characterization of Ligand Binding by NMR Spectroscopy

1.2.1 Integration of NMR in the Drug Development Process

NMR has become a more and more attractive tool in any stage of drug development, which is reflected by the large number of reviews available (see e.g. Pellecchia et al. 2008). The reason therefore can be found in the strong progress in the field of hard- and software development, such as high field spectrometers, cryogenic probes and modern software packages for data evaluation (Güntert 2009), respectively. Additionally the sensitivity of NMR has improved by modern pulse sequences, such as the TROSY-spectroscopy (Zhu and Yao 2008) and more and more information about interactions is available due to the extended use of different NMR parameters, such as residual dipolar couplings (RDCs) (Bax and Grishaev 2005, Bouvignies et al. 2005) and cross correlated relaxation (CCR) rates (Reif et al. 1997). Moreover combinatorial chemistry approaches deliver large amounts of substances with high diversity, which can be tested in the early stage of drug design in order to obtain initial hits. Automation is straight forward in NMR spectroscopy by now allowing for high throughput applications. In general advantages of the method can be found in its high sensitivity and the possibility to investigate biomolecules under physiological conditions without disturbing the sample.

Structural characterization of the target molecule by NMR spectroscopy represents several advantages over conventional X-ray crystallography, such as the possibility to gain information about the dynamics of the protein by relaxation experiments (Kay 1998) or the solvent accessibility by examining amide proton exchange rates for example (Gemmecker et al. 1993, Dyson et al. 2008), both necessary for the identification of druggable areas in the protein. As soon as the target is identified and sufficiently characterized primary screening is employed in order to identify so-called hits. Binding activity of a ligand can either be detected in receptor- or ligand-based methods by monitoring changes of NMR parameters of either the receptor in the presence of the ligand or vice versa. Initial methods were based on the observation of the chemical shifts or line width of the target resonances in 2D NMR spectroscopy, which was very time and sample consuming. Meanwhile 1D spectroscopy observing the ligand signals is applied in most of the cases. The advantages are obvious. There is no need of isotope labelling, data collection time is reduced as well as the amount of protein one needs. Several primary NMR screening techniques have been reported, such as WaterLOGSY (Dalvit et al. 2001), transferred NOE (Meyer et al. 1997), NOE pumping (Chen and Shapiro 1999 2000) or STD (saturation transfer difference) spectroscopy (see section 1.2.2). In all these methods weak binders are identified, which have to be further characterized in terms of their binding position and further modified concerning their binding affinity by for example INPHARMA (Sánchez-Pedregal et al. 2005) or SAR (structure activity-relationship) by NMR (Shuker et al. 1996, Hajduk 2006). In the latter approach fragments binding to nearby sites in the protein are identified by

[^1H , ^{15}N]-HSQC experiments and optimized concerning their binding properties. Both fragments are then linked together with the aim to give a high affinity ligand.

1.2.2 Saturation Transfer Difference Spectroscopy

1.2.2.1 The Transferred NOE-Effect

Macromolecules and small molecules differ in their nuclear Overhauser enhancement (NOE) characteristics due to their different correlation times τ_c . Low molecular mass substances have short correlation times ($\tau_c < 10^{-10}$ s) and therefore exhibit positive or very small negative NOEs, while large molecules have long correlation times ($\tau_c > 10^{-8}$ s) and consequently strongly negative NOEs. In the complex with a protein the ligand adopts the correlation time of the macromolecule and consequently its NOE characteristics. This observation is termed the transferred NOE (trNOE) effect (Balaram et al. 1972a 1972b) and reflects the bound state of the ligand. As soon as the ligand dissociates from the target it carries the information of binding into solution, where it can be detected by the loss of signal intensity (Clare and Gronenborn 1982 1983). The trNOE effect has successfully been used for the identification of binding compounds in screening experiments (Meyer et al. 1997). One major problem occurs in the case of aggregation of the ligand molecules, which results also in negative NOEs not obtained due to the binding of the macromolecule. Akasaka (1979) found that selective saturation of the muscle protein myosin also influenced the signal intensity of the ligand ADP due to the transfer of saturation from the protein to the bound ligand via intermolecular cross relaxation. In saturation transfer difference (STD) spectroscopy (Klein et al. 1999, Mayer and Meyer 1999), which relies on the trNOE effect, magnetization is transferred from the protein to the bound ligand, which ‘remembers’ the saturation in its free state, where it is detected. Comparison with a standard experiment directly reveals binding ligands.

1.2.2.2 The STD NMR Experiment

Saturation transfer difference spectroscopy consists of two experiments. In the first one, the off-resonance experiment, a common spectrum is recorded with an irradiation frequency of about 30 ppm, which is far away from the signals of any compound in the sample. In the second experiment (the on-resonance experiment) magnetization is introduced into the protein by selective radio frequency pulses and spreads through the entire molecule via spin diffusion (Kalk and Berendsen 1976). Binding to the protein leads to a transfer of magnetization from the macromolecule to the ligand, which in turn results in a loss of signal intensity of the ligand resonances in the on-resonance spectrum. Subtraction of the on-resonance spectrum from the off-resonance (or reference) spectrum gives the difference spectrum. Only signals from ligands with binding activity appear in

the difference spectrum. A schematic representation of the experiment is given in Figure 1.16. It is clear that the on-resonance spectrum has to ensure that only the protein resonances will be saturated. Due to their strong line broadening protein resonances are also present outside the spectral window of the ligand in the negative ppm range or at ppm-values > 10 . Commonly on-resonance irradiation is performed at around -1 ppm, but at least 1.2 ppm away from the closest ligand signal. It has to be noted that the size of the signal in the difference spectrum cannot be used as a direct measure of binding affinity. It strongly depends on the off-rate of the bound ligand from its complex with the protein, the saturation time and the excess of ligand in the sample. In the difference spectrum also the signals from the protein appear. In order to prevent an overlap of the protein resonances with the ones from the ligand a relaxation filter, the so-called $T_{1\rho}$ -filter can be integrated in the pulse sequence. The STD scheme can in principle be implemented to any NMR experiment (Nagaraja 2006). STD NMR spectroscopy offers several advantages. Neither the ligand nor the protein needs to be labelled. Likewise there is no upper size limitation for the protein, since saturation is rather more efficient the larger the receptor molecule is. The major advantage is represented by the low amount of protein one needs, which can be down to 20 μM . The large excess of ligand, commonly 100-fold in primary screening gives spectra with good quality. Moreover mixtures of compounds with different spectra can be screened.

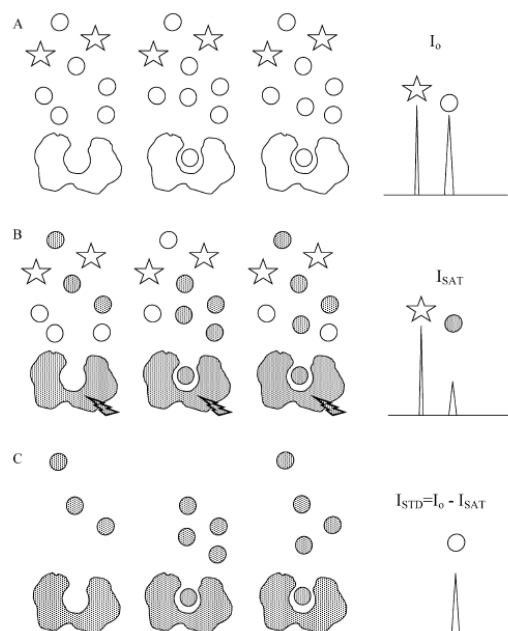


Figure 1.16: Schematic representation of the STD experiment. The binding and non-binding compounds are represented by circles and stars, respectively. (A) During the off-resonance experiment neither receptor nor ligand are saturated and the spectrum gives the intensity I_0 . (B) Selective irradiation of the receptor leads to saturation of the resonance from bound ligands. From the on-resonance spectrum I_{sat} is derived. (C) Subtraction of the on- from the off-resonance spectrum gives the difference spectrum. Only binding components appear with the intensity $I_{STD} = I_{off} - I_{on}$ (taken from Peng et al. 2004).

1.2.2.3 Quantification and Characterization of Ligand Binding

Saturation of the protein spin system is very fast and happens within about 100 ms, the saturation time of the ligand is usually performed in a time period of around 2-5 s. If a large excess of a ligand with a high off-rate is present one protein molecule can saturate more than one ligand molecule, meaning the effect becomes amplified. This effect explains the range of binding affinity, which can be detected by STD NMR spectroscopy. If the affinity is very high ($K_D \leq 100$ nM), the ligand rests for a longer period of time in the binding pocket and the equilibrium is strongly shifted towards the bound state of the ligand. Consequently the information of binding is neither sufficiently carried into solution nor amplified. On the other side for very weak binders ($K_D > 10$ mM) it is less probable that enough binding events happen during the experiment. Titration studies can be used to value the binding constant of a ligand by STD by using the so-called STD amplification factor (Mayer and Meyer 1999).

Like most ligand-based methods direct identification of binding compounds is limited to low and medium affinity binders. This is generally desired in primary NMR screening, since the first hits will be further optimized anyway. However, it is also possible to detect and quantify high affinity ligands. The only requirement is a known weak binding ligand at the binding site of interest, the so-called reporter ligand (Jahnke et al. 2002). In competitions experiments the STD signals of a known weak binder are followed during the titration with a ligand with higher affinity and allow for the determination of the K_D -value. Additionally to its binding strength also information about the orientation of the bound ligand in complex with the macromolecule is obtained (Mayer and Meyer 2001, Peikert et al. 2004). Moieties of the ligand closer to the binding interface exhibit a stronger relative STD effect compared to those parts of the molecule further away from the binding pocket. Consequently parts of the molecule, which are closer to the binding pocket can be identified, which is of special interest by the development of lead substances.

1.2.3 Chemical Shift Perturbation Mapping in 2D NMR Spectroscopy

2D experiments like [^1H , ^{15}N]-HSQC spectroscopy can be used in order to obtain site specific information about the binding of a ligand to a target molecule. To do so ^{15}N enriched protein has to be available. Each backbone (except proline) and side chain NH group of the protein is represented by a cross peak. Upon binding of a ligand the chemical environment of residues directly affected by binding or by conformational changes induced by the binding differs, which is directly reflected by changes of the NMR signals of those residues depending on the exchange processes. One has to discriminate between slow, intermediate and fast exchange processes on the NMR time scale, which result in different observations for the chemical shifts of the residues affected by binding. Slow exchange processes include a reduction of the cross peak intensity at the initial position and the observation of a new cross peak at a different position. Intermediate exchange leads to line broadening and therefore to a decrease in signal intensity, which is not accompanied by the

appearance of a new cross peak for a given residue. If fast exchange processes on the NMR time scale prevail only a single cross peak is observed for the free and complexed form of a given residue with a chemical shift at the population averaged position. All these effects have to be monitored very accurately in order to prevent errors during data evaluation (see next paragraph). If fast exchange is present the combined chemical shift changes (Schumann et al. 2007) can directly be monitored as a function of the ligand concentration. In the case of slow and intermediate exchange signal intensities or the line widths, respectively have to be evaluated. In the first case the relative signal intensity of the new cross peak representing the bound conformation is normalized for the overall signal intensity of both cross peaks belonging to the same residue. In the case of intermediate exchange the change of the line width depending on the ligand concentration is consulted for evaluation. Each NMR parameter can be used in order to determine the binding affinity by plotting the change against the ligand concentration.

1.2.4 Paramagnetic Relaxation Enhancement

Paramagnetic systems, such as transition metal complexes or free radicals contain at least one unpaired electron. Both the chemical shift and the line width of NMR active nuclei can be affected through the interaction with the unpaired electron spins. Consequently paramagnetic substances are subdivided into shift and relaxation reagents, respectively. The latter ones accelerate the relaxation rates of the NMR active nuclei, a phenomenon known as paramagnetic relaxation enhancement (PRE), originally described by Solomon (1955). As a consequence the corresponding signals in the NMR spectrum are strongly broadened depending on the distance to the paramagnetic centre. This effect can be so strong that the signals disappear in the noise level and they are so-called ‘bleached’. The transition metal ion Cu^{2+} exhibits a very fast relaxation rate. Proton signals in a distance less than 11 Å are affected (Arnesano et al. 2003). For that reason the binding sites of the small organic molecule metal(II)-cyclen, which is known to selectively stabilize the weak binding state in active Ras (see section 1.1.6.4) has been investigated in titration studies using the paramagnetic derivative Cu^{2+} -cyclen (T. Graf 2006).

As described in paragraph 1.2.3.1 line broadening is not only caused by the presence of a paramagnetic centre, but can also be observed, when exchange processes, which are slow or intermediate compared to the NMR time scale occur. For that reason data from binding studies using a paramagnetic derivative of the ligand have to be evaluated taking these possible effects into account in order to give reliable results. The best approach herein is to directly compare the data with the ones obtained in titration studies with a diamagnetic derivative of the ligand. Line broadening observable in the presence of both derivatives cannot clearly be assigned to the distance-dependent paramagnetic effect, but may also represent structural changes induced by the binding of the ligand elsewhere in the protein.

2 MATERIALS

2.1 Chemicals

The basic equipment in the laboratory is purchased from the companies Fluka (Neu-Ulm, Germany), Merck (Darmstadt), Roche (Mannheim), Novabiochem (Läufelingen, Switzerland), Acros Organics (Geel, Belgium), Roth (Karlsruhe), Pharma-Waldorf (Düsseldorf) and Sigma (Deisenhofen) with analytical grade.

The metal(II)-cyclen and metal(II)-derivatives and the peptide LIGGR have been synthesized at the chair of Organic Chemistry (Prof. B. König) at the University of Regensburg.

The peptides with consensus Ras binding sequences (CCAVFRL, CCFFRRRL) have been synthesized by the company GenScript Corporation (Piscataway, USA) with purity between 95% and 98%.

2.2 Enzymes

Alkaline Phosphatase	Boehringer/Roche (Mannheim, Germany)
DNase I	Boehringer/Roche (Mannheim, Germany)
Lysozyme	Sigma (Deisenhofen, Germany)
Thrombin	Sigma (Deisenhofen, Germany)

2.3 Frequently Used Buffer Solutions

Buffer A	32 mM Tris/HCl pH 7.4, 10 mM MgCl ₂ , 1 mM DTE
Buffer B	64 mM Tris/HCl pH 7.4, 10 mM MgCl ₂ , 400 mM NaCl, 2 mM DTE, 0.1 mM GDP
Buffer C	50 mM Tris/HCl pH 7.4, 150 mM NaCl, 5 mM EDTA, 5 mM DTE, 1 mM PMSF
Buffer D	50 mM Tris/HCl pH 7.4, 150 mM NaCl, 5 mM DTE
Buffer E	40 mM HEPES/NaOH pH 7.4, 10 mM MgCl ₂ , 150 mM NaCl, 2 mM DTE
Buffer F	40 mM Tris/HCl pH 7.4, 10 mM MgCl ₂ , 2 mM DTE

2.4 Plasmids

For the expression of the different truncated (aa 1 - 166) and full length (aa 1 - 189) human H-Ras proteins ptac-vectors have been used. The expression of the Ras binding domain of Raf-kinase (aa 51-131) was carried out using pGEX-4T-vectors.

2.5 Bacteria Strains

Escherichia coli CK600K supE, hsdM⁺, hsdR⁻, kan^R (Hoffmann-Berling, Heidelberg, Germany)

Escherichia coli BL21(DE3) F⁻, opmT, hsdS (r_B⁻, m_B⁻), gal (38,39) (Stratagene, Heidelberg, Germany)

2.6 Media and Antibiotics

Luria-Bertani (LB)-medium 10 g bacto-tryptone
 5 g yeast extract
 10 NaCl
 were filled up to 1 L with millipore H₂O. After adjusting the pH to 7.0 by 5 mmol L⁻¹ NaOH the medium was autoclaved.

SL-6 stock solution 100 mg ZnSO₄ x 7 H₂O
 30 mg MnCl₂
 300 mg HBO₃
 200 mg CoCl₂ x 6 H₂O
 10 mg CuCl₂ x 2 H₂O
 20 mg NiCl x 6 H₂O
 30 mg Na₂MoO₄
 were filled up to 1 L with millipore water and autoclaved. The stock solution can be stored for long-term at 4 °C.

SL-4 stock solution 500 mg EDTA
 200 mg FeSO₄ x 7 H₂O
 were filled up to 90 mL with millipore water. This solution has to be prepared freshly.

SL-mix	1 mL	SL-6 stock solution
	0.9 mL	SL-4 stock solution
	were filled up to 10 mL with millipore water and sterile filtered.	
Minimal medium	7.5 g	NaHPO ₄
	3 g	KH ₂ PO ₄
	0.5 g	NaCl
	0.25 g	MgSO ₄ x 7 H ₂ O
	0.014 g	CaCl ₂ x 2 H ₂ O
	were filled up to 900 mL with millipore water and autoclaved.	
New minimal medium (NMM)	900 mL	minimal medium
	10 mL	SL-mix
	4 g	glucose
	1 g	NH ₄ Cl
	were filled up to 1 L with sterile millipore water.	

Each antibiotic was purchased from GERBU Biotechnik GmbH (Gaiberg, Germany).

2.7 Protein Standard

SDS7

(66/45/36/29/24/20.1/14.2 kDa) Sigma (Deisenhofen, Germany)

2.8 Expendable Materials

Bradford reagent	Biorad (München, Germany)
NMR sample tubes	
5 mm	Norell Inc. (Landsville, NJ, USA)
8 mm	Shigemi Co. LTD (Tokyo, Japan)
Quart glass cells	Perkin Elmer (Waltham, MA, USA)
Vivaspin ultrafiltration units	Vivascience (Hannover, Germany)

2.9 Columns

Nucleosil 100 C18 precolumn	Bischoff Chromatography (Leonberg, Germany)
ODS hypersil C18 column	Beckman Coulter (Fullerton, CA, USA)
Q-sepharose	Amersham Pharmacia (Freiburg, Germany)
Q-sepharose fast flow	Amersham Pharmacia (Freiburg, Germany)
Superdex G-75 prep grade	Amersham Pharmacia (Freiburg, Germany)

2.10 Instruments

Beckman HPLC-system Gold	Beckman (München, Germany)
FPLC-System	Amersham Pharmacia (Freiburg, Germany)
Luminescence spectrometer LC-50	Perkin Elmer (Waltham, MA, USA)
NMR spectrometer	
Avance 500	Bruker (Karlsruhe, Germany)
Avance 600	Bruker (Karlsruhe, Germany)
Avance 800	Bruker (Karlsruhe, Germany)
Ultrasonic device Sonifier 250/450	Branson (Schwäbisch Gmünd, Germany)
UV/Vis-Spectrometer Uvikon 933	Kontron (Neufahrn, Germany)

2.11 Data Analysis and Graphical Software

Auremol 2.4.0	www.auremol.de
CorelDraw 12	Corel Corporation (Ottawa, Canada)
Origin 6.0	Microcal Software Inc. (Northampton, MA, USA)
PyMOL	DeLano Scientific (San Francisco, CA, USA)
Topspin 2.0	Bruker (Karlsruhe, Germany)
ViewerLite 4.2	Accelrys Inc. (San Diego, CA, USA)

3 METHODS

3.1 Molecular Biology

3.1.1 Expression and Purification of Unlabeled Ras Proteins

Overexpression of human H-Ras was performed according to Tucker et al. (1986) by using ptac-vectors in the *E. coli* strain CK600K. 10 L of the standard LB medium containing 100 mg L⁻¹ carbenicilline and 25 mg L⁻¹ kanamycin was inoculated with 100 mL of an overnight culture. Incubation was carried out at 37 °C and a shaker speed of 180 rpm. Expression was induced at an OD₆₀₀-value between 0.8 and 1 with 1 mM IPTG. Centrifugation of the culture was performed after overnight incubation (about 14 to 18 hours). The precipitate was frozen and stored at -20 °C.

The unfrozen cell pellet was resuspended in cell disruption buffer (32 mM Tris/HCl pH 7.4, 5 mM EDTA, 2 mM DTE and 1 mM PMSF) and cell disruption was initiated by addition of lysozyme (1 mg per mL cell suspension). After 30 minutes of incubation 10 mM MgCl₂ and 20 mg DNase I per 100 mL cell suspension were added and the mixture was allowed to incubate another 30 minutes at 4 °C. Sedimentation of the cell fragments was achieved by 60 minutes of centrifugation with 18.000 g. The clear supernatant was brought on a Q-sepharose column (500 mL volume), which has been equilibrated with buffer A (32 mM Tris/HCl pH 7.4, 10 mM MgCl₂, 1 mM DTE) before. Upon washing with 1.5 column volumes of buffer A a linear salt gradient (0 - 800 mM NaCl in buffer A) was run over an overall volume of 4 L with 4 mL min⁻¹. All steps have been carried out at 4 °C. Fractions containing the Ras protein were identified by SDS-PAGE following the Lämmli protocol (see section 3.2.1), pooled, concentrated and purified further using a Sephadex G-75 prep grade column equilibrated with buffer B (64 mM Tris/HCl pH 7.4, 10 mM MgCl₂, 400 mM NaCl, 2 mM DTE, 0.1 mM DTE). Again SDS-PAGE according to Lämmli (section 3.2.1) allowed for the identification of the fractions containing pure Ras. The corresponding fractions were pooled and concentrated up to about 20 - 50 mg mL⁻¹. Quantification of the protein solution was done by HPLC as described in section 3.2.2. Aliquots of the solution have been frozen in liquid nitrogen and stored at -80 °C.

3.1.2 Expression and Purification of Uniformly ¹⁵N-Labeled Ras

Overexpression of uniformly ¹⁵N-labeled protein was performed by using T7-vectors in the *E. coli* strain BL21(DE3). A cell pellet derived from the sedimentation of an overnight culture prepared in LB medium containing carbenicilline with a final concentration of 25 mg L⁻¹ was washed with new minimal medium (NMM, see section 2.6) twice and dissolved in NMM. The cell suspension was transferred into NMM containing 1 g L⁻¹ ¹⁵NH₄Cl as the sole nitrogen source (Neidhardt et al. 1974). Per 1 L main culture

100 mL overnight starter culture was used. The bacteria were allowed to grow in ^{15}N -enriched NMM at 37 °C and a shaker speed of 200 rpm. Expression of Ras was induced by addition of IPTG (final concentration 0.4 mM). The culture was incubated further at 30 °C and a shaker speed of 180 rpm over night. The following steps were carried out as described for unlabeled Ras in section 3.1.1.

3.1.3 Expression and Purification of Raf-RBD

Raf-RBD (amino acids 51 - 131) was expressed as GST-fusion protein using a pGex-4T-vector in the *E. coli* strain BL21(DE3). 10 L LB medium containing 100 mg carbenicilline per liter were inoculated with 100 mL of an overnight culture and incubated at 37 °C using a shaker speed of 180 rpm. Protein expression was induced at an OD₆₀₀-value of 0.6 with IPTG (final concentration 0.3 mM). Overnight incubation at 30 °C was followed by centrifugation of the culture media. The precipitate was frozen and stored at -20 °C.

The unfreezed cell pellet was resuspended in buffer C (50 mM Tris/HCl pH 7.4, 150 mM NaCl, 5 mM EDTA, 5 mM DTE, 1 mM PMSF) and disrupted as described above for the Ras protein (section 3.1.1). Additionally ultrasound was applied at the end of the disruption process. The cell fragments have been sedimented by 30 minutes of centrifugation with 25.000 g.

The clear supernatant was brought on a GSH column, which has been equilibrated with buffer D (50 mM Tris/HCl pH 7.4, 150 mM NaCl, 5 mM DTE) before with a flow rate of 1 mL min⁻¹. The column material carries immobilized glutathione on the surface, which binds the GST-domain of the fusion protein. Upon washing with 3 to 5 column volumes of buffer D unspecifically proteins binding have been eluted. For the cleavage of Raf-RBD from the GST-tag 1 U thrombin per 2 mg protein was brought on the column and the cleaving reaction was allowed to proceed slowly (0.3 mL min⁻¹) at 4 °C over night. The fractions of the eluate containing Raf-RBD have been identified by SDS-PAGE according to Schägger and v. Jagow (see section 3.2.1), pooled and concentrated. Further purification was done by gel filtration using a Sephadex G-75 column, which has been equilibrated with buffer E (40 mM HEPES/NaOH pH 7.4, 10 mM MgCl₂, 150 mM NaCl, 2 mM DTE). The fractions containing pure Raf-RBD were identified by SDS-PAGE according to Schägger and v. Jagow (1987), pooled and concentrated again with a final concentration of 40 - 80 mg mL⁻¹. Determination of the protein concentration was done using the Bradford reagent (see section 3.2.2). Aliquots of Raf-RBD have been frozen in liquid nitrogen and stored at -80 °C.

3.1.4 Nucleotide Exchange

3.1.4.1 Nucleotide Exchange against GTP

The Ras protein is loaded with GDP after the above described purification steps. By ultrafiltration Ras·GDP was transferred into exchange buffer (50 mM Tris/HCl pH 7.4, 2 mM DTE), which does not contain Mg^{2+} -ions in order to weaken the binding of GDP. Addition of 200 mM $(NH_4)_2SO_4$ and 20 mM EDTA to the sample further destabilized nucleotide binding via coordination of Mg^{2+} . A 50- to 60-fold excess of GTP was added to the Ras·GDP sample. Upon 3 to 4 hours of incubation on ice the protein was loaded with about 90% GTP as determined by HPLC (see section 3.2.2). Free nucleotides were separated by size exclusion chromatography using a Sephadex G-25 PD 10 column, which has been preincubated with buffer F (40 mM Tris/HCl pH 7.4, 10 mM $MgCl_2$, 2 mM DTE) and loaded with the concentrated sample. Fractions of 750 μ M volume have been collected. The fractions containing the protein have been identified by using the Bradford reagent (see section 3.2.2), pooled and concentrated. The purification step was repeated for a second time. The final concentration of the protein and its relative loading with GTP and GDP was determined by HPLC (see section 3.2.2). Appropriate aliquots of the final sample were frozen in liquid nitrogen and stored at -80 °C or directly transferred into the NMR sample tube.

3.1.4.2 Nucleotide Exchange against GppNHp and GTP γ S

The exchange of GDP against the stable GTP-analogues GppNHp or GTP γ S was done using alkaline phosphatase treatment (John et al. 1990). Upon transferring the Ras·GDP sample into exchange buffer (50 mM Tris/HCl pH 7.4, 2 mM DTE) 200 mM $(NH_4)_2SO_4$ and a 2-fold excess of GppNHp or GTP γ S over GDP were added. In addition 2 U alkaline phosphatase per mg Ras·GDP were present in the sample facilitating the dephosphorylation of GDP, but not GppNHp or GTP γ S. The sample was allowed to incubate at 4 °C overnight. Separation of the desired protein sample from the free nucleotides was done as described for Ras·GTP in section 3.1.4.1.

3.2 Biochemical Methods

3.2.1 SDS-Polyacrylamide Gel Electrophoresis (SDS-PAGE)

SDS-PAGE was used for the identification of the fractions containing Ras or Raf-RBD, respectively during the different purification steps. The different components of the protein mixture are separated according to their molecular weight. A 6 μ L sample of each fraction was added to 18 μ L of 4 x SDS-sample buffer (150 mM Tris/HCl pH 6.8, 2% (w/v) SDS, 20% glycerol, 0.1% (w/v) bromine-phenol-blue, 10 mM DTE) and subsequently denatured by heat for about 5 minutes at 95 °C. 18 μ L of the denatured protein sample were put into the pockets of the stacking gel. A standard protein mixture (L7, see section 2.7) was run in

parallel. For the identification of Ras fraction further steps have been carried out according to Lämmli et al. (1970). The content of acryl amide was 15% in the running gel and 5% in the stacking gel, respectively. The running buffer was composed of 25 mM Tris-base/ 200 mM glycine/ 0.1% (w/v) SDS. The gels were run with a constant current of 36 mA per gel for about 50 - 60 minutes. The proteins on the gel were visualized using Coomassie Brilliant Blue.

During the purification of Raf-RBD gel electrophoresis was done following the Schagger and v. Jagow system (1987) due to its molecular weight of less than 10 kDa. The acryl amide content was 16.5% in the running gel and 5% in the stacking gel. The anode buffer consisted of 200 mM Tris/HCl pH 8.9. The cathode buffer was composed of 100 mM Tris, 100 mM tricine and 0.1% (w/v) SDS. The gels were allowed to run at a constant voltage of 100 mV for about 70 - 90 minutes. Visualization of the protein was achieved as described before.

3.2.2 Determination of Protein Concentrations

After removal of free nucleotides reversed phase HPLC was utilized for the quantification of the Ras concentration via the bound guanine nucleotides, which can be detected at a wavelength of 254 nm. Additionally the distinct retention times of the different nucleotides (GMP, GDP, GTP and the corresponding analogues) on the column allow for the determination of their relative loading on Ras. The running buffer consisted of 100 mM K_2HPO_4/KH_2PO_4 pH 6.4, 10 mM TBA, 8% aceto nitrile. Calibration was done with GDP-stock solutions with known concentration derived via UV-measurements ($\lambda = 254$ nm, $\epsilon_{254}(GDP) = 13700 \text{ cm}^{-1} \text{ M}^{-1}$).

For the determination of the concentration of Raf-RBD the Bradford reagent (Bradford 1976) was used. The binding of basic or aromatic amino acid residues in the protein to Coomassie Blue G 250 is detected and quantified at a wavelength of 595 nm. Calibration was carried out with samples containing BSA in defined concentrations.

3.3 NMR Spectroscopy

3.3.1 Saturation Transfer Difference Spectroscopy

3.3.1.1 Sample Preparation, Data Collection and Processing

For STD spectroscopy the samples originally contained 50 μM c'Ras(T35A)·GppNHp in 40 mM Tris/HCl pH 7.4, 10 mM $MgCl_2$, 5% D_2O and 0.2 mM DSS as a reference standard, if not otherwise stated. In binding studies the ligands were dissolved in the sample buffer and titrated to the protein sample.

The on-resonance irradiation frequency was set to a chemical shift value between -2 ppm and 0.3 ppm. Off-resonance irradiation was applied at +30 ppm. The protein was selectively saturated by a train of 40 Gauss-shaped 90° pulses of 50 ms length giving a

total saturation time of 2 s. On- and off-resonance experiments have been performed in an interlaced fashion. Water suppression was achieved using a delay $d19$ of 100 μ s for binomial water suppression. Prior to acquisition a so-called $T_{1\rho}$ -filter consisting of a spinlock pulse with 50 ms length and an attenuation of 15 dB was implemented in order to suppress protein proton resonances, which eases data evaluation (Scherf and Anglister 1993). The experiments were performed on a Bruker Avance 600 MHz spectrometer equipped with a 5 mm triple resonance cryo probe at 278 K. 32k data points have been collected, zero-filled to 64k and multiplied by an exponential line broadening function of 0.3 Hz. After splitting the data into on- and off-resonance both spectra were processed and phased identically. Baseline correction was done automatically using a polynomial of degree 5. Processing was performed using topspin 2.0 software.

3.3.1.2 Quantification of Ligand Binding

Quantification of ligand binding by STD NMR spectroscopy was done by using the so-called STD amplification factor A_{STD} introduced by Mayer and Meyer (1999). A_{STD} is defined as the relative STD effect multiplied by the ligand excess (Equation 3.1).

$$A_{STD} = \frac{I_0 - I}{I_0} \cdot \text{ligand excess}$$

Equation 3.1

A_{STD} was plotted against the total ligand concentration, which gives a normal binding isotherm, which can be used to derive the K_D value following Equation 3.2 with α_{STD} being the maximum A_{STD} and $[L]$ the total ligand concentration.

$$A_{STD} = \frac{\alpha_{STD} \cdot [L]}{[L] + K_D}$$

Equation 3.2

Determination of the STD effect was achieved via the relative intensities determined using the Topspin 2.0 software. Fitting of the data was done using Microcal Origin.

3.3.2 ^{31}P NMR Spectroscopy

For ^{31}P NMR spectroscopy the protein or nucleotide, respectively was dissolved in 40 mM Tris/HCl pH 7.5, 10 mM MgCl_2 , 2 mM DTE and 0.1 mM DSS and 5% D_2O , if not otherwise stated. In the titration studies with Raf-RBD the sample additionally contained 150 mM NaCl to avoid aggregation of Raf-RBD. An 8 mm Shigemi sample tube containing 0.7 - 1.2 mL protein solution with a concentration between 0.5 and 2 mM Ras

or nucleotide was used for the measurements. The NMR spectra were recorded with a Bruker Avance-500 NMR spectrometer operating at a ^{31}P frequency of 202 MHz using a 70° pulse and a repetition time of 6 s. Measurements were performed in a 10 mm selective ^{31}P probe using 8 mm Shigemi sample tubes at various temperatures. Protons were decoupled during data acquisition by a GARP sequence (Shaka et al. 1985) with strength of the B_1 -field of 830 Hz. A γ -value of 0.4048073561 reported by Maurer and Kalbitzer (1996) was used which corresponds to 85% external phosphoric acid contained in a spherical bulb. Temperature was controlled using the line separation (methylene-hydroxyl) of external ethylene glycol for calibration (Raiford et al. 1979). The absolute accuracy of the temperatures given in this work is better than ± 0.5 K. All ^{31}P NMR measurements have been carried out at 278 K.

3.3.3 [^1H , ^{15}N]-(-TROSY)-HSQC Spectroscopy

3.3.3.1 Sample Preparation and Data Collection

2D NMR measurements used for the titrations with the different metal(II)-chelate complexes and the peptide LGGIR were performed on approximately 1 mM ^{15}N labeled Ras·Mg $^{2+}$ ·GppNHp samples in 40 mM Tris/HCl pH 7.4, 10 mM MgCl $_2$, 2 mM DTE, 0.1 mM DSS and 5% D $_2$ O. In the binding studies with the peptides CCAVFRL and CCFFFRRL the protein samples were dissolved in 20 mM Na $_2$ HPO $_4$ -NaH $_2$ PO $_4$ pH 5.5, 10 mM MgCl $_2$, 2 mM DTE, 0.2 mM DSS and 5% D $_2$ O. In each titration the ligand was dissolved in the same buffer as the protein sample and added stepwise. The data with metal(II)-BPA were collected with a Bruker AVANCE-600 spectrometer equipped with a TXI cryoprobe at operating frequencies of 600.13 MHz for ^1H and 60.81 MHz for ^{15}N . Measurements with the peptides were performed on a Bruker AVANCE-800 spectrometer equipped with a TXI cryoprobe operating at a proton frequency of 800.12 MHz and 81.08 MHz for ^{15}N . All NMR spectra within the titration studies were acquired at 293 K. At every titration step a standard [^1H , ^{15}N]-HSQC experiment with sensitivity improvement (Palmer et al. 1969) was performed. Each 2D spectrum was recorded as a complex data matrix comprised of 128, 256 or 516 x 2048 points using a sweep width of 8400 Hz or 9600 Hz in the ^1H dimension and 2400 Hz or 2800 Hz in the ^{15}N dimension. A recycle delay of 3.4 s was used with 16 scans/FID. Before each 2D experiment a standard ^1H NMR spectrum was recorded. ^1H chemical shifts were directly and ^{15}N chemical shifts indirectly referenced to DSS as described by Wishart et al. (1995).

3.3.3.2 Data Processing and Evaluation

All NMR spectra were processed using the TOPSPIN 2.0 software (Bruker Biospin). The assignment of the amide resonances for Ras(wt)·Mg $^{2+}$ ·GppNHp was performed with regard to the assignment published by Ito et al. (1997). The cross peaks of Ras(T35S) and Ras(T35A) bound to Mg $^{2+}$ ·GppNHp were assigned by F. Schumann (University of

Regenburg, to be published elsewhere). Within the single titrations steps the assignment was transferred using AUREMOL-SHIFTOPT (Baskaran et al. 2009). Combined amino acid specific chemical shift differences $\Delta\delta_{\text{comb}}$ of the amino acids j were calculated using the program AUREMOL. $\Delta\delta_{\text{comb}}$ is defined by Equation 3.3, where $\Delta\delta_{\text{H},j}$ and $\Delta\delta_{\text{N},j}$ are the chemical shift differences of the amide proton and nitrogen of amino acid j in the partly complexed and free protein, respectively. The weighting factors $w_{\text{H},j}$ and $w_{\text{N},j}$ are specific for the kind of atom and the type of amino acid in position j .

$$\Delta\delta_{\text{comb},j} = \sqrt{\frac{1}{2}((w_{\text{H},j}\Delta\delta_{\text{H},j})^2 + (w_{\text{N},j}\Delta\delta_{\text{N},j})^2)}$$

Equation 3.3

Chemical shift changes $\Delta\delta_{\text{comb},j}$ were considered as significant when they were larger than the corrected standard deviation σ_0^{corr} to zero (Schumann et al. 2007).

3.3.3.3 Determination of Binding Constants

For the determination of the dissociation constant of the peptide LGGIR the combined chemical shift changes $\Delta\delta_{\text{comb}}$ for an amino acid j was plotted against the total ligand concentration $[L]$. The data were fitted using a simple one-site binding isotherm following Equation 3.4. $\Delta\delta_{\text{comb}}$ of amino acid j was calculated as described above. $\Delta\delta_{\text{comb},j\text{max}}$ is the maximum combined chemical shift change.

$$\Delta\delta_{\text{comb},j} = \frac{\Delta\delta_{\text{comb},j\text{max}} \cdot [L]}{K_D + [L]}$$

Equation 3.4

3.3.4 High Pressure NMR Spectroscopy

3.3.4.1 Sample Preparation and Data Collection

The pressure series with $\text{Ras(wt)} \cdot \text{Mg}^{2+} \cdot \text{GppNHp}$ were carried out at 278 K between 3 MPa and 200 MPa and at 303 K between 3 MPa and 180 MPa. The samples contained 1.05 mM (278 K) and 1.84 mM (303 K) ^{15}N -labeled $\text{Ras(wt)} \cdot \text{Mg}^{2+} \cdot \text{GppNHp}$ in 40 mM Tris/HCl pH 7.4, 10 mM MgCl_2 , 2 mM DTE and 12% D_2O . In the sample for the pressure series recorded at 278 K additionally 0.1 mM DSS was present as internal reference standard. For the pressure series carried out at 278 K the sample was transferred into a glass capillary with an outer diameter of 5 mm and an inner diameter of 1.2 mm. The measurements at 303 K were performed on a ceramic cell with an outer diameter of 4 mm and an inner diameter of 1.1 mm as described by Beck-Erlach et al. (manuscript submitted). The samples were pressurized using the Yamada glass cell method (Yamada 1974). To protect

the spectrometer probe from damage, the glass capillary or ceramic cell was placed into a short polished Teflon tube (50 mm length, 5 mm inner diameter, 0.5 mm walls).

Measurements were performed on a Bruker AVANCE-800 spectrometer equipped with a TXI cryo probe operating at a frequency of 800.12 MHz for protons and 81.08 MHz for ^{15}N . At every pressure step a phase-sensitive [^1H , ^{15}N]-HSQC experiment was performed. Each 2D spectrum was recorded as a complex data matrix comprised of 2048 x 512 points using a sweep width of 8400 Hz in the ^1H -dimension and 2400 Hz in the ^{15}N -dimension. A recycle delay of 3.4 s was used with 8 scans/FID and 16 scans/FID at the series performed at 278 K and 303 K, respectively. At 278 K additionally experiments with 32 scans/FID have been recorded at 3 MPa and 200 MPa. Before and after each 2D experiment a standard ^1H NMR spectrum was recorded. ^1H chemical shifts were directly and ^{15}N chemical shifts indirectly referenced to DSS at the pressure series at 278 K and to the signal of Tris at the pressure series at 303 K.

3.3.4.2 Data Processing and Evaluation

The assignment of the amide resonances for Ras(wt)·Mg²⁺·GppNHp was performed with regard to the assignment published by Ito et al. (1997). Additionally pH and temperature series recorded by M. Spörner (University of Regensburg) have been included in the assignment of the spectra, since the temperature or the pH value differed from the conditions within the assignment performed by Ito et al. (1997). All NMR spectra were processed using the TOPSPIN 2.0 software. Data analysis was performed using the Auremol software. The data have been evaluated as described in the following paragraphs.

3.3.4.3 Analysis of the Chemical Shifts

The pressure dependence of the chemical shift values of the amide protons and nitrogen atoms in the [^1H , ^{15}N]-HSQC spectra of the protein was fitted in two different ways. Using a second order Taylor expansion (Equation 3.4) the first and second order pressure coefficients B_1 and B_2 , respectively can be derived.

$$\delta(p, T_0) = \delta_0(p_0, T_0) + B_1(p_0, T_0)(p - p_0) + B_2(p_0, T_0)(p - p_0)^2$$

Equation 3.4

δ_0 is the chemical shift at ambient pressure p_0 at temperature T_0 . The chemical shifts of the amide protons were corrected by the known pressure response of random-coil peptides (Gly-Gly-X-Ala) of the corresponding amino acid (Arnold et al. 2002, Kremer et al. 2004) giving the corrected coefficients B_1^* and B_2^* .

If there is an equilibrium between two conformations of the protein, which are in fast exchange on the time scale of the NMR experiment, the observed chemical shifts are the weighted average of the chemical shifts of the two states 1 and 2. With an equilibrium constant for the conformational exchange K_{12} defined by the probabilities N_1 and N_2 to be in state 1 and 2

$$K_{12} = \frac{N_2}{N_1} = \exp\left(-\frac{\Delta G_{12}}{RT}\right)$$

Equation 3.5

the chemical shift δ is given by

$$\delta = \frac{1}{1 + K_{12}} \delta_1 + \frac{K_{12}}{1 + K_{12}} \delta_2 = \frac{\delta_1 + \delta_2 \exp\left(-\frac{\Delta G_{12}}{RT}\right)}{1 + \exp\left(-\frac{\Delta G_{12}}{RT}\right)}$$

Equation 3.6

Since in addition to the main process always classical continuous chemical shifts by compression of the molecule occur, these (small) effects can be accounted for by assuming an additional pressure dependence of the chemical shift values $\delta_1(p)$ and $\delta_2(p)$ or by correcting the experimental values before fitting by suitable data such as random-coil pressure induced shifts (see above). The free energy at ambient pressure $\Delta G_{12}^0 = \Delta G_{12}(p_0)$ can be determined by fitting the data to Equation 3.7.

$$\Delta G_{12} = \Delta G_{12}^0 + \Delta V_{12}^0(p - p_0) + \frac{1}{2} \Delta \beta_{12}(p - p_0)^2$$

Equation 3.7

Here, $\Delta V_{12}^0 = \Delta V_{12}(p_0) = V_2(p_0) - V_1(p_0)$ is the difference of the partial molar volumes and $\Delta \beta_{12}$ the difference of the partial molar compressibilities. For the calculations of the $\Delta G_{12}(p_0)$ values the quadratic term in Equation 3.7 was neglected giving Equation 3.8.

$$\Delta G_{12} = \Delta G_{12}^0 + \Delta V_{12}^0(p - p_0)$$

Equation 3.8

Equations 3.6 and 3.8 can be generalized for a n-state process with the chemical shifts $\delta_1, \delta_2, \dots, \delta_n$ by

$$\delta = \frac{\delta_1 + \sum_{i=2}^n \delta_i \exp\left(-\frac{\Delta G_{li}^0 + \Delta V_{li}^0 (p - p_0)}{RT}\right)}{1 + \sum_{i=2}^n \exp\left(-\frac{\Delta G_{li}^0 + \Delta V_{li}^0 (p - p_0)}{RT}\right)}$$

Equation 3.9

3.3.4.4 Analysis of the Signal Volumes

As described in section 4.8.3.1 the observed intensity in the [^1H , ^{15}N]-HSQC spectra recorded at different pressure are higher than the actual ones caused by the compression of the sample. Thus the area of the signal of the Tris buffer in the sample was used as an internal correction factor. The plot of the relative signal area $A_p / A_{3 \text{ MPa}}$ against the applied pressure p was regressed linearly according to Equation 3.10.

$$\frac{A}{A_{3 \text{ MPa}}} = a \cdot p + b$$

Equation 3.10

The slope a and the intercept b obtained by the fit according to Equation 3.10 were used for the correction of the observed intensity I in the single [^1H , ^{15}N]-HSQC spectra giving the corrected intensity I_{corr} following Equation 3.11, which was used in the further evaluation.

$$I_{\text{corr}} = \frac{I}{a \cdot p + b}$$

Equation 3.11

Is there a conformational exchange between two states 1 and 2 which is slow relative to the time scale of the NMR experiment ($|\omega_2 - \omega_1| \gg 1/\tau_{\text{ex}}$, τ_{ex} exchange correlation time) the signal volume I_i of state i ($i = 1, 2$) is proportional to its population N_i . Assuming a two-state transition for the change of the conformational equilibrium with increased pressure, the equilibrium constant K_{12} can be calculated from the relative cross-peak intensities of the HSQC spectra by Equation 3.12 (Akasaka 2006). $I_i(p)$ is the cross-peak intensity at pressure p and I_0 is defined by $I_0 = I_1 + I_2$.

$$K_{12} = \frac{I_2}{I_1} = \frac{1 - \frac{I(p)}{I_0}}{\frac{I(p)}{I_0}}$$

Equation 3.12

With Equation 3.5 the observed intensity I is given by

$$I_1(p) = \frac{I_0}{1 + \exp\left(-\frac{\Delta G_{12}}{RT}\right)}$$

Equation 3.13

The free energy at ambient pressure ΔG_{ii} is defined by Equation 3.8, when neglecting the quadratic term in Equation 3.7. When only one of the two cross peaks is observable, I_0 can be used as additional fit parameter.

4 RESULTS

4.1 Saturation Transfer Difference Spectroscopy

4.1.1 General Considerations

Since oncogenic Ras proteins are key players in aberrant signalling contributing to cancer development its inhibition is of high medicinal interest (Wittinghofer and Waldmann 2000). One promising strategy herein is the stabilization of conformational state (1) of activated oncogenic Ras (see section 1.1.6.4). A calculated structure of the binding site of metal(II)-cyclen in the partial loss-of-function mutant Ras(T35A) complexed to Mg^{2+} ·GppNHp is available (T. Graf 2006). Using the computer program LUDI S. Kreitner (University of Regensburg) is working on the structure-based virtual screening for *de novo* ligands binding at the same position as does the metal(II)-cyclen and additionally for small fragments binding in a defined distance to the metal(II)-cyclen, which can be linked to the compounds. Potential hits identified in this approach will be further investigated concerning their actual binding activity by STD NMR spectroscopy and therefore the method was optimized for the Ras protein.

The experiments have been carried out with Ras(T35A)· Mg^{2+} ·GppNHp for several reasons. First, this mutant was also used in the virtual screening, secondly each compound being capable of stabilizing conformational state (1) should also preferentially bind to a mutant existing in this state. Third, the [^1H , ^{15}N]-HSQC assignment for this mutant is available allowing for further investigations of identified Ras ligands in terms of their binding site(s).

4.1.2 Determination of Measurement Parameters

Saturation transfer difference spectroscopy consists of two experiments, which are acquired in an interleaved fashion. The off-resonance spectrum represents a common spectrum with on-resonance irradiation far away from the resonances of any compound in the screening mixture containing the protein and different potential ligands. It was set to 30 ppm in each experiment, which is commonly applied (Mayer and Meyer 1999). The on-resonance spectrum ensures selective irradiation of some protein proton resonances leading to the saturation of the entire protein via spin diffusion and additionally of bound ligands via intermolecular cross relaxation. In order to obtain reliable results one has to ensure the selective and sufficient saturation of the protein. Important parameters herein are the on-resonance irradiation frequency for the saturation of the protein and the attenuation of the saturation pulse. Different on-resonance irradiation frequencies have been tested as well as different attenuations. As soon as the saturation is efficient one expects the same or at least similar protein signal intensity in the difference spectrum as in the reference spectrum. Additionally signals from nonbinding compounds should not appear in the

difference spectrum avoiding false positive results. Figure 4.1 shows the difference spectra obtained with different on-resonance irradiation frequencies.

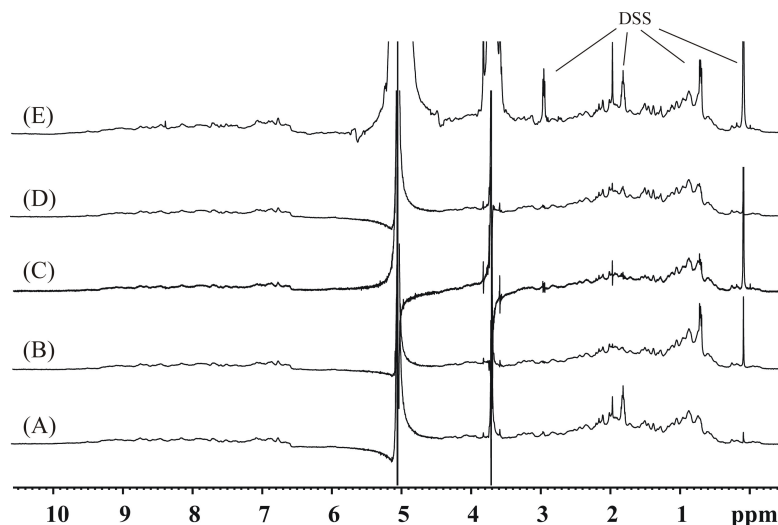


Figure 4.1: Variation of the on-resonance irradiation frequency for saturation. Shown are the difference spectra obtained from STD experiments with an on-resonance irradiation frequency of 1.4 ppm (A), 0.3 ppm (B), -0.4 ppm (C) and -1 ppm (D) with an attenuation of 40 dB, respectively. In spectrum (E) the reference spectrum is shown for comparison. 20 mM Ras(T35A)-Mg²⁺-GppNHp in 40 mM Tris/HCl pH 7.4, 10 mM MgCl₂, 0.2 mM DSS and 5% D₂O. All spectra have been recorded at 278 K.

Within the different frequencies applied no significant differences are observed in terms of the degree of saturation, but concerning the selectivity for the protein over other sample additives. As one can see very clearly the different resonance signals belonging to DSS appear in the difference spectrum depending on the on-resonance frequency. Irradiation at 850 Hz (1.4 ppm at a spectrometer operating at 600 MHz) leads to the direct saturation of the pentet signal of DSS at 1.75 ppm (Figure 4.1 (A)). Setting the on-resonance irradiation frequency to 200 Hz (0.33 ppm) leads to the appearance of a triplet signal at 0.63 ppm assigned to DSS in the difference spectrum (Figure 4.1 (B)). Irradiating at 600 Hz (1 ppm) gives a difference spectrum showing only signals from the protein, except the signal of the nine methyl protons of DSS (0 ppm), which is also present when irradiating at -600 Hz (-1 ppm). As described in section 1.2.2.2 the on-resonance irradiation frequency should be set to a value, which is at least 1.2 ppm away from the closest ligand signal. If one wants to study peptide ligands for example an on-resonance irradiation frequency of -1 ppm might not be far enough from the peptide resonances and on-resonance irradiation has to be performed at an even lower frequency range. For that reason the attenuation for the shaped pulse for saturation was adjusted such that both selective and sufficient saturation is achieved even with on-resonance frequencies at higher fields. The corresponding difference spectra obtained with an on-irradiation frequency of -2 ppm with different power levels are shown in Figure 4.2. As one can see an attenuation of 30 dB is sufficient for the saturation of the protein resonances. The protein appears with a similar signal intensity compared to the reference spectrum, whereas signals from DSS except the

one at 0 ppm do not appear in the reference spectrum. The saturation spreads over the entire protein, signals of the aromatic region and the backbone and side chain H^N are also showing up with a signal intensity comparable to the reference spectrum. Consequently sufficient and selective saturation of the protein signals is achieved. Additionally the saturation obtained with an attenuation of 40 dB is sufficient for the experiments.

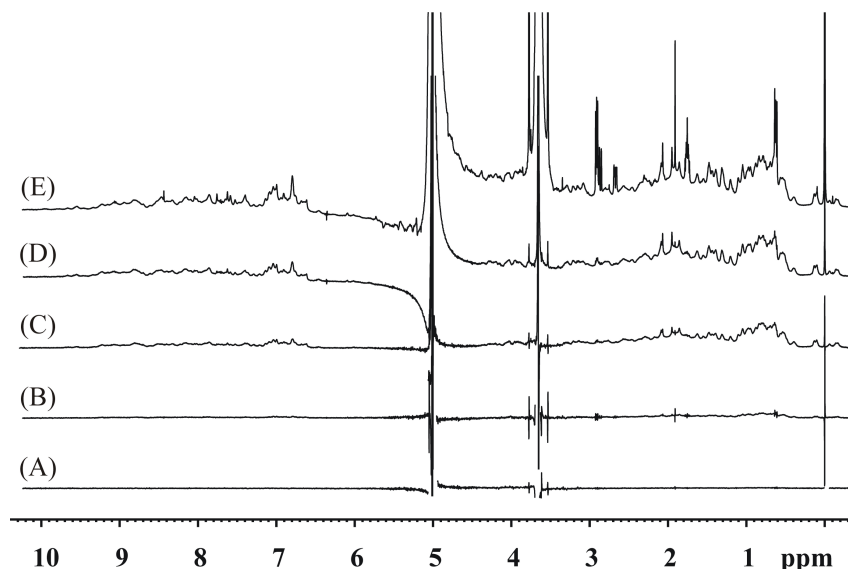


Figure 4.2: Comparison of different power levels (sp13) for the saturation of the protein resonances at an on-resonance frequency of -2 ppm. Difference spectra of a sample containing 50 μ M Ras(T35A)·Mg²⁺·GppNHp in 40 mM Tris/HCl pH 7.4, 10 mM MgCl₂, 0.2 mM DSS and 5% D₂O obtained with a power level of 60 dB (A), 50 dB (B), 40 dB (C) and 30 dB (D) for protein saturation in the on-resonance spectrum, respectively. The reference spectrum (E) is shown for comparison. All spectra have been recorded at 278 K.

Irradiation closer to the methylen signals of the protein at 30 dB does neither alter the degree of saturation nor the relative signal intensity of the DSS signal at 0 ppm significantly as shown in Figure 4.3. DSS obviously binds to the Ras protein with its signal around 0 ppm showing the biggest response.

STD NMR is a so-called ligand-based method, i.e. changes of the NMR parameters of the ligand are observed. In order to ease the evaluation of the spectra a spinlock filter can be implemented to the STD pulse sequence prior to acquisition eliminating protein resonances in the spectra eventually overlapping with ligand signals (Mayer and Meyer 2001). Figure 4.4 shows the difference spectrum of the same sample recorded with and without a spinlock filter. As one can see very clearly, no protein resonances are visible in the difference spectrum, when a spin lock filter $T_{1\rho}$ is applied. Again, the DSS signal at 0 ppm appears in the difference spectrum and additional the pentet signal around 1.75 ppm. The sample additionally contained DTE, commonly used as reducing agent for disulfide bonds in protein samples. In the difference spectrum the signals representing DTE and its oxidized disulfide from around 2 ppm and 2.8 ppm do not give signals. This again shows that saturation is achieved selectively.

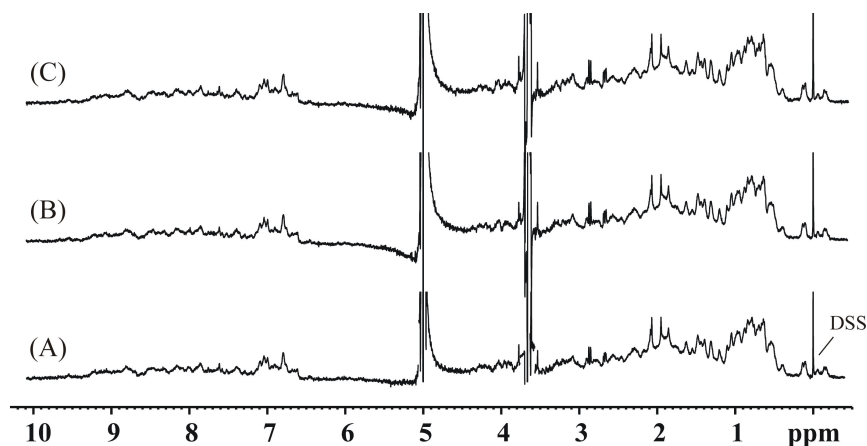


Figure 4.3: Different on-resonance irradiation frequencies used at 30 dB. Shown are the difference spectra obtained from STD experiments with a sample containing 50 μM Ras(T35A) $\cdot\text{Mg}^{2+}\cdot\text{GppNHp}$ in 40 mM Tris/HCl pH 7.4, 10 mM MgCl_2 , 0.2 mM DSS and 5% D_2O with on-resonance irradiation frequency set to -2 ppm (A), -1.3 ppm (B) and -1 ppm (C), respectively. All spectra have been recorded at 278 K.

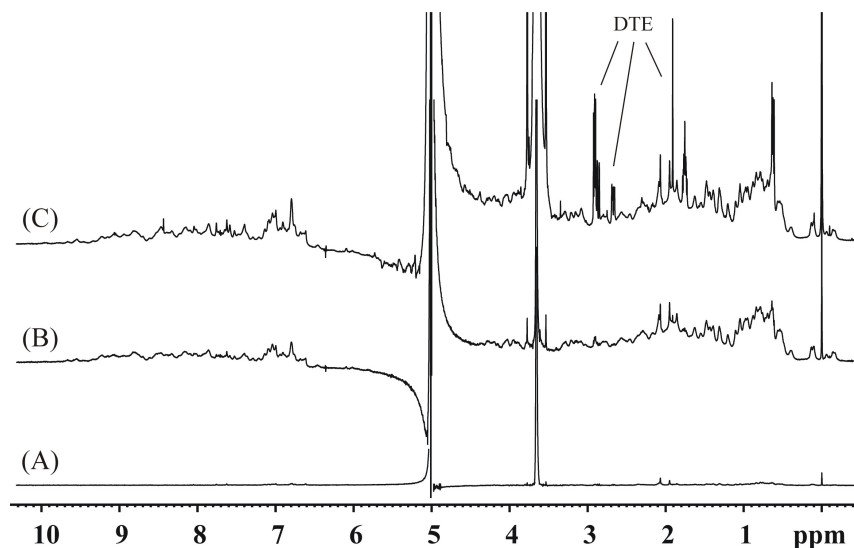


Figure 4.4: Integration of the spinlock filter into the STD experiment. The difference spectrum of sample containing 50 μM Ras(T35A) $\cdot\text{Mg}^{2+}\cdot\text{GppNHp}$ in 40 mM Tris/HCl pH 7.4, 10 mM MgCl_2 , 0.2 mM DSS and 5% D_2O is shown in with (A) and without (B) a spinlock filter $T_{1\rho}$ of 50 ms at 25 dB. The reference spectrum of the sample (C) is shown for comparison.

4.1.3 STD NMR Spectroscopy with the Known Ras Ligand Zn^{2+} -Cyclen

As described in section 1.1.6.4 the small organic compound Zn^{2+} -cyclen has been identified as Ras ligand. In order to know whether the above determined parameters are appropriate for the detection of binding activity for Ras the experiment was carried out with Zn^{2+} -cyclen. The latter compound was present in a 100-fold excess over $\text{Ras(T35A)} \cdot \text{Mg}^{2+} \cdot \text{GppNHp}$ in the sample. This ratio of protein to ligand is commonly used in screening experiments (Meyer and Peters 2003) using STD. Figure 4.5 shows the spectra obtained with $\text{Ras(T35A)} \cdot \text{Mg}^{2+} \cdot \text{GppNHp}$ with Zn^{2+} -cyclen.

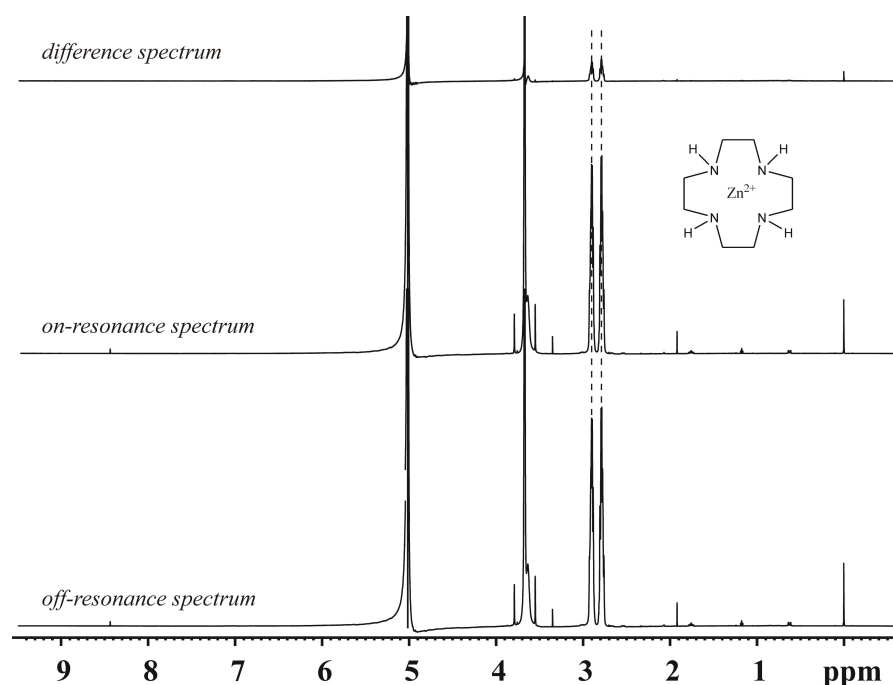


Figure 4.5: STD experiment with $\text{Ras(T35A)} \cdot \text{Mg}^{2+} \cdot \text{GppNHp}$ and Zn^{2+} -cyclen. The sample contained 50 μM $\text{Ras(T35A)} \cdot \text{Mg}^{2+} \cdot \text{GppNHp}$ in 40 mM Tris/HCl pH 7.4, 10 mM MgCl_2 , 0.2 mM DSS and 5% D_2O and 5 mM Zn^{2+} -cyclen $\cdot 2 \text{Cl}^-$. On-resonance irradiation was performed at -2 ppm at 30 dB. A spinlock filter was implemented (50 ms at 15 dB). All spectra were recorded at 278 K.

As one can see the resonance signals of the compound are visible in the difference spectrum. For the determination of the dissociation constant Zn^{2+} -cyclen was titrated to Ras(T35A) bound to $\text{Mg}^{2+} \cdot \text{GppNHp}$ and the STD amplification factor A_{STD} was calculated after each step according to Equation 3.1. The obtained binding curve is shown in Figure 4.6. The results have been fitted according to Equation 3.2 yielding an overall K_D -value of $9.65 \pm 1 \text{ mM}$.

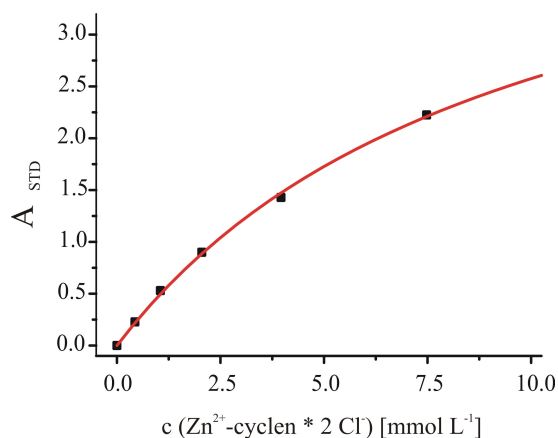


Figure 4.6: Plot of A_{STD} against the concentration of Zn^{2+} -cyclen. The amplification factor was calculated from data obtained in STD titrations experiments with a sample originally containing $50 \mu\text{M}$ $\text{Ras(T35A)} \cdot \text{Mg}^{2+} \cdot \text{GppNHp}$ in 40 mM Tris-D11/HCl pH 7.4, 10 mM MgCl_2 , 0.2 mM DSS and 5% D_2O . On-resonance irradiation was performed at -2 ppm at 40 dB . A spinlock filter was implemented (50 ms at 15 dB). All spectra were recorded at 278 K . The data were fitted according to Equation 3.2 giving a K_D -value of $9.65 \pm 1 \text{ mM}$. The fit is given by the red line.

4.1.4 Identification of Zn^{2+} -BPA as Ras Ligand

Zn^{2+} -cyclen has been found to bind close to the bound nucleotide in conformational state (1) of active Ras. Receptors based on metal(II)-bis(2-picoly)amine (subsequently referred to as metal(II)-BPA) are known in molecular recognition for phosphate sensing (Sakamoto et al. 2009). Consequently the compound class was initially tested in terms of its binding activity for $\text{Ras(T35A)} \cdot \text{Mg}^{2+} \cdot \text{GppNHp}$ using STD NMR spectroscopy. The on-resonance irradiation frequency was set to 0.3 ppm at 40 dB in the experiment with Zn^{2+} -BPA since this frequency should be far away enough from the closest Zn^{2+} -BPA signal around 4 ppm . However, the experiment was carried out both with a sample containing the ligand in the absence and the presence of the protein. Figure 4.7 shows the obtained spectra. The only resonance visible in the difference spectrum of the experiment in the absence of Ras (Figure 4.7 (B)) is the one belonging to DSS, which is very close to the on-resonance irradiation frequency and became saturated directly. No resonances belonging to Zn^{2+} -BPA appear and consequently false positive results should not be obtained in the presence of the protein. The same experiment was carried out with a sample containing additionally $50 \mu\text{M}$ $\text{Ras(T35A)} \cdot \text{Mg}^{2+} \cdot \text{GppNHp}$. Now the signals from Zn^{2+} -BPA show up in the difference spectrum (Figure 4.7 (C)) and the compound can clearly be identified as a binding ligand. Note that in the difference spectrum the DSS signal at 0 ppm is also appearing again in contrast to the difference spectrum obtained in the sample without Ras.

Zn^{2+} -BPA was titrated to $\text{Ras(T35A)} \cdot \text{Mg}^{2+} \cdot \text{GppNHp}$ up to a 320-fold molar excess over Ras and the STD amplification factor A_{STD} has been determined at each step according to Equation 3.1. Figure 4.8 shows the plot of A_{STD} for the single proton resonances against

the ligand concentration. Fitting the data according to Equation 3.2 gives a dissociation constant of 2.07 ± 0.25 mM.

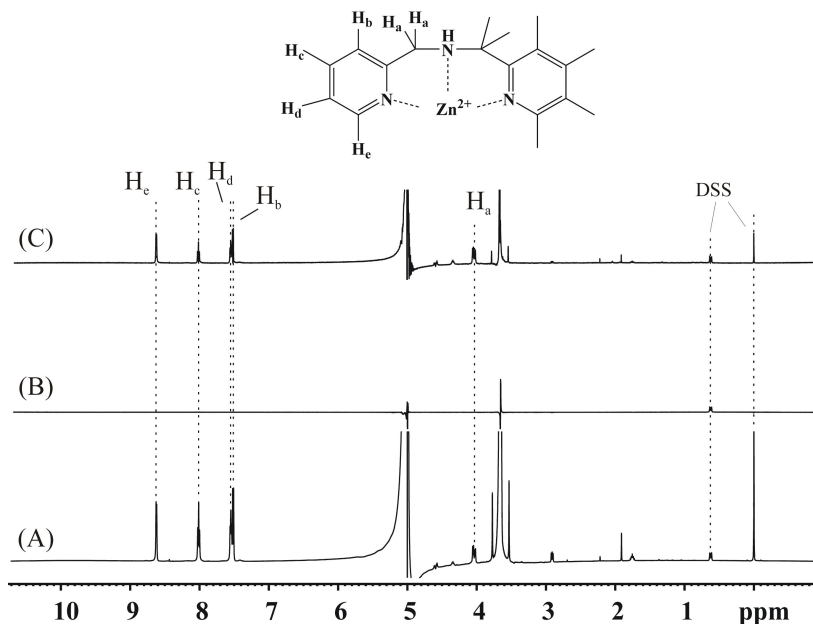


Figure 4.7: Identification of Zn^{2+} -BPA as Ras ligand. (A) Reference spectrum of a sample containing 5 mM Zn^{2+} -BPA in 40 mM Tris/HCl pH 7.4, 10 mM MgCl_2 , 0.2 mM DSS and 5% D_2O recorded with an off-resonance irradiation frequency of 30 ppm. (B) and (C) show the difference spectra obtained in the absence and presence of 50 μM Ras(T35A)- Mg^{2+} -GppNHp, respectively. On-resonance irradiation was performed at 0.3 ppm. A spinlock filter of 50 ms at 15 dB was implemented in order to avoid overlapping between protein and ligand resonances. All spectra were recorded at 278 K.

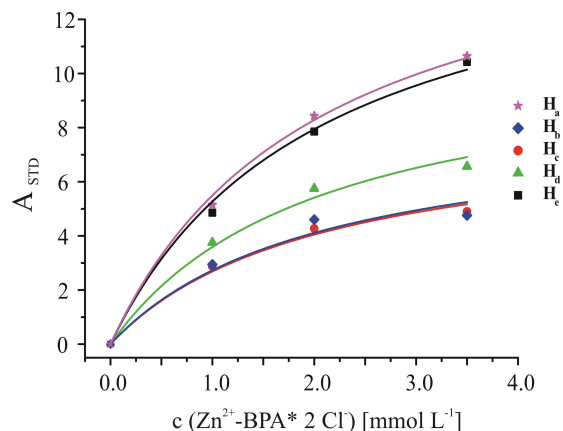


Figure 4.8: Plot of the STD amplification factor obtained for each ligand proton against the ligand concentration. The amplification factors were calculated from data obtained in STD titrations experiments with a sample originally containing 50 μM Ras(T35A)- Mg^{2+} -GppNHp in 40 mM Tris/HCl pH 7.4, 10 mM MgCl_2 , 0.2 mM DSS and 5% D_2O . On-resonance irradiation was set to 0.3 ppm in this case. All spectra have been recorded at 278 K. The data were fitted according to Equation 3.2 giving a K_D -value of 2.07 ± 0.25 mM.

4.2 ^{31}P NMR Spectroscopic Investigations on the Influence of Metal(II)-Cyclen and -BPA on Ras

4.2.1 Binding of Metal(II)-Cyclen and -BPA to $\text{Mg}^{2+}\cdot\text{GppNHp}$

Zn^{2+} -cyclen binds in close proximity to the bound nucleotide, when Ras is complexed to $\text{Mg}^{2+}\cdot\text{GppNHp}$ (Rosnizeck et al., accepted). In this section the influence of the compound to GppNHp in free form is studied by ^{31}P NMR spectroscopy under identical conditions compared to the experiments of the Ras-nucleotide complex, i.e. at 278 K and pH 7.4 with 10 mM MgCl_2 being present in the sample. The spectra of $\text{Mg}^{2+}\cdot\text{GppNHp}$ in the presence of increasing concentrations of Zn^{2+} -cyclen are shown in Figure 4.9. An upfield shift is observed for the β -phosphate resonance, while the shift direction of the γ -phosphate signal is downfield. For the α -phosphate resonance no significant shift differences are observed. Additionally significant line broadening is observed for each signal with the strongest effects for the β - and the γ -phosphate, respectively. The shift behaviour of the resonances is in good agreement with that observed, when $\text{Mg}^{2+}\cdot\text{GppNHp}$ is complexed to the Ras protein (Spoerner et al. 2005c). GppNH₂ and inorganic phosphate P_i , which are the hydrolysis products of GppNHp were also present in the sample. As one can see, also significant shift differences are observed for both the phosphate peak and the resonance representing the β -phosphate group of GppNH₂ around -0.9 ppm.

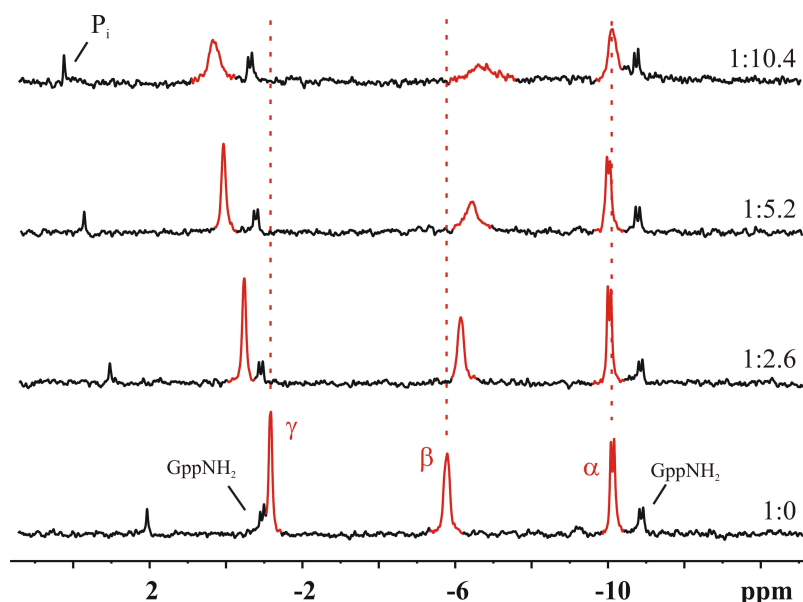


Figure 4.9: Complex formation between $\text{Mg}^{2+}\cdot\text{GppNHp}$ and Zn^{2+} -cyclen. ^{31}P NMR spectra of a sample containing 2 mM GppNHp in 40 mM Hepes/NaOH pH 7.4, 10 mM MgCl_2 , 0.2 mM DSS and 5% D_2O in the absence and presence of increasing concentrations of Zn^{2+} -cyclen. All spectra have been recorded at 278 K. Data processing using an exponential filter led to an additional line broadening of 8 Hz.

The same experiment was also carried out with Zn^{2+} -BPA. The obtained spectra are given in Figure 4.10. Again, an upfield and a downfield shift are observed for the signals representing the β - and the γ -phosphate group, respectively. In contrast to the results obtained in the presence of Zn^{2+} -cyclen significant shift differences are also observed for the α -phosphate group, actually being stronger than the effects observed for the β -phosphate group. The observed results are summarized in Table 4.1.

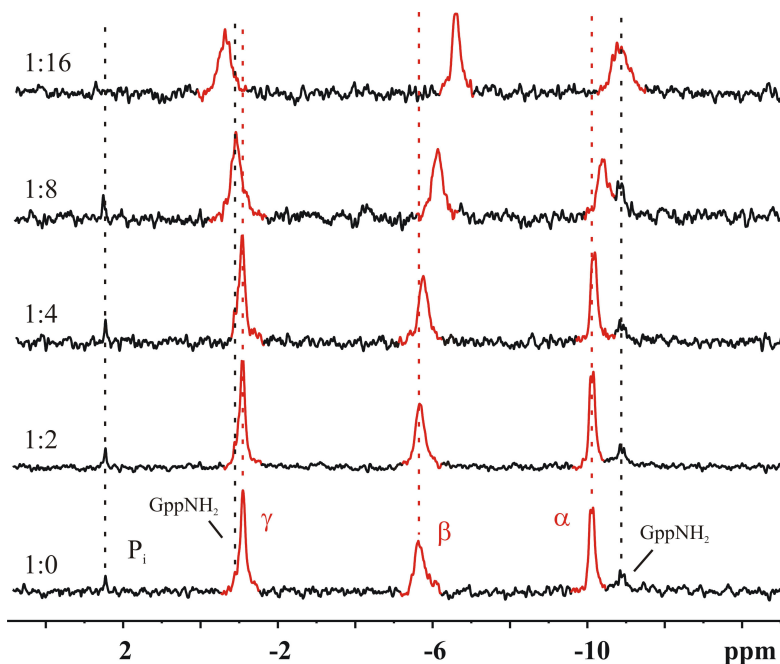


Figure 4.10: Complex formation between Mg^{2+} -GppNHp and Zn^{2+} -BPA. ^{31}P NMR spectra of a sample containing 0.5 mM GppNHp in 40 mM Tris/HCl pH 7.4, 10 mM MgCl_2 , 0.2 mM DSS and 5% D_2O in the absence and presence of increasing concentrations of Zn^{2+} -BPA. All spectra have been recorded at 278 K. Data processing using an exponential filter led to an additional line broadening of 8 Hz.

Table 4.1: Chemical shift changes and line width obtained in the ^{31}P NMR spectra of Mg^{2+} -GppNHp in the presence of Zn^{2+} -cyclen and -BPA, respectively.

Zn^{2+} -	n:l	α -phosphate		β -phosphate		γ -phosphate	
		δ [ppm]	$\Delta\nu_{1/2}$ [Hz] ^a	δ [ppm]	$\Delta\nu_{1/2}$ [Hz] ^a	δ [ppm]	$\Delta\nu_{1/2}$ [Hz] ^a
cyclen	1:0	-10.12	22	-5.78	24.0	-1.16	11
	1:10	-10.12	39	-6.71	142	0.31	51
BPA	1:0	-10.12	24	-5.66	43	-1.10	19
	1:8	-10.93	74	-6.61	36	-0.64	56
	1:16	-11.17	57	-6.86	28	-0.26	41

^a the line width was corrected with respect to the exponential filter applied during data processing

4.2.2 Binding of Zn^{2+} -BPA to $\text{Ras}(\text{wt})\cdot\text{Mg}^{2+}\cdot\text{GppNHp}$

STD NMR spectroscopy clearly revealed the binding activity of Zn^{2+} -BPA for $\text{Ras}(\text{T35A})\cdot\text{Mg}^{2+}\cdot\text{GppNHp}$. It was also shown that the compound binds to $\text{Mg}^{2+}\cdot\text{GppNHp}$. For these reasons it was of interest whether the compound binds close to the active centre and might influence the dynamic equilibrium in active Ras in any way. Zn^{2+} -BPA was titrated to wild type Ras complexed to $\text{Mg}^{2+}\cdot\text{GppNHp}$ up to a molar ratio of 1:28. During the titration precipitation was observed and resonances representing $\text{Mg}^{2+}\cdot\text{GppNHp}$ showed up and shifted upfield in the corresponding ^{31}P NMR spectra. SDS-Page analysis of the precipitant after the last titration step clearly revealed that Ras precipitated. Figure 4.11 shows the obtained spectra.

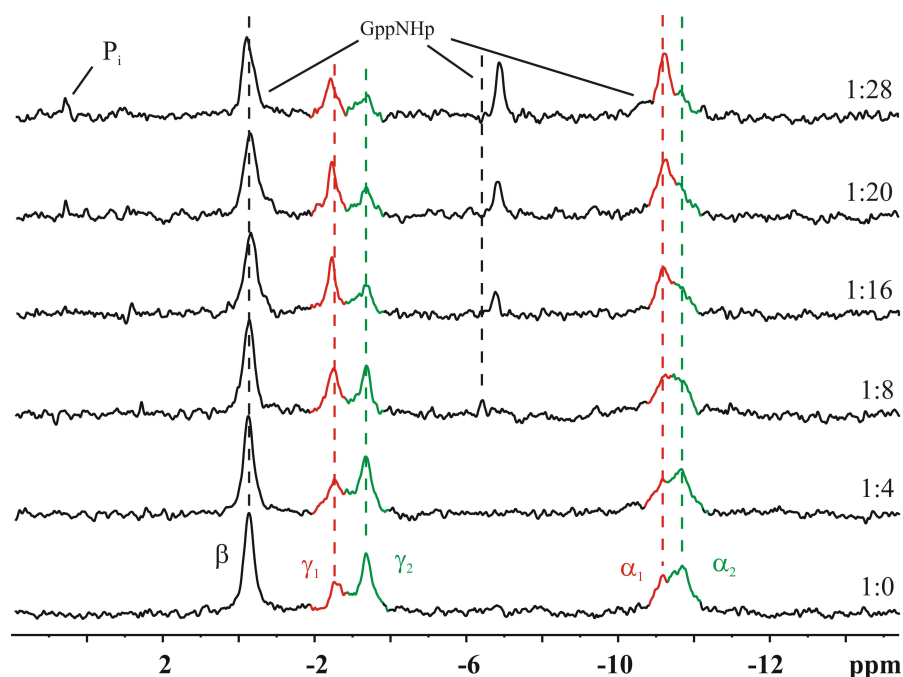


Figure 4.11: Influence of Zn^{2+} -BPA on the dynamic equilibrium of $\text{Ras}(\text{wt})\cdot\text{Mg}^{2+}\cdot\text{GppNHp}$. ^{31}P NMR spectra of 0.4 mM $\text{Ras}(\text{wt})\cdot\text{Mg}^{2+}\cdot\text{GppNHp}$ in 40 mM Tris/HCl pH 7.4, 10 mM MgCl_2 , 2 mM DTE, 0.2 mM DSS and 5% D_2O in the absence and presence of Zn^{2+} -BPA. The molar ratios Ras:BPA are indicated. All spectra have been recorded at 278 K. Experimental data were filtered exponentially resulting in an additional line broadening of 15 Hz.

Qualitatively is clear from these spectra that Zn^{2+} -BPA selectively binds to conformational state (1) when looking at the γ - and α -phosphate signals. The resonances representing conformational state (1) gain in population. At the same time a loss in the peak area is observed for resonances assigned to conformational state (2). In contrast to Zn^{2+} -cyclen a significant shift change is not observed for any of the signals. Quantification of the observed effect is quite cumbersome due to the poor quality and the lack of knowledge about the exact concentrations. However the data have been evaluated ignoring the precipitated fraction and the results are given in Table 4.2.

Table 4.2 Chemical shifts observed for Ras(wt)·Mg²⁺·GppNHp in the presence of Zn²⁺-BPA.

p:l	α -phosphate		β -phosphate ^a		γ -phosphate		K_{12} ^b
	δ_1 [ppm]	δ_2 [ppm]	δ_1 [ppm]	δ_2 [ppm]	δ_1 [ppm]	δ_2 [ppm]	
1:0	-11.18	-11.67		-0.27 ^a	-2.59	-3.37	1.74
1:4 ^c	-11.15	-11.69		-0.30 ^a	-2.60	-3.35	1.27
1:28 ^d	-11.20	-11.50 ^e		-0.33 ^e	-2.43	-3.33	0.58

^a signals for conformational state (1) and (2) overlap at the magnetic field used.

^b K_{12} was calculated from the relative peak areas observed for the γ -phosphate resonance: $K_{12} = A_{(\gamma 2)}/A_{(\gamma 1)}$

^c precipitation was not observed at this ligand excess

^d Ras started to precipitate at this ligand excess

^e could not be determined accurately due to the overlap with the α -phosphate signal from free Mg²⁺·GppNHp

4.2.3 Binding of Cu²⁺-BPA to Wild Type Ras and Ras(T35A) Complexed to Mg²⁺·GppNHp

Whereas in the presence of Zn²⁺-cyclen the change of the relative population of conformational state (1) over state (2) is accompanied by large chemical shift changes for the resonances representing state (1) this is not the case for Zn²⁺-BPA. The question remaining was, whether stabilization of conformational state is achieved with metal(II)-BPA by binding in the active centre or whether long range conformational changes induced by a binding elsewhere in the protein influences the dynamic equilibrium, which is then detected in the ³¹P NMR spectra. The presence of a paramagnetic centre leads to the enhancement of the relaxation rates of NMR active nuclei. The latter effect can be observed by strong line broadening of the affected resonances in a distance-dependent manner. Consequently the effect of the paramagnetic derivative Cu²⁺-BPA on the ³¹P resonance signals of active Ras has been investigated like we have done with the metal(II)-cyclens (Rosnizeck et al., accepted). Metal(II)-BPA might bind to active Ras in a comparable manner, i.e. close to the bound nucleotide in conformational state (1). Consequently the resonances belonging to the latter state should be influenced to a larger extend in wild type Ras·Mg²⁺·GppNHp than the one representing the effector-binding state (2). Additionally the expected effects should be stronger in the Ras mutant T35A, which predominantly exists in conformational state (1). Cu²⁺-BPA was titrated to wild type Ras and Ras(T35A) complexed to Mg²⁺·GppNHp up to a molar ratio of 1:8. The obtained spectra are shown in Figure 4.12 and 4.13, the results are summarized in Table 4.3. No significant shift changes are observed in both titrations. The lines of the β - and γ -phosphate peaks are broadened to a much greater extend than the one of the α -phosphorus in each case. The strongest effects are observed for the resonances belonging to conformational state (1). This becomes apparent when comparing the results obtained for wild type Ras and Ras(T35A).

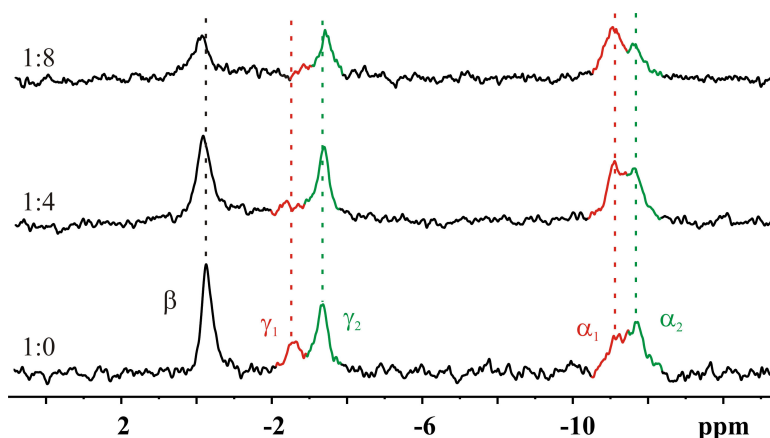


Figure 4.12: Influence of Cu^{2+} -BPA on $\text{Ras(wt)}\cdot\text{Mg}^{2+}\cdot\text{GppNHp}$. ^{31}P NMR spectra of 0.4 mM $\text{Ras(wt)}\cdot\text{Mg}^{2+}\cdot\text{GppNHp}$ in 40 mM Tris/HCl pH 7.4, 10 mM MgCl_2 , 2 mM DTE, 0.2 mM DSS and 5% D_2O in the absence and presence of Cu^{2+} -BPA. The molar ratios Ras:BPA are indicated. All spectra have been recorded at 278 K. Experimental data were filtered exponentially leading to an additional line broadening of 15 Hz.

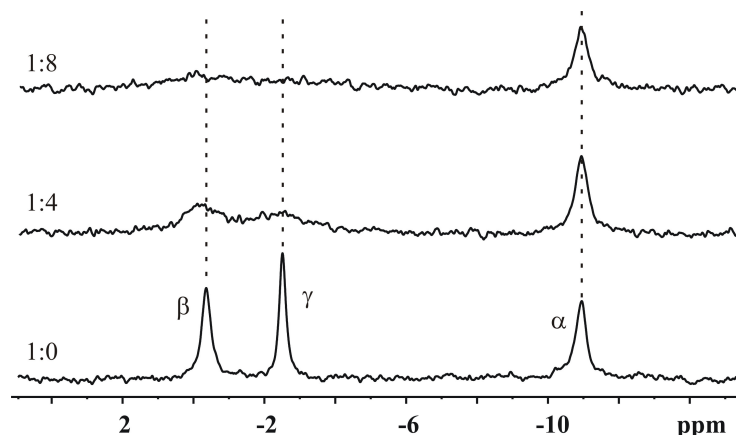


Figure 4.13: Influence of Cu^{2+} -BPA on $\text{Ras(T35A)}\cdot\text{Mg}^{2+}\cdot\text{GppNHp}$. ^{31}P NMR spectra of 0.7 mM $\text{Ras(T35A)}\cdot\text{Mg}^{2+}\cdot\text{GppNHp}$ in 40 mM Tris/HCl pH 7.4, 10 mM MgCl_2 , 2 mM DTE, 0.2 mM DSS and 5% D_2O in the absence and presence of Cu^{2+} -BPA. The molar ratios Ras:BPA are indicated. All spectra have been recorded at 278 K. Exponential filtering of experimental data led to additional line broadening of 15 Hz.

At a molar ratio of 1:8 the β - and γ -phosphate peaks are almost broadened beyond detection in the latter mutant. In wild type Ras the selectivity for conformational state (1) over (2) can be seen very clearly. The γ -phosphate signal of state (1) becomes significantly broadened and is no longer detectable at molar ratio of Ras:BPA of 1:8. At a 4-fold excess the line width is 563 Hz compared to 71 Hz in the absence of the compound. Additionally the α -phosphate resonance, which is not significantly influenced by the Cu^{2+} -centre in terms of line broadening clearly reveals a shift of the dynamic equilibrium towards the weak effector-binding state in the wild type protein.

Table 4.3: Chemical shift differences and relative peak areas observed for Ras complexed to Mg^{2+} ·GppNHp in the absence and presence of Cu^{2+} -BPA.

Fig. 1. GppNHp in the absence and presence of Ca^{2+} DPA.								
	p:l	K_{12}	α -phosphate		β -phosphate		γ -phosphate	
			α_1	α_2	β_1	β_2	γ_1	γ_2
Ras(wt)·Mg ²⁺ ·GppNHp								
δ [ppm]	1:0	2.00 ^a	-11.14	-11.67	-0.28 ^b		-2.58	-3.34
	1:8	0.45 ^c	-11.07	-11.66	-0.12 ^b		n.d. ^d	-3.43
$\Delta\nu_{1/2}$ [Hz]	1:0		65	85	47 ^b		71	58
	1:8		92	77	118 ^b		n.d. ^d	86
Ras(T35A)·Mg ²⁺ ·GppNHp								
δ [ppm]	1:0		-10.93		-0.36		-2.51	
	1:8	>0.05 ^e	-10.94		-0.18		-3.09	
$\Delta\nu_{1/2}$ [Hz]	1:0		60		47		29	
	1:8		84		474		603	

^a K_{12} was calculated from the relative peak areas observed for the γ -phosphate resonance: $K_{12} = A_{(\gamma 2)}/A_{(\gamma 1)}$

^b resonances representing conformational state (1) and (2) are not separated for the β -phosphate group at the magnetic field used

^c K_{12} was calculated from the relative peak areas observed for the γ -phosphate resonance: $K_{12} = A_{(\alpha 2)}/A_{(\alpha 1)}$

^d resonances already broadened beyond detection. At molar ratio of 1:4 following values have been obtained: $\delta(\gamma 1) = -2.42$, $\Delta\nu_{1/2} = 563$ Hz.

^e taking into account the signal to noise ratio the limit for K_{12} can be estimated

4.2.4 Binding of Zn^{2+} -Cyclen and -BPA to Ras(G12V) Complexed to Mg^{2+} ·GTP and Mg^{2+} ·GppNHp

The small organic compound Zn^{2+} -cyclen selectively binds the weak binding state of Ras(wt)· Mg^{2+} ·GppNHp and is able to shift the dynamic equilibrium completely towards this state (Spoerner et al. 2005c). The same was shown for Zn^{2+} -BPA. The effect of both metal(II)-chelates on the oncogenic mutant Ras(G12V) in its active conformation was also investigated. Bound to Mg^{2+} ·GppNHp the dynamic equilibrium is slightly shifted towards state (1) with $K_{12} = 0.9$ (Spoerner et al. 2004 2005) in the oncogenic mutant compared to wild type with $K_{12} = 1.9$. Ras(G12V)· Mg^{2+} ·GppNHp shows a similar free activation energy for exchange compared to wild type Ras· Mg^{2+} ·GppNHp. Zn^{2+} -cyclen and -BPA were titrated to Ras(G12V)· Mg^{2+} ·GppNHp followed by ^{31}P NMR spectroscopy. The reference and final spectra are shown in Figures 4.14 and 4.15, respectively. Regarding the relative population of conformational state (1) over state (2) the effect of Zn^{2+} -BPA is stronger than the one observed for Zn^{2+} -cyclen. At a molar ratio of 1:10 the shift towards state (1) is almost complete, whereas a 32-fold excess in the case of Zn^{2+} -cyclen is still not sufficient. Zn^{2+} -cyclen influences the resonances of the all three phosphate groups in terms of their chemical shift. The shift direction is comparable with the ones observed in wild type Ras, i.e. the α - and γ -phosphate resonances shift downfield and the β -phosphate peak shifts upfield. However, quantitatively the shift effect is stronger in Ras(wt)· Mg^{2+} ·GppNHp. For

Zn^{2+} -BPA no significant shift differences can be observed. At a molar ratio of about 1:10 the protein starts to precipitate as already observed in the titration with $\text{Ras}(\text{wt})\cdot\text{Mg}^{2+}\cdot\text{GppNHp}$ and for that reason the experiment was not carried out at higher concentrations for Zn^{2+} -BPA.

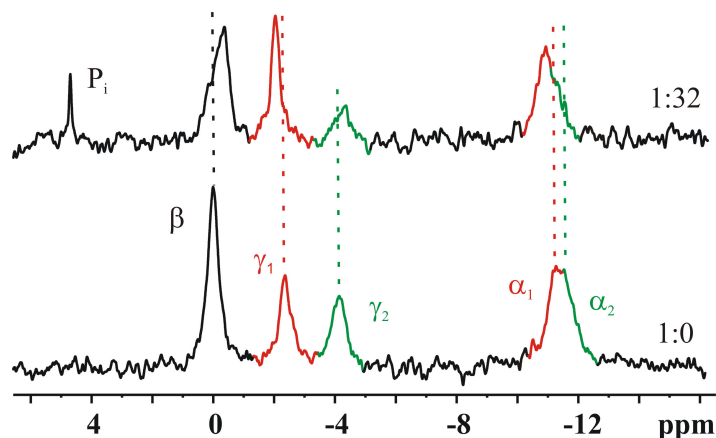


Figure 4.14: Influence of Zn^{2+} -cyclen on the dynamic equilibrium of $\text{Ras}(\text{G12V})\cdot\text{Mg}^{2+}\cdot\text{GppNHp}$. ^{31}P NMR spectra 1 mM $\text{Ras}(\text{G12V})\cdot\text{Mg}^{2+}\cdot\text{GppNHp}$ in 40 mM Tris/HCl pH 7.4, 10 mM MgCl_2 , 2 mM DTE, 0.2 mM DSS and 5% D_2O in the absence and presence of Zn^{2+} -cyclen. The molar ratios are indicated. All spectra have been recorded at 278 K. Experimental data were fitted exponentially leading to an additional line broadening of 15 Hz.

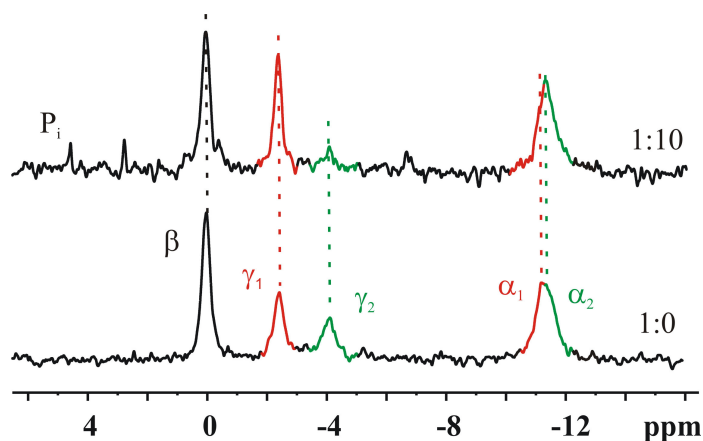


Figure 4.15: Influence of Zn^{2+} -BPA on the dynamic equilibrium of $\text{Ras}(\text{G12V})\cdot\text{Mg}^{2+}\cdot\text{GppNHp}$. ^{31}P NMR spectra of 0.6 mM $\text{Ras}(\text{G12V})\cdot\text{Mg}^{2+}\cdot\text{GppNHp}$ in 40 mM Tris/HCl pH 7.4, 10 mM MgCl_2 , 2 mM DTE, 0.2 mM DSS and 5% D_2O in the absence and presence of Zn^{2+} -BPA. The molar ratios are indicated. All spectra have been recorded at 278 K. Experimental data were fitted exponentially leading to an additional line broadening of 15 Hz.

$\text{Ras}(\text{G12V})$ is an oncogenic mutant of Ras and consequently exhibits a very slow hydrolysis rate of 0.0017 min^{-1} (Ahmadian et al. 1999) allowing to study the active conformation of Ras complexed to its physiological nucleotide GTP. $\text{Ras}(\text{wt})\cdot\text{Mg}^{2+}\cdot\text{GTP}$ predominantly exists in a conformation corresponding to state (2). Saturation transfer ^{31}P NMR experiments reveal the existence of a conformational equilibrium with a second conformational state, which is found in the partial loss-of-function mutants T35A and

T35S complexed to Mg^{2+} ·GTP (Spoerner et al., unpublished results). The same is true for $\text{Ras(G12V)}\cdot\text{Mg}^{2+}$ ·GTP. It was investigated whether the two chelate complexes are able to shift the dynamic equilibrium towards the weak effector-binding state of (G12V) complexed to Mg^{2+} ·GTP. Figure 4.16 and 4.17 show the influence of Zn^{2+} -cyclen and -BPA on $\text{Ras(G12V)}\cdot\text{Mg}^{2+}$ ·GTP.

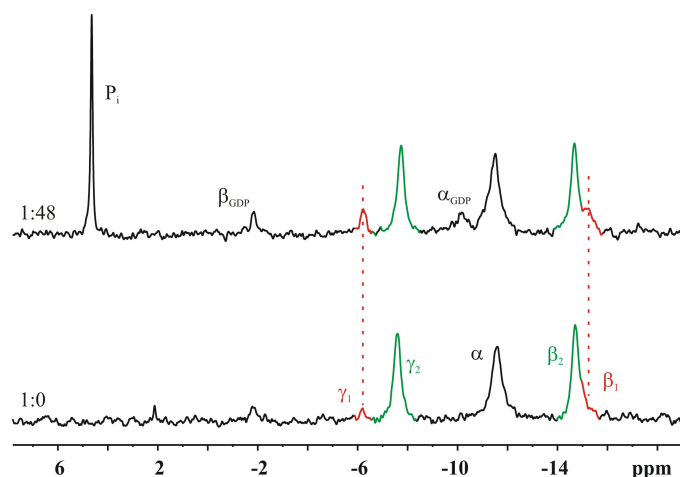


Figure 4.16: Influence of Zn^{2+} -cyclen on the conformational equilibrium of Ras(G12V) complexed to Mg^{2+} ·GTP. ^{31}P NMR spectra of 0.8 mM $\text{Ras(G12V)}\cdot\text{Mg}^{2+}$ ·GTP in 40 mM Hepes/NaOH pH 7.4, 10 mM MgCl_2 , 2 mM DTE, 0.2 mM DSS and 5% D_2O in the absence and presence of Zn^{2+} -cyclen recorded at 278 K. The molar ratios are indicated. Experimental data were filtered exponentially leading to an additional line broadening of 15 Hz.

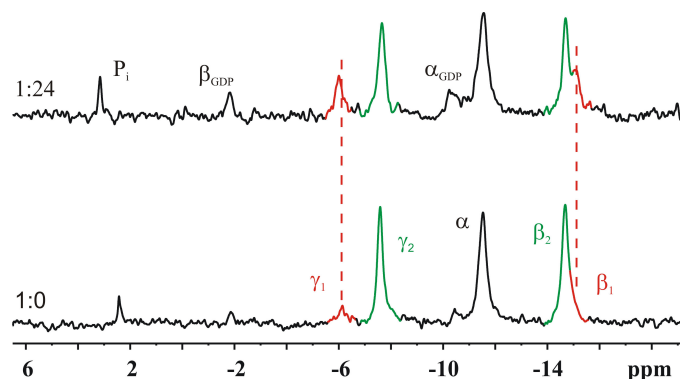


Figure 4.17: Influence of Zn^{2+} -BPA on the conformational equilibrium of Ras(G12V) complexed to Mg^{2+} ·GTP. ^{31}P NMR spectra of 0.6 mM $\text{c'Ras(G12V)}\cdot\text{Mg}^{2+}$ ·GTP in 10 mM Tris/HCl pH 7.4, 10 mM MgCl_2 , 2 mM DTE, 0.2 mM DSS and 5% D_2O in the absence and presence of Zn^{2+} -BPA recorded at 278 K. The molar ratios are indicated. Experimental data were filtered exponentially leading to an additional line broadening of 15 Hz.

The results clearly reveal the selective stabilization of conformational state (1) in the protein. However the affinity is much lower than to the protein in complex with Mg^{2+} ·GppNHp. Again, qualitatively one can say that the effect is stronger in the case of Zn^{2+} -BPA. The same was also observed for Ras(G12V) complexed to Mg^{2+} ·GppNHp. It is

noteworthy that in the presence of Zn^{2+} -cyclen, but not -BPA a resonance line representing free inorganic phosphate is observed at higher concentrations. The obtained results from the titration of Ras(G12V) complexed to Mg^{2+} ·GppNHp and Mg^{2+} ·GTP, respectively with the two Zn^{2+} -chelates are summarized in Table 4.4.

Table 4.4: Chemical shift differences and relative peak areas observed for Ras(G12V)· Mg^{2+} ·GppNHp and Ras(G12V)· Mg^{2+} ·GTP in the absence and presence of Zn^{2+} cyclen and Zn^{2+} -BPA, respectively.

			α -phosphate		β -phosphate		γ -phosphate	
Zn^{2+} -	p:l	K_{12}^{b}	δ_1 [ppm]	δ_2 [ppm]	δ_1 [ppm]	δ_2 [ppm]	δ_1 [ppm]	δ_2 [ppm]
Ras(G12V)·Mg ²⁺ ·GppNHp								
cyclen	1:0	0.95	-11.23	-11.63	0.00 ^a		-2.36	-4.12
	1:32	0.40	-10.93		0.25 ^a		-2.05	
BPA	1:0	0.86	-11.19	-11.50	0.04 ^a		-2.40	-4.06
	1:10	0.29	-11.31	-11.66	0.05 ^a		-2.37	
Ras(G12V)·Mg ²⁺ ·GTP								
cyclen	1:0	15.3 ^c	-11.57		-15.07	-14.72	-6.18	-7.59
	1:48	3.96	-11.48		-15.33		-6.23	
BPA	1:0	6.97 ^c	-11.53		-14.92	-14.68	-6.12	-7.59
	1:24	2.86	-11.53		-15.09		-6.02	

^a the signals representing the two conformational states in active Ras are not separated at the magnetic field used

^b K_{12} was calculated from the relative peak areas observed for the γ -phosphate resonance: $K_{12} = A_{(\alpha 2)}/A_{(\alpha 1)}$

^c the value for K_{12} is afflicted with large errors since conformational state (1) is only sparsely populated

4.2.5 Binding of Metal(II)-Cyclens to Mg^{2+} ·GTP γ S in Free Form and Complexed to Ras

The ^{31}P NMR spectrum of Ras(T35A)· Mg^{2+} ·GTP γ S reveals two substates of the weak effector-binding state, which are in a slow conformational equilibrium (Spoerner et al. 2007). Since Zn^{2+} -cyclen is capable of stabilizing state (1) its influence on both substates was studied by ^{31}P NMR spectroscopy.

Initially Mg^{2+} ·GTP γ S was titrated with Zn^{2+} - and Cu^{2+} -cyclen up to a molar ratio of Mg^{2+} ·GTP γ S:metal(II)-cyclen of 1:20 and 1:6.4, respectively and the effect was followed by ^{31}P NMR spectroscopy. The obtained spectra and the derived chemical shifts are depicted and summarized in Figure 4.18 and Table 4.5, respectively. In the presence of Cu^{2+} -cyclen the signals of all three phosphate groups are significantly broadened with the strongest effects observed for the γ -phosphate, which is already broadened beyond detection at a molar excess of 1:0.2 and the β -phosphate showing a line width of 330 Hz at a molar ratio of GTP γ S: Cu^{2+} -cyclen of 1:6.4 compared to 82 Hz in the reference spectrum.

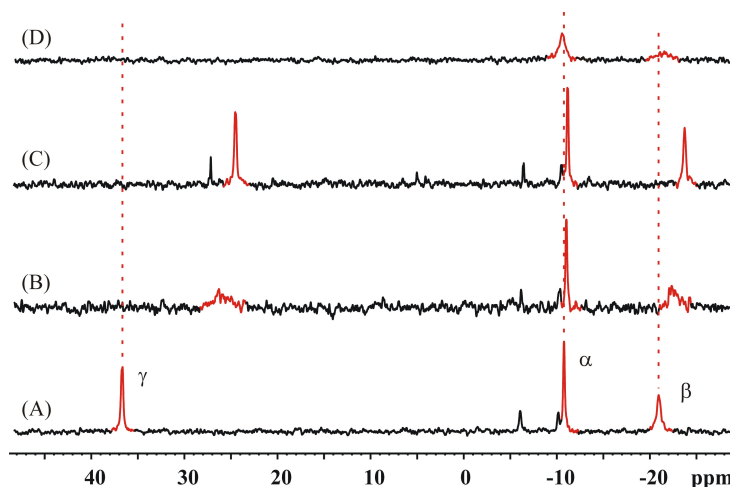


Figure 4.18: Binding of metal(II)-cyclens to Mg^{2+} -GTP γ S. ^{31}P NMR spectra of 1 mM GTP γ S in 40 mM Tris/HCl pH 7.4, 10 mM MgCl_2 , 2 mM DTE, 0.2 mM DSS and 5% D_2O in the absence (A) and presence of Zn^{2+} -cyclen with a molar excess of 5 (B) and 20 (C) and Cu^{2+} -cyclen with a molar excess 6.4 (D), respectively. All spectra have been recorded at 278 K. The experimental have been filtered exponentially leading to an additional line broadening of 20 Hz.

Table 4.5: Chemical shift differences and line broadening observed for Mg^{2+} -GTP γ S upon addition of metal(II)-cyclens.

-cyclen	n:l	α -phosphate		β -phosphate		γ -phosphate	
		δ [ppm]	$\Delta\nu_{1/2}$ [Hz] ^a	δ [ppm]	$\Delta\nu_{1/2}$ [Hz] ^a	δ [ppm]	$\Delta\nu_{1/2}$ [Hz] ^a
Cu^{2+} -	1:0	-10.77	21	-20.96	82	36.70	36
	1:6.4	-10.59	140	-21.45	329	n.d. ^b	
Zn^{2+} -	1:0	-10.67	16	-20.68	93	36.77	41
	1:5	-11.05	18	-23.55	136	24.32	293
	1:20	-11.16	21	-23.72	43	24.51	36

^a the line width was corrected with respect to the exponential filter applied during data processing

^b lines for the γ -phosphate group were already broadened beyond detection at a molar ratio of n:l = 1:0.2. At a molar excess of 0.1 the following values are obtained: $\delta(\gamma)$ = 36.52 ppm, $\Delta\nu_{1/2}$ = 1018 Hz.

In the presence of the diamagnetic derivative each signals shifts upfield to a different extend. The strongest effects are again observed for the γ - and the β -phosphate resonance, whereas the influence on the α -phosphate is very small with 0.6 ppm compared to 2.9 ppm and 12.3 ppm for the β - and γ -phosphate signal, respectively. During the titration with Zn^{2+} -cyclen also intermediate exchange processes can be observed for the γ - and the β -phosphate signals at a molar ratio of Mg^{2+} -GTP γ S: Zn^{2+} -cyclen between 1:1 and 1:5. The signals are almost broadened beyond detection for the γ -phosphate signal and show up again at a molar excess of 1:10 without being significantly broadened compared to the reference spectrum. An example is shown in Figure 4.18 and the corresponding data are given in Table 4.5.

In the next step $\text{Ras(T35A)} \cdot \text{Mg}^{2+} \cdot \text{GTP}\gamma\text{S}$ was titrated with Cu^{2+} -cyclen up to a molar ratio of 1:4. The strongest line broadening effects are again observed for the γ - and β -phosphate group. The dynamic equilibrium is shifted towards state (1a). $\text{Ras(T35A)} \cdot \text{Mg}^{2+} \cdot \text{GTP}\gamma\text{S}$ was further titrated with the diamagnetic derivative Zn^{2+} -cyclen up to a molar excess of Zn^{2+} -cyclen of 20 (see Figure 4.20). It is striking that in this titration the resonances assigned to state (1a) are mainly affected. Additionally one can see that between an ratio of metal(II)-cyclen to Ras of 1:2 and 1:4 also a strong line broadening is observed for the resonance of the γ -phosphate belonging to substate (1a). The latter resonance is broadened beyond detection at the same molar ratio as in the case of the titration with the paramagnetic derivative. In order to ensure that the bleaching effect observed in the titration with Cu^{2+} -cyclen can clearly be related to its paramagnetism the titration was repeated with molar ratios of 1:0, 1:4, 1:10 and 1:20. The obtained spectra are shown in Figure 4.19 together with the spectra from the previous titration.

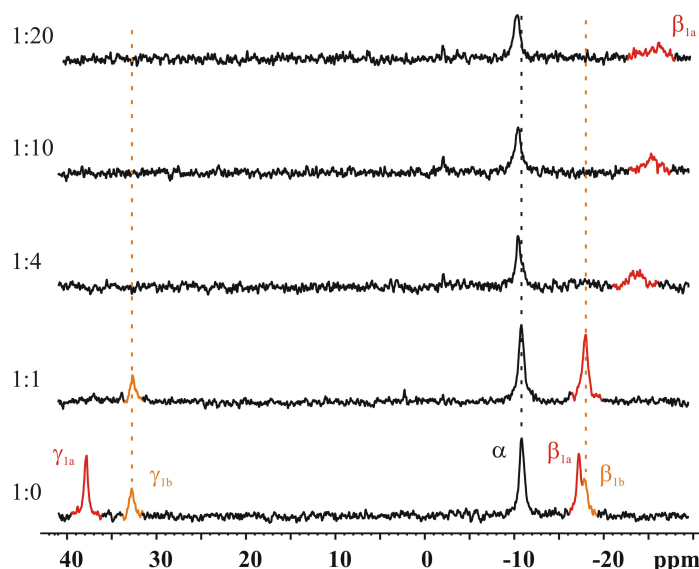


Figure 4.19: Binding of Cu^{2+} -cyclen to Ras(T35A) complexed to $\text{Mg}^{2+} \cdot \text{GTP}\gamma\text{S}$. ^{31}P NMR spectra of 0.76 mM $\text{Ras(T35A)} \cdot \text{Mg}^{2+} \cdot \text{GTP}\gamma\text{S}$ in 40 mM Tris/HCl pH 7.4, 10 mM MgCl_2 , 2 mM DTE, 0.2 mM DSS and 5% D_2O in the absence and presence of increasing concentrations of Cu^{2+} -cyclen. The molar ratios between Ras and metal(II)-cyclen are indicated. All spectra have been recorded at 278 K. The experimental have been filtered exponentially leading to an additional line broadening of 20 Hz.

The γ -resonance representing substate (1a) does not appear again indicating strong line broadening effects caused by the paramagnetic Cu^{2+} -ion of the ligand than rather by exchange phenomena. For the β -phosphate peak further line broadening and an extended upfield shift is observed. The resonances belonging to substate (1b) are disappearing in the case of the β - and γ -phosphate due to the shift of the dynamic equilibrium towards state (1a). The obtained results are summarized in Table 4.6.

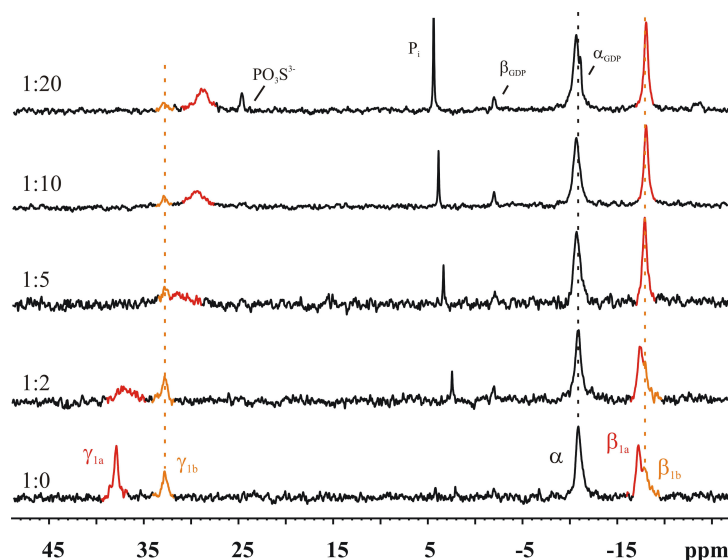


Figure 4.20: Influence of Zn^{2+} -cyclen on the dynamic equilibrium in Ras(T35A) complexed to Mg^{2+} -GTP γ S. ^{31}P NMR spectra of 0.88 mM Ras(T35A)· Mg^{2+} -GTP γ S in 40 mM Tris/HCl pH 7.4, 10 mM MgCl_2 , 2 mM DTE, 0.2 mM DSS and 5% D_2O in the absence and presence of increasing concentrations of Zn^{2+} -cyclen. The molar ratios of Ras:metal(II)-cyclen are indicated. All spectra have been recorded at 278 K. Experimental have been filtered exponentially leading to an additional line broadening of 20 Hz.

Table 4.6: Chemical shift values and line widths observed for Ras(T35A)· Mg^{2+} -GTP γ S upon addition of metal(II)-cyclens.

		α -phosphate ^a		β -phosphate		γ -phosphate	
	p:l	α_{1a}	α_{1b}	β_{1a}	β_{1b}	γ_{1a}	γ_{1b}
Cu ²⁺ -cyclen							
δ [ppm]	1:0	-10.88		-17.20	-17.85	37.96	32.74
	1:20	-10.35		-26.07	n.d. ^b	n.d. ^c	n.d. ^b
$\Delta v_{1/2}$ [Hz] ^d	1:0	75		65	111	64	84
	1:20	149		551	n.d. ^b	n.d. ^c	n.d. ^b
Zn ²⁺ -cyclen							
δ [ppm]	1:0	-10.92		-17.25	-17.98	37.92	32.78
	1:20	-10.71		-18.06	n.d. ^e	28.78	32.88
$\Delta v_{1/2}$ [Hz] ^d	1:0	108		85	108	74	89
	1:20	147		83	n.d. ^e	259	72

^a the signals representing the two conformational states are not separated at the magnetic field used

^b could not be determined. The equilibrium is completely shifted towards state (1a) at a molar ratio of 1:4

^c could not be determined. The signal is already broadened beyond detection after the first titration step

^d the line width was corrected with respect to the exponential filter used during data processing.

^e could not be determined due to the overlap with the signal of $\gamma(1a)$

From this titrations it is clear that the small compound binds in close proximity of the γ - and β -phosphate group and herein selectively to conformational state (1a). Interestingly the line broadening effects strongly indicating slow exchange between the free and the bound form are also observed for the free nucleotide. The resonances belonging to state (1b) are not affected in terms of their chemical shift in both titrations. The only effect observed is a loss in peak intensity or area, respectively, which is caused by the stabilization of the conformational substate (1a).

GTP γ S is probably most similar to the physiological nucleotide GTP compared to GppNHp or GppCH₂p, especially in terms of the conformational equilibrium in active Ras (Spoerner et al. 2007). Mainly conformational state (2) is found in wild type Ras complexed to Mg²⁺·GTP γ S (Spoerner et al. 2007) and Mg²⁺·GTP (M. Spoerner, unpublished results). In section 4.2.4 it was shown that in the oncogenic mutant Ras(G12V) complexed to Mg²⁺·GTP the same conformational state is found as in the wild type protein. Upon addition of a large excess of Zn²⁺-cyclen resonances representing conformational state (1) appeared in the ³¹P NMR spectrum. Consequently the oncogenic mutant was complexed to Mg²⁺·GTP γ S in order to see, whether also mainly conformational state (2) is found. The corresponding spectrum is shown in Figure 4.21 and compared to Ras(T35A)·Mg²⁺·GTP γ S.

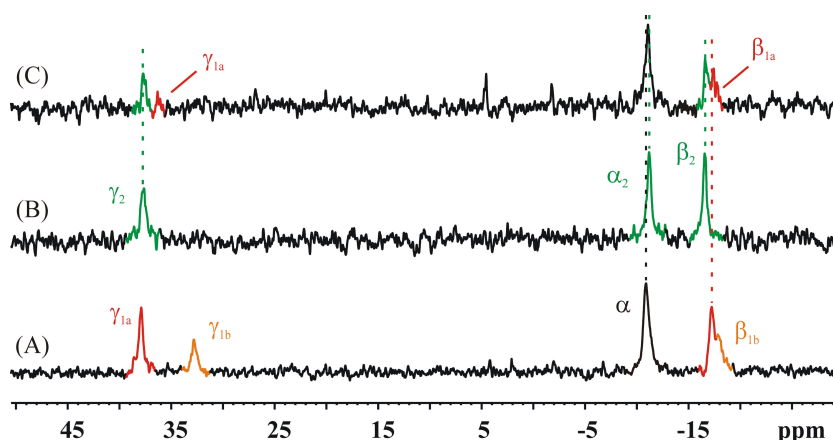


Figure 4.21: Influence of Zn²⁺-cyclen on the dynamic equilibrium in Ras(G12V) complexed to Mg²⁺·GTP γ S. ³¹P NMR spectra of 0.58 mM Ras(G12V)·Mg²⁺·GTP γ S in 40 mM Tris/HCl pH 7.4, 10 mM MgCl₂, 2 mM DTE, 0.2 mM DSS and 5% D₂O in the absence (B) and presence (C) of Zn²⁺-cyclen with a molar ratio of Ras:metal(II)-cyclen of 1:20. The ³¹P NMR spectrum of Ras(T35A)·Mg²⁺·GTP γ S is shown for comparison (A). All spectra have been recorded at 278 K. Experimental have been filtered exponentially leading to an additional line broadening of 15 Hz ((B), (C)) and 20 Hz (A), respectively.

Indeed as expected one resonance signal for each phosphate group representing conformational state (2) is found. In the next step Zn²⁺-cyclen was titrated to the sample. As one can see additional resonances appear with chemical shift values of 36.3 ppm and -17.80 ppm, when a molar excess for Zn²⁺-cyclen of 20 is present. In the case of the β -phosphate group this chemical shift value is in good agreement with the one found for

substate (1a) in Ras(T35A)·Mg²⁺·GTPγS. The latter state has already been shown to be selectively bound by the small compound compared to state (1b). The signal representing conformational state (1a) is strongly shifts upfield in the presence of Zn²⁺-cyclen. Thus, the signal appearing at 36.3 ppm at a molar excess of Zn²⁺-cyclen over Ras of 20 is most probably representing conformational substate (1a) in complex with Zn²⁺-cyclen. However, data quality is not sufficient for quantification.

4.2.6 Binding of Cyclens and Metal(II)-BPA to Ras·Mg²⁺·GDP

High field EPR and ³¹P NMR studies could show that also the GDP bound “off” state of Ras exists in two different conformational states (Rohrer et al. 2001). For that reason and due to suggestion that conformational state (1) of active Ras is structurally similar to the inactive conformation of Ras, the effect of Cu²⁺-cyclen on Ras(wt)·Mg²⁺·GDP has already been investigated. Neither significant line broadening nor chemical shift differences have been observed at molar ratios between Ras(wt)·Mg²⁺·GDP and Cu²⁺-cyclen, where already strong effects are observed in the active conformation (Spoerner et al. 2005c). To complete the picture the effect of different cyclens on the partial loss-of-function mutant Ras(T35A) complexed to Mg²⁺·GDP was investigated. Figure 4.22 shows the spectra obtained in the presence of molar excess of 16 of cyclen, Zn²⁺-cyclen and Cu²⁺-cyclen. Chemical shift differences and line broadening have been evaluated, the results are summarized in Table 4.7. Slight line broadening effects and chemical shift changes can be observed for the α-phosphate resonances in the presence of Zn²⁺- and Cu²⁺-cyclen. The β-phosphate resonances are not affected significantly.

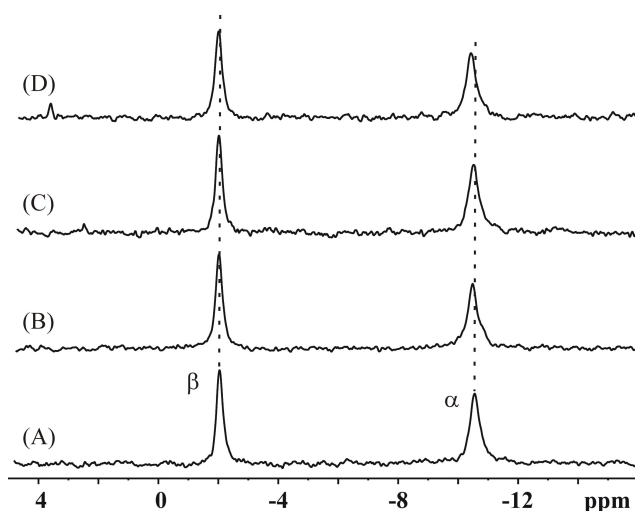


Figure 4.22: Influence of different cyclen derivatives on the ³¹P NMR spectra of Ras(T35A)·Mg²⁺·GDP. ³¹P NMR spectra of 1 mM Ras(T35A)·Mg²⁺·GDP in 40 mM Tris/HCl pH 7.4, 10 mM MgCl₂, 2 mM DTE, 0.2 mM DSS and 5% D₂O in the absence (A) and presence of cyclen (B), Zn²⁺-cyclen (C) and Cu²⁺-cyclen (D) with a molar ratio of Ras:cyclen of 1:16. All spectra were recorded at 278 K. Experimental data were filtered exponentially leading to an additional line broadening of 15 Hz.

Table 4.7: Chemical shift values and line broadening of the phosphate resonances of Ras(T35A)·Mg²⁺·GDP in the absence and presence of different cyclen derivatives.

	p:l	α -phosphate		β -phosphate	
		δ [ppm]	$\Delta\nu_{1/2}$ [Hz] ^a	δ [ppm]	$\Delta\nu_{1/2}$ [Hz] ^a
Zn²⁺-cyclen	1:0	-10.55	61	-2.03	33
	1:16	-10.32	70	-2.00	35
Cu²⁺-cyclen	1:0	-10.55	64	-2.04	33
	1:16	-10.44	69	-2.02	37
cyclen	1:0	-10.55	68	-2.06	35
	1:16	-10.51	66	-2.02	35

^a the line width was corrected with respect to the exponential filter used in data processing

The effect of metal(II)-BPAs on the inactive conformation of wild type and mutant Ras complexed to Mg²⁺·GDP was studied for the same reasons as in the case of the metal(II)-cyclens. The experiments have been carried out with wild type and mutant Ras·Mg²⁺·GDP. The obtained spectra are given in Figure 4.23.

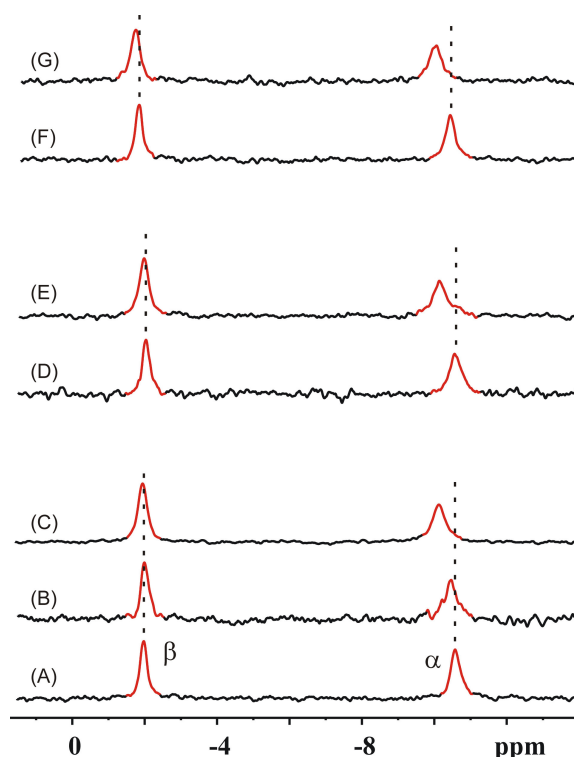


Figure 4.23: Influence on metal(II)-BPA on Ras complexed to Mg²⁺·GDP. ³¹P NMR spectra of Ras·Mg²⁺·GDP in 40 mM Tris/HCl pH 7.4, 10 mM MgCl₂ and 2 mM DTE, 0.2 mM DSS and 5% D₂O. (A), (B), (C) 0.48 mM Ras(wt) in the absence and presence of Zn²⁺-BPA and Cu²⁺-BPA, respectively with a molar excess of 16. (E) and (D) 0.57 mM Ras(T35A) in the absence and presence of a 16-fold excess of Cu²⁺-BPA. (F) and (G) 0.71 mM Ras(G12V) in the absence and presence of an 18-fold excess of Cu²⁺-BPA. All spectra have been recorded at 278K. Experimental data have been filtered exponentially leading to an additional line broadening of 15 Hz.

Ras(wt)·Mg²⁺·GDP was titrated with Zn²⁺- and Cu²⁺-BPA. The resonance of the β -phosphate group is not influenced significantly by the presence of the two compounds concerning both the line width and the chemical shift. For the α -phosphate peak a downfield shift can be observed upon addition of both compounds, with the effect being stronger in the presence of Cu²⁺-BPA. The line width of the α -phosphate signal is also not influenced significantly.

Additionally the Ras mutants T35A and G12V complexed to Mg²⁺·GDP have been titrated with Cu²⁺-BPA. Again in both cases the β -phosphate resonance is not influenced significantly, whereas the signals of the α -phosphate shift downfield. The effects are comparable for both Ras mutants with a chemical shift difference of 0.43 and 0.39 ppm for T35A and G12V, respectively between Ras·Mg²⁺·GDP in the absence and presence of a 16-fold and 18-fold ligand excess, respectively. This is also in good agreement with wild type Ras, where a downfield shift of 0.45 ppm is observed upon addition of a 16-fold excess Cu²⁺-BPA. Significant line broadening can not be observed for both signals. Table 4.8 summarizes the effects of metal(II)-BPA on Ras·Mg²⁺·GDP.

Table 4.8: Chemical shift values and line broadening of the phosphate resonances of Ras(T35A)·Mg²⁺·GDP in the absence and presence of different BPA derivatives.

Ras·Mg ²⁺ ·GDP	p:l	α-phosphate		β-phosphate	
		δ [ppm]	Δν _{1/2} [Hz] ^a	δ [ppm]	Δν _{1/2} [Hz] ^a
Cu ²⁺ -BPA					
wild type	1:0	-10.59	47	-1.97	30
	1:16	-10.14	72	-1.95	43
T35A	1:0	-10.59	59	-2.04	30
	1:16	-10.16	78	-1.98	44
G12V	1:0	-10.42	45	-1.83	29
	1:18	-10.03	70	-1.80	45
Zn ²⁺ -BPA					
wild type	1:0	-10.59	47	-1.97	30
	1:16	-10.46	66	-2.01	33

^a the line width was corrected with respect to the exponential filter used during data processing

4.3 Perturbation of the Ras-Raf-RBD Interaction by Metal(II)-Chelates

4.3.1 General Considerations

As described in section 1.1.5.2 conformational state (1) of active Ras shows drastically reduced affinity for effector molecules. The above characterized metal(II)-chelates have been shown to selectively recognize and stabilize conformational state (1) of active Ras. Consequently it should also be possible to perturb the Ras-effector interaction by both mutants via stabilization of conformational state (1). This was already shown by ITC, where a drop of the apparent affinity constant of Raf-RBD for Ras(wt)·Mg²⁺·GppNHp in the presence of Zn²⁺-cyclen and Cu²⁺-cyclen is observed (Roznizeck et al., accepted). No data are available about the association kinetics between Ras and Raf-RBD in the presence of both compounds. Additionally their mode of inhibition is not known. Since Raf-RBD can bind both conformational states of active Ras the question remains, whether a heterotrimeric complex is formed consisting of Ras·Mg²⁺·GppNHp in conformational state (1), Raf-RBD and Zn²⁺-cyclen or whether the effector and the metal(II)-chelate bind separately to Ras. To address these questions the Ras-Raf-RBD association in the presence of the two compounds was studied further by ³¹P NMR spectroscopy.

4.3.2 ³¹P NMR Titration of Ras(T35S)·Mg²⁺·GppNHp Complexed to Raf-RBD with Zn²⁺-Cyclen and Zn²⁺-BPA

The partial loss-of-function mutant Ras(T35S)·Mg²⁺·GppNHp predominately exists in the weak effector-binding state. Upon addition of effector the signals corresponding to conformational state (2) appear in the corresponding ³¹P NMR spectrum. The signals representing conformational state (1) and (2) for the γ -phosphate group in Ras(T35S)·Mg²⁺·GppNHp are very well separated allowing the determination of the proportion of the single states quite easily via the peak areas. Ras(T35S)·Mg²⁺·GppNHp was complexed to Raf-RBD and the displacement of the latter was studied by ³¹P NMR titration with the two Zn²⁺-chelates. Figure 4.24 shows the results obtained with Zn²⁺-cyclen. The three phosphate groups in Ras(T35S)·Mg²⁺·GppNHp are represented by one signal each. Upon addition of Raf-RBD the equilibrium is almost completely shifted towards the effector-binding state. The line widths of the signals representing conformational state (2) are broadened by a factor of 1.43, 1.41 and 1.44 for the α -, the β - and the γ -phosphate peak in complex with Raf-RBD compared to conformational state (1). This relates very well with the increase of the molecular mass by a factor of 1.46, when effector is bound. To the present complex between Ras(T35S)·Mg²⁺·GppNHp and Raf-RBD Zn²⁺-cyclen was added up to a 48-fold molar excess. As one can see very clearly

the signals representing conformational state (1) of Ras(T35A)·Mg²⁺·GppNHp increase with increasing concentrations of Zn²⁺-cyclen accompanied by an upfield shift for the β -phosphate peak and an downfield shift for the α - and γ -resonance, respectively. At the same time the population of the resonances belonging to the effector-binding state (2) decreases. No significant shift changes are observed for the signals of the α - and γ -phosphate group representing state (2). The resonances of both conformational states can be separated for the β -phosphate peak at a molar ratio of Ras:cyclen of 1:16.

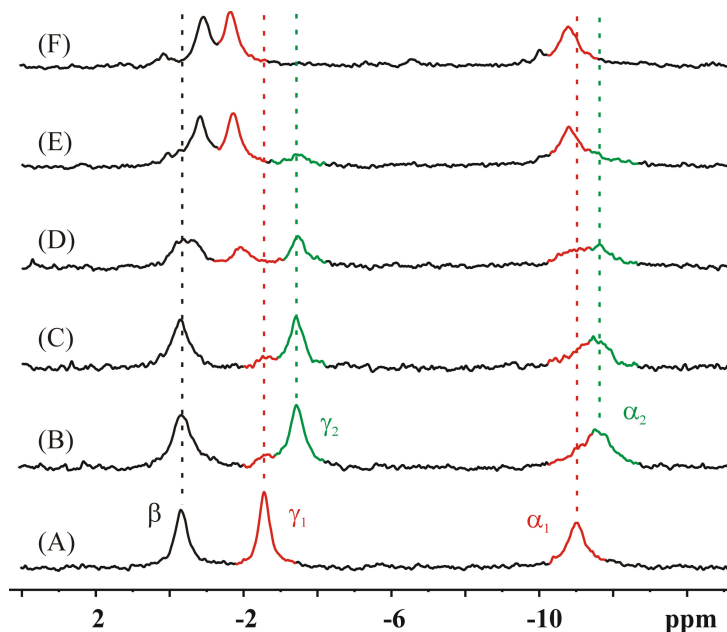


Figure 4.24: Displacement of Raf-RBD from Ras(T35S)·Mg²⁺·GppNHp by Zn²⁺-cyclen.

Ras(T35S)·Mg²⁺·GppNHp in the absence (A) and presence of a 1.5-fold excess of Raf-RBD (B) and subsequent addition of a 4-fold (C), 16-fold (D), 32-fold (E) and 48-fold (F) excess of Zn²⁺-cyclen, respectively. The sample initially contained 2.1 mM Ras(T35S)·Mg²⁺·GppNHp in 40 mM Tris/HCl pH 7.4, 10 mM MgCl₂, 2 mM DTE, 0.2 mM DSS and 5% D₂O. All spectra have been recorded at 278 K. Experimental data have been filtered exponentially leading to an additional line broadening of 15 Hz.

The same experiment was carried out with Zn²⁺-BPA. A precipitation of Ras was observed upon addition of increasing amounts of the ligand, which was already observed in the titration of Ras(wt)·Mg²⁺·GppNHp. For that reason the titration was only performed up to a molar excess of BPA of 11-fold. The obtained spectra are given in Figure 4.25. Upon complex formation with Raf-RBD the line width increases by a factor of 1.9, 1.53 and for the α - and β -phosphate peak compared to the reference peak and by a factor of 1.42 for the γ -phosphate representing conformational state (2). Stepwise addition of Zn²⁺-BPA to the complex leads to an increase of the population of conformational state (1) and at the same time to a decrease of state (2). No significant shift changes are observed for either resonances representing state (1) or (2), respectively. The poor data quality did not allow for accurate evaluation of the line widths and chemical shifts for every resonance,

especially the α -phosphate resonances. The results obtained for the γ - and β -phosphorus resonances are given in Table 4.9. Increasing concentrations of Zn^{2+} -BPA lead to a decrease of the line width for the β -phosphate resonance. The signal from the γ -phosphorus in conformational (1) state is not broadened significantly during the titration.

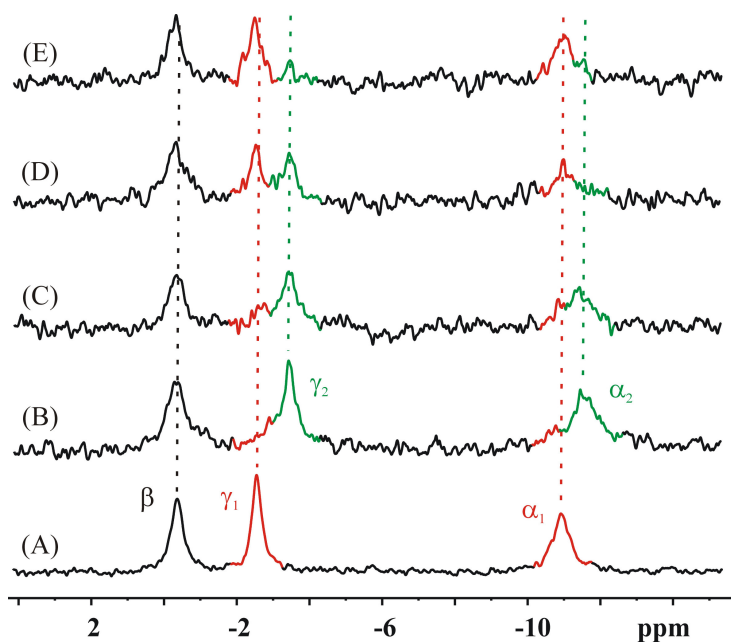


Figure 4.25: Displacement of Raf-RBD from Ras(T35S)·Mg²⁺·GppNHp by Zn²⁺-BPA.

Ras(T35S)·Mg²⁺·GppNHp in the absence (A) and presence of a 1.5-fold excess of Raf-RBD (B) and subsequent addition of a 4-fold (C), 7-fold (D), and 11-fold (E) excess of Zn²⁺-BPA, respectively. The sample initially contained 0.98 mM Ras(T35S)·Mg²⁺·GppNHp in 40 mM Tris/HCl pH 7.4, 10 mM MgCl₂, 2 mM DTE, 0.2 mM DSS and 5% D₂O. All spectra have been recorded at 278 K. Experimental data have been filtered exponentially leading to an additional line broadening of 15 Hz.

Table 4.9 Chemical shift changes and line widths observed in Ras(T35S)·Mg²⁺·GppNHp in the presence of Raf-RBD and after subsequent addition of Zn²⁺-cyclen and Zn²⁺-BPA, respectively.

		Ras(T35S)	+ Raf-RBD	+ Zn ²⁺ -cyclen	
molar excess			1.5	32	48
δ [ppm]	$\alpha(1)$	-11.01	-11.02	-10.82	-10.80
	$\alpha(2)$		-11.60	-11.62	n.d. ^a
	$\beta(1)$	-0.32	-0.34 ^b	-0.81	-0.90
	$\beta(2)$			-0.14	n.d. ^a
	$\gamma(1)$	-2.56	-2.59	-1.73	-1.66
	$\gamma(2)$		-3.44	-3.49	n.d. ^a
$\Delta\nu_{1/2}$ [Hz] ^c	$\alpha(1)$	101	92	n.d. ^d	112
	$\alpha(2)$		132		n.d. ^a
	$\beta(1)$			78	66
	$\beta(2)$	69	104 ^b	128	n.d. ^a
	$\gamma(1)$	54	50	74	74
	$\gamma(2)$		80	116	n.d. ^a
		Ras(T35S)	+ Raf-RBD	+ Zn ²⁺ -BPA	
molar excess			1.5	7	11
δ [ppm]	$\alpha(1)$	-10.93	-11.55 ^b	-11.05	-11.00
	$\alpha(2)$			-11.72	-11.66
	$\beta(1)$	-0.36	-0.32 ^b	-0.31 ^b	-0.27 ^b
	$\beta(2)$				
	$\gamma(1)$	-2.55	-2.55	-2.51	-2.41
	$\gamma(2)$		-3.43	-3.40	-3.40
$\Delta\nu_{1/2}$ [Hz] ^c	$\alpha(1)$	91	173 ^b	n.d. ^d	n.d. ^d
	$\alpha(2)$				
	$\beta(1)$	64	107 ^b	97 ^b	89 ^b
	$\beta(2)$				
	$\gamma(1)$	50	53	50	61
	$\gamma(2)$		78	100	n.d. ^d

^a peaks representing conformational state (2) are not observed at this molar excess of Zn²⁺-cyclen

^b the signals representing the two conformational states are not separated

^c the line width was corrected with respect to the exponential filter used during data processing

^d could not be determined accurately

4.3.3 Competitive ^{31}P NMR Titrations of $\text{Ras}(\text{T35A})\cdot\text{Mg}^{2+}\cdot\text{GppNHp}$ with Raf-RBD and Zn^{2+} -Cyclen

The titration studies with $\text{Ras}(\text{T35S})\cdot\text{Mg}^{2+}\cdot\text{GppNHp}$ complexed to Ras clearly reveal that the effector can be displaced from its complex with Ras in state (2). The question remains, whether Raf-RBD is afterwards bound to state (1), which is stabilized by Zn^{2+} -cyclen. For that reason displacement studies have also been carried out with the T35A mutant (see Figure 4.26). This mutant cannot be shifted towards conformational state (2) in the presence of Raf-RBD (Spoerner et al. 2001) and exists in conformational state (1) during the whole titration. Binding of Raf-RBD to $\text{Ras}(\text{T35A})\cdot\text{Mg}^{2+}\cdot\text{GppNHp}$ is accompanied by a broadening of the signals due to the enhanced molecular mass.

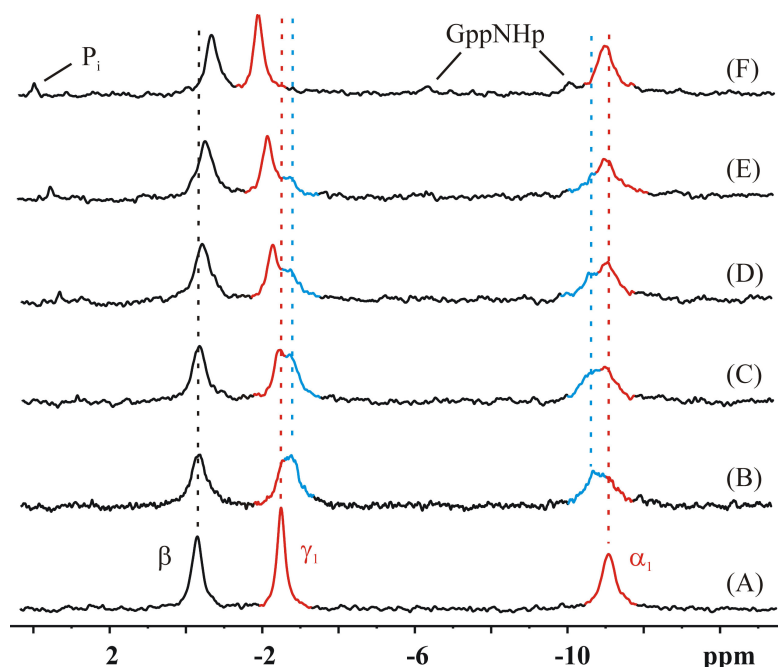


Figure 4.26: Displacement of Raf-RBD from $\text{Ras}(\text{T35A})\cdot\text{Mg}^{2+}\cdot\text{GppNHp}$ by Zn^{2+} -cyclen.

$\text{Ras}(\text{T35A})\cdot\text{Mg}^{2+}\cdot\text{GppNHp}$ in the absence (A) and presence of a 2-fold excess of Raf-RBD (B) and subsequent addition of a 4-fold (C), 8-fold (D), 12-fold (E) and 24-fold (F) excess of Zn^{2+} -cyclen, respectively. The sample initially contained 1.1 mM $\text{Ras}(\text{T35A})\cdot\text{Mg}^{2+}\cdot\text{GppNHp}$ in 40 mM Tris/HCl pH 7.4, 10 mM MgCl_2 , 2 mM DTE, 0.2 mM DSS and 5% D_2O . All spectra have been recorded at 278 K. Experimental data have been filtered exponentially leading to an additional line broadening of 15 Hz.

Upon binding of Zn^{2+} -cyclen to this mutant chemical shift changes can be observed for each signal. As soon as Raf-RBD and Zn^{2+} -cyclen bind simultaneously to the weak binding state one would expect the existence of only one signal for each phosphate group during the whole titration. These signals should be broadened since the effector is complexed to Ras and additionally shift because of the presence of Zn^{2+} -cyclen. If both compounds can only bind separately to Ras a different behaviour is expected. Two distinct resonances

representing Ras(T35A)·Mg²⁺·GppNHp with Raf-RBD or Zn²⁺-cyclen bound should be observed. The signal representing the Ras-Raf-RBD complex should decrease in the presence of increasing amounts of Zn²⁺-cyclen without significant shift changes, while the other one should gain in population accompanied by the shift changes commonly observed in Ras in the presence of the compound. Ras(T35A)·Mg²⁺·GppNHp was complexed with Raf-RBD followed by addition of increasing concentrations of Zn²⁺-cyclen up to a molar excess over Ras of 24-fold. The obtained spectra are depicted in Figure 4.26. Addition of Raf-RBD to Ras leads to line broadening of the signals representing the effector-bound conformational state of Ras(T35A)·Mg²⁺·GppNHp. With increasing amounts of Zn²⁺-cyclen two lines can be observed for the α - and γ -phosphate group, of which one increases, while the other one is decreasing. For the increasing signal of the γ -phosphate group also a downfield shift can be observed. For the β -phosphate resonance only one signal shifting upfield is observed over the whole titration. The results are summarized in Table 4.10.

Table 4.10 Chemical shift changes and line widths observed in Ras(T35A)·Mg²⁺·GppNHp in the presence of Raf-RBD and upon subsequent addition of Zn²⁺-cyclen.

		Ras(T35A)	+ Raf-RBD	+ Zn ²⁺ -cyclen	
molar excess			2	12	24
δ [ppm]	$\alpha(1)$	-11.08	-11.17	-10.98 ^a	-10.99 ^a
	$\alpha(2)$		-10.78		
	$\beta(1)$	-0.29	-0.34 ^a	-0.52 ^a	-0.68
	$\beta(2)$				
	$\gamma(1)$	-2.49	-2.51	-2.14	-1.9
	$\gamma(2)$		-2.79	-2.69	
$\Delta\nu_{1/2}$ [Hz] ^b	$\alpha(1)$	67	67	87 ^a	118 ^c
	$\alpha(2)$		113		
	$\beta(1)$	50	77 ^a	75 ^a	57 ^a
	$\beta(2)$				
	$\gamma(1)$	34	40	48	45
	$\gamma(2)$		77	83	

^a the signals representing the two conformational states are not separated

^b the line width was corrected with respect to the exponential filter used during data processing

^c could not be determined accurately

If the experiment is carried out the other way around, i.e. first Zn²⁺-cyclen is complexed to Ras and then Raf-RBD is added with increasing concentrations the same results should be observed. Upon addition of Raf-RBD the population of the Ras-Zn²⁺-cyclen complex should be diminished while the one representing the effector-bound complex should

increase. Additionally the resonances belonging to the Ras-Zn²⁺-cyclen complex should shift in the opposite direction due to the decreased concentration of the complex. Consequently Ras(T35A)·Mg²⁺·GppNHp was pre-complexed with Zn²⁺-cyclen and Raf-RBD was added stepwise. The obtained spectra are given in Figure 4.27.

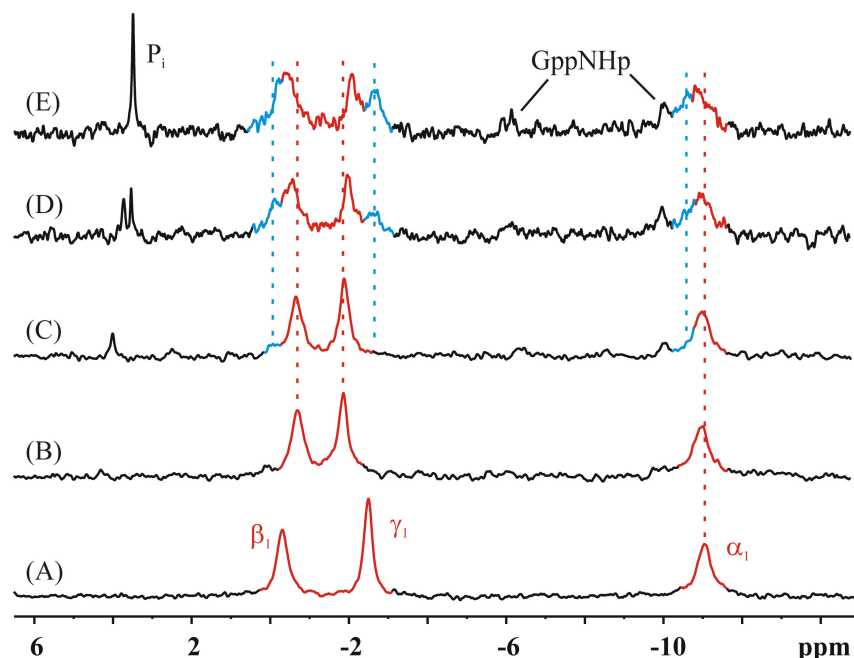


Figure 4.27: Displacement of Zn²⁺-cyclen from Ras(T35A)·Mg²⁺·GppNHp Raf-RBD.

Ras(T35A)·Mg²⁺·GppNHp in the absence (A) and presence of a 30-fold excess of Zn²⁺-cyclen (B) and subsequent addition of a 1-fold (C), 4-fold (D) and 7-fold (E) of Raf-RBD, respectively. All spectra have been recorded at 278 K. Experimental data have been filtered exponentially leading to an additional line broadening of 15 Hz. The sample initially contained 0.99 mM Ras(T35A)·Mg²⁺·GppNHp in 40 mM Tris/HCl pH 7.4, 10 mM MgCl₂, 2 mM DTE, 0.2 mM DSS and 5% D₂O.

At a 1-fold molar excess of Raf-RBD over Ras and higher precipitation was observed in the NMR sample. Additionally signals characteristic for Mg²⁺·GppNHp are observed in the ³¹P NMR spectra. The precipitant was subject to SDS-Page analysis, which revealed Ras as precipitant. In the final spectrum a peak probably representing inorganic phosphate is coming up. Surprisingly the shift direction of the P_i-peak is opposite to the one commonly observed for inorganic phosphate in the presence of Zn²⁺-cyclen. Due to the poor data quality the effects observed are not quantified. Qualitatively the expected results are obtained. Addition of Zn²⁺-cyclen lead to the above described shift of the β- and γ-phosphate. Upon addition of Raf signals representing the Raf-Ras complex show up and increase in population compared to the signals of the Ras-Zn²⁺-cyclen-complex. Additionally the signals representing the latter complex shift upfield for the γ- and downfield for the β-phosphate group.

4.4 Localization of the Binding Sites of the Metal(II)-Chelates in Ras(T35A)·Mg²⁺·GppNHp

4.4.1 General Procedure

³¹P NMR spectroscopic investigations clearly revealed an effect of the substances in the active centre of the protein (see section 4.2). Additionally it could be shown that at least one binding position must be located in proximity to the active site close to the bound nucleotide by paramagnetic relaxation enhancement studies. The question remaining is about the exact position and the residues affected by binding. Likewise it can be possible that additional binding sites beside the one in the active centre might exist, which is the case for metal(II)-cyclen (T. Graf 2006).

The location and number of the binding sites was determined in [¹H, ¹⁵N]-HSQC titrations. Experiments have been carried out with both a paramagnetic and a diamagnetic derivative of the chelate complexes. The presence of a paramagnetic centre as represented by Cu²⁺ has a strong effect on the relaxation of NMR active nuclei leading to the bleaching of the corresponding NMR signal depending on the distance to the paramagnetic centre as described in section 1.2.4. Also exchange phenomena can give rise to line broadening and must not be neglected. For that reason each study for the investigation of the binding positions of the compounds has been carried out with both the paramagnetic Cu²⁺- and the diamagnetic Zn²⁺-derivative and the results have been directly compared.

4.4.2 Backbone Assignment of Ras(T35A)·Mg²⁺·GppNHp at pH 7.5

The backbone of Ras(T35A)·Mg²⁺·GppNHp has not been assigned sequentially until present. For that reason the assignment of Ras(T35S)·Mg²⁺·GppNHp at pH 5.5 has been transferred to the T35A mutant with the aid of additional triple resonance spectra (F. Schumann, University of Regensburg). Any studies concerning the Ras protein and its possible ligands have been carried out at pH 7.4. For that reason Ras(T35A)·Mg²⁺·GppNHp was titrated from pH 5.5 to 7.4 and the resonances of the individual peaks have been followed by [¹H, ¹⁵N]-HSQC spectroscopy (T. Graf 2006). The correct assignment of the backbone resonances is of high importance since it is the basis for several titration studies within this work. For that reason the obtained spectra have been evaluated again in order to minimize errors. Figure 4.28 (A) shows the combined chemical shift changes observed between pH 5.5 and 7.4. Not surprisingly the largest differences are observed for histidine residues, e.g. His²⁷ and His⁹⁴ and aspartate residues like Asp⁵⁴ and residues in their close proximity. During titration studies peak overlapping complicates the assignment of the chemical shifts after each titration step. In order to ensure that the titration was followed in the right way the chemical shift changes were plotted against the pH value and it was checked, whether the curves resembles the common pH dependence. An example is given in Figure 4.28 (B) for histidine⁹⁴.

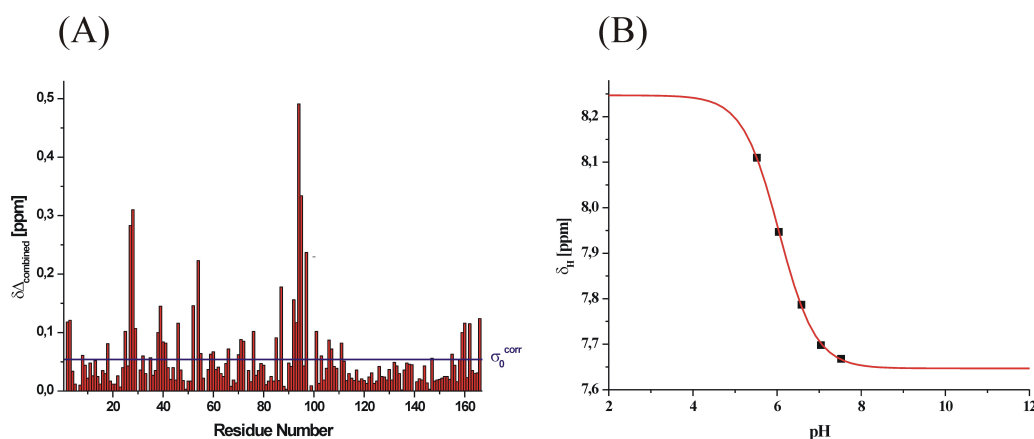


Figure 4.28: Combined Chemical Shifts Changes $\Delta\delta_{\text{combined}}$ observed in Ras(T35A)·Mg²⁺·GppNHp between pH 5.5 and pH 7.4 (A) and exemplarily for the proton signals for histidine⁹⁴ plotted against the pH value (B). The corrected standard deviation to zero (σ_0^{corr}) is given by the blue line.

4.4.3 Results Obtained for Metal(II)-Cyclen

As described in paragraph 1.1.6.4 ³¹P NMR spectroscopy directly revealed the binding position of the metal(II)-cyclens to be in close proximity to the γ -phosphate group in the active centre of the protein. Three binding sites for the metal(II)-cyclens have been determined in the partial loss-of-function mutant Ras(T35A)·Mg²⁺·GppNHp by [¹H, ¹⁵N]-HSQC titrations, whereby one is close to the active centre in good agreement with the results from the ³¹P NMR measurements (T. Graf 2006). However, during data evaluation of the titrations carried out slow exchange processes have not been taken under consideration. For that reason the obtained data have been re-evaluated and compared with the analogues experiments with the diamagnetic derivative. Cu²⁺-cyclen was titrated to ¹⁵N Ras(T35A)·Mg²⁺·GppNHp up to a molar ratio of 5:1 (T. Graf, University of Regensburg). In Figure 4.29 a small section of the HSQC-spectrum of ¹⁵N Ras(T35A) complexed to Mg²⁺·GppNHp in the absence and presence of Cu²⁺-cyclen is shown. The signal intensities of the resonances of Gly¹³, located in the P-loop, and of Gly⁶⁰, located in switch II are decreased substantially whereas those of other resonances are not perturbed. The titration with the diamagnetic derivative was carried out up to a 50-fold excess of the ligand. The corresponding ¹H spectra clearly reveal that the protein starts to precipitate at a ligand excess of 20-fold. For that reason only the data obtained up to a 15-fold excess of Zn²⁺-cyclen over Ras(T35A)·Mg²⁺·GppNHp have been evaluated. Several residues also show a significant decrease in cross peak volume, when Zn²⁺-cyclen is titrated to Ras due to exchange processes, which can be intermediate or slow compared to the NMR time scale. Slow exchange is accompanied by the appearance of a novel peak for a given amino acid, while the intensity of the original one is decreasing. An example is given by isoleucine²⁴ and glycine¹¹⁵ in Figure 4.30 If a residue exchanges between two chemical environments in an intermediate manner compared to the NMR time scale, its cross peak volume is decreased without the appearance of a novel one. This can for example be

observed for phenylalanine²⁸ and is depicted in Figure 4.31 This residue was considered to be part of the third binding site in Ras(T35A)·Mg²⁺·GppNHp together with histidine²⁷ due to the loss of signal intensity in the presence of Cu²⁺-cyclen. Both residues are also bleached out in the titration with Zn²⁺-cyclen.

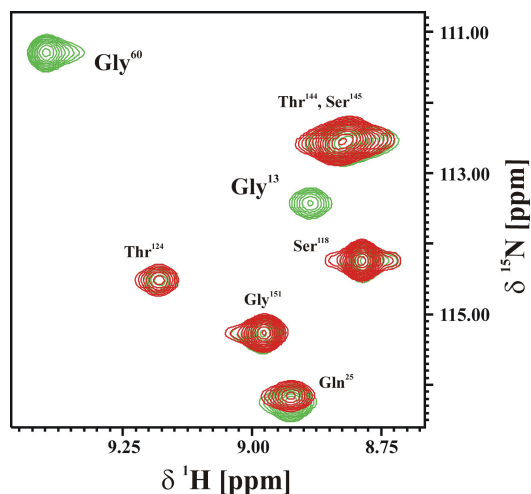


Figure 4.29: Effect of Cu²⁺-cyclen on [¹H, ¹⁵N]-HSQC NMR spectra of Ras(T35A)·Mg²⁺·GppNHp. Section of the [¹H, ¹⁵N]-HSQC NMR spectra of 1.3 mM Ras(T35A)·Mg²⁺·GppNHp in 40 mM Hepes/NaOH, pH 7.5, 10 mM MgCl₂, 2 mM DTE, and 5% D₂O at 293 K in the absence (green) and presence of 6.5 mM Cu²⁺-cyclen (red) at the same conditions.

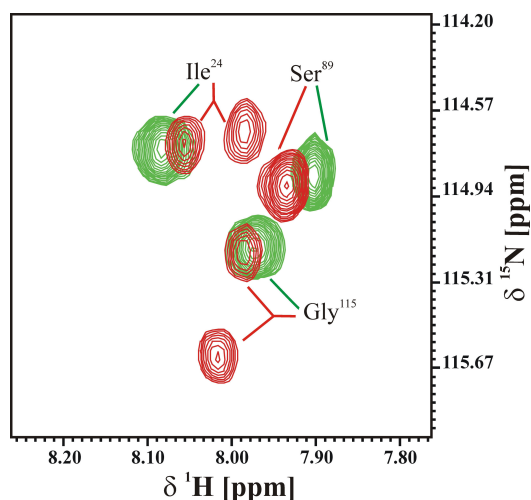


Figure 4.30: Exchange processes observed in Ras(T35A)·Mg²⁺·GppNHp upon addition of Zn²⁺-cyclen. Section of the [¹H, ¹⁵N]-TROSY-HSQC NMR spectra of 0.78 mM Ras(T35A)·Mg²⁺·GppNHp in 40 mM Hepes/NaOH, pH 7.4, 10 mM MgCl₂, 2 mM DTE, and 10% D₂O at 293 K in the absence (green) and presence of 11.66 mM Zn²⁺-cyclen (red) at the same conditions.

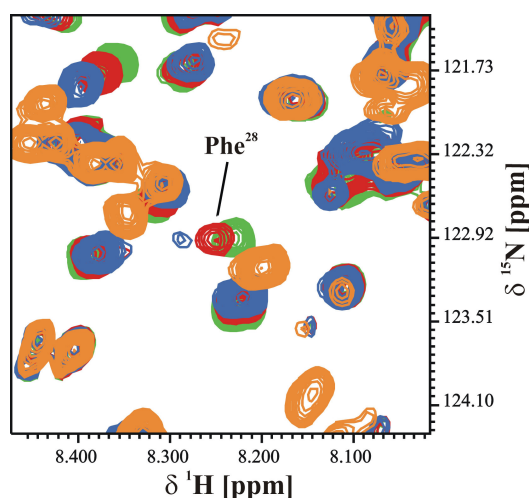


Figure 4.31: Exchange processes observed for phenylalanine²⁸ in the presence of Zn²⁺-cyclen.

Section of the [¹H, ¹⁵N]-TROSY-HSQC NMR spectra of 0.78 mM Ras(T35A)·Mg²⁺·GppNHp in 40 mM Hepes/NaOH, pH 7.4, 10 mM MgCl₂, 2 mM DTE, 0.2 mM DSS and 10% D₂O at 293 K in the absence (green) and presence of increasing concentrations of Zn²⁺-cyclen (red, blue and orange) at the same conditions.

It is possible that His²⁷ and Phe²⁸ are in slow exchange, but the new peak is not be identified and clearly assigned. Likewise for these residues intermediate exchange may happen. However, residues exhibiting significant signal reduction in both titrations cannot be clearly related to the paramagnetic distance-dependent effect of the Cu²⁺ ion. For that reason one has to compare the results from both titrations. In Table 4.11 those residues, exhibiting a signal reduction $I(j)/I_0(j) < 1 - \sigma_0$ in the presence of Cu²⁺-cyclen definitely caused by paramagnetic relaxation enhancement are listed.

Table 4.11: Residues clearly affected by the paramagnetic central Cu²⁺-ion chelated by cyclen assigned to the two binding sites identified.

	Site 1	Site 2
$(I-I_0)/I_0 > \sigma_0$	13, 32, 59-61	105-109, 111, 165, 166
not assigned	1, 4, 30, 34, 53, 57, 66, 73, 79, 100, 110, 140, 163	

These residues give two spatially well separated binding sites, when mapped onto the surface of the crystal structure of Ras(wt)·Mg²⁺·GppNHp (Figure 4.33). Binding site 1 (Figure 4.33(A)) is close to the γ -phosphate group of the bound nucleotide in accordance to the ³¹P NMR data and the previous results. Residues most affected are Gly¹³, Tyr³², Ala⁵⁹, Gly⁶⁰ and Gln⁶¹ (Table 4.11), located in the P-loop (amino acid 10-18), the PM3-motif (57-61) and in switch II (60-72), respectively. The second binding site (Figure 4.33 (B)) centres in the negatively charged loop L7 comprising Asp¹⁰⁵, Ser¹⁰⁶, Asp¹⁰⁷, Asp¹⁰⁸, Val¹⁰⁹, Met¹¹¹ and at the C-terminal residues Gln¹⁶⁵ and His¹⁶⁶. The third binding site identified by T. Graf (2006) is not supported by this evaluation. If fast exchange processes compared to the NMR time scale prevail only a single cross peak is observed representing both

chemical environments with a chemical shift at the population averaged position. Figure 4.32 shows the combined chemical shift changes observed in Ras(T35A)·Mg²⁺·GppNHp in the presence of Zn²⁺-cyclen. Table 4.12 summarizes the effects observed in the [¹H, ¹⁵N]-HSQC spectrum of Ras(T35A)·Mg²⁺·GppNHp in the presence of Zn²⁺-cyclen. Large shift perturbations are observed for Ala³⁵, Ile³⁶ and Asp³⁸, which are part of the switch I region, Ile¹⁶³ from the C-terminal end of the protein and Asp¹⁰⁸ and Met¹¹¹ from loop L7. This agrees very well with the results obtained in the titration with Cu²⁺-cyclen. Most of these residues become significantly broadened in the latter experiment. Residues, which are significantly perturbed in their chemical shift upon addition of Zn²⁺-cyclen have mapped onto the surface of the wild type crystal structure (Figure 4.33).

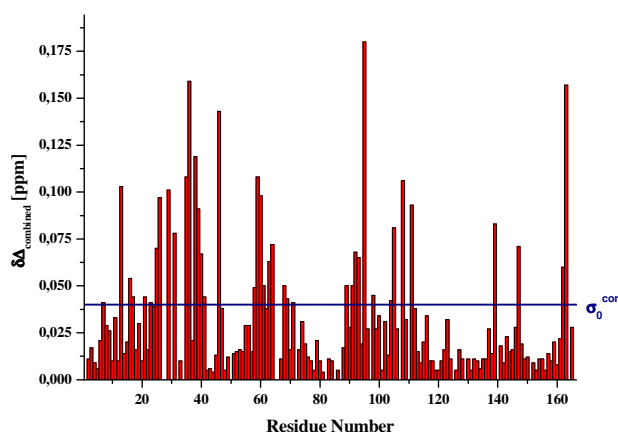


Figure 4.32: Combined chemical shift changes observed in Ras(T35A)·Mg²⁺·GppNHp in the presence of Zn²⁺-cyclen with a molar excess of 15. The corrected standard deviation to zero (σ_0^{corr}) is represented by the blue line (Schumann et al. 2007).

Table 4.12: Exchange processes and combined chemical shift changes observed in Ras(T35A)·Mg²⁺·GppNHp in the presence of Zn²⁺-cyclen.

	Site 1	Site 2
$k \gg \delta_A - \delta_B^b$	13, 16, 21, 23, 25, 26, 29, 31, 35, 36, 37, 38, 58, 59, 60, 61, 63, 64, 68, 76, 89, 98, 147	104, 105, 106, 108, 111, 139, 162, 163, 164, 166
$k \ll \delta_A - \delta_B^c$	8, 11-13, 17-21, 24-26, 31, 39, 46, 56, 58, 80, 83, 84, 85, 87, 88, 91, 112, 114, 115, 117, 119-121, 124, 125, 127-134, 139, 141, 142, 147, 148, 151-154, 157, 158, 159, 160, 162, 166	

^a fast exchange processes

^b slow exchange processes

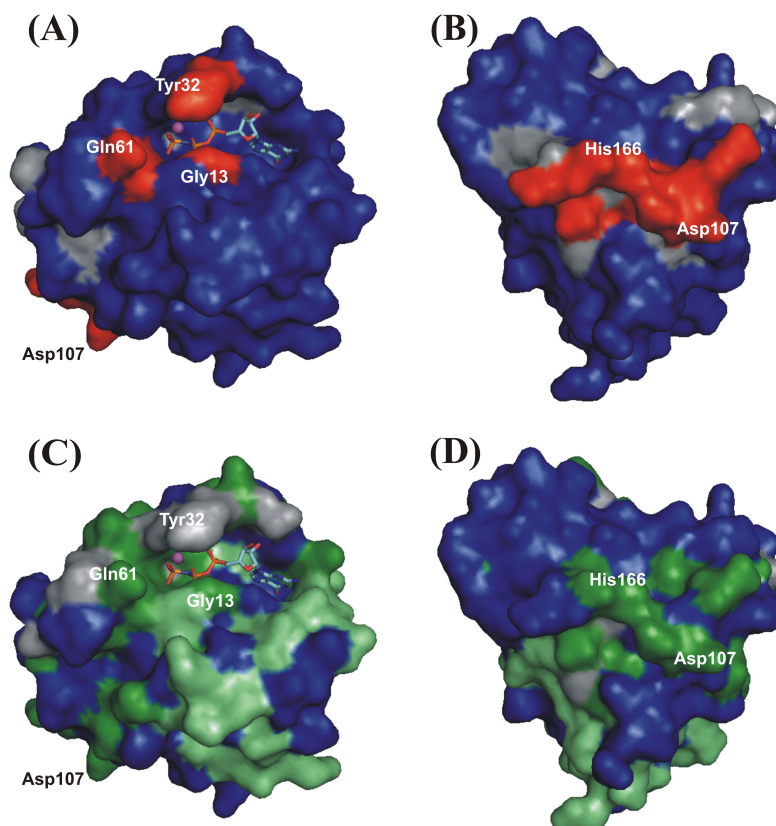


Figure 4.33: Binding sites of metal(II)-cyclen in active Ras. (A) and (B) amino acids clearly affected by the paramagnetic distance-dependent Cu(II)-effect mapped onto the surface of the crystal structure of Ras(wt)·Mg²⁺·GppNHp (pdb 5p21). Residues exhibiting a significant relative signal reduction $I(j)/I_0(j) < 1 - \sigma_0$ are colored red, not clearly assignable residues are shown in gray. (C) and (D) amino acids showing significant shift perturbations in the presence of Zn²⁺-cyclen mapped onto the surface of the crystal structure of Ras(wt)·Mg²⁺·GppNHp (pdb 5p21). Residues with a significant combined chemical shift change $\Delta\delta_{\text{comb}} > \sigma_0$ are colored green, residues showing a line splitting by binding of Zn²⁺-cyclen typical for a slow exchange process are shown in light green, not clearly assignable residues are shown in gray.

4.4.4 Results Obtained for Metal(II)-BPA

³¹P NMR investigations with Zn²⁺-BPA already revealed that at least one binding position should be in close proximity to the bound nucleotide in the active centre. The compound selectively recognizes conformational state (1) in active Ras as shown for different mutants by NMR spectroscopy. This stabilization is not accompanied by large chemical shift changes for the phosphorus resonances, which would be expected if a compound like BPA carrying two aromatic rings is in binding distance. Consequently [¹H, ¹⁵N]-HSQC titration studies with both the paramagnetic and diamagnetic derivative of BPA were carried out. Initially Cu²⁺-BPA was titrated to Ras(T35A)·Mg²⁺·GppNHp up to a molar excess of 1.2 and its effect was followed by [¹H, ¹⁵N]-HSQC-spectroscopy. In contrast to the corresponding titration with Cu²⁺-cyclen the bleaching of several residues is already

observed at a molar ratio of Ras:Cu(II)-BPA of 1:0.2. In order to allow for proper information about the relative effect of single amino acid residues in the protein, the data obtained at that molar ration have been used for the determination of the binding sites. In Figure 4.34 the relative signal intensity of the reference intensity observed upon addition of a 0.2-fold excess of Cu(II)-BPA is plotted against the amino acid sequence of Ras(T35A).

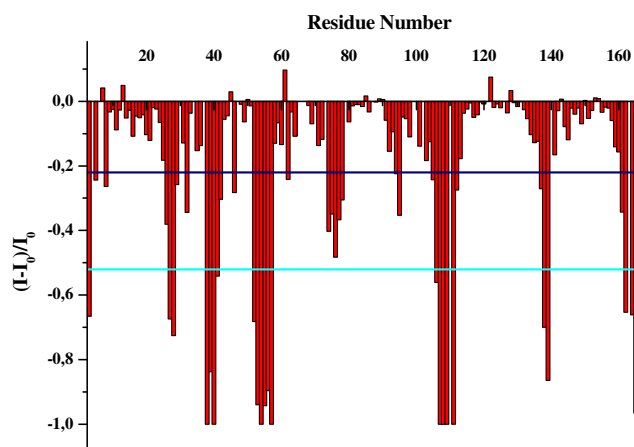


Figure 4.34: Relative signal intensities observed in the $[^1\text{H}, ^{15}\text{N}]$ -HSQC spectrum of Ras(T35A) complexed to Mg^{2+} -GppNHp in the presence of a 0.2-fold excess of Cu^{2+} -BPA. The mean value is given by the blue line. The line colored cyan represents the mean value plus the standard deviation.

The cross peaks of residues Tyr³⁸, Asp⁴⁰, Asp¹⁰⁷, Asp¹⁰⁸, Val¹⁰⁹ and Met¹¹¹ are already bleached and cannot be detected anymore. Strong effects are also observed for residues 52-55, which are part of the PM3 motif and the C-terminal residues 162-165 as well as residues 103-105, which are part of loop L7. Residues exhibiting a relative signal reduction larger than the mean value have been color coded according to their effect and mapped onto the surface of the structure of Ras(T35S)· Mg^{2+} -GppNHp, which was solved by NMR spectroscopy at the department (F. Schumann, unpublished results). Two binding sites can be identified for metal(II)-BPA. One of the binding sites is located at the C-terminal end of Ras and loop L7 and was also found for metal(II)-cyclen both by NMR spectroscopy and by X-ray crystallography (Roznizeck et al., accepted). The second one is located close to the active centre, which is presumably the one responsible for the stabilization of conformational state (1) in active Ras. However, its position differs from the binding site obtained for metal(II)-cyclen. Metal(II)-BPA is located on the other site of the nucleotide binding pocket compared to metal(II)-cyclen. The binding sites identified are depicted in Figure 4.36.

In the next step Ras(T35A)· Mg^{2+} -GppNHp was also titrated with the diamagnetic derivative Zn^{2+} -BPA. At a molar ratio of Ras:BPA of 1:16 the protein started to precipitate, which was already observed in the ^{31}P NMR experiments. Consequently further titration steps have not been carried out and the change of the chemical shift values was evaluated with the results obtained with an 8-fold molar excess of Zn^{2+} -BPA over Ras. During the

titration slow exchange processes have not been observed. Consequently the results derived from the Cu^{2+} -titration need not to be corrected. Figure 4.35 shows the combined chemical shift changes observed in the presence of the diamagnetic derivative.

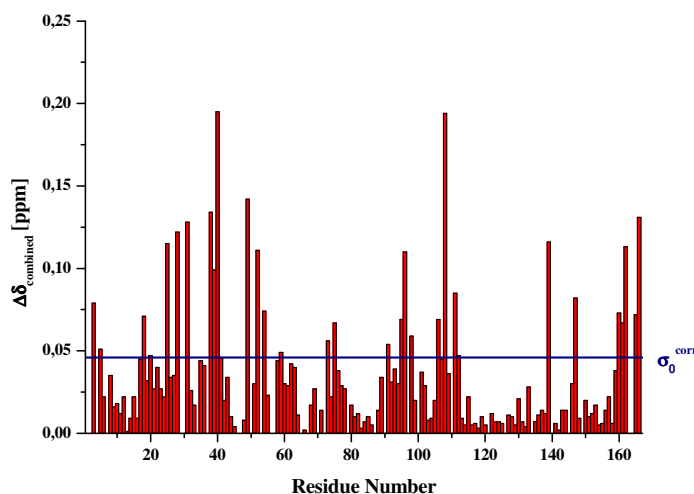


Figure 4.35: Combined chemical shift changes observed in the $[\text{}^1\text{H}, \text{}^{15}\text{N}]$ -HSQC spectrum of **Ras(T35A)·Mg²⁺·GppNHp** in the presence of an 8-fold excess of **Zn²⁺-BPA**. The corrected standard deviation to zero (σ_0^{corr}) is given by the blue line.

The strongest effects are observed for residues Asp³⁸, Ser³⁹ and Tyr⁴⁰, which are part of the binding position in proximity to the active centre as well as the C-terminal residues Ile¹⁶³, Gln¹⁶⁵ and His¹⁶⁶. Additionally large changes can be found for Ile¹³⁹, which is in close proximity to the C-terminal end and loop L7 and thus part of the second binding position and for Lys¹⁴⁷, which supports nucleotide binding by the G1 motif. Phe²⁸, which represents the G1 motif and forms strong hydrophobic interaction with the guanine base is also affected significantly together with residues in its neighbourhood.

Residues showing chemical shift changes $\Delta\delta_{\text{combined}} > \sigma_0^{\text{corr}}$ have been normalized to the value calculated for Arg⁴¹, which shows the strongest effect, color-coded and mapped onto the surface of Ras(T35S)·Mg²⁺·GppNHp. As one can see very clearly in Figure 4.36 the results obtained with both derivatives agree very well. Significant effects are observed in both cases for residues around the C-terminus and loop L7, which compromise one binding position and residues of switch I and the PM3 motif.

A summary of the results obtained from the $[\text{}^1\text{H}, \text{}^{15}\text{N}]$ -HSQC titrations with metal(II)-BPA is given in Table 4.13. The affected residues are assigned to the binding sites identified.

Table 4.13: Relative signal intensities and combined chemical shift changes observed in Ras(T35A)·Mg²⁺·GppNHp in the presence of Cu²⁺-BPA and Zn²⁺-BPA, respectively.

		Site 1	Site 2
Cu²⁺-BPA^b	0.00 < (I-I₀)/I₀ < 0.25^a		
	0.25 < (I-I₀)/I₀ < 0.50^a	5, 8, 26, 29, 32, 42, 46, 62, 74-76, 78	94, 95, 105, 112, 137, 161
	0.50 < (I-I₀)/I₀ < 0.75^a	3, 27, 28, 41, 52	106, 138, 162, 164
	0.75 < (I-I₀)/I₀ < 1.00^a	39, 40, 53-58	107-111, 165, 166
Zn²⁺-BPA^d	0.00 < Δδ_{comb} < 0.25^c	20, 41	112
	0.25 < Δδ_{comb} < 0.50^c	3, 5, 18, 54, 59, 73, 75	91, 95, 98, 106, 111, 147, 160, 165
	0.50 < Δδ_{comb} < 0.75^c	25, 28, 31, 38, 39, 49, 52	96, 139, 162, 166
	0.75 < Δδ_{comb} < 1.00^c	40	108

^a combined chemical shift changes observed for the residues have been normalized for the residue giving the biggest response and subgrouped according to the relative shift effect

^b the results listed are obtained at a molar ratio of Ras:Cu²⁺-BPA = 1:0.2

^c relative signal intensities have been subgrouped according to the maximum relative signal loss of 1

^d the results listed are obtained at a molar of Ras:Zn²⁺-BPA = 1:8

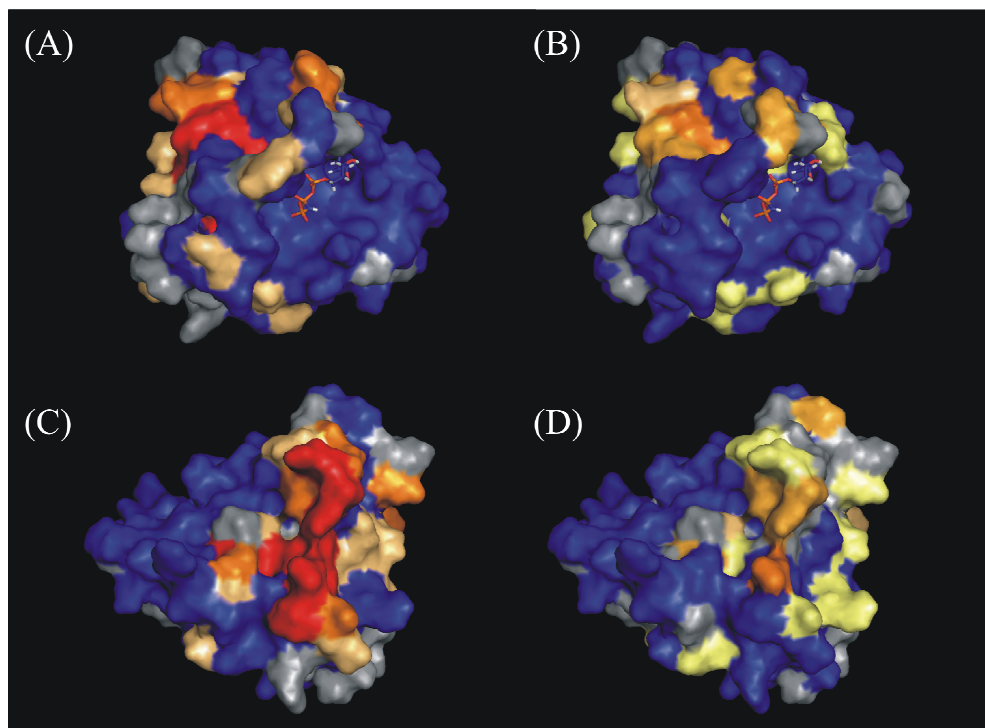


Figure 4.36: Intensity loss and chemical shift changes observed in Ras(T35A)·Mg²⁺·GppNHp in the presence of Cu²⁺- and Zn²⁺-BPA, respectively. (A), (B) Binding site 1. (C), (D) Binding site 2. The effects in the presence of Cu²⁺-BPA ((A), (C)) and Zn²⁺-BPA ((B), (D)) are colored according to the subgroups listed in Table 4.13. The stronger the observed effect the darker the residues are colored. Prolines and not assigned residues are shown in gray. The NMR structure of Ras(T35S)·Mg²⁺·GppNHp is shown (F. Schumann, unpublished results).

4.5 Development of Bivalent Ras Ligands

4.5.1 Linkage of Zn^{2+} -Cyclen and Zn^{2+} -BPA to a Peptide with a Consensus Ras Binding Sequence

The metal(II)-chelates Zn^{2+} -cyclen and Zn^{2+} -BPA influence the dynamic equilibrium of active Ras by selectively stabilizing conformational state (1). Additionally it was shown by ^{31}P NMR spectroscopy that it is possible to influence the Ras-effector interaction by these compounds. Their application is limited by their low affinity, which has been determined to be in the millimolar range and the fact, that more than one binding position is present in Ras for both compounds. In order to increase both the affinity and the selectivity of Zn^{2+} -cyclen and Zn^{2+} -BPA at the binding site in the active centre of Ras, which is responsible for the stabilization of conformational state (1) bivalent Ras ligands have been designed. State (1) is assumed to be close related to the conformation of Ras found in complex with its exchange factor SOS (Ford et al. 2005, Kalbitzer et al. 2009). Consequently the crystal structure of the Ras-SOS complex (Boriack-Sjodin et al. 1998) was used as basis for the design of a peptide possibly interacting with Ras and bivalent Ras ligands have been designed. The peptide consists of amino acids from the sequence of the exchange factor SOS directly interacting with Ras close to the active centre. Single amino acids in between, not contributing to the interaction with Ras have been displaced by glycines in order to allow for more flexibility. Figure 4.37 illustrates the structural basis for the design of the peptide with the sequence LGGIR.

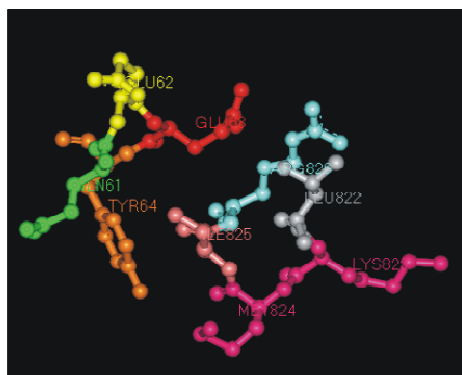


Figure 4.37: Part of the crystal structure of Ras in complex with SOS (1bkd). Direct contacts with Ras switch II residues Glu⁶², Glu⁶³ and Tyr⁶⁴ are provided by Arg⁸²⁶, Ile⁸²⁵ and Leu⁸²² from SOS. Residues Lys⁸²³ and Met⁸²⁴ do not contribute to the interaction.

The short peptide LGGIR was synthesized at the chair of Prof. B. König and investigated in terms of its binding position using $[^1\text{H}, ^{15}\text{N}]$ -HSQC titration studies with Ras(T35A)· Mg^{2+} ·GppNHp at our department. Figure 4.38 shows the histogram of the observed chemical shift changes induced by binding of the small peptide.

The largest chemical shift changes are observed for residues 62-65 (switch II), which are at the desired binding position of the peptide. Figure 4.39 shows the binding curve for the peptide obtained for residues Glu⁶² and Glu⁶³. The binding affinity has been determined to be 3.66 ± 1.3 mM according to Equation 3.4.

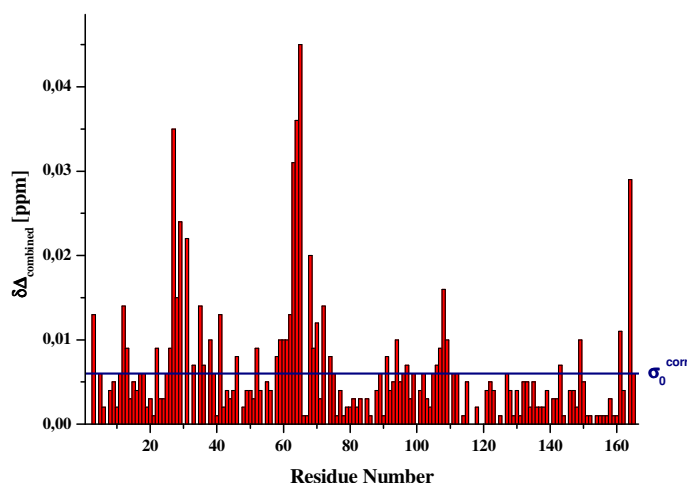


Figure 4.38: Combined chemical shift changes observed in Ras(T35A)·Mg²⁺·GppNHp in the presence of LGGIR. Given are the chemical shift changes observed in the [¹H, ¹⁵N]-TROSY-HSQC spectrum of a sample originally containing 0.8 mM ¹⁵N c-Ras(T35A)·Mg²⁺·GppNHp in 40 mM Tris/HCl pH 7.4, 10 mM MgCl₂, 2 mM DTE, 0.2 mM DSS and 5% D₂O upon addition of a 32-fold excess of the peptide LGGIR dissolved in the same buffer. The spectra have been recorded at 293 K at a spectrometer operating at 800 MHz proton frequency. The corrected standard deviation to zero (σ_0^{corr}) is given by the blue line (Schumann et al. 2007).

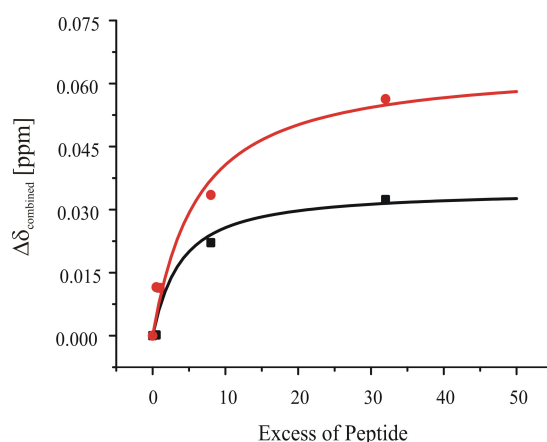


Figure 4.39: Plot of the chemical shift changes obtained for Ras residues Glu⁶² (black squares) and Glu⁶³ (red dots) against the excess of the peptide LGGIR. The data have been fitted by a one-site binding model according to Equation 3.4 giving a K_D -value of 3.66 mM. The obtained fit is given by the black and the blue line for Glu⁶² and Glu⁶³, respectively.

Consequently the distance between the binding position of the metal(II)-chelates at the active centre and the peptide was estimated and the peptide was thereupon linked to both metal(II)-chelates at the chair of Prof. König. Figure 4.40 shows the designed bivalent ligands.

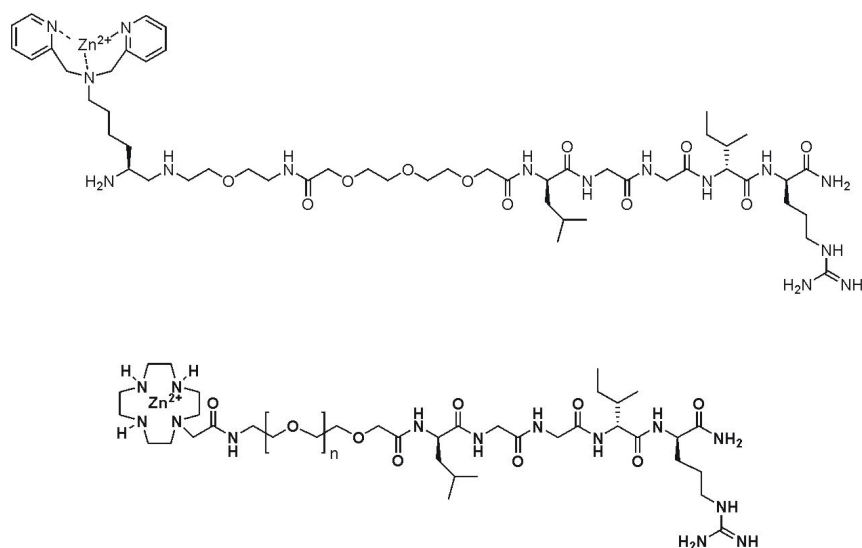


Figure 4.40: Designed bivalent ligands for Ras. Both Zn^{2+} -chelates have been linked to the small peptide LGGIR giving the hybide ligands H181 (above) and RHC-5-1 (bottom, $n = 3$) and RHC-6-1 (bottom, $n = 2$).

4.5.2 Determination of the Affinity of the Bivalent Ligands by STD NMR

The designed hybide ligands carry a peptide moiety and consequently the on-resonance irradiation frequency in the STD experiment has to be chosen carefully as already described in section 4.1.2. It has been shown that it is possible to saturate Ras entirely and selectively at -2 ppm. This frequency should be far enough from the signals from the peptides. However to make sure that reliable results are obtained the compounds were initially measured without Ras being present. In the next step $\text{Ras(T35A)} \cdot \text{Mg}^{2+} \cdot \text{GppNHp}$ was added to the sample and the same experiment was carried out followed by the titration with H181, RHC-5-1 and RHC-6-1 up to a molar excess of 333, 480 and 190, respectively. Peaks representative for the metal(II)-chelate moiety of the molecule have been used for evaluation. Figure 4.41 and 4.42 show the obtained plot of the amplification factor against the concentration of the hybide ligand carrying either a Zn^{2+} -cyclen or a Zn^{2+} -BPA moiety. The binding curve does not reach saturation at molar ratios between Ras and the hybide ligands of 333, 480 and 190. From these data is it clear that the designed hybide ligands do not have higher affinity for Ras than the metal(II)-chelates alone.

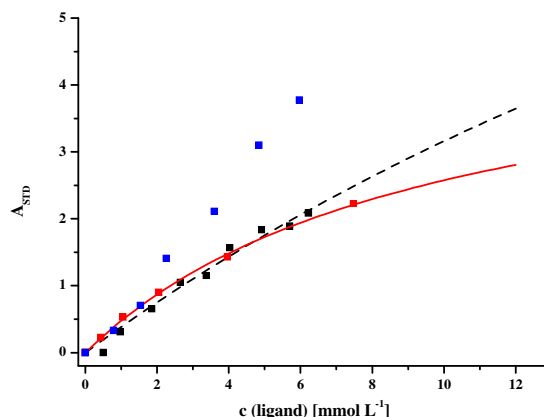


Figure 4.41: Plot of the STD amplification factor against the molar excess of Zn^{2+} -cyclen and the hybrid ligands RHC-5-1 and RHC-6-1. Shown are the amplification factors obtained from a STD titration with a sample originally containing $50 \mu\text{M}$ Ras(T35A)·Mg $^{2+}$ ·GppNHp in 40 mM Tris/HCl pH 7.4 and 10 mM MgCl $_2$ with Zn^{2+} -cyclen (red dots), RHC-5-1 (blue dots) and RHC-6-1 (black dots), respectively. In each experiment on-resonance irradiation was performed at -2 ppm and a spinlock filter was implemented (50 ms at 15 dB). In the titration of RHC-5-1 the on-resonance irradiation was performed with an attenuation of 30 dB resulting in higher A_{STD} -values compared to the titrations with Zn^{2+} -cyclen and RHC-6-1 (the attenuation was set to 40 dB) due to the more effective saturation of the protein. The obtained values for A_{STD} have been multiplied by a factor of 0.1 in the case of RHC-5-1 in order to allow for a better comparison with the data obtained for Zn^{2+} -cyclen and RHC-6-1. All spectra were recorded at 278 K at 600 MHz proton frequency. In each case the signals representing the Zn^{2+} -cyclen moiety have been used for evaluation. The data have been fitted according to Equation 3.2. The corresponding fits are represented by the red (Zn^{2+} -cyclen) and the black line (RHC-6-1). For Zn^{2+} -cyclen a K_{D} -value of $9.65 \pm 1 \text{ mM}$ is derived. For the RHC-6-1 the K_{D} -value can be estimated to be larger than 40 mM . The data for RHC-5-1 do not allow for an estimation or quantification of the K_{D} -value.

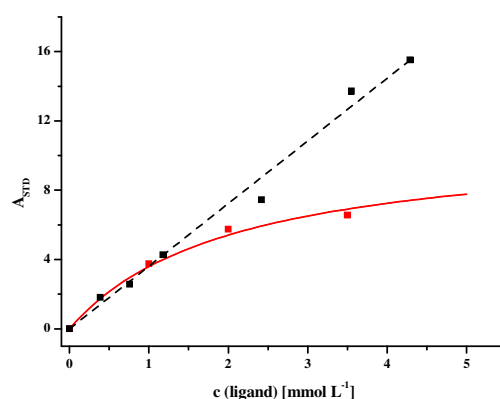


Figure 4.42: Plot of the STD amplification factor against the molar excess of Zn^{2+} -BPA and the hybrid ligand H181. Shown are the amplification factors obtained from a STD titration with a sample originally containing $50 \mu\text{M}$ Ras(T35A)·Mg $^{2+}$ ·GppNHp in 40 mM Tris/HCl pH 7.4 and 10 mM MgCl $_2$ with Zn^{2+} -BPA (red dots), RHH 181 (black dots), respectively. The on-resonance irradiation was set to -2 ppm with an attenuation of 30 dB (H181) and 0.3 ppm with an attenuation of 40 dB (Zn^{2+} -BPA). A spinlock filter was implemented (50 ms at 15 dB) in order to suppress protein proton resonances potentially overlapping with the ligand signals. The data obtained in the titration with Zn^{2+} -BPA have been fitted according to Equation 3.2 giving a K_{D} -value of $2.07 \pm 0.25 \text{ mM}$. The corresponding fit is represented by the red line. The data for H181 do not allow for an estimation or quantification of the K_{D} -value. The liner regression of the data is shown by the dashed black line.

4.6 Characterization of the Interaction between Ras and Peptides Derived from Raf-RBD

4.6.1 Localization of the Binding Site in Ras(wt)·Mg²⁺·GppNHp and Ras(T35A)·Mg²⁺·GppNHp

In section 1.1.6.3 peptides derived from the Ras binding domain of the Ras effector Raf and their modified analogues have been described, which potentially interfere with the Ras-Raf association (Barnard et al. 1995, 1998). The peptide CCAVFRL comprising Raf-RBD residues 95-101 and the peptide CCFFFRRL obtained from computational design were investigated in more detail by NMR spectroscopy since the binding position of these peptides and also their mode of inhibition have not been elucidated so far. For that reason the two peptides have been subject to chemical shift perturbation studies with both wild type Ras and the T35A mutant complexed to Mg²⁺·GppNHp. For the wild type mutant an assignment was only available for pH 5.5 at this point of time (Ito et al. 1997). In order to allow for a good comparison all investigations have been carried out at this pH value. CCAVFRL and CCFFFRRL were first titrated to wild type Ras complexed to Mg²⁺·GppNHp up to a molar excess of 4 and 3.2, respectively and the effect was followed by [¹H, ¹⁵N]-HSQC spectroscopy. Figure 4.43 shows the combined chemical shift changes observed in wild type Ras·Mg²⁺·GppNHp in the presence of the two peptides.

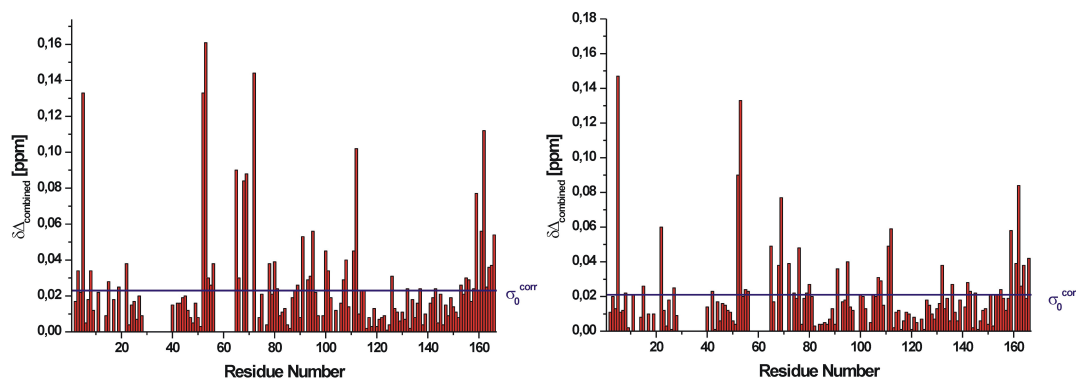


Figure 4.43: Combined chemical shift changes observed in wild type Ras·Mg²⁺·GppNHp in the presence of the peptide CCAVFRL (left panel) and CCFFFRRL (right panel). Given are the chemical shift changes observed in a sample originally containing 1.2 mM ¹⁵N c-Ras(wt)·Mg²⁺·GppNHp in 20 mM Na₂HPO₄-NaH₂PO₄ pH 5.5, 10 mM MgCl₂, 2 mM DTE, 0.2 mM DSS and 5% D₂O upon addition of a 4-fold and 4.8-fold excess of the peptides CCAVFRL and CCFFFRRL dissolved in the same buffer, respectively. All spectra have been recorded at 293 K at 800 MHz proton frequency. The corrected standard deviation to zero (σ₀^{corr}) is given by the blue line (Schumann et al. 2007).

The largest changes are observed for residues Lys⁵, Leu⁵³ and Ile⁵⁵ in both cases. A strong effect is also observed for residues Ser⁶⁵, Arg⁶⁸, Asp⁶⁹ and Met⁷², which are part of the switch II region and the C-terminal residues Arg¹⁶¹ and Glu¹⁶². The residues affected are normalized with regard to the residue exhibiting the strongest combined chemical shift change and listed in Table 4.14. They do not cluster at one position of the protein. Either more than one binding position is present in the protein for the peptides or structural changes happening upon binding of the peptide might be the case.

Due to the lack of H^N cross peaks of the switch regions in active wild type Ras the titration was also carried out with the partial loss-of-function mutant Ras(T35A)·Mg²⁺·GppNHp, which gives signals for all backbone residues in the protein. CCAVFRL and CCFFRRL were titrated to Ras(T35A)·Mg²⁺·GppNHp up to a molar excess of 4.8 and 4, respectively. Figure 4.44 shows the combined chemical shift changes. Again residues 52 to 54 of the PM3 motif show the largest perturbation similar to the results in wild type Ras. In the presence of the peptide CCFFRRL the effects observed in that region are larger relative to the other residues affected. Additionally the absolute values for the chemical shift changes are greater, when CCFFRRL is present. At a molar excess of 4 the effect observed for Leu⁵³ is higher by a factor of 1.25 compared to the results obtained with CCAVFRL at a molar excess of 4.8. Residues most affected in both titrations are listed in Table 4.14. They are again normalized relative to the residue showing the strongest shift change. In Figure 4.45 the effect of the peptide CCAVFRL observed in the [¹H, ¹⁵N]-HSQC spectrum of Ras(T35A)·Mg²⁺·GppNHp is shown graphically.

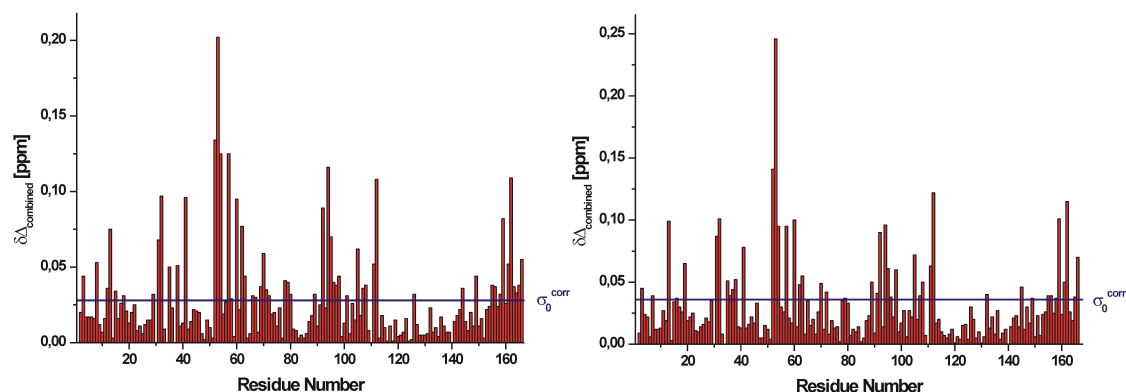


Figure 4.44: Combined chemical shift changes observed in Ras(T35A)·Mg²⁺·GppNHp in the presence of the peptide CCAVFRL (left panel) and CCFFRRL (right panel). Given are the chemical shift changes observed in a sample originally containing 0.6 mM (left panel) and 0.7 mM (right panel) ¹⁵N c Ras(T35A)·Mg²⁺·GppNHp in 20 mM Na₂HPO₄-NaH₂PO₄ pH 5.5, 10 mM MgCl₂, 2 mM DTE, 0.2 mM DSS and 5% D₂O upon addition of a 3.2-fold and 4-fold excess of the peptides CCAVFRL and CCFFRRL dissolved in the same buffer, respectively. All spectra have been recorded at 293 K at 800 MHz proton frequency. The corrected standard deviation to zero (σ_0^{corr}) is given by the blue line (Schumann et al. 2007).

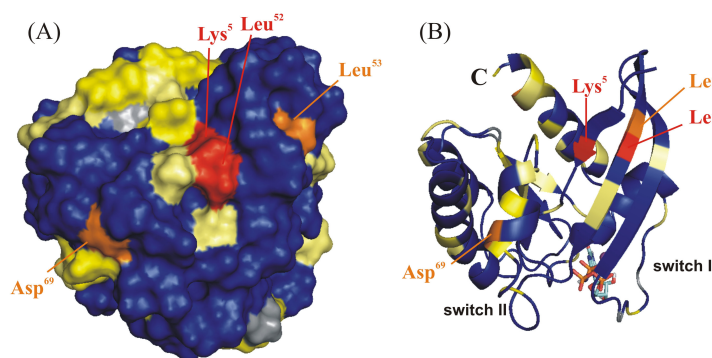


Figure 4.45: Combined chemical shift changes observed in Ras(T35A)·Mg²⁺·GppNHp in the presence of the peptide CCAVFRL. Residues exhibiting combined chemical shift changes $\Delta\delta_{\text{comb}} > \sigma_0^{\text{corr}}$ have been color-coded according to Table 4.14 and mapped on the structure of Ras(T35A)·Mg²⁺·GppNHp calculated when complexed to Cu²⁺-cyclen (T. Graf 2006). Shown is the surface representation (A) and the ribbon plot (B). The stronger the observed effect the darker the residues are colored. Prolines and not assigned residues are shown in gray.

Table 4.14: Combined chemical shift changes observed in wild type Ras and Ras(T35A) complexed to Mg²⁺·GppNHp in the presence of the peptides CCAVFRL and CCFFFRRL, respectively.

Ras(wt)·Mg ²⁺ ·GppNHp		Ras(T35A)·Mg ²⁺ ·GppNHp
CCAFVRL	p:l	1:4
0.00 < $\Delta\delta_{\text{comb}}$ < 0.25^a	3, 8, 15, 19, 22, 54-56, 66, 78, 80, 81, 88, 89, 93, 94, 101, 107, 108, 114, 115, 126, 132, 137, 143, 153, 155, 156, 158, 160, 163-165,	8, 15, 27, 42, 55, 56, 74, 79, 80, 91, 100, 107, 108, 136, 142, 143, 145, 151, 153, 155, 163
0.25 < $\Delta\delta_{\text{comb}}$ < 0.50^a	91, 95, 100, 111, 161, 166	65, 68, 72, 76, 95, 111, 112, 132, 159, 161, 164, 166
0.50 < $\Delta\delta_{\text{comb}}$ < 0.75^a	65, 68, 69, 112, 162	52, 69, 162
0.75 < $\Delta\delta_{\text{comb}}$ < 1.00^a	5, 52, 53, 72	5, 53
CCFFFRRL	p:l	1:4
0.00 < $\Delta\delta_{\text{comb}}$ < 0.25^a	3, 12, 15, 18, 29, 35, 58, 63, 67, 69, 71, 72, 78, 79, 80, 89, 96, 97, 98, 101, 107, 108, 126, 144, 149, 155, 156, 158, 163-165	3, 7, 16, 35-38, 62, 63, 70, 72, 79, 89, 91, 95, 96, 98, 107, 108, 132, 145, 149, 155, 156, 158, 161, 165,
0.25 < $\Delta\delta_{\text{comb}}$ < 0.50^a	8, 13, 31, 32, 38, 41, 60, 62, 70, 92, 95, 105, 111, 159, 161, 166	13, 19, 31, 32, 41, 54, 57, 60, 92, 94, 112, 159, 162
0.50 < $\Delta\delta_{\text{comb}}$ < 0.75^a	52, 54, 57, 94, 162	52
0.75 < $\Delta\delta_{\text{comb}}$ < 1.00^a	53	53

^a combined chemical shift changes observed for the signals residues have been normalized for the residue giving the biggest response and subgrouped according to the relative shift effect.

4.6.2 ^{31}P NMR Titration of Ras(wt)·Mg $^{2+}$ ·GppNHp with CCAVFRL

The [^1H , ^{15}N]-HSQC titration studies of the peptide CCAVFRL reveals its binding to Ras(T35A)·Mg $^{2+}$ ·GppNHp. Since the latter mutant predominantly exists in the weak effector-binding state (1) a possible influence on the dynamic equilibrium in active Ras was checked. For that purpose the peptide CCAVFRL was titrated to Ras(wt)·Mg $^{2+}$ ·GppNHp up to a molar excess of 2. At this ratio effects should be observed in the ^{31}P NMR spectra since the compound has been shown to bind to Ras(wt)·Mg $^{2+}$ ·GppNHp in the micromolar range (D. Filchtinski, personal communication). Figure 4.46 shows the spectra in the absence and presence of the peptide. Neither the chemical shift nor the line width or the relative populations of the two conformational states are affected significantly. At this ratio already strong effects are observed in the corresponding [^1H , ^{15}N]-HSQC spectra.

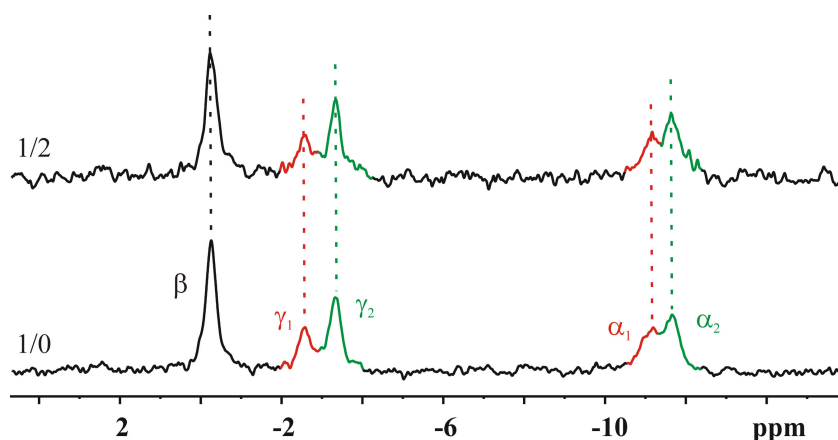


Figure 4.46: Influence of the peptide CCAVFRL on the dynamic equilibrium in Ras(wt)·Mg $^{2+}$ ·GppNHp. ^{31}P NMR Spectra of 0.8 mM Ras(wt)·Mg $^{2+}$ ·GppNHp in 40 mM Tris/HCl pH 7.4, 10 mM MgCl $_2$, 2 mM DTE, 0.2 mM DSS and 5% D $_2$ O in the absence and presence of CCAVFRL. The molar ratios are indicated. All spectra have been recorded at 278 K. Experimental data have been filtered exponentially leading to an additional line broadening of 15 Hz.

4.7 Comparison of the [^1H , ^{15}N]-TROSY-HSQC Spectra of the Ras Mutants T35S and T35A Complexed to Mg $^{2+}$ ·GppNHp

The NMR structure of Ras(T35S)·Mg $^{2+}$ ·GppNHp was solved at the department (F. Schumann, unpublished results). It is assumed that the partial loss-of-function Ras mutants T35A and T35S share the same structural principles and most probably differ in their dynamics. Changes in the chemical environment are very sensitively sensed by the chemical shifts of corresponding residue. In order to obtain detailed information about region with a different chemical environment between the two Ras mutants [^1H , ^{15}N]-HSQC spectra of both mutants have been measured under identical conditions.

The identical buffer solution was used for the sample, the data were recorded at the same spectrometer at the same temperature and the same settings for the experiments (M. Spoerner, Regensburg). Subsequently the chemical shifts have been directly compared. Figure 4.47 shows the chemical shift differences between Ras(T35S) and Ras(T35A) complexed to Mg^{2+} -GppNHp as a function of the primary sequence. Not surprisingly the largest differences can be observed for residue 35, which is the mutated one and residues in its close proximity. Residues with an observed combined differences between the chemical shifts $\Delta\delta_{\text{comb}} > \sigma_0^{\text{corr}}$ are given in Table 4.16. Residues affected by the mutation can be found in both switch regions and around helix $\alpha 3$. In Figure 4.48 these residues are mapped on the NMR structure of Ras(T35S)· Mg^{2+} -GppNHp (F. Schumann, unpublished results).

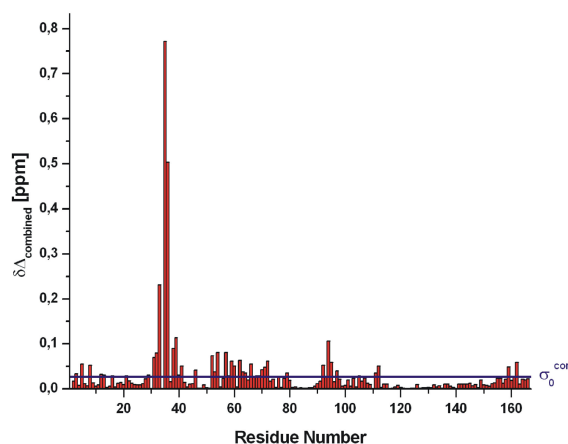


Figure 4.47: Chemical shift differences observed between the $[\text{}^1\text{H}, \text{}^{15}\text{N}]$ -TROSY-HSQC spectra of the Ras mutants T35S and T35A complexed to Mg^{2+} -GppNHp. Data have been obtained from experiments under identical conditions. (M. Spörner, University of Regensburg). The samples contained 0.75 mM Ras(T35S)· Mg^{2+} -GppNHp and 0.7 mM Ras(T35A)· Mg^{2+} -GppNHp in 20 mM NaP_i pH 5.5, 10 mM MgCl_2 , 2 mM DTE, 0.2 mM DSS and 5% D_2O . All spectra have been recorded at 293 K. The corrected standard deviation to zero (σ_0^{corr}) is given by the blue line.

Table 4.16: Residues exhibiting a significant difference in the combined chemical shifts between the $[\text{}^1\text{H}, \text{}^{15}\text{N}]$ -HSQC spectra of the Ras mutants T35A and T35S complexed to Mg^{2+} -GppNHp. The mutated residue is given in bold letters.

$$\Delta\delta_{\text{comb}} > \sigma_0^{\text{corr}}$$

3, 5, 8, 12, 13, 16, 21, 29, 32, 33, **35**, 36, 38, 39, 40, 41, 46, 52, 53, 54, 57, 58, 59, 60, 62, 63, 64, 66, 68, 69, 70, 71, 72, 76, 79, 92, 93, 94, 95, 97, 105, 111, 112, 159, 161, 162

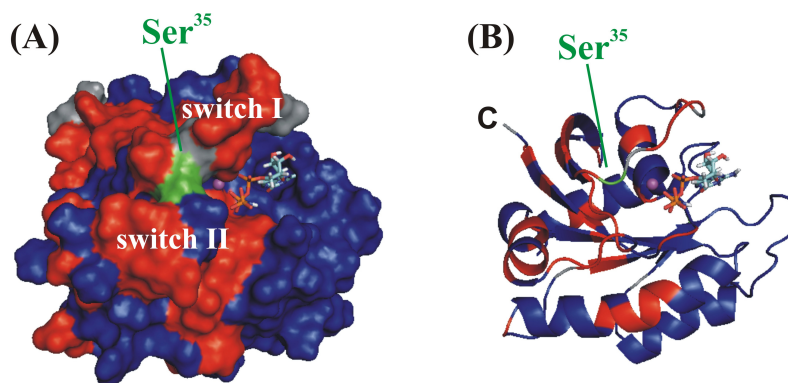


Figure 4.48: Residues showing significant combined chemical changes in the $[^1\text{H}, ^{15}\text{N}]$ -HSQC-spectra of Ras(T35A) and Ras(T35S) complexed to Mg^{2+} -GppNHp. Residues exhibiting a combined chemical shift difference $\Delta\delta_{\text{comb}}$ larger than the standard deviation to zero are shown in red. Ser³⁵ is shown in green. Prolines and not assigned residues are shown in gray.

4.8 High Pressure NMR Spectroscopic Investigations on Ras(wt)·Mg²⁺·GppNHp

As described in section 1.1.5.3 under high pressure the dynamic equilibrium in wild type Ras·Mg²⁺·GppNHp is shifted from the strong effector-binding substate (2) towards conformational state (1), which is recognized by GEFs (Kalbitzer et al. 2009). The functional cycle of Ras as described in section 1.1.1 requires the coexistence of more than the two conformational substates (1) and (2), which are sensed by ³¹P NMR spectroscopy by different chemical shifts for the α - and γ -phosphate group (Geyer et al. 1996, Spoerner et al. 2004 2005a 2007). The GAP-binding conformation has not been detected so far and additionally local unfolding states and the completely unfolded state have not been investigated. In order to obtain information about the different conformational substates coexisting in the Ras protein in solution at atomic resolution, the pressure effect was followed using $[^1\text{H}, ^{15}\text{N}]$ -HSQC spectroscopy. For a better comparison the 2D experiments have first been carried out at the same experimental conditions with regard to the ³¹P pressure series, i.e. at a pH value of 7.4 and a temperature of 278 K. Additionally a pressure series at 303 K was recorded. Due to the poor signal to noise ratio achieved in the pressure series at 278 K mainly the experimental data from the pressure series recorded at 303 K have been used for evaluation. $[^1\text{H}, ^{15}\text{N}]$ -HSQC spectra have been recorded at 0.3 MPa and up to 200 MPa and 180 MPa, respectively. The pressure series recorded at 303 K was only performed up to a pressure of 180 MPa due to the “explosion” of the ceramic cell at a pressure of 200 MPa. The results are given in the following paragraphs.

4.8.1 Pressure Dependence of the Chemical Shifts

Increasing pressure results in chemical shift changes of all resonances at both temperatures. The observed shift directions are qualitatively the same at both temperatures. Figure 4.49 shows the overlay of the $[^1\text{H}, ^{15}\text{N}]$ -HSQC spectra of Ras(wt)·Mg²⁺·GppNHp under different pressures at both temperatures.

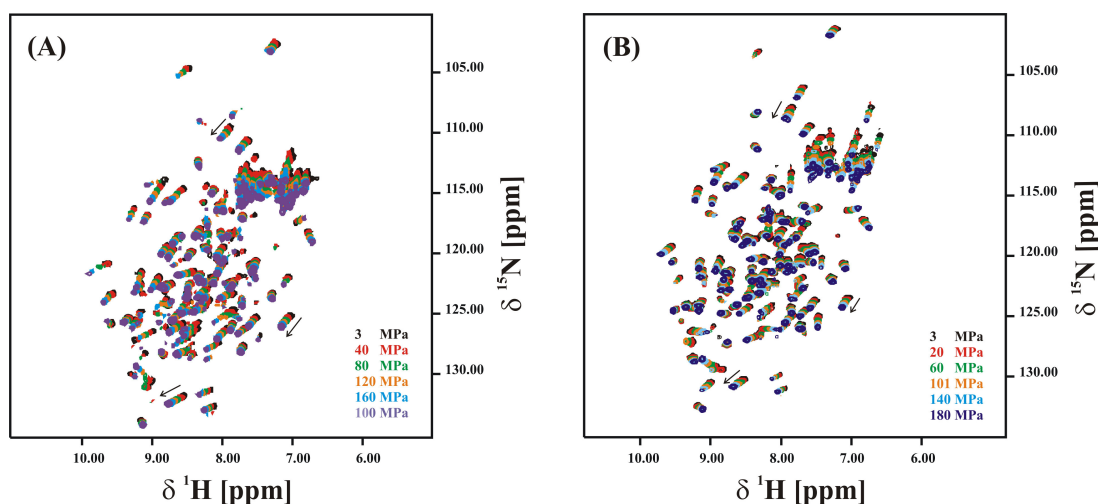


Figure 4.49: Pressure dependent shifts in Ras(wt)·Mg²⁺·GppNHp: (A) Overlay of the $[^1\text{H}, ^{15}\text{N}]$ -HSQC spectra of 1.05 mM Ras(wt)·Mg²⁺·GppNHp in 40 mM Tris/HCl pH 7.4, 10 mM MgCl₂, 2 mM DTE, 0.1 mM DSS and 12% D₂O recorded at 278 K under different pressures between 3 and 200 MPa. (B) Overlay of the $[^1\text{H}, ^{15}\text{N}]$ -HSQC spectra of 1.84 mM Ras(wt)·Mg²⁺·GppNHp in 40 mM Tris/HCl pH 7.4, 10 mM MgCl₂, 2 mM DTE and 12% D₂O recorded at 303 K under increasing pressures of 3 MPa and 180 MPa. The direction of chemical shift with increasing pressure is indicated by the arrows. All spectra have been recorded at 800 MHz proton frequency.

In general the chemical shift changes induced by the local and global conformational changes are a non-linear function of the pressure. The chemical shift changes induced by pressure can be described by a 2nd order Taylor expansion according to Equation 3.4 (see section 3.3.4.3). The pressure effects are composed of two contributions, an unspecific effect, which is also observed in random coil peptides and a specific effect, characteristic for a certain protein. Consequently the chemical shifts of the amide protons were corrected by the known pressure response of random-coil peptides (Arnold et al. 2002) and fitted according to Equation 3.4. Unfortunately the corresponding information for the correction of the nitrogen shifts in random-coil peptides is missing, but work is currently going on at the department. The first order conformation dependent pressure coefficients $|B_1^*(\text{H}^{\text{N}})|$ and $|B_1(\text{N})|$ determined for the single residues in wild type Ras complexed to Mg²⁺·GppNHp at 303 K are depicted in Figure 4.50 as a function of the sequence position. Figure 4.51 shows the second order coefficients $|B_2^*(\text{H}^{\text{N}})|$ and $|B_2(\text{N})|$, respectively.

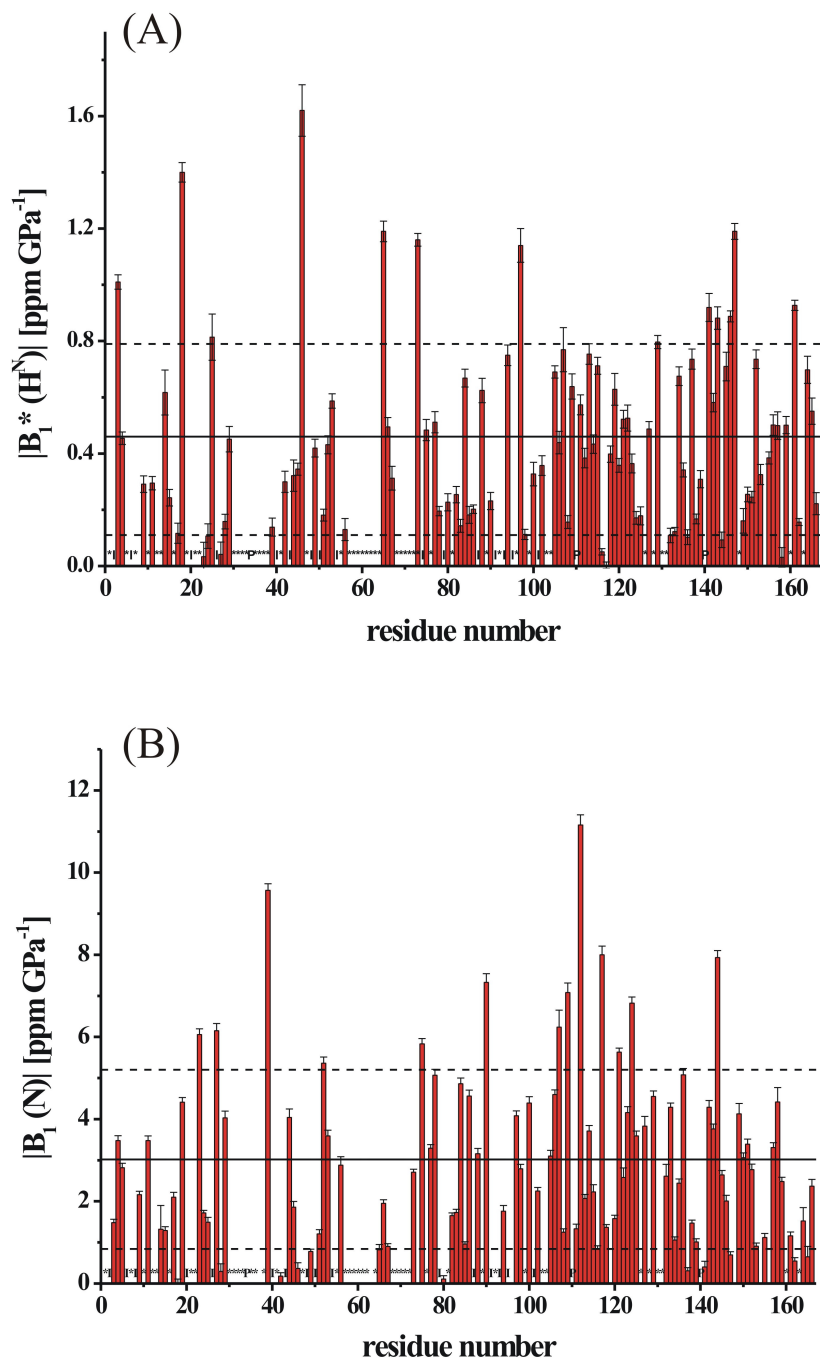


Figure 4.50: First order pressure coefficients of wild type Ras-Mg²⁺-GppNHp derived from a pressure series at 303 K. Shown are the absolute values of the first order pressure coefficients of H^N (corrected by the standard values derived from model peptides) (A) and N (B) as a function of the primary sequence. The mean value (straight line) and the mean value plus /minus the standard deviation (dashed lines) are shown. Prolines are marked with P, not assigned or not assignable residues, respectively with * and residues, for which the coefficients could not be determined due the loss of signal intensity within the pressure series are marked with I.

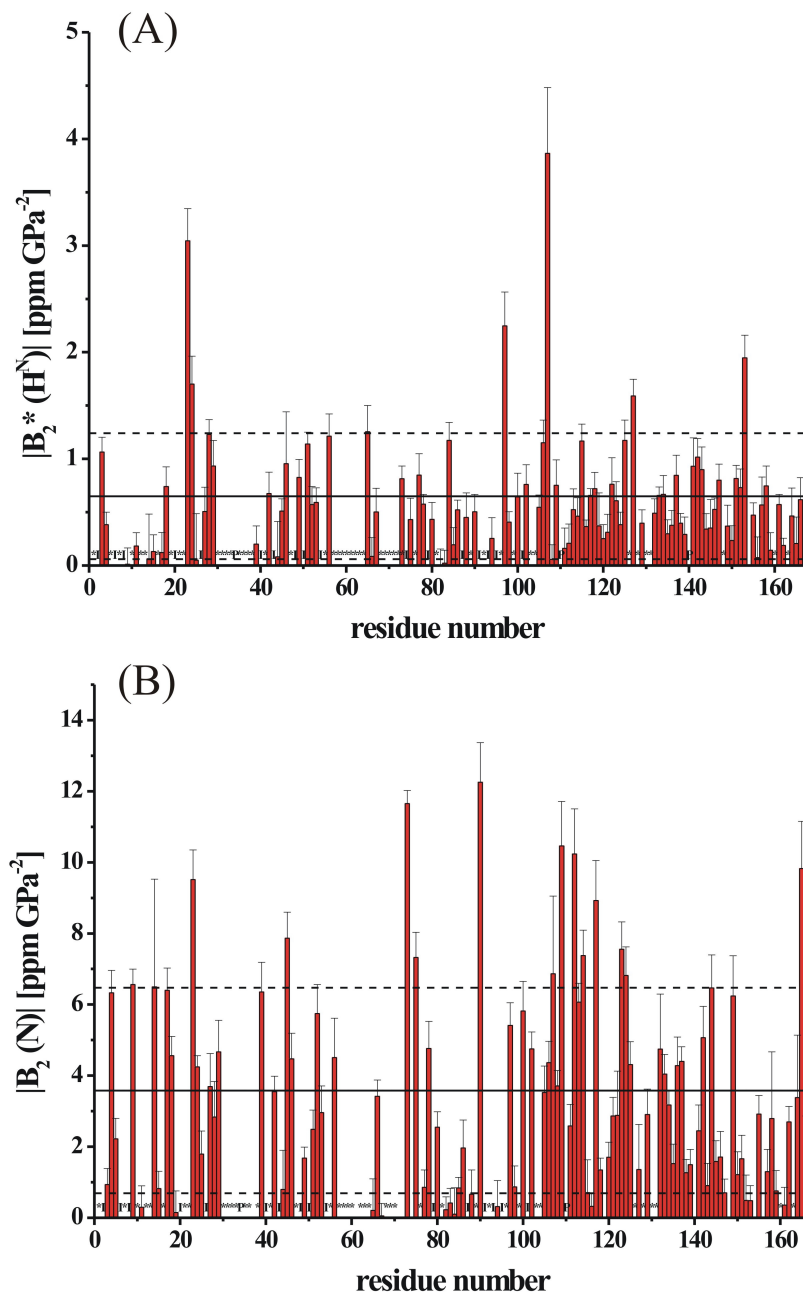


Figure 4.51: Second order pressure coefficients of wild type Ras·Mg²⁺·GppNHp derived from a pressure series at 303 K. Shown are the absolute values of the second order pressure coefficients of H^N (corrected by the standard values derived from model peptides) (A) and N (B) as a function of the primary sequence. The mean value (straight line) and the mean value plus / minus the standard deviation (dashed lines) are shown. Prolines are marked with P, not assigned or not assignable residues, respectively with * and residues, for which the coefficients could not be determined due the loss of signal intensity within the pressure series are marked with I.

From the pressure series recorded at 278 K the derived mean first order and second order pressure coefficients are 0.45 ppm/GPa ($|B_1^*(H^N)|$), 0.46 ppm/GPa² ($|B_2^*(H^N)|$), 3.50 ppm/GPa ($|B_1(N)|$) and 3.42 ppm/GPa² ($|B_2(N)|$), respectively. At a temperature of 303 K the mean first order and second order pressure coefficients are 0.50 ppm/GPa ($|B_1^*(H^N)|$), 0.65 ppm/GPa² ($|B_2^*(H^N)|$), 3.02 ppm/GPa ($|B_1(N)|$) and 3.58 ppm/GPa² ($|B_2(N)|$), respectively. These data agree very well and are summarized in Table 4.16.

Table 4.16: Mean absolute values of the first and second order pressure coefficients for the chemical shifts determined according to equation 3.4 in Ras(wt)·Mg²⁺·GppNHp from a pressure series recorded at 278 K and 303 K, respectively.

	$ B_1^*(H^N) $ [ppm /GPa]	$ B_1(N) $ [ppm /GPa]	$ B_2^*(H^N) $ [ppm /GPa ²]	$ B_2(N) $ [ppm /GPa ²]
278 K	0.45 ± 0.25	3.50 ± 1.96	0.50 ± 0.42	3.42 ± 2.70
303 K	0.46 ± 0.33	3.02 ± 2.18	0.65 ± 0.59	3.58 ± 2.89

The pressure-dependent chemical shift changes observed in wild type Ras·Mg²⁺·GppNHp are of different magnitude within the single residues. Since chemical shift changes reflect local changes in the environment of a given residue they strongly correlate with structural rearrangements. Hence residues with pressure coefficients significantly larger than the mean value are likely to sense a conformational change happening under increased pressure. In Table 4.17 those residues, for which pressure coefficients between the mean value and the mean value plus the standard deviation or even larger than the mean value plus the standard deviation have been determined are listed. Within these residues a lot participate in the binding of the nucleotide in the active centre, such as Lys¹¹⁷, Ser¹¹⁸, Asp¹¹⁹ from the KKXD-motif or residues Ala¹⁴⁶ and Lys¹⁴⁷, which are part of the SAK-motif and residues in their close proximity. The same is true for residues like Val¹⁴ and Ala¹⁸, which are located within or close to the PM1 motif or P loop, which is involved in the binding of the β- and γ-phosphate group of the bound nucleotide (Pai et al. 1990). Although most of the residues belonging to the both switch regions in Ras do not give cross peaks signals in the [¹H, ¹⁵N]-HSQC-spectrum of Ras(wt)·Mg²⁺·GppNHp (Ito et al. 1997) residues in their close proximity exhibit large pressure coefficients, such as Ala⁶⁶, Gly⁷⁵ and Gly⁷⁷, respectively. Additionally residues Asp¹⁰⁵, Asp¹⁰⁷, Val¹⁰⁹ and Met¹¹¹ building the negatively charged loop L7 show high pressure sensitivities and also residues at the N- and C-terminal part of the protein like Glu³, Arg¹⁶⁴ and Gln¹⁶⁵. Figure 4.52 gives a graphical view of the residues exhibiting large pressure coefficients around the active centre of Ras.

Table 4.17: Residues in Ras(wt)·Mg²⁺·GppNHp exhibiting significant large pressure coefficients determined from the pressure series performed at 303 K.

$ B_1^* (H^N) $		$ B_2^* (H^N) $	
Group 1^a	Glu ³ , Ala ¹⁸ , Gln ²⁵ , Ile ⁴⁶ , Ser ⁶⁵ , Arg ⁷³ , Arg ⁹⁷ , Gln ¹²⁹ , Tyr ¹⁴¹ , Glu ¹⁴³ , Ala ¹⁴⁶ , Lys ¹⁴⁷ , Arg ¹⁶¹		Glu ³ , Ala ¹⁸ , Leu ²³ , Ile ²⁴ , Ser ⁶⁵ , Arg ⁹⁷ , Asp ¹⁰⁷ , Ser ¹²⁷ , Glu ¹⁵³
	Val ¹⁴ , Leu ⁵³ , Ala ⁶⁶ , Gly ⁷⁵ , Gly ⁷⁷ , Ile ⁸⁴ , Asp ¹⁰⁵ , Asp ¹⁰⁷ , Val ¹⁰⁹ , Met ¹¹¹ , Leu ¹¹³ , Gly ¹¹⁵ , Asp ¹¹⁹ , Ala ¹²¹ , Ala ¹²² , Ser ¹²⁷ , Ala ¹³⁴ , Tyr ¹³⁷ , Ile ¹⁴² , Ser ¹⁴⁵ , Val ¹⁵² , Phe ¹⁵⁶ , Tyr ¹⁵⁷ , Leu ¹⁵⁹ , Arg ¹⁶⁴ , Gln ¹⁶⁵		Phe ²⁸ , Val ²⁹ , Lys ⁴² , Ile ⁴⁶ , Glu ⁴⁹ , Cys ⁵¹ , Asp ⁵⁶ , Arg ⁷³ , Gly ⁷⁷ , Ile ⁸⁴ , Asn ⁸⁵ , Arg ¹⁰² , Ser ¹⁰⁶ , Val ¹⁰⁹ , Gly ¹¹⁵ , Lys ¹¹⁷ , Ser ¹¹⁸ , Ala ¹²² , Val ¹²⁵ , Leu ¹³³ , Ala ¹³⁴ , Tyr ¹³⁷ , Tyr ¹⁴¹ , Ile ¹⁴² , Glu ¹⁴³ , Lys ¹⁴⁷ , Gly ¹⁵¹ , Val ¹⁵² , Thr ¹⁵⁸
$ B_1 (N) $		$ B_2 (N) $	
Group 1^a	Leu ²³ , His ²⁷ , Ser ³⁹ , Leu ⁵² , Gly ⁷⁵ , Phe ⁹⁰ , Asp ¹⁰⁷ , Val ¹⁰⁹ , Val ¹¹² , Lys ¹¹⁷ , Ala ¹²¹ , Thr ¹²⁴ , Thr ¹⁴⁴		Val ⁹ , Val ¹⁴ , Leu ²³ , Val ⁴⁵ , Arg ⁷³ , Gly ⁷⁵ , Phe ⁹⁰ , Asp ¹⁰⁷ , Val ¹⁰⁹ , Val ¹¹² , Val ¹¹⁴ , Lys ¹¹⁷ , Arg ¹²³ , Thr ¹²⁴ , Gln ¹⁶⁵
	Tyr ⁴ , Ala ¹¹ , Leu ¹⁹ , Val ²⁹ , Val ⁴⁴ , Leu ⁵³ , Gly ⁷⁷ , Phe ⁷⁸ , Ile ⁸⁴ , Asn ⁸⁶ , Lys ⁸⁸ , Arg ⁹⁷ , Ile ¹⁰⁰ , Asp ¹⁰⁵ , Ser ¹⁰⁶ , Val ¹¹⁴ , Arg ¹²³ , Val ¹²⁵ , Ser ¹²⁷ , Gln ¹²⁹ , Leu ¹³³ , Ser ¹³⁶ , Ile ¹⁴² , Glu ¹⁴³ , Arg ¹⁴⁹ , Gln ¹⁵⁰ , Gly ¹⁵¹ , Tyr ¹⁵⁷ , Thr ¹⁵⁸		Tyr ⁴ , Ser ¹⁷ , Ala ¹⁸ , Ile ²⁴ , His ²⁷ , Val ²⁹ , Ser ³⁹ , Ile ⁴⁶ , Asp ⁵⁶ , Phe ⁷⁸ , Arg ⁹⁷ , Ile ¹⁰⁰ , Arg ¹⁰² , Ser ¹⁰⁶ , Asp ¹⁰⁸ , Leu ¹¹³ , Val ¹²⁵ , Asp ¹³² , Leu ¹³³ , Ser ¹³⁶ , Tyr ¹³⁷ , Ile ¹⁴² , Thr ¹⁴⁴ , Arg ¹⁴⁹

^a residues exhibiting a pressure coefficient larger than the mean value plus the standard deviation.^b residues exhibiting a pressure coefficient in between the mean value and the mean value plus the standard deviation.

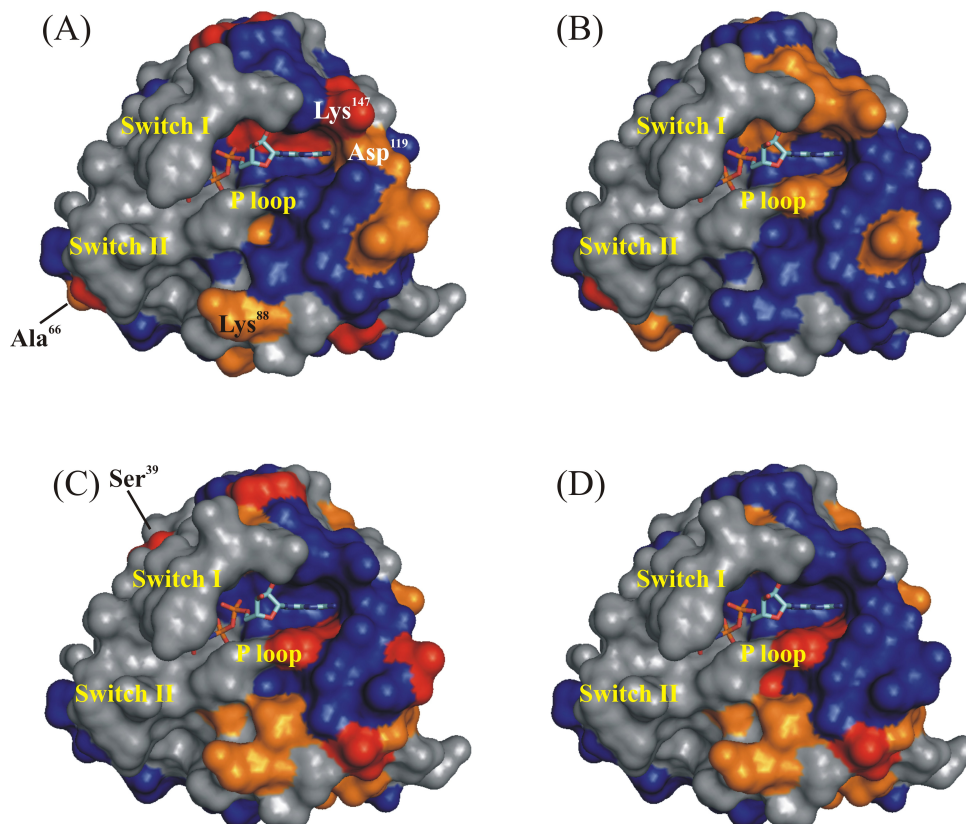


Figure 4.52: Pressure-sensitive residues in Ras(wt)·Mg²⁺·GppNHp. Residues exhibiting significant large first and second order pressure coefficients for the amide protons (A, B) and amide nitrogen atoms (C, D) mapped onto the surface of the crystal structure of Ras(wt)·Mg²⁺·GppNHp (Pai et al. 1990, pdb 5p21). Residues with a value for the pressure coefficient from group 1 (as defined in Table 4.16) and group 2 are colored red and orange, respectively. Amino acids, which are not assigned in the [¹H, ¹⁵N]-HSQC-spectrum of Ras(wt)·Mg²⁺·GppNHp or could not be followed within the pressure series are shown in gray. The other parts of the protein are colored blue.

4.8.2 Pressure Response of the Chemical Shifts and Related Gibbs Free Energies

For some of the residues a strong non-linear pressure dependence of the chemical shift together with an asymptotic behaviour can be observed. This is typical for a two-state transition in fast exchange on the NMR time scale. In this model, at ambient pressure either one main conformational state N1 exists, which is shifted towards conformation N2 with increasing pressure. Likewise the two conformational states N1 and N2 coexist at ambient pressure and one certain conformation is preferred at higher pressures. Both types can be differentiated by the shape of the curve obtained by plotting the chemical shift against the applied pressure. The molar free energy (ΔG^0) for this local transition can be derived from the chemical shift change by Equation 3.9. As already stated above, prior to

the calculation of the Gibbs free energies ΔG^0 the observed pressure-induced chemical shift was corrected according to random coil standard peptides (Arnold et al. 2002). Since this is only possible for the proton shifts, the pressure dependence of the nitrogen chemical shifts have not been evaluated. Figure 4.53 gives an example for residues exhibiting pressure dependent shift changes characteristic for a two-state model at both temperatures.

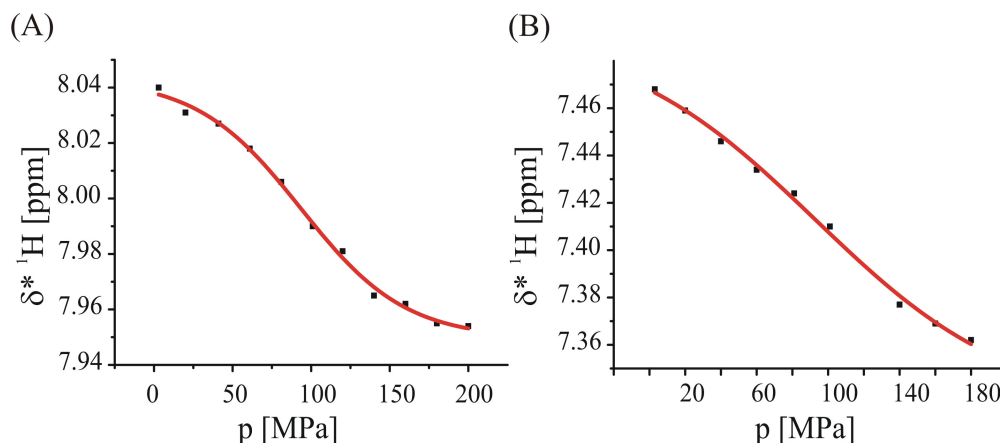


Figure 4.53: Pressure dependent chemical shift changes observed in Ras(wt)·Mg²⁺·GppNHp. Given are the corrected proton chemical shifts δ^*H of Gly¹¹⁵ observed at 278 K (A) and Val¹⁴ observed at 303 K (B) as a function of pressure. The fits of the data according to Equation 3.9 are represented by the red line.

Concerning the transition from conformational substate (2) into substate (1) as investigated by ³¹P NMR spectroscopy two facts are known. First, at ambient pressure both conformations are already populated with an equilibrium constant K_{12} of 1.9 for Ras(wt)·Mg²⁺·GppNHp (Geyer et al. 1996, Spoerner et al. 2001). Secondly the ³¹P NMR pressure series on Ras(wt)·Mg²⁺·GppNHp showed that at a pressure of 200 MPa the equilibrium is not completely shifted towards the weak effector-binding state. Hence the detection of this transition via the chemical shifts is quite cumbersome since the expected curve does neither have a plateau at ambient pressure nor at 200 or 180 MPa, respectively. However molar free energy ΔG^0 for this transition of 1.48 kJ mol⁻¹ (Spoerner et al. 2005a) and the difference in the molar volume $\Delta V^0 = 17.2$ mL mol⁻¹ derived from the ³¹P NMR pressure series (Kalbitzer et al. 2009) might allow for the identification of residues participating in this transition. Consequently the pressure response of the chemical shift has been fitted according to Equation 3.9 with a constant value for ΔG^0 of 1.48 kJ mol⁻¹. As soon as the obtained fit gives a difference in the specific volume ΔV^0 in agreement with the one obtained from the ³¹P NMR experiments within the range of error the corresponding residues is likely to sense the transition from the strong effector-binding state (2) to the weak effector-binding state (1). Doing so amino acid residues Asn²⁶, Tyr⁹⁶, Gly¹³⁸ and Ile¹³⁹ (278 K) and Val⁹, Val¹⁴, Gln²⁵ and Ala⁶⁶ (T = 303 K) could be identified to take part in the described process, which is subsequently defined by the transition from

conformation C(1) to conformation C(2). The obtained values for ΔV^0 are given in Table 4.18.

Table 4.18: Residues giving a value for ΔV^0 in agreement with the one obtained from the ^{31}P NMR pressure series by fitting the pressure response of their chemical shifts according to Equation 3.9 with a value for ΔG^0 of 1.48 kJ mol^{-1} (Spoerner et al 2005a).

278 K		303 K	
Residue	$\Delta V^0 [\text{mL mol}^{-1}]$	Residue	$\Delta V^0 [\text{mL mol}^{-1}]$
Asn ²⁶	-17.0 ± 4.0	Val ⁹	-18.1 ± 7.2
Tyr ⁹⁶	-14.9 ± 2.7	Val ¹⁴	-18.6 ± 8.8
Gly ¹³⁸	-18.0 ± 6.4	Gln ²⁵	-19.2 ± 6.4
Ile ¹³⁹	-17.4 ± 3.1	Ala ⁶⁶	-19.0 ± 7.2
		His ⁹⁴	-19.4 ± 4.2

Figure 4.54 shows the residues with fast exchange processes describing a two-state transition under increasing pressure for both temperatures, which have not been identified to sense the transition from C(1) to C(2). Fitting these data simultaneously according to Equation 3.9 one derives a molar free energy ΔG^0 for this transition, of $3.9 \pm 0.8 \text{ kJ mol}^{-1}$ from the data obtained at 278 K. The difference in the specific volume between the two conformations is $-37 \pm 8 \text{ mL mol}^{-1}$.

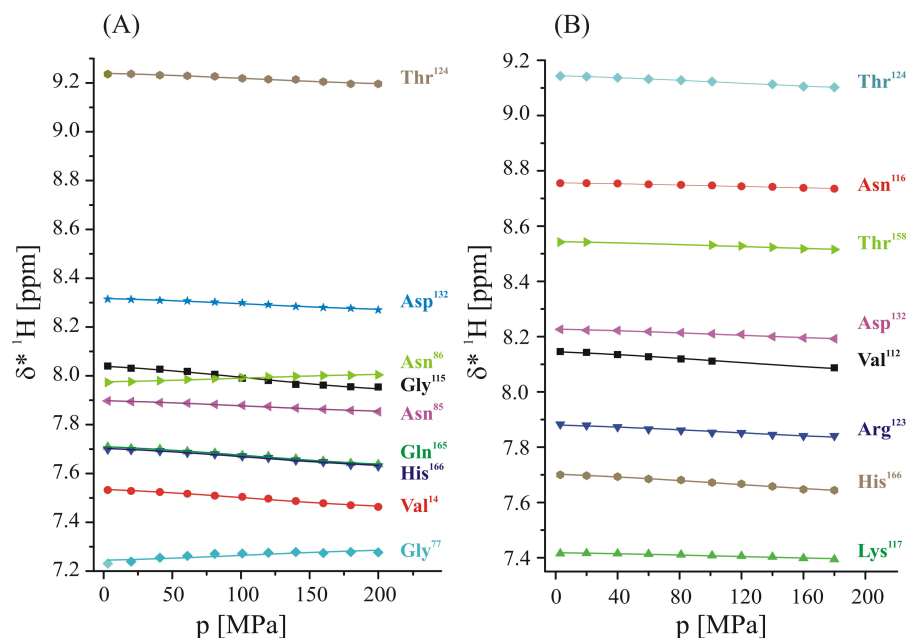


Figure 4.54: Residues exhibiting a chemical shift dependence on pressure typical for a two-state transition with a fast exchange regime on the NMR time scale. Residues from the pressure series recorded at 278 K (A) and 303 K (B) have been fitted according to Equation 3.9. The corresponding results are given in Table 4.18.

The data obtained from the pressure series at 303 K give a molar free energy ΔG^0 for the transition of 3.9 ± 0.8 kJ mol⁻¹. The difference in the specific volume between the two conformations is -35 ± 10 mL mol⁻¹. This transition will subsequently be defined as the transition from C(1) to C(3). The results derived from the pressure series at the two different temperatures agree very well and are summarized in Table 4.19.

Table 4.19: Molar free energies and specific volumes determined from the pressure-response of the chemical shifts describing a two-state model in the fast exchange regime according to Equation 3.9.

	ΔG^0 [kJ mol ⁻¹]	ΔV^0 [mL mol ⁻¹]
278 K	3.9 ± 0.8	-37 ± 8
303 K	3.9 ± 0.8	-35 ± 10
mean	3.9 ± 0.8	-36 ± 9

Additionally some of the peaks, namely Leu¹⁹, Val⁴⁵, Ser⁸⁹, Lys¹¹⁷, Val¹²⁵ and Ala¹³⁰ (278 K) and Cys⁵¹, Val¹²⁵, Leu¹³³ and Glu¹⁵³ (303 K) exhibit a pressure dependence regarding their chemical shift, which cannot sufficiently be described by a simple two-state model. An example is given by Lys¹¹⁷ and Cys⁵¹ in Figure 4.55. These residues obviously sense two different transitions with increasing pressure and by taking a closer look at the corresponding plot it becomes clear that neither at ambient pressure nor at the end of the pressure series one main conformation is present.

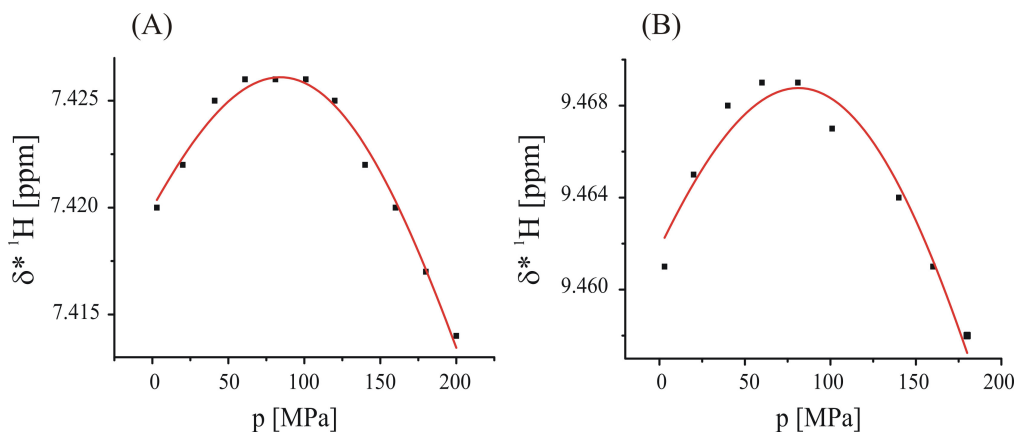


Figure 4.55: Pressure dependent chemical shift changes indicating more than one conformational transition in Ras(wt)·Mg²⁺·GppNHp. Given are the corrected proton chemical shifts $\delta^* \text{H}$ for Lys¹¹⁷ observed at 278 K (A) and Cys⁵¹ obtained at 303 K (B) as a function of the pressure. The data have been fitted according to Equation 3.9 with $n = 3$. The data known for the transition from conformational state (2) to state (1) (Spoerner et al. 2005a, Kalbitzer et al. 2009) have been taken as values for one of the processes described. The data obtained from the fit described above (see Table 4.17) have been taken as values for the second process sensed.

Consequently it is likely that again one of the transitions sensed by these residues might be the one from the strong effector-binding substate (2) to the weak effector-binding substate (1), i.e. from C(1) to C(2) and other one equals the transition from C(1) to C(3) identified above with a molar free energy of 3.9 kJ mol^{-1} and a mean change in specific volume of -36 mL mol^{-1} . In order to proof that assumption the data have evaluated in two different ways either by using ΔG_{12}^0 , ΔV_{12}^0 , ΔG_{13}^0 and ΔV_{13}^0 free fit parameter or by fixing the values for ΔG_{12}^0 , ΔV_{12}^0 , ΔG_{13}^0 and ΔV_{13}^0 with the ones obtained from the ^{31}P NMR pressure series and the results from the analysis of the pressure-dependent chemical shift changes from the transition from C(1) to C(3) (see Table 4.18). Only the latter method enabled a sufficient fit of the residues sensing two transitions. Examples are given Figure 4.55.

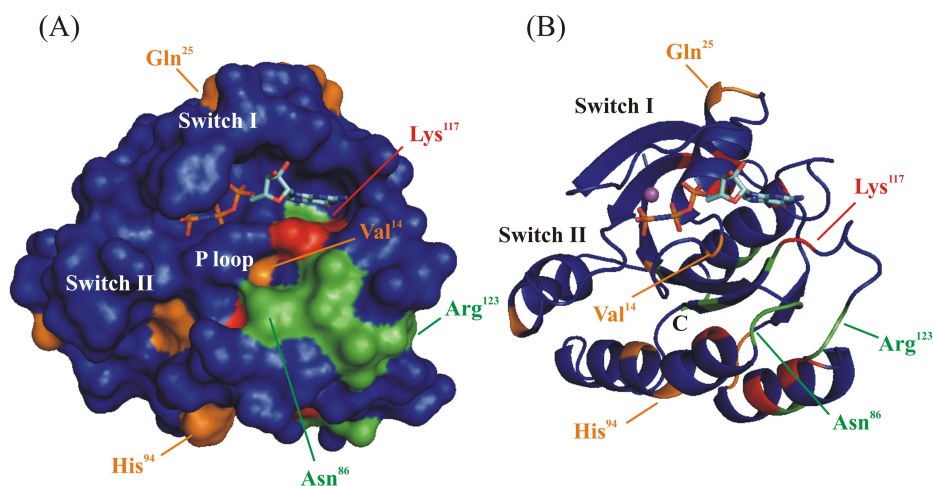


Figure 4.56: Residues participating in two different transitions in Ras(wt)·Mg²⁺·GppNHp derived from analysis of the chemical shifts at 278 K and 303 K. Surface (A) and ribbon plot (B) of the crystal structure of Ras(wt)·Mg²⁺·GppNHp (Pai et al. 1990, pdb 5p21). Residues participating in transition C(1)→C(2) in Ras(wt)·Mg²⁺·GppNHp are colored orange, residues taking part in transition C(1)→C(3) are shown in green. Residues sensing both transitions are colored red. The results shown here graphically are summarized in Table 4.18.

The results obtained from the evaluation of the pressure response of the chemical shifts at both temperatures are summarized in Table 4.20. In Figure 4.56 the residues participating in the two different transitions are mapped onto the surface of the crystal structure of Ras(wt)·Mg²⁺·GppNHp (Pai et al. 1990).

Table 4.20: Conformational transitions observed in Ras(wt)·Mg²⁺·GppNHp by analysis of the pressure-dependent chemical shift changes.

transition	C(1) → C(2)	C(1) → C(3)
ΔG^0 [kJ mol ⁻¹]	1.48 ^a	3.9 ± 0.8
ΔV^0 [mL mol ⁻¹]	-18.0 ± 1.4	-36 ± 9
residues involved	Val ⁹ , Val ¹⁴ , Gln ²⁵ , Asn ²⁶ , Ala ⁶⁶ , His ⁹⁴ , Tyr ⁹⁶ , Gly ¹³⁸ , Ile ¹³⁹	Gly ⁷⁷ , Asn ⁸⁵ , Asn ⁸⁶ , Val ¹¹² , Gly ¹¹⁵ , Asn ¹¹⁶ , Arg ¹²³ , Thr ¹²⁴ , Asp ¹³² , Gln ¹⁶⁵ , His ¹⁶⁶
	Leu ¹⁹ , Val ⁴⁵ , Cys ⁵¹ , Ser ⁸⁹ , Lys ¹¹⁷ , Val ¹²⁵ , Ala ¹³⁰ , Leu ¹³³ , Glu ¹⁵³	

^a data taken from Spoerner et al. (2005a)

4.8.3 Pressure Response of the Signal Intensities and Related Gibbs Free Energies

Another possible pressure response is a change in signal intensity caused by exchange processes. Increasing pressure leads to a compression of the sample and thus to an increase of the effective protein concentration observable within the active volume in the probe head. Consequently the observed intensities are higher and have to be corrected before evaluating their pressure response. The pressure dependent increase of the peak integral of the buffer signal of Tris has been used for the determination of an internal correction factor. In Figure 4.57 the relative peak area of the signal is shown as a function of the pressure.

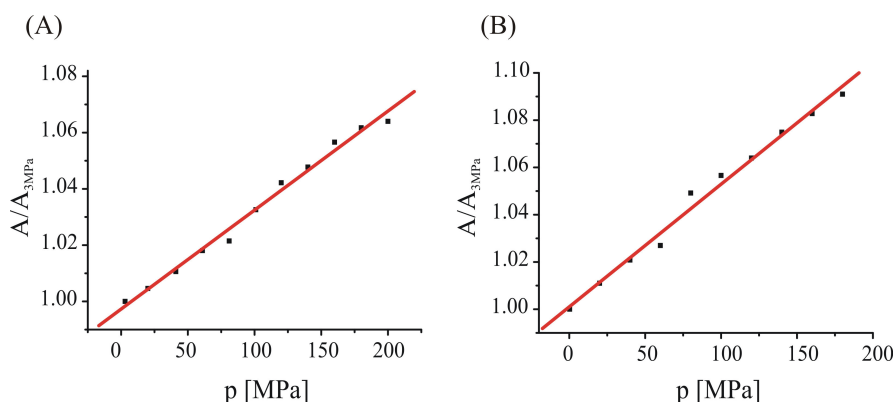


Figure 4.57: Pressure dependent peak area of the signal for Tris buffer at 278 K (A) and 303 K (B). The linear fits according to Equation 3.10 (red line) give the parameters for the correction of the signal intensities in the corresponding [¹H, ¹⁵N]-HSQC-spectra. The isothermal compressibility of the sample can be derived to be 0.35 ± 0.01 GPa⁻¹ and 0.51 ± 0.02 GPa⁻¹ at 278 K and 303 K, respectively.

Linear regression according to Equation 3.10 of the data allows for the correction of the signal intensities in the corresponding $[^1\text{H}, ^{15}\text{N}]$ -HSQC spectra following Equation 3.11. In order to obtain reliable results additionally long time experiments have been carried out at 3 MPa and 200 MPa at the end of the pressure series at 278 K. Due to the explosion of the ceramic cell at a pressure of 200 MPa long term experiments are missing for the pressure series recorded at 303 K. At 278 K almost each residue shows a change in signal intensity with increasing pressure, which is either a loss or an increase as shown schematically in Figure 4.58. New peaks can be observed in the $[^1\text{H}, ^{15}\text{N}]$ -HSQC spectrum of Ras(wt)·Mg²⁺·GppNHp at 200 MPa in the case of the long time experiment recorded at 278 K. Comparison with the $[^1\text{H}, ^{15}\text{N}]$ -HSQC spectrum of Ras(T35A)·Mg²⁺·GppNHp, which gives cross peaks signals for each amino acid in the protein (except prolines) allows for the assignment of these residues to represent Gly¹⁰, Gly¹² and Gly¹³, which are all part of the phosphate binding loop. An example is given in Figure 4.59. Unfortunately these peaks are not observed in the pressure series recorded with 8 scans per increment due to the poor signal to noise ratio and thus quantification is not possible.

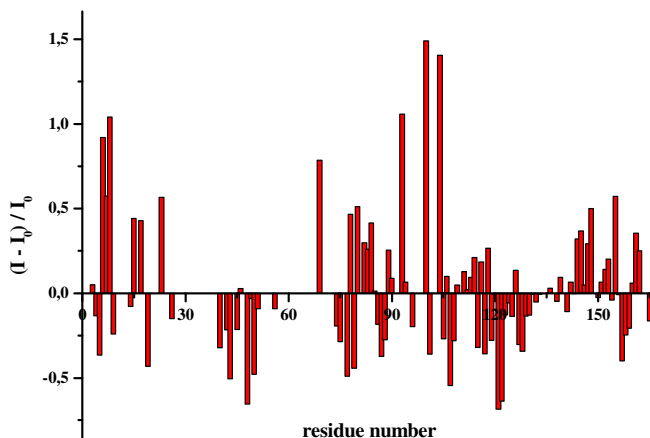


Figure 4.58: Observed changes in signal intensity at high pressure in Ras(wt)·Mg²⁺·GppNHp at 278 K. Shown is the change of the signal intensities observed in the $[^1\text{H}, ^{15}\text{N}]$ -HSQC spectrum of 1.05 mM ^{15}N Ras(wt)·Mg²⁺·GppNHp in 40 mM Tris/HCl pH 7.4, 10 mM MgCl₂, 2 mM DTE, 0.1 mM DSS and 12% D₂O at 200 MPa relative to the reference spectrum recorded at 3 MPa as a function of the residue position. Both spectra have been recorded at 278 K at 800 MHz proton frequency. The change of the concentration of Ras in the active probe volume caused by the compression of the sample was corrected using the signal of Tris as an internal standard (see section 3.3.4.4).

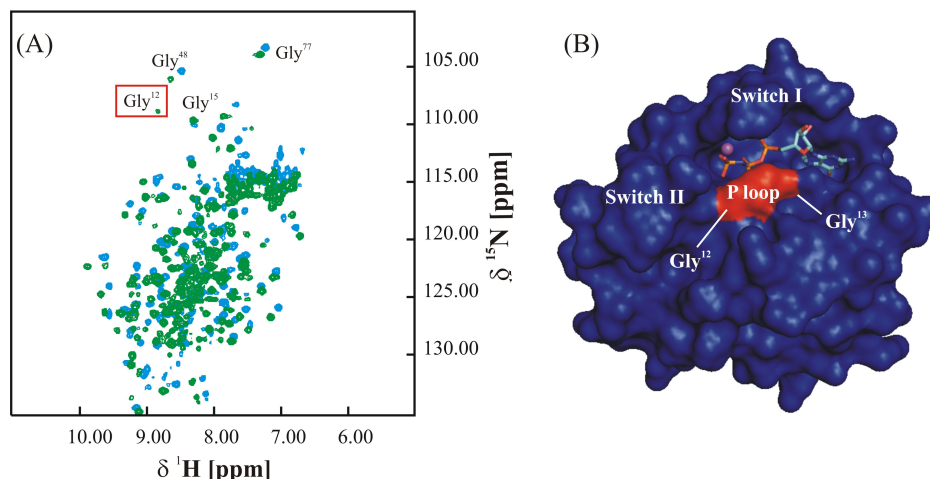


Figure 4.59: New cross peak signals observed in Ras(wt)·Mg²⁺·GppNHp at 278 K at high pressure.

(A) Overlay of the [¹H, ¹⁵N]-HSQC spectra of 1.05 mM Ras(wt)·GppNHp in 40 mM Tris/HCl pH 7.4, 10 mM MgCl₂, 2 mM DTE, 0.1 mM DSS and 12% D₂O recorded at 3 MPa (blue) and 200 MPa (green), respectively. The experiments have been performed at 278 K at 800 MHz proton frequency with 32 scans per increment. (B) New cross peaks for Gly¹² and Gly¹³ observed at 200 MPa mapped onto the surface of the crystal structure of Ras(wt)·Mg²⁺·GppNHp (Pai et al. 1990, pdb 5p21).

Comparing the cross peak intensities between 3 MPa and 180 MPa from the pressure series recorded at 303 K gives a different picture. The only observed effect is a loss in signal intensity. As already stated above it was not possible to record a spectrum at higher pressures than 180 MPa at 303 K for technical reasons. Additionally long time experiments are missing. Due to signal overlap within the pressure series not each assigned residue can be evaluated according its pressure-dependent signal intensity. A plot of the intensity against the applied pressure gives three different types of curves, which are depicted in Figure 4.60.

- 1) At ambient pressure one certain conformation of the protein is sensed by the residue, which loses population with increasing pressure. The conformation favoured at higher pressures is not completely stabilized at a pressure of 180 MPa (Figure 4.60 (A)).
- 2) Two conformations are already present at ambient pressure with favour of one certain conformational state (Figure 4.60 (B)).
- 3) At ambient pressure an equilibrium between two conformations is sensed by the residue. In contrary to the case described in 2) the favour for a certain conformational state is not the case and the conformation preferred at higher pressures becomes almost completely stabilized at 180 MPa (Figure 4.60 (C)).

The residues have been subgrouped according to the examples given in Figure 4.59. In order to ensure that the observed effects are caused by slow exchange processes additionally the pressure-response of the line widths of these residues have been evaluated. In the fast exchange regime with $|\omega_2 - \omega_1| \ll 1/\tau_{ex}$ the cross peak volumes should not be dependent on the relative populations of the two states. However, when the exchange

correlation time gets larger additional line broadening proportional to $N_1 N_2 (\omega_2 - \omega_1)^2$ occurs. This leads to a possible loss of intensity during the INEPT polarization transfer, and when only peak amplitudes A not volumes are measured to a more pronounced decrease in A . A maximum additional line broadening is expected for $N_1 = N_2 = 0.5$, i.e. when both conformations involved in the transition are equally populated. In addition, pressure may modify the exchange correlation times themselves and thus also the exchange line broadening. An increase in $1/\tau_{\text{ex}}$ leads in the fast exchange regime to a decrease of line broadening, in the slow exchange regime to an increase of line broadening.

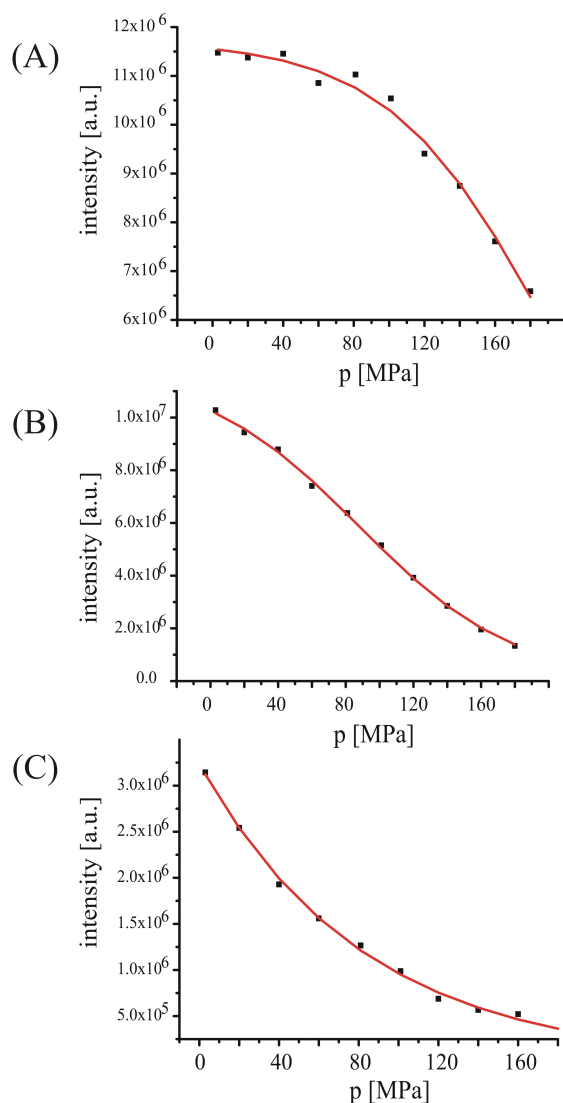


Figure 4.60: Pressure response of the signal intensities observed in Ras(wt)·Mg²⁺·GppNHp at 303 K for leucine⁵³ (A), alanine¹⁸ (B) and threonine²⁰ (C). The data have been fitted according to Equation 3.13. The corresponding fits are given by the red lines. The change of the concentration of Ras in the active probe volume caused by the compression of the sample was corrected using the signal of Tris as an internal standard (see section 3.3.4.4).

Group A covers the largest number of residues. Concerning residues assigned to this group a significant change in the line widths of ^1H or ^{15}N , respectively cannot be observed. The maximum increase of the line width is 16% for ^1H and 15% for ^{15}N with a mean value for the relative line widths $\text{LB}/\text{LB}_{\text{Ref}}$ of 0.89 ± 0.14 for ^1H and 0.99 ± 0.11 for ^{15}N . Consequently the loss in signal intensity reflects a loss in signal volume and thus a reduced population of the conformation sensed by these residues at ambient pressure. Thus the pressure response of the signal intensities of these residues can be fitted by Equation 3.13 assuming a two-state transition in the slow exchange regime. Figure 4.61 shows the distribution of the values for ΔG^0 and ΔV^0 obtained from the corresponding fits. As one can see very nicely amino acids belonging to group A describe one certain process with a molar free energy of $\Delta G^0 = 8.6 \pm 1.8 \text{ kJ mol}^{-1}$ and a change in the specific volumes ΔV^0 between the two conformations of $-43.7 \pm 8.4 \text{ mL mol}^{-1}$.

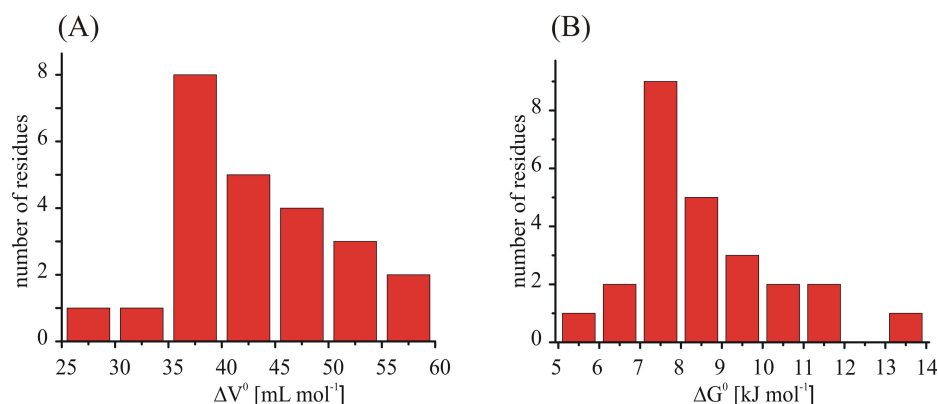


Figure 4.61: Distribution of the molar free energies ΔG^0 and the changes in the specific volumes ΔV^0 determined by Equation 3.13 from the pressure response of residues assigned to group A.

For the residues assigned to group B at higher pressures the loss of intensity or volume is almost 100% and thus the determination of the line widths is afflicted with higher errors. Consequently the line widths of the signals obtained at 80 MPa have been evaluated. At this pressure the loss in signal intensity for these residues is about 50%. If this was caused by strong line broadening effects this should also be observed at 80 MPa. A mean value for the relative line widths $\text{LB}/\text{LB}_{\text{Ref}}$ of 1.05 ± 0.15 for ^1H and 0.97 ± 0.06 for ^{15}N is observed. As described above for the residues assigned to group A this again reveals a two state transition in the slow exchange regime. Five residues have been found exhibiting a pressure response according their signal intensity as shown in Figure 4.60 (B). They have been fitted simultaneously by Equation 3.13 (Figure 4.62). For the process sensed by these residues a value of $4.4 \pm 0.6 \text{ kJ mol}^{-1}$ for ΔG^0 and of $-48.4 \pm 3.3 \text{ mL mol}^{-1}$ for ΔV^0 has been determined.

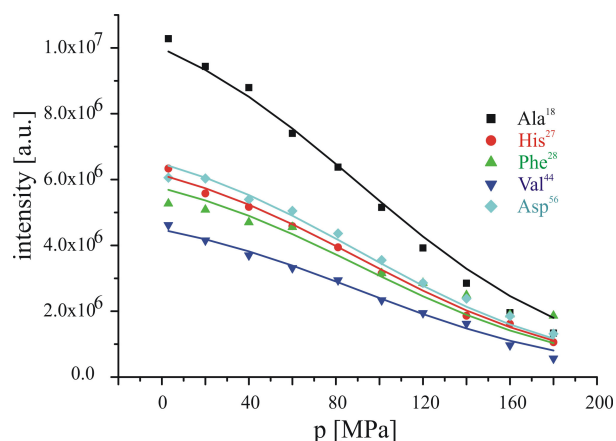


Figure 4.62: Residues in Ras(wt)·Mg²⁺·GppNHp exhibiting a pressure-dependence of their signal intensities as described for group B. The data have been fitted simultaneously according to Equation 3.13 giving a value for ΔG^0 of $4.4 \pm 0.6 \text{ kJ mol}^{-1}$ and for ΔV^0 of $-48.4 \pm 3.3 \text{ mL mol}^{-1}$ for the sensed transition.

Group C covers nine amino acids. Due to the poor signal to noise ratio for these residues neither the signal volume nor the line width can be determined automatically with sufficient accuracy. The line width might be constant over the pressure range studied and thus the data can be fitted by Equation 3.13 just like it was done with the data derived from the residues assigned to group A and B, respectively. Likewise the volume of the peak might be constant and the lines get broadened due to fast exchange. In the latter case quantification with Equation 3.13 is not possible. However for completeness the data have been fitted simultaneously by Equation 3.13 (Figure 4.63) deriving a value of $-28.9 \pm 2.4 \text{ mL mol}^{-1}$ for ΔV^0 .

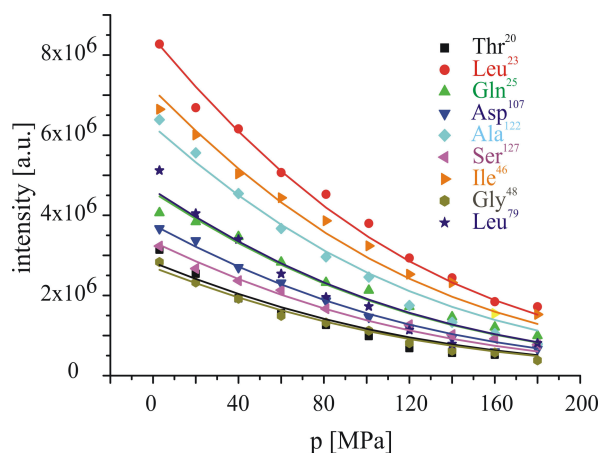


Figure 4.63: Residues in Ras(wt)·Mg²⁺·GppNHp exhibiting a pressure-dependence of their signal intensities as described for group B. The data have been fitted simultaneously according to Equation 3.13 giving a value for ΔV^0 of $-28.9 \pm 2.4 \text{ mL mol}^{-1}$ for the sensed transition. Due to the shape of the curves ΔG^0 could not be determined with sufficient accuracy.

A quantification of ΔG^0 was not possible with the data available. Also the determination of the peak volume was not possible with enough accuracy.

Comparing the results obtained from both analyses the values obtained for ΔG^0 and ΔV^0 obtained from analysis of the pressure response of the signal intensity from residues assigned to group B agree within the range of error with the transition from conformation C(1) to C(3) obtained from the analysis of the chemical shifts.

Table 4.21 gives a summary about the single transitions determined in Ras(wt)·Mg²⁺·GppNHp and the residues involved.

Table 4.21 Conformational transitions and corresponding molar free energies ΔG^0 and molar volumes ΔV^0 in Ras(wt)·Mg²⁺·GppNHp determined by analysis of pressure NMR series performed at 278 K and 303 K.

	ΔG^0 [kJ mol ⁻¹]	ΔV^0 [mL mol ⁻¹]	residues involved ^a
C(1) → C(2) ^c	1.48 ^b	-18.0 ± 1.4	Val ⁹ , Val ¹⁴ , Leu¹⁹ , Gln ²⁵ , Asn ²⁶ , Val⁴⁵ , Cys⁵¹ , Ala ⁶⁶ , Ser⁸⁹ , His ⁹⁴ , Tyr ⁹⁶ , Lys¹¹⁷ , Val¹²⁵ , Ala¹³⁰ , Leu¹³³ , Gly ¹³⁸ , Ile ¹³⁹ , Glu¹⁵³
C(1) → C(3) ^c	3.9 ± 0.8	-36.0 ± 9.0	Leu¹⁹ , Val⁴⁵ , Cys⁵¹ , Gly ⁷⁷ , Asn ⁸⁵ , Asn ⁸⁶ , Ser⁸⁹ , Val ¹¹² , Gly ¹¹⁵ , Asn ¹¹⁶ , Lys¹¹⁷ , Arg ¹²³ , Thr ¹²⁴ , Val¹²⁵ , Ala¹³⁰ , Asp ¹³² , Leu¹³³ , Glu¹⁵³ , Gln ¹⁶⁵ , His ¹⁶⁶
C(1) → C(3) ^d	4.4 ± 0.6	-48.4 ± 3.3	Ala ¹⁸ , His ²⁷ , Phe ²⁸ , Val ⁴⁴ , Asp ⁵⁶
C(1) → C(4) ^d	8.6 ± 1.8	-43.7 ± 8.4	Glu ³ , Gly ¹⁵ , Lys ¹⁷ , Ser ³⁹ , Lys ⁴² , Val ⁴⁵ , Glu ⁴⁹ , Leu ⁵³ , Gly ⁷⁷ , Phe ⁸² , Ile ⁸⁴ , Asn ⁸⁵ , Met ¹¹¹ , Leu ¹²⁰ , Ala ¹³⁰ , Leu ¹³³ , Ala ¹³⁴ , Arg ¹³⁵ , Ser ¹³⁶ , Gly ¹³⁸ , Tyr ¹⁴¹ , Glu ¹⁴³ , Ala ¹⁴⁶ , Lys ¹⁴⁷ , Arg ¹⁶¹

^a residues sensing two transitions are given in bold letters.

^b taken from Spoerner et al. (2005a)

^c determined by analysis of the pressure-dependent chemical shift changes according to Equation 3.9

^d determined by analysis of the pressure-dependent changes in signal intensity according to Equation 3.13

5 DISCUSSION

5.1 Saturation Transfer Difference Spectroscopy

Ras is a quite interesting target in medicinal chemistry due to its involvement in the development of about 30% of all human tumors (Barbacid 1987). Several approaches are followed for the inhibition of its signaling (see e.g. Wittinghofer 2000). A novel promising strategy is the stabilization of a conformational substate in active Ras with decreased effector affinity. The small organic compound Zn^{2+} -cyclen is capable of doing so (Spoerner et al. 2005c) and to date no other substance has been reported. A structure of the binding site of Zn^{2+} -cyclen in the partial loss-of-function mutant Ras(T35A) in its active GppNHp-bound conformation is available (Rosnizeck et al., accepted). This can be taken as basis for the structure-based virtual screening at our department following two approaches: first, the *de novo* design for compounds binding at the same position as does the Zn^{2+} -cyclen and secondly, the screening for fragments binding in a defined distance to the active centre. Potential hits derived from the screening will subsequently be investigated using NMR-based screening for their actual binding activity. Both binding positions shall further be linked in order to give high affinity ligands.

A diverse array of methods is reported for the detection of ligand binding via NMR (see e.g. Peng et al. 2004, Pellechia et al. 2008). Within the ligand-based methods, INPHARMA (Sánchez-Pedregal et al. 2005) for example utilizes protein-mediated interligand NOEs for the identification of compounds competing for the identical binding pocket in the protein. This would represent an interesting approach for the detection of ligands binding at the same position as does Zn^{2+} -cyclen. However, small fragments are also screened for binding in a defined distance to the binding site of Zn^{2+} -cyclen. Additionally it was shown that Zn^{2+} -cyclen binds at two distinct positions in Ras (Rosnizeck et al., accepted) and hence the obtained results will not exclusively reflect the competition for the desired position at the active centre. In the WaterLOGSY method magnetization is transferred from bulk water (Dalvit et al. 2000 2002, Shimotakahara et al. 2005) within the protein-ligand surface. Irradiation is either realized by the direct saturation of the water resonances or by inverting the water resonance signal using for example the NOE-ePHOGSY scheme (Bertini et al. 1997). The overlap of the water resonance with for example H^α protons can lead to cumulative effects limiting the selectivity of the method. Additionally signals from binding and non-binding compounds, which have different signs in the resulting spectrum, can cancel each other out. In general the method is recommended for targets exhibiting a low proton density and systems with the ligand or receptor being strongly hydrated, e. g. RNA-ligand complexes (Peng et al. 2004). For the screening of potential Ras ligands in this work saturation transfer difference spectroscopy (Mayer and Meyer 1999) was the method of choice. It is adequate for the identification of ligands with affinities ranging from 10^{-3} and 10^{-8} M.

Additionally competitive experiments also allow for the identification of compounds binding at a desired position for which a ligand is already known (Jahnke et al. 2002). Moreover STD NMR is capable for the characterization of the binding epitope of the ligand molecule (Mayer and Meyer 2001, Peikert et al. 2004). The latter feature can be utilized for the further optimization of the identified Ras ligands, which has already been reported for sugar-derived Ras ligands (Peri et al. 2005, Airoidi et al. 2007). Such information is in principle also provided by the WaterLOGSY method (Dalvit et al. 2000 2002, Shimotakahara et al. 2005), but primary reflects the water contact surface of the ligand and not its interaction pattern with the target molecule. STD NMR can in principle be combined with any NMR pulse sequence (Vogtherr and Peters 2000, Nagaraja 2006). One of the major advantages of STD NMR spectroscopy are the smaller amount of protein needed, which is very low with 0.1 nmol compared to 25 nmol in WaterLOGSY or inverse NOE pumping and of course compared to receptor-based methods like SAR by NMR or diffusion editing, which require 25 nmol and 100 nmol, respectively (Meyer and Peters 2003). In general receptor-based methods are usually limited by the size of the macromolecule. This is not the case in STD NMR spectroscopy since the saturation is even more efficient for large proteins and even membrane-bound or immobilized proteins have been successfully investigated (Klein et al. 1999, Meinecke and Meyer 2001).

As described in section 1.2.2.2 the STD experiment consists of a reference spectrum and an on-resonance spectrum, which ensures the selective irradiation of the protein signals. Binding ligands appear with decreased intensity in the on-resonance spectrum. A $T_{1\rho}$ -filter was implemented in the pulse sequence (Mayer and Meyer 2001). With the use of this spinlock relaxation filter the protein proton resonances are filtered out from the spectrum, which eases the evaluation of the difference spectra due to less overlap of protein signals with potential ligand signals. In this work different on-resonance irradiation frequencies have been tested and used. During the experiments with the different on-resonance irradiation frequencies it became apparent that the reference standard DSS present in the sample binds to Ras(T35A)·Mg²⁺·GppNHp. When irradiating at -2 ppm the signal of the nine methyl protons of DSS at 0 ppm show up in the difference spectrum only when Ras is present in the sample. It has been reported that the compound does bind to hydrophobic cavities in proteins (Laurents et al. 2005). DSS might also tend to aggregate and is for that reason directly saturated when irradiating at -2 ppm. In the active centre of the Ras protein a lot of charges are present due to the strong polar interactions between the active centre and the nucleotide (Pai et al. 1990). Thus it is less probable that DSS competes against the ligands used within this work and would thus falsify the obtained results. Even if this would be case it will still be possible to detect appropriate ligands since they are present in a much higher excess than DSS. In each NMR experiment carried out with Ras at the department DSS is used as internal reference and hence this substance was further used in the STD experiments allowing for better comparison. However, before starting new screening experiments one might consider to use a reference standard, which has been tested according to its potential binding to Ras before. An example can be given by

dioxane (Wishart et al. 1995). Alternatively the water signal can be used for referencing the spectra as reported for the STD experiments carried out by Peikert et al. (2004).

STD spectroscopy has been successfully applied for the identification of the Ras ligand Zn^{2+} -BPA in this work by irradiating at 0.3 ppm, which is in a distance of more than 3.3 ppm from the closest BPA-resonance and guaranteed the selective irradiation of the protein resonances over the ligand resonances. The signals of the compound appear in the corresponding difference spectrum only upon addition of Ras. Peri et al. (2005) and Airoldi et al. (2007) selectively saturated Ras·GDP by irradiating in the aliphatic region around 1 ppm in their studies on inhibitors for the nucleotide exchange reaction mediated by GEFs. The identification of Zn^{2+} -BPA by STD NMR does not give any information about the binding position in the protein. If one is interested, whether the compound does bind towards the protein at the same site as another known ligand, competition experiments can be carried out (Jahnke et al. 2002). This was not done in this case, since Zn^{2+} -cyclen binds to more than one position in active Ras (Roznizeck et al., accepted). Whenever it is possible to displace Zn^{2+} -cyclen from Ras in STD NMR one will not obtain explicit information according the binding position. Dissociation constants were determined using the so-called STD amplification factor introduced by Mayer and Meyer (1999) giving a K_D -value of 9.65 mM and 2.07 mM for Zn^{2+} -cyclen and Zn^{2+} -BPA, respectively.

Bivalent Ras ligands have been investigated according their binding activity towards Ras(T35A)· Mg^{2+} ·GppNHp. These ligands carry a peptide moiety and thus the on-irradiation frequency was set to -2 ppm in order to avoid direct saturation of the ligand and thus wrong positive results. Preliminary experiments with Ras(T35A)· Mg^{2+} ·GppNHp in the absence and presence of the known Ras ligand Zn^{2+} -cyclen proofed the efficacy and selectivity of the method when irradiating at -2 ppm. This frequency is also recommended for primary NMR screening with a large number of potential ligands covering a large spectral window.

The above described experiments and results show that Ras can be successfully applied for the identification of binding ligands using STD NMR spectroscopy. In future screening experiments with potential ligands the on-resonance irradiation frequency can be set to -2 ppm, which will be sufficient for the detection of ligands giving signals in the common spectral window. However, it is suggested to perform a negative control with a sample without the protein being present in order to avoid false positive results, since some compounds might tend to aggregate and can thus also be saturated directly since their spectral window can be widened due to line broadening effects caused by an increased molecular mass upon aggregation. Additionally it was shown that the reference standard DSS does bind to Ras. One should be aware that this might influence the results obtained in the screening as soon as the potential ligands competes with DSS for the same binding position.

5.2 Modulation of the Conformational Equilibrium in Active Ras by Metal(II)-Chelates

^{31}P NMR spectroscopy reveals the existence of at least two distinct conformational states in active wild type Ras, which are in dynamic equilibrium (Geyer et al. 1996, Spoerner et al. 2001). The equilibrium constant strongly depends on the nature of the bound nucleotide and mutations in the protein (Spoerner et al. 2004 2005a 2007). One of these states, namely state (1) shows drastically reduced affinity towards effector molecules (Spoerner et al. 2001) and hence its stabilization by suitable ligands represents a promising approach in the disruption of aberrant Ras signalling. To date one compound, Zn^{2+} -cyclen has been reported to selectively bind to this weak-effector binding state and thus shifts the dynamic equilibrium completely to state (1) (Spoerner et al. 2005c). Using STD NMR spectroscopy Zn^{2+} -BPA has been identified as a ligand for active Ras in this work. ^{31}P NMR titration studies clearly reveal that this compound also selectively recognizes the weak effector-binding conformation in active Ras. In doing so no significant chemical shift changes can be observed for the phosphorus resonances of the bound nucleotide in $\text{Ras}(\text{wt})\cdot\text{Mg}^{2+}\cdot\text{GppNHp}$, which is the case in the corresponding experiment with Zn^{2+} -cyclen. In the latter titration each signal shifts by more than 1 ppm (Spoerner et al. 2005c). At increasing concentrations of Zn^{2+} -BPA the protein starts to precipitate and resonances of $\text{Mg}^{2+}\cdot\text{GppNHp}$ show up in the respective ^{31}P NMR spectrum accompanied by an upfield shift for the β -phosphate group of the free nucleotide. The latter observation is likely to be caused by the complex formation between Zn^{2+} -BPA and the free nucleotide. A comparable shift response is observed in the titration of free $\text{Mg}^{2+}\cdot\text{GppNHp}$ with Zn^{2+} -BPA. In principle different explanations can be given for the precipitation of Ras and the resulting appearance of signals representing free $\text{Mg}^{2+}\cdot\text{GppNHp}$ in the ^{31}P NMR spectra. Zn^{2+} -BPA might pull the nucleotide out of its active site in the protein by directly binding to the latter. Likewise the compound could also stabilize the Ras protein in a conformation, which weakens nucleotide binding and thus facilitates the dissociation of $\text{Mg}^{2+}\cdot\text{GppNHp}$ from the active site in Ras. Additionally impurities in the stock solution of Zn^{2+} -BPA such as free ZnCl_2 left from the complexation of BPA with Zn^{2+} might cause protein denaturation and consequently the observed release of free nucleotide. It is not likely that the nucleotide is pulled out of its binding position in the active centre of Ras. The ^{31}P NMR titration of $\text{Mg}^{2+}\cdot\text{GppNHp}$ with Zn^{2+} -BPA indicates only a weak complex formation with an affinity in the millimolar range, whereas the protein binds the nucleotide very tightly with picomolar affinity (John et al. 1990). A possible participation of impurities like ZnCl_2 in the precipitation of Ras can be excluded. The corresponding ^{31}P NMR titrations of $\text{Ras}(\text{T35A})\cdot\text{Mg}^{2+}\cdot\text{GppNHp}$ with ZnCl_2 show that concentrations as high as 6.5 mM of ZnCl_2 are tolerated. At this concentration neither significant chemical shift changes of the resonances of the bound nucleotide nor the appearance of signals representing free $\text{Mg}^{2+}\cdot\text{GppNHp}$ can be observed (M. Spoerner, personal communication). The most probable mechanism leading to the above described effects in the ^{31}P NMR

spectra of Ras(wt)·Mg²⁺·GppNHp the presence of Zn²⁺-BPA can be given by the stabilization of the weak effector-binding conformational state (1) by the compound, which does not proceed via a direct coordination of the bound nucleotide in state (1) as it is the case for Zn²⁺-cyclen. This assumption is supported by the fact that no significant shift changes can be observed for the single phosphorus resonances of the bound nucleotide, while the relative peak areas of the signals representing the single phosphorus resonances clearly reveal an increase of the population of state (1) in the presence of Zn²⁺-BPA. It is known that the dissociation of the nucleotide is enhanced in conformational state (1) of active Ras (Spoerner et al. 2001). The same observation can be made when Ras(wt)·Mg²⁺·GppNHp is titrated with the chaotropic compound GdmCl in an unfolding experiment: the dynamic equilibrium is shifted towards the weak effector-binding state (1) accompanied by the denaturation of the protein and the observation of resonances representing Mg²⁺·GppNHp in the corresponding ³¹P NMR spectra (Kalbitzer et al. 2009).

A good explanation for the different effects of Zn²⁺-cyclen and Zn²⁺-BPA observed in the ³¹P NMR experiments can be derived when looking at their binding positions in the partial loss-of-function mutant Ras(T35A)·Mg²⁺·GppNHp. Both compounds bind at two distinct positions in the protein, which can be deduced from [¹H, ¹⁵N]-HSQC titrations with both a paramagnetic and a diamagnetic derivative of the metal(II)-complexes. One of the binding positions is identical for both compounds. It centres between the negatively charged loop L7 and the C-terminal end of Ras. The driving force for this interaction is assumable a strong ionic attraction between the central metal ion of the complexes and the negatively charged amino acids within loop L7 (Asp¹⁰⁵, Asp¹⁰⁷ and Asp¹⁰⁸). This binding position was also identified in crystals of the complex between Ras(wt)·Mg²⁺·GppNHp and Zn²⁺-cyclen (Rosnizeck et al. accepted). The second binding position accountable for the stabilization of conformational state (1) differs for Zn²⁺-cyclen and Zn²⁺-BPA. Zn²⁺-cyclen binds in close proximity of the γ-phosphate group of the bound nucleotide, which is so to say sandwiched between the protein and the compound. This binding position is only accessible for Ras in conformational state (1) probably for steric reasons. In Ras proteins, which predominantly exist in conformation (1) from the spectroscopic view like the Mg²⁺·GppNHp-complexes of the Ras mutants G60A (Ford et al. 2005), T35S (F. Schumann, unpublished results) and M-Ras (Ye et al. 2005) the switch I region adopts a more opened conformation similar to the one of nucleotide-free Ras in complex with its exchange factor SOS (Boriack-Sjodin et al. 1998).

In contrary, the second binding position of Zn²⁺-BPA is located at the PM3 motif of Ras with residues 53 to 58 giving the strongest response in the titration with Cu²⁺-BPA, thus revealing the closest proximity of this region to the paramagnetic metal centre. This binding position of Zn²⁺-BPA is composed of several hydrophobic amino acids like Leu⁵³ and Ile⁵⁵, which can interact with the aromatic rings of BPA. Additionally negative charges are present (Asp⁵⁶ and Asp⁵⁷) possibly interacting with the central metal ion of the chelate complex. The compound approaches the nucleotide binding site from the opposite direction compared to metal(II)-cyclen. The nucleotide is not sandwiched between its

binding pocket in the active Ras and the compound, which is the case, when looking at the calculated HADDOCK structure for the binding site of metal(II)-cyclen (Rosnizeck et al., accepted). In the corresponding titration with Zn^{2+} -BPA large chemical shift changes are observed within switch I indicating structural rearrangements in this region. Obviously metal(II)-BPA stabilizes conformational state (1) by fixing the switch I region in its more opened conformation, which results in a weakened binding of the nucleotide. Additionally residues, which take part in the coordination of the nucleotide in active Ras are strongly affected in the presence of both metal(II)-BPAs, e.g. Phe²⁸ and Lys¹⁴⁷ which form strong stabilizing interactions with the guanine base of the bound nucleotide in active wild type Ras (Wittinghofer and Waldmann 2000). Phe²⁸ also drastically changes its position in complex with SOS easing the exchange of the nucleotide (Boriack-Sjodin et al. 1998). Measuring the dissociation rate of the nucleotide in the presence of Zn^{2+} -BPA might be an appropriate approach to study the influence of the compound on the affinity of Ras towards the nucleotide. Additionally the determination of the distance of the Cu^{2+} -ion to the phosphorus nuclei by measuring the T_1 relaxation in the presence of Cu^{2+} -BPA might provide further information about the binding position of the compound.

These discriminative binding positions close to the active centre of Ras(T35A)· Mg^{2+} ·GppNHp also explain very nicely the different effects of Zn^{2+} -cyclen and Zn^{2+} -BPA, respectively on the dynamic equilibrium of the oncogenic Ras mutant G12V complexed to Mg^{2+} ·GppNHp. In the latter mutant the dynamic equilibrium is slightly shifted towards the weak binding conformation with a K_{12} value of 0.9 compared to 1.9 for the wild type protein (Spoerner et al 2005a). Consequently one would expect a stronger influence of both compounds on the dynamic equilibrium in the oncogenic mutant. This is indeed the case for Zn^{2+} -BPA. At a molar ratio of Ras: Zn^{2+} -BPA of 1:10 the dynamic equilibrium is almost completely shifted towards the weak effector-binding state ($K_{12} = 0.29$), whereas such a shift is not achieved at the same excess in the wild type protein. The situation is vice versa for Zn^{2+} -cyclen. A 20-fold molar excess is sufficient for a complete shift of the equilibrium towards the weak effector-binding state in the wild type protein (Spoerner et al. 2005c), whereas K_{12} equals 0.4 in the presence of a 32-fold excess of Zn^{2+} -cyclen in the oncogenic mutant. In contrast to the titration with the wild type protein large chemical shift changes are not observed, when Zn^{2+} -cyclen is titrated to Ras(G12V)· Mg^{2+} ·GppNHp indicating a perturbed interaction with the active site of the protein and the nucleotide bound. Additionally the bleaching of the ³¹P NMR resonance of the γ -phosphate group in Ras(G12V)· Mg^{2+} ·GppNHp requires a very high excess of Cu^{2+} -cyclen over the protein of 30-fold compared to 5-fold in Ras(wt)· Mg^{2+} ·GppNHp (T. Graf 2006). The mutation of Gly¹² to Val also influences the ³¹P chemical shifts of the bound nucleotide. The resonance signal of the γ -phosphate group representing state (1) is shifted downfield by 0.23 ppm and the one corresponding to state (2) is shifted highfield by 0.76 ppm compared to the wild type protein. For the β -phosphorus resonance an upfield shift of 0.24 ppm is observed (Spoerner et al. 2005a). This strongly indicates a perturbation

of the chemical environment of the β - and γ -phosphate group both in conformational state (1) and (2), respectively. Comparison of the crystal structure of Ras(G12V)·Mg²⁺·GppNHp and Ras(wt)·Mg²⁺·GppNHp shows that structural differences can be found in the phosphate binding loop around amino acids Gly¹² and Gly¹³ and additionally for residues Gly⁶⁰ and Gln⁶¹, which are slightly pushed away from the nucleotide binding site, whereas the overall topology of the protein is maintained (Krengel et al. 1990). Thus the mainly affected residues correspond for the most part with the residues involved in binding of the metal(II)-cyclen and hence the binding position for the compound in the Ras(G12V)·Mg²⁺·GppNHp might be less attractive to the small compound even though switch I opens up somewhat. In contrast the binding position of metal(II)-BPA is not affected by this mutation and the latter compound can bind without any difficulties.

Both compounds are also capable of stabilizing conformational state (1) in the oncogenic mutant complexed to its physiological nucleotide GTP. The ³¹P NMR spectrum of Ras(wt) complexed to Mg²⁺·GTP shows one peak for each phosphorus signal, which can be assigned to conformational state (2). By ³¹P NMR saturation transfer spectroscopy it could be shown that this state is in equilibrium with a second one assigned to conformational state (1). The latter one is very little populated and thus only sparsely visible (Spoerner et al., unpublished results). The same is true for Ras(G12V)·Mg²⁺·GTP. Upon addition of a high excess of the Zn²⁺-chelates a second set of resonances shows up in the corresponding spectra for the γ - and β -phosphate group, which have been assigned to conformational state (1). The effect is again stronger in the presence of Zn²⁺-BPA probably again for the above described reasons.

Besides the conformational equilibrium between conformational states (1) and (2) as described above a slow conformational exchange between two substates of conformational state (1) is found in the mutants Ras(T35A) and Ras(T35S) in complex with Mg²⁺·GTP γ S (Spoerner et al. 2007). The equilibrium constant K_{1a1b} equals 0.5. Three different coordination spheres are possible for GTP γ S, when complexed to the protein. The sulphur is either not coordinated or by the Mg²⁺-ion and the main chain NH of Thr³⁵ or by the main chain NH of Gly⁶⁰ and Lys¹⁶ (Spoerner et al. 2007). A schematic representation is given in Figure 5.1. The side chain coordination of the Mg²⁺-ion cannot take place, when Thr³⁵ is replaced by alanine. It is suggested that the loss of this coordination is accompanied by a break of the hydrogen bond between the main chain NH of amino acid at position 35 and the γ -phosphate group of the bound nucleotide (Allin et al. 2001). All three coordination spheres are possible for the state (1) mutant Ras(T35A). It is assumed by Spoerner et al. (2007) that arrangement A and B are preferred since the side chain of lysine¹⁶ can coordinate an oxygen in each case. Within both, structure A is preferred since additionally the Mg²⁺-ion is coordinated to an oxygen instead of an sulphur, which is preferred following the hard soft [Lewis] acid base (HSAB) principle (Pearson 1963). For that reason conformational substate (1a), which is populated to a higher extend most probably resembles structure A and in turn substate (1b) is reflected by the coordination

pattern B. Metal(II)-cyclens represent an attractive tool in order to obtain additional insight into the coordination pattern in the active centre since it binds to the γ -phosphate group. Titration studies with both the paramagnetic and the diamagnetic metal(II)-cyclen derivative clearly reveal that substrate (1a) is selectively recognized. This is not surprising since the sulphur atom is available for coordination in structure A, whereas the electron pairs of the non coordinated oxygen of the thiophosphate group in structure B are not available for coordination due their delocalization strongly supporting the proposed interaction pattern assigned to the two substrates by Spoerner et al. (2007).

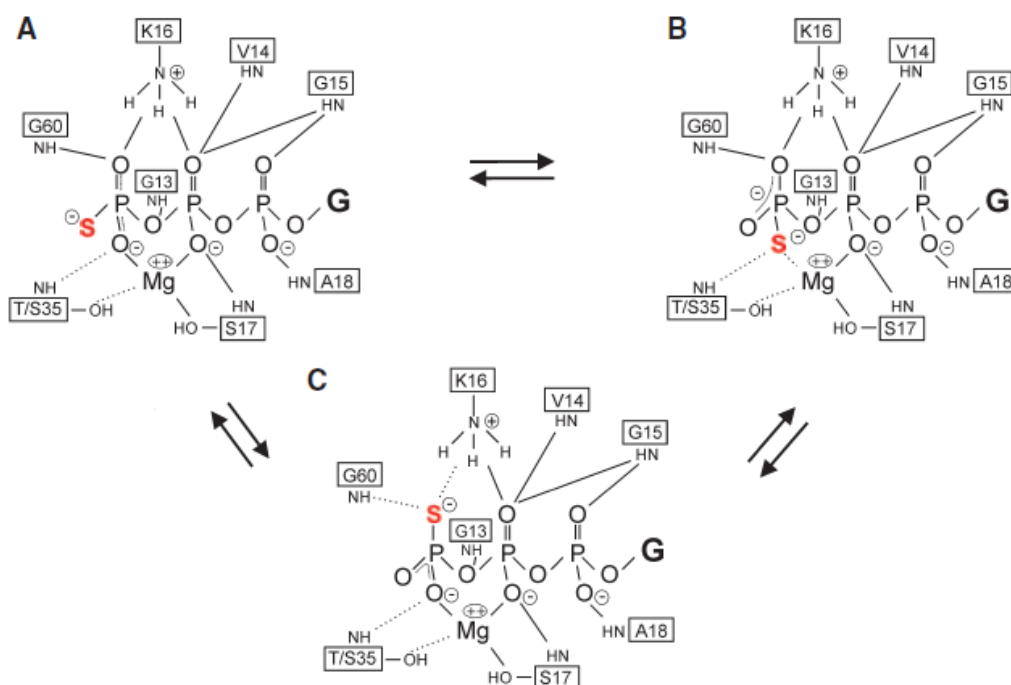


Figure 5.1: Schematic representation of the coordination sphere of the phosphate groups and the thiophosphate of GTP γ S complexed to wild type and mutant Ras. Bonds that probably exists only in state (1) or are weakened or abolished in the thiophosphate group are represented by broken lines (taken from Spoerner et al. 2007).

The present coordination pattern also gives an explanation for the observed stronger effect of Cu²⁺-cyclen compared to Zn²⁺-cyclen, which is observed in the respective ³¹P NMR titrations. Following the HSAB theory Zn²⁺ and Cu²⁺ differ in their Lewis acidity. While Zn²⁺ is an intermediate acid, Cu²⁺ is a weak acid. Consequently the latter one is stronger coordinated by sulphur, which is a weak Lewis base. Both compounds affect the γ -phosphorus resonance in the corresponding ³¹P NMR titration the strongest. When Cu²⁺-cyclen is present additionally strong effects are observed for the β -phosphate group in terms of both its chemical shift and its line width for electronic reasons caused by the stronger influence on the coordination sphere of the β -phosphate group. A direct coordination of the β -phosphate hardly is the reason for the latter effect since it is less

accessible for the metal(II)-cyclen and effects in the presence of both derivatives should be observed as it is the case in the corresponding titration with free $\text{Mg}^{2+}\cdot\text{GTP}\gamma\text{S}$.

The preference of Zn^{2+} -cyclen for substate (1a) was also shown in the mutant $\text{Ras}(\text{G12V})\cdot\text{GTP}\gamma\text{S}$, which predominantly exists in conformational state (2). In the presence of Zn^{2+} -cyclen a second set of resonances shows up in the corresponding spectra for the γ - and β -phosphate group, which can be assigned to conformational state (1a). However, the affinity towards this mutant is much lower as already described.

$\text{GTP}\gamma\text{S}$ is a less stable analogue of GTP compared to GppNHp and GppCH_2p . An abnormal hydrolysis mechanism was observed for $\text{GTP}\gamma\text{S}$ in the presence of Ras giving protein bound GDP as expected and inorganic phosphate and H_2S instead of thiophosphate (Spoerner et al. 2007). In the titration with Zn^{2+} -cyclen the expected hydrolysis product is obtained and shifts due to the complex formation with Zn^{2+} -cyclen, which might avoid the hydrolysis of thiophosphate. Additionally a high intensity peak representing inorganic phosphate is observed, which is not likely to be a hydrolysis product of thiophosphate since the amount of the latter matches quite well with the protein bound GDP and H_2S was not detected by its smell at the end of the experiment.

In the above described titrations of different Ras mutants such a high intensity peak representing inorganic phosphate appears only in the presence of Zn^{2+} -cyclen, not Zn^{2+} -BPA independent from the bound nucleotide. This observation has been made before in experiments with Ras and its effectors and regulators such as SOS and NF1 (M. Spoerner, personal communication) or with Arf1 and ArnoSec7 (Kremer et al. 2004). Interestingly the signal for P_i is not observed in each sample itself, but can be detected after adding them together. To date no explanation can be given. It is possible that the Ras protein carries an additional phosphate molecule, which is not detectable due to intermediate exchange between the free and the protein-bound state, but released in the presence of certain regulators. Probably Zn^{2+} -cyclen can also do so. It does bind to inorganic phosphate leading to a downfield shift of the resonance of the latter, as derived from several experiments. Since this effect is not observed in the presence of Zn^{2+} -BPA it is strongly suggested that this potential additional phosphate molecule is positioned close to the binding site of Zn^{2+} -cyclen at the active centre.

High field EPR and ^{31}P NMR studies also indicate the existence of two different conformational states in the $\text{Ras}\cdot\text{Mg}^{2+}\cdot\text{GDP}$ complex (Rohrer et al. 2001). ^{31}P NMR titrations of $\text{Ras}\cdot\text{Mg}^{2+}\cdot\text{GDP}$ with metal(II)-cyclen do not reveal any significant effects of the compound. A different picture is obtained for the α -phosphate signal in the presence of metal(II)-BPA. In the presence of Cu^{2+} -BPA the line width of the α -resonance signal is not affected, but significant downfield shifts can be observed in wild type Ras, $\text{Ras}(\text{G12V})$ and $\text{Ras}(\text{T35A})$. $\text{Ras}(\text{wt})\cdot\text{Mg}^{2+}\cdot\text{GDP}$ was also titrated with Zn^{2+} -BPA. A slight downfield shift is observed for the α -phosphate signal, whereas the β -phosphorus signal remains unperturbed. This observation strongly indicates that there is a binding position for metal(II)-BPA in inactive $\text{Ras}\cdot\text{Mg}^{2+}\cdot\text{GDP}$, which perturbs the chemical environment of the α -phosphate group but does not influence the β -phosphate group considerable.

It can be deduced from the ^{31}P NMR experiments that both metal(II)-cyclen and metal(II)-BPA bind to Ras with millimolar affinity. Hybrid ligands composed of a chelate moiety and a peptide with a consensus Ras binding sequence have been designed with the aim to enhance both the selectivity and the affinity of the compounds in cooperation with G. Dirscherl and F. Schmidt from the chair of Prof. König (Institute for Organic Chemistry, University of Regensburg). The peptide was derived from the interaction surface of the guanine nucleotide exchange factor SOS (Boriack-Sjodin et al. 1998) since conformational state (1) of Ras is structurally closer related to the conformation of Ras in its complex with SOS (Ford et al. 2005). [^1H , ^{15}N]-HSQC titration revealed the binding of the peptide at the desired position, namely around Glu⁶² and Glu⁶³ and hence both metal chelates have been connected to the peptide by an appropriate linker at the chair of Prof. König. STD NMR titrations clearly show that the compounds still bind towards Ras but with reduced affinity. In the case of the hybrid ligand carrying Zn^{2+} -cyclen as chelate moiety the reason for the reduced binding affinity can be of steric origin. As described above for the oncogenic mutant Ras(G12V)· Mg^{2+} ·GppNHp the binding position of the metal(II)-cyclen reacts very sensitively on changes in its environment. The additional binding module obviously enlarges the ligand spatially such that it is not able to enter its binding pocket. Probably only the binding position at loop L7 is recognized accompanied by a reduced affinity due to the attached second site ligand. It is also likely for both hybrid ligands that the linker length was not chosen appropriately, i.e. the peptide does not reach its binding position in the desired way. Likewise the linker might affect the binding potential of the hybrid ligands. Additionally the peptide part of the designed bivalent ligands might be orientated the other way around than expected from the Ras-SOS complex structure.

Both metal(II)-chelates represent attractive lead compounds for the development of Ras inhibitors following the novel strategy of stabilizing the weak effector-binding conformation of active Ras. The compounds differ in their binding position responsible for this stabilization, which widens the range of the design for novel ligands with increased affinity. Advancements in the binding site of Zn^{2+} -cyclen are most probably achieved by the modification of known phosphate sensing compound, such as linear and bismacrocylic octaamines (Le Bris et al. 2007). One has to be aware of the fact that any compound, which is known to bind towards triphosphates is not necessarily able to do so, when the nucleotide is bound to the protein. The application of the Zn^{2+} -cyclens is limited for steric reasons as shown by its decreased affinity towards the oncogenic mutant Ras(G12V)· Mg^{2+} ·GppNHp. This is not the case for metal(II)-BPAs. Taking all the NMR results with the metal(II)-BPA into account one could calculate a HADDOCK structure of the Ras-ligand complex for the subsequent structure-based design of a second class of compounds stabilizing conformational state (1) via a different mechanism as it was done with the ligand Zn^{2+} -cyclen (Rosnizeck et al., accepted).

The existence of a conformational equilibrium seems to be a common feature of Ras family GTPases and has been reported for Ran (Geyer et al. 1999), Rho (Dias and Cerione 2007), Rap and Ral (Liao et al. 2008). Due to their involvement in the development of several diseases (Lu et al. 2009, Minato and Hattori 2009, Smith and Theodorescu 2009, Abe et al. 2008) their interaction with effectors or regulators might also be controlled by the stabilization of a certain conformational states.

5.3 Perturbation of the Ras-Effector Interaction by Zn^{2+} -Cyclen and Zn^{2+} -BPA

^{31}P NMR spectroscopy clearly revealed that metal(II)-cyclen and metal(II)-BPA selectively bind to conformational state (1) of active Ras as described in the previous paragraph. Conformational state (1) is also known as weak effector-binding state due to its reduced affinity towards effector molecules (Spoerner et al. 2001) and hence its stabilization by suitable ligands represents a promising approach in the inhibition of Ras-Raf signaling. Isothermal calorimetric titration studies showed that the binding affinity of Raf-RBD to wild type Ras· Mg^{2+} ·GppNHp is decreased in the presence of Zn^{2+} - and Cu^{2+} -cyclen, respectively (Rosnizeck et al., accepted).

In this work it was shown by ^{31}P NMR spectroscopy that both Zn^{2+} -cyclen and Zn^{2+} -BPA, respectively are capable of shifting the dynamic equilibrium back towards conformational state (1), when Raf-RBD is present. This becomes apparent by the analysis of the peak areas in the experiment with Ras(T35S)· Mg^{2+} ·GppNHp. In this mutant the resonance signals representing state (1) and state (2), respectively are very well separated by 0.5 ppm and 0.84 ppm for the α - and the γ -phosphorus resonance allowing the accurate determination of the peak areas, which are a direct measure of the population of each state. Upon addition of increasing concentrations of Zn^{2+} -cyclen or Zn^{2+} -BPA, respectively an increase of the population of conformational state (1) accompanied by the decrease of the population of conformational state (2) is observed. Only the signals assigned to conformational state (1) shift in the presence of Zn^{2+} -cyclen. The shift directions are identical to the ones found for the signals representing the weak effector-binding state in the titration of Ras(wt)· Mg^{2+} ·GppNHp with Zn^{2+} -cyclen without Raf-RBD being present (Spoerner et al. 2005c). Significant shift changes are not observed for the resonances representing conformational state (2) as expected since it has been shown that Zn^{2+} -cyclen does not bind towards the latter conformation.

From suitable experiments it was also possible to deduce that the mode of inhibition does not proceed via the formation of a heterotrimeric complex consisting of Ras in conformational state (1), Raf-RBD and Zn^{2+} -cyclen, which was expected since Raf-RBD can also bind the weak binding state (Spoerner et al. 2001). Evidence for the separate binding of Zn^{2+} -cyclen and Zn^{2+} -BPA is derived from analysis of the line widths of the resonances assigned to both conformational states in the experiment with Ras(T35S)· Mg^{2+} ·GppNHp. The signals representing conformational state (2) are

significantly broadened compared to the ones assigned to conformational state (1) during the titration with the compounds. This directly reflects the larger mass of Ras in conformational state (2) due to its complex with Raf-RBD. If the above described heterotrimeric complex was formed also the lines representing the weak effector-binding state should be significantly broadened due to this increased molecular mass.

Additional data supporting the assumed separated binding of Raf-RBD and the compounds is given by experiments with the partial loss-of-function mutant Ras(T35A)·Mg²⁺·GppNHp, which stays in conformational state (1) even in the presence of Raf-RBD (Spoerner et al. 2001). Upon addition of Zn²⁺-cyclen to the complex between this Ras mutant and Raf-RBD the fractions of Ras in conformational state (1) with Raf-RBD and Zn²⁺-cyclen, respectively are represented by distinct resonances for the α - and γ -phosphate group. From the analysis of the line width and the chemical shifts one can exclude the formation of a heterotrimeric complex. First, within the whole titration the α - and γ -phosphorus resonances reflecting the effector-bound fraction are broadened by a factor of about 1.8 compared to the ones representing the Zn²⁺-cyclen-bound fraction. The latter line widths correspond very well with the ones observed for the signals of Ras(T35A)·Mg²⁺·GppNHp in absence of Raf-RBD within the whole titration. Secondly, a significant shift can only be observed for the resonances assigned to the Zn²⁺-cyclen-bound fraction. At a molar ratio of Ras:cyclen of 1:24 the resonances of the effector-bound fraction can no longer be detected. The signals representing both fractions cannot be separated at the magnetic field used for the β -phosphate group. Nevertheless they also point out that a formation of a heterotrimeric complex does not occur. A shift of the signal is observed with increasing concentrations of Zn²⁺-cyclen and additionally the line width decreases, which directly reflects the decrease of the effector-bound fraction. Again, at the endpoint of the titration the β -phosphate resonance appears with a line width comparable to free Ras(T35A)·Mg²⁺·GppNHp.

From the experiment carried out the other way around, i.e. the displacement of Zn²⁺-cyclen by Raf-RBD the same conclusions can be drawn. Both fractions are again represented by two sets of resonances for the α - and γ -phosphate group and only the signals representing the Zn²⁺-cyclen-bound fraction shift. The direction is opposite compared to the contrariwise titration as expected and directly reflects the decrease of the Zn²⁺-cyclen-bound fraction upon addition of increasing concentrations of Raf-RBD. An increase in signal volume of the resonance representing Ras(T35A)·Mg²⁺·GppNHp complexed to the effector is observed, whereas the Zn²⁺-cyclen-bound fraction decreases as deduced from the loss of the corresponding peak areas. Unfortunately the results can only be consulted qualitatively due to the observed precipitation of Ras.

The experiments with Ras(T35A)·Mg²⁺·GppNHp have not been carried out with Zn²⁺-BPA due to the observed precipitation of Ras in the presence of the compound. However, it is very likely that this compound follows the same mode of inhibition. This can already be explained by the results obtained in the competitive titration of Ras(T35S)·Mg²⁺·GppNHp with Raf-RBD and Zn²⁺-BPA, which agree very well with the respective experiment with

Zn²⁺-cyclen, i.e. the increased line width of resonances representing conformational state (2) compared to the ones assigned to state (1).

The ³¹P NMR data are in good agreement with the results obtained from D. Filchtinski using fluorescence titration. In the presence of Raf-RBD the relative fluorescence of the Ras mutant Y32C/C118S which the IEDANS fluorophore attached at position 32 increases by a factor of 2.5. Upon addition of both Zn²⁺-cyclen and Zn²⁺-BPA a decrease in fluorescence is observed due to the release of the effector (D. Filchtinski, personal communication).

5.4 Peptide Ligands for Ras·Mg²⁺·GppNHp Derived from the Primary Sequence of Raf-RBD

The small peptide CCAVFRL has been found to inhibit the Ras-Raf-RBD interaction (Barnard et al. 1998). It represents the truncated version of a peptide sequence derived from the primary sequence of Raf-RBD which is capable of interfering with Ras-Raf-RBD association (Barnard et al. 1995). This peptide compromises Raf-RBD residues 95 to 101 and is located about 15 Å away from the binding interface between Ras and Raf-RBD in the crystal structure (Nassar et al. 1996, Zeng et al. 1999). Since the interaction with the RBD of RalGDS is also influenced by the peptide it is strongly suggested that its mode of action is caused by binding towards Ras (Barnard et al. 1998). In cooperation with D. Filchtinski from the group of Prof. Herrmann (Ruhr University Bochum) this peptide was studied using ITC, fluorescence titration and [¹H, ¹⁵N]-HSQC NMR. Additionally the peptide CCFFFRRL, which has been designed by Zeng et al. (2001) using a computational combinatorial algorithm was subject to investigations. A *K_D*-value of 12 μM was obtained for CCAVFRL by ITC. In competitive titrations with Raf-RBD a *K_D*-value of 6.5 μM and 3.5 μM was extracted for the peptides CCAVFRL and CCFFFRRL, respectively (D. Filchtinski, unpublished results).

Both peptides have been investigated further at our department according to their binding sites using [¹H, ¹⁵N]-HSQC-titrations. Since in the [¹H, ¹⁵N]-HSQC spectrum of the wild type protein not every residue of the switch regions is represented by a cross peak the investigations have additionally been carried out with the mutant Ras(T35A). Significant chemical shift changes are observed for several residues, which do not clearly reveal one distinct binding position in the protein. Two explanations can be suggested. Either the small peptides do bind at more than one position in active Ras or large structural changes are induced by the binding of the small peptides in the protein, which are reflected by the chemical shift perturbations. In each titration the residues most affected are Leu⁵² and Leu⁵³. In the wild type protein also Lys⁵ is strongly affected by the presence of both peptides. These residues are part of the so-called interaction surface in Ras comprising residues Lys⁵-Val⁸ and Leu⁵²-Asp⁵⁶, bridging the effector loop and switch II (Zeng and Treutlein 1999). In the crystal structure the Ras-Raf-RBD complex Raf residues Lys⁸⁴

and Arg⁸⁹ form salt bridges with Glu³³ and Asp³⁸ of the effector loop (Nassar et al 1996). Consequently Zeng et al. (2001) extended the Ras binding helix in a computational approach for peptide design by taking potential interactions with the effector region, switch II and the interaction surface of Ras as a basis yielding the peptide CCFFFRRL among others. The relative shift effect on residues of the interaction surface is stronger in both mutants when CCFFFRRL is present. Barnard et al. (1998) could show that the replacement of the arginine in CCAVFRL against a hydrophobic residue strongly enhances the inhibitory effect. In the CCFFFRRL this position is occupied by a phenylalanine. They also showed that mutations of residues 98-100 (with respect to the primary sequence of Raf-RBD) are tolerated. Obviously the introduced phenylalanine strongly contributes to the interaction with Leu⁵³ in Ras since the absolute effect for this residue is stronger in the presence of CCFFFRRL compared to CCAVFRL.

The incorporation of a paramagnetic label in the peptide might ease the identification of the exact binding position(s) of the peptide. Detailed analysis of the peptide by Barnard et al. (1998) exclude a direct participation of the thiol groups of both cysteine residues for the interaction, even though they are indispensable for the inhibitory effect of the peptide. However a covalently attached label might largely influence the interaction pattern of such a small peptide and thus the incorporation of a paramagnetic module into the peptide sequence represents a more promising approach. Several unnatural amino acids carrying a nitroxide paramagnetic moiety, which can be readily used in the solid phase synthesis of the peptide are reported in literature (Toniolo et al. 1998, Tominga et al. 2001, Balog et al. 2003, Lindfors et al. 2008). The major drawback of these labels is the need of their synthesis. Carboxy-PROXYL in contrast is commercially available, but can only be attached at the N-terminal end of the peptide due to the lack of an amine group. Since this does not limit our application the latter compound might be appropriate for the desired investigations concerning the binding position of CCAVFRL in active Ras. Figure 5.2 shows the designed paramagnetic labelled peptide.

Another question remaining is, whether the peptide sequence is also in binding contact with Ras, when part of the effector. To date no crystal structure is available for the Ras-Raf-RBD complex. A widely accepted model is given by the Ras-Raf-RBD complex (Nassar et al. 1996). The sequence homology within the effector region forming an intermolecular β -sheet with Raf β 2 is 95% with Ras. However, the overall sequence homology is only 50% and additional contributions from other parts in Ras for the interaction with Raf-RBD can not be excluded. Mutations in the switch II regions of Ras, e.g. D57A and A59T have been found to abolish the interaction with Raf-RBD (Shirouzo et al. 1994). These residues are close to the interaction surface of Ras. Additionally the so-called cysteine rich region of Raf-RBD requires an intact switch II region for its binding activity (Drugan et al. 1996). Recently Stieglitz et al. (2008) solved the crystal structure of Ras and the RBD of the Ras effector NORE 1. Strong hydrophobic interaction between an N-terminal extension of the RBD and Ras switch II are necessary

for the association. Information about a possible contact of the region in Raf containing the peptide sequence CCAVFRL can for example be obtained by introducing a paramagnetic label into Raf-RBD at one of the cysteine residues. Mutagenesis analysis showed that free SH- groups of the cysteine residues in the peptides are not necessary for the inhibitory effect (Barnard et al. 1998) and consequently a covalently attached label might not disturb the interaction, when part of the complete RBD. Likewise alanine scanning within Raf residues 95 to 101 represents an alternative. If this sequence is contributing to the interaction with Ras the overall affinity should drop, when certain residues are mutated to alanine.

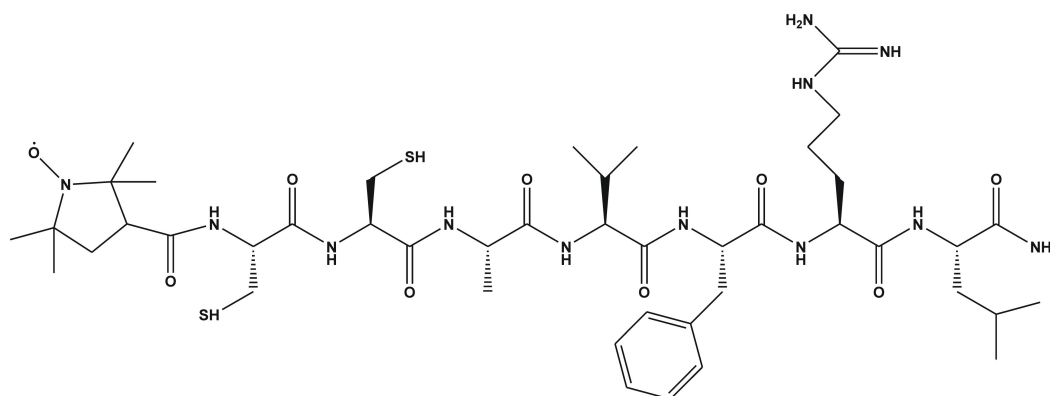


Figure 5.2: The small peptide CCAVFRL with a paramagnetic label covalently attached to the N-terminus.

5.5 High Pressure NMR Spectroscopy on Wild Type Ras Complexed to Mg^{2+} ·GppNHp

The active wild type Ras protein complexed to Mg^{2+} ·GppNHp exists in at least two distinct conformational states as sensed by different chemical shifts for the α - and γ -phosphorus resonance of the bound nucleotide in ^{31}P NMR spectroscopy (Geyer et al. 1996, Spoerner et al. 2005a). Both conformations are in dynamic equilibrium with exchange rates in the millisecond time scale at room temperature. As described in section 1.1.5.2 state (2) becomes stabilized by the interaction with the Ras binding domains of Ras effectors, such as Raf-RBD. State (1) represents a conformation, which is recognized by guanine nucleotide exchange factors, such as SOS (Kalbitzer et al. 2009).

High pressure NMR spectroscopy represents a powerful tool for the investigation of conformational processes in biomolecules at atomic resolution (Akasaka 2006, Kremer 2006). In general conformations with a smaller specific volume become stabilized when high pressure is applied to the protein sample. The structure of the Ras-SOS complex reveals a more opened switch I region in Ras and thus a smaller specific volume of the

protein (Boriack-Sjodin et al. 1998). ^{31}P NMR investigations on $\text{Ras}(\text{wt})\cdot\text{Mg}^{2+}\cdot\text{GppNHp}$ show that conformational state (1) of Ras indeed becomes stabilized at higher pressures giving a difference in the specific volume ΔV^0 between state (2) and state (1) of -17.2 mL mol^{-1} (Kalbitzer et al. 2009). Since state (1) also represents an interesting target for drugs interfering with aberrant Ras signaling (see section 1.1.6.4) knowledge of the residues involved in the transition from conformational state (2) to state (1) can aid structure-based inhibitor design. When looking at the functional cycle of Ras as shown in Figure 1.1 (section 1.1.1) one can deduce that Ras necessarily requires at least one other conformational state, which is recognized by GTPase activating proteins.

For these reasons the pressure response of $\text{Ras}(\text{wt})\cdot\text{Mg}^{2+}\cdot\text{GppNHp}$ was investigated using $[\text{}^1\text{H}, \text{}^{15}\text{N}]$ -HSQC spectroscopy. Pressure series have been recorded at 278 K and 303 K from 3 MPa to 200 MPa and 180 MPa, respectively. Both the changes in the chemical shifts induced by pressure as well as the signal intensities of the cross peaks have been subject to evaluation. In $\text{Ras}(\text{wt})\cdot\text{Mg}^{2+}\cdot\text{GppNHp}$ large parts of both switch regions and the P loop are not represented by cross peaks in the corresponding $[\text{}^1\text{H}, \text{}^{15}\text{N}]$ -HSQC spectrum. At 278 K and a pressure of 200 MPa new cross peaks appear in the spectrum, namely Gly^{10} , Gly^{12} and Gly^{13} , which are all part of the phosphate binding loop. It is likely that these residues sense the same transition as the phosphate groups do in the corresponding ^{31}P NMR pressure studies (Kalbitzer et al. 2009). Unfortunately these peaks only become detectable, when collecting a respective number of scans. Since only the reference spectrum and the one at the highest pressure applied have been repeated with more scans per increment quantification of the effect is not possible.

Due to the poor signal to noise ratio yielded in the pressure series performed at 278 K only the effect on the chemical shifts was followed quantitatively. In the experiments carried out at 303 K with more scans/FID and a higher concentrated protein sample the pressure response of the signal intensities cannot give information about the transition from the strong effector-binding state (2) to the weak effector-binding state (1). At 303 K the exchange rate between conformational state (2) and (1) is 1800 s^{-1} (Spoerner et al. 2005a) and consequently the exchange between the two conformations is always fast compared to the NMR time scale, when recorded at that temperature and at a spectrometer operating at 800 MHz proton frequency. Information about the transition from conformational state (2) to (1) as described was only derived by the evaluation of the chemical shift data. The signal intensities from the data at 278 K, could not be evaluated due to the poor signal to noise ratio.

The chemical shift data could be evaluated by the use of the results reported by Kalbitzer et al. (2009) from the ^{31}P NMR pressure series. Amino acids Val^{14} , Leu^{19} , Gln^{25} , Asn^{26} , Val^{45} , Cys^{51} , Ala^{66} , Ser^{89} , His^{94} , Tyr^{96} , Lys^{117} , Val^{125} , Ala^{130} , Leu^{133} , Gly^{138} , Ile^{139} , Glu^{153} have been identified to sense the transition from the state (2) to state (1). These residues are in close proximity of the active centre of Ras as depicted in Figure 4.56 (see section 4.8.2). Val^{14} for example is part of the so-called phosphate binding loop and in the neighbourhood of Gly^{12} . Mutating the latter residue to valine gives an oncogenic mutant, which has lost the ability to be switched off either intrinsically or by GAPs.

^{31}P NMR spectroscopy also reveals that the dynamic equilibrium between state (2) and state (1) is directly influenced by this mutation with slight preference of state (1) over state (2) (Spoerner et al. 2005a). Lys¹¹⁷ plays a crucial role in the stabilization of nucleotide binding (Pai et al. 1990). Unfortunately, as already mentioned residues from both switch regions, which are expected to undergo large structural changes during that process do not give cross peak signals in the [^1H , ^{15}N]-HSQC spectrum of the wild type protein.

From the chemical shift data a second transition (C(1) to C(3)), which compromises a difference in the specific volume ΔV^0 of $-36 \pm 9 \text{ mL mol}^{-1}$ and in the molar free energy ΔG^0 of $3.9 \pm 0.8 \text{ kJ mol}^{-1}$ could be identified compromising residues Gly⁷⁷, Asn⁸⁵, Asn⁸⁶, Val¹¹², Gly¹¹⁵, Asn¹¹⁶, Arg¹²³, Thr¹²⁴, Asp¹³², Gln¹⁶⁵, His¹⁶⁶. Out of the analysis of the peak intensities additional residues can be found, which are involved in this transition. The obtained values for ΔG^0 of $4.4 \pm 0.6 \text{ kJ mol}^{-1}$ and for ΔV^0 of $-48.4 \pm 3.3 \text{ mL mol}^{-1}$ agree very well within the range of error with the ones obtained by analysis of the chemical shift data. Plotting the chemical shifts and the intensities against the applied pressure also gives a comparable curve describing a two-state transition. For the latter transition as well as for the transition from state (2) to state (1) the equilibrium is not completely in favour of one of these states neither at ambient pressure nor at 200 and 180 MPa, respectively. Interestingly, several residues, namely Leu¹⁹, Val⁴⁵, Cys⁵¹, Ser⁸⁹, Lys¹¹⁷, Val¹²⁵, Ala¹³⁰, Leu¹³³ and Glu¹⁵³ could be identified to sense both transitions as derived from the pressure-dependence of their chemical shifts. Using the values obtained for the two above described transitions enables the fit of these data describing a conformational exchange between three conformations. They are located in between the residues sensing either the transition from C(1) to C(2) or C(3), respectively.

Analysis of the peak intensities reveals a third transition (C(1) to C(4)), which differs from the one described above. This is already clear when looking at the pressure response qualitatively. At ambient pressure one main conformation is clearly sensed by the residues. At a pressure of 180 MPa the equilibrium is equally populated by the original conformation and the one stabilized by high pressure. A large number of residues sense this transition. They are again involved in key interaction patterns of Ras and part of important structural motifs. The transition is characterized by a change in the molar volume ΔV^0 of $-43.7 \pm 8.4 \text{ mL mol}^{-1}$, which corresponds with the value obtained for the transition from C(1) to C(3) within the range of error. However, when looking at the molar free energy ΔG^0 of $8.6 \pm 1.8 \text{ kJ mol}^{-1}$ describing this transition it is obvious that one talks of two different processes. Keeping the functional cycle of Ras in mind one of the conformations stabilized at higher pressure is likely to be recognized by GAPs. The GAP mechanism involves a transition state, which becomes stabilized by a so-called arginine finger provided by GAP (Scheffzek et al. 1997). Consequently there should exist two different GAP-binding conformations. Assuming that the molar volumes of these conformations should not differ largely the conformations C(3) and C(4) stabilized under high pressure might represent two different GAP binding conformations.

Finally a group of residues exhibiting a completely different pressure response have been identified. Unfortunately, quantitative description of their pressure response is not possible

accurately for the reasons described in section 4.8.3. The main question remaining is whether these residues sense a process, which is slow or fast on the NMR time scale, which would in principle both be possible. Adequate data regarding the peak volume and the line widths of these residues would give more information. In general two different explanations can be given for their pressure response. If the transition sensed is slow on the NMR time scale there is already an equilibrium between two conformational states at ambient pressure. In this case the line width should not be influenced significantly by the applied pressure, but only the peak volume reflecting a change of the populations. This can in turn be observed by a loss in signal intensity and the data can be fitted by Equation 3.13 describing a two-state transition in the slow exchange regime. Likewise the volume of the peak does not change significantly but the lines get broadened. This is the case, when the exchange is fast on the NMR time scale. As described in section 4.8.3 maximum line broadening is expected when both conformations are equally populated. This gives a completely different interpretation of the curve observed for these residues. At ambient pressure one certain conformation is represented. The lines get broadened until both conformations are populated equally and would then get smaller again. In this case qualitatively the same pressure dependence is observed as in the transition from conformation C(1) to conformation C(4).

High pressure NMR spectroscopy is also used for the study of protein folding and unfolding. At higher pressures the unfolded state of a protein is preferred due to its smaller specific volume compared to the folded structure. Likewise folding intermediates or local unfolding processes can be detected (Kachel et al. 2006, Inoue et al. 2000). In principle each of the transitions described above could also reflect local unfolding of these residues. Unfolded protein parts resemble a random-coil structure and give cross peak signals at a characteristic chemical shift region of the [^1H , ^{15}N]-HSQC spectrum, namely between 7.9 and 8.6 ppm for ^1H and 120 - 128 ppm for ^{15}N . Taking a closer look at the overlay of the reference spectrum and the spectrum recorded with the highest pressure in the series one cannot find new cross peaks appearing in this region. This is true for the pressure series at both temperatures. Since the pressure induced loss in signal intensity for the single residues is at least 50% independently from the subgroup according to the pressure response these residues should be visible. Many of the residues involved in the single transitions observed are located in close proximity to the bound nucleotide and the switch regions. If local unfolding processes would be the case in these regions one would expect the release of the nucleotide. This was not observed in the ^{31}P NMR pressure series (Kalbitzer et al. 2009) and is thus also not likely to happen here.

6 SUMMARY

The small guanine nucleotide binding protein Ras is essentially involved in the regulation of cell proliferation, differentiation and apoptosis. Alternating between an inactive GDP and an active GTP-bound form, Ras acts as molecular switch, whereby two classes of regulatory proteins determine the lifetime of these two states: guanine nucleotide exchange factors (GEFs) and GTPase activating proteins (GAPs). In about 30% of all human tumors Ras exhibits point mutations at either position 12, 13 or 61. These mutants are insensitive to GAP activation and are therefore locked in the active GTP-bound form, which contributes to tumor formation. Ras is part of a complex signaling network, which requires the coexistence of multiple functional states allowing for the fast transition into a certain conformation. ^{31}P NMR spectroscopy using the bound nucleotide as probe reveals the dynamic equilibrium between at least two distinct conformational substates in active Ras, namely state (1) and state (2), which interconvert in the millisecond timescale. State (2) becomes stabilized by binding of effectors like Raf kinase. State (1) is recognized by guanine nucleotide exchange factors and shows a drastically reduced affinity towards effectors. The relative population of the two states is directly influenced by mutations in Ras and the nature of the bound nucleotide. Chaotropic compounds, high pressure and metal(II)-cyclens shift the dynamic equilibrium towards conformational state (1). Since oncogenic Ras is a key player in human malignancies the selective stabilization of conformational state (1) by suitable ligands, such as metal(II)-cyclens represents a promising approach for the inhibition of aberrant Ras signaling.

Two binding positions could be identified in $\text{Ras(T35A)}\cdot\text{Mg}^{2+}\cdot\text{GppNHp}$ for metal(II)-cyclen. One binding site centres between loop L7 and the C-terminal part of the protein. The second binding site responsible for the stabilization of conformational state (1) is located in close proximity of the γ -phosphate group of the bound nucleotide. In this work a promising second alternative lead structure for the inhibition of Ras signalling was identified. By saturation transfer difference spectroscopy metal(II)-bis(2-picolyl)amine (short: metal(II)-BPA) was identified as Ras ligand. Its binding affinity to $\text{Ras(T35A)}\cdot\text{Mg}^{2+}\cdot\text{GppNHp}$ was determined to be 2.07 ± 0.25 mM. The compound selectively recognizes the weak effector-binding state in active Ras as revealed by ^{31}P NMR spectroscopy. Combining paramagnetic relaxation enhancement (PRE) and chemical shift perturbation (CSP) mapping two binding sites were identified for this lead structure. One binding site is located around loop L7 and the C-terminal end and is also found for the metal(II)-cyclens. In contrary, the second binding site differs for the two compound classes even though they share the same stabilizing effect regarding conformational state (1) of Ras. It is located in the PM3 motif around residues Leu⁵³ to Thr⁵⁸. In this work it was shown that both compound classes differ in their stabilizing efficacy for state (1) in the oncogenic mutant $\text{Ras(G12V)}\cdot\text{Mg}^{2+}\cdot\text{GppNHp}$. The observed effect is stronger for the novel ligand metal(II)-BPA, most probably due to its different binding site responsible for

stabilization of conformational state (1). This is not influenced sterically by mutations of residues such as Gly¹² around the bound nucleotide.

In order to increase both the affinity and the selectivity of metal(II)-cyclen and metal(II)-BPA for state (1) bivalent ligands have been designed. They consist of a peptide derived from the primary sequence of the guanine nucleotide exchange factor SOS and a metal(II)-chelate moiety. The first hybrid ligands did not give the desired results most probably because the linker was not chosen appropriately according to its length. However, the ligands are synthetically accessible and can be further improved.

In this work the impact of Zn²⁺-cyclen and Zn²⁺-BPA on the Ras-effector interaction was studied. Both compounds are capable of replacing Raf-RBD from its complex with conformational state (2) of active Ras, which can be attributed to the stabilization of state (1) and an associated shift of the equilibrium towards this state. Interestingly ³¹P NMR displacement experiments with suitable Ras mutants reveal at least for Zn²⁺-cyclen that also the binding of the effector towards Ras in state (1) is influenced by the compound. Zn²⁺-cyclen and Raf-RBD cannot bind simultaneously to Ras in conformation (1). Additionally to its stabilizing effect regarding conformational state (1) Zn²⁺-cyclen also behaves as an allosteric inhibitor for the binding of Raf-RBD to state (1) since its binding site is not located in the interaction surface of Ras for Raf-RBD.

Additionally peptides directly derived or modified from the primary sequence of Raf-RBD have been investigated. They are known to interfere with the Ras-Raf-RBD interaction but their binding position was left to be unclear and thus chemical shift perturbation mapping was applied in this work with both the active wild type protein and the mutant Ras(T35A). The largest chemical shift changes are observed for residues Leu⁵², Leu⁵³ and Asp⁵⁴ at the PM3 motif strongly indicating the binding of the peptides at this position. However, also amino acids elsewhere in the protein are influenced by the addition of the peptides. The explanation can be the existence of more than one binding site or a strong structural change induced by binding of the peptides at the PM3 motif. The incorporation of a paramagnetic labelled amino acid into the sequence of the peptide can give detailed information of the binding site by use of paramagnetic relaxation enhancement studies.

As already mentioned the dynamic equilibrium of active Ras can also be modulated by the application of pressure in favour of state (1) as studied by ³¹P NMR spectroscopy. Within this work the influence of pressure on Ras(wt)-Mg²⁺-GppNHp was investigated at atomic resolution by [¹H, ¹⁵N]-HSQC spectroscopy. Chemical shift analysis of the data obtained from pressure series carried out at 278 K and 303 K enabled the identification of residues involved in the transition from conformational state (2) to state (1), namely Val⁹, Val¹⁴, Leu¹⁹, Gln²⁵, Asn²⁶, Val⁴⁵, Cys⁵¹, Ala⁶⁶, Ser⁸⁹, His⁹⁴, Tyr⁹⁶, Lys¹¹⁷, Val¹²⁵, Ala¹³⁰, Leu¹³³, Gly¹³⁸, Ile¹³⁹, Glu¹⁵³ which are either directly or indirectly involved in binding of the nucleotide or part of the switch regions. At least two further transitions can be derived from analysis of the pressure response of both the chemical shifts and the signal intensities. For one of the transitions the values derived for ΔG^0 are 3.9 ± 0.8 kJ mol⁻¹ and 4.4 ± 0.6 kJ mol⁻¹ and the difference in the specific volume ΔV^0 between the two conformations involved in the process is -36.0 ± 9.0 mL mol⁻¹ and -48.4 ± 3.30 mL mol⁻¹

as determined from analysis of the chemical shifts and the signal intensities, respectively. The other process does not involve a significantly different change in the specific volume, which has been determined to be $-43.7 \pm 8.4 \text{ mL mol}^{-1}$, but is described by a different molar free energy of $8.6 \pm 1.8 \text{ kJ mol}^{-1}$. It is likely that one of the processes describes the stabilization of the GAP-binding conformation at higher pressure, which has not been detected so far. Conformational states of Ras, which are not visible under ambient pressure become stabilized at high pressure. These states are of special interest for example in the above described approach for the inhibition of Ras signaling. Calculating the structure of these states from NMR data obtained at higher pressure might offer novel opportunities in structure-based drug design. Comparison with the pressure response of different Ras mutants, such as T35A or T35S might allow to interpret and discriminate the data obtained from the investigations on Ras(wt)·Mg²⁺·GppNHp more easily.

7 REFERENCES

- Abe, H., Kamai, T., Shirataki, H., Oyama, T., Arai, K., Yoshida, K.** (2008) High expression of Ran GTPase is associated with local invasion and metastasis of human clear cell renal carcinoma. *Int. J. Canc.* **122**, 2391-2397.
- Ader, C., Spoerner, M., Kalbitzer, H.R., Brunner, E.** (2007) Solid-state ^{31}P NMR spectroscopy of precipitated guanine-nucleotide binding protein Ras in complexes with its effector molecules Raf kinase and RalGDS. *J. Phys. Chem. B.* **111**, 2752-2757.
- Ahmadian, M.R., Wiesmüller, L., Lautwein, A., Bischoff, F.R., Wittinghofer, A.** (1996) Structural differences in the minimal catalytic domain of the GTPase-activating protein p120^{GAP} and Neurofibromin. *J. Biol. Chem.* **271**, 16409-16415.
- Ahmadian, M.R., Hoffmann, U., Goody, R., Wittinghofer, A.** (1997) Individual rate constants for the interaction of Ras proteins with GTPase-activating proteins determined by fluorescence spectroscopy. *Biochemistry* **36**, 4535-4541.
- Ahmadian, M.R., Zor, T., Vogt, D., Kabsch, W., Selinger, Z., Wittinghofer, A., Scheffzek, K.** (1999) Guanosine triphosphate stimulation of oncogenic Ras mutants. *Proc. Natl. Acad. Sci. USA.* **96**, 7065-7070.
- Airoidi C., Palmioli A., D'Urzo A., Colombo S., Vanoni M., Martegani E., Peri F.** (2007) Glucose-derived Ras pathway inhibitors: evidence of Ras-ligand binding and Ras-GEF (Cdc25) interaction inhibition. *ChemBioChem* **8**, 1376-1379.
- Akasaka, K.** (1979) Intermolecular spin diffusion as a method for studying macromolecule-ligand interactions. *J. Magn. Reson.* **36**, 135-140.
- Akasaka, K., Tamada, M., Wang, F., Kariya, K., Shima, F., Kikuchi, A., Yamamoto, M., Shirouzu, M., Yokoyama, S., Kataoka, T.** (1996) Differential requirements for the interaction of Ras proteins with its distinct downstream effectors. *J. Biol. Chem.* **271**, 5353-5360.
- Akasaka, K., Li, H.** (2001) Low-lying excited states of proteins revealed from nonlinear pressure shifts in ^1H and ^{15}N NMR. *Biochemistry* **40**, 8665-8671.
- Akasaka, K.** (2006) Probing conformational fluctuation of proteins by pressure perturbation. *Chem. Rev.* **106**, 1814-1835.
- Allin, C., Ahmadian, M.R., Wittinghofer, A., Gerwert, K.** (2001) Monitoring the GAP catalyzed H-Ras GTPase reaction at atomic resolution in real time. *Proc. Natl. Acad. Sci. USA.* **98**, 7754-7759.
- Almoguera, C., Shibata, D., Forrester, K., Martin, J., Arnheim, N., Preucho, M.** (1988) Most human carcinomas of the exocrine pancreas contain mutant c-K-ras genes. *Cell* **53**, 549-554.
- Arnesano, F., Banci, L., Bertini, I., Felli, I.C., Luchinat, C., Thompsett, A.R.** (2003) A strategy for the NMR characterization of type II copper(II) proteins: the case of the copper trafficking protein CopC from pseudomonas syringae. *J. Am. Chem. Soc.* **125**, 7200-7208.

- Arnold, M.R., Kremer, W., Lüdemann, H.-R., Kalbitzer, H.R.** (2002) ^1H -NMR parameters of common amino acid residues measured in aqueous solutions of the linear tetrapeptides Gly-Gly-X-Ala at pressures between 0.1 and 200 MPa. *Biophys. Chem.* **96**, 129-140.
- Balaram, P., Bothner-By, A.A., Dadok, J.** (1972a) Negative nuclear overhauser effects as probes of macromolecular structure. *J. Am. Chem. Soc.* **94**, 4015-4017.
- Balaram, P., Bothner-By, A.A., Dadok, J.** (1972b) Localization of tyrosine at the binding site of neurophysin II by negative nuclear overhauser effects. *J. Am. Chem. Soc.* **94**, 4017-4018.
- Balog, M., Kálei, T., Jekó, J., Berente, Z., Steinhoff, H.-J., Engelhard, M., Hideg, K.** (2003) Synthesis of new conformationally rigid paramagnetic α -amino acids. *Tetrahedron Lett.* **44**, 9213-9217.
- Barbacid, M.** (1987) Ras genes. *Annu. Rev. Biochem.* **56**, 779-827.
- Barnard, D., Hettich, L., Chuang, E., Zhang, X.-F., Avruch, J., Marshall, M.S.** (1995) Identification of interaction sites between c-Raf-1 and Ras-GTP. *Oncogene* **10**, 1283-1290.
- Barnard, F., Sun, H., Baker, L., Marshall, M.S.** (1998) In vitro inhibition of Ras-Raf association by short peptides. *Biochem. Biophys. Res. Commun.* **247**, 176-180.
- Baskaran, K., Kirchhöfer, R., Huber, F., Trenner, J., Brunner, K., Gronwald, W., Neidig, K.-P., Kalbitzer, H.R.** (2009) Chemical shift optimization in multidimensional NMR spectra by AUREMOL-SHIFTOPT. *J. Biomol. NMR* **43**, 197-210.
- Basso, A., Kirshmeier, P., Bishop, W.R.** (2006) Farnesyltransferase inhibitors. *J. Lipid. Res.* **47**, 15-31.
- Bax, A., Grishaev, A.** (2005) Weak alignment NMR: a hawk-eyed view of biomolecular structure. *Curr. Opin. Struct. Biol.* **15**, 563-570.
- Beck-Erlach, M., Munte, C.E., Kremer, W., Hartl, R., Rochelt, D., Niesner, D., Kalbitzer, H.R.** Ceramic cells for high pressure NMR spectroscopy on protein. *submitted*
- Bellew, B.F., Halkides, C.J., Gerfen, G.J., Griffin, R.G., Singel, D.J.** (1996) High frequency (139.5 GHz) electron paramagnetic resonance characterization of $\text{Mn(II)}\text{-H}_2^{17}\text{O}$ interactions in GDP and GTP forms of p21 *ras*. *Biochemistry* **35**, 12186-12193.
- Bertini, I., Dalvit, C., Huber, J.G., Luchinat, C., Piccioli, M.** (1997) ePHOGSY experiments on a paramagnetic protein: location of the catalytic water molecule in the heme crevice of the oxidized form of heart cytochrome *c*. *FEBS Lett.* **415**, 45-48.
- Boriack-Sjodin, P.A., Margarit, S.M., Bar-Sagi, D., Kuriyan, J.** (1998) The structural basis for the activation of Ras by SOS. *Nature* **394**, 337-343.
- Bos, J.** (1989) Ras oncogenes in human cancer: a review. *Cancer Res.* **49**, 4682-4689.
- Bouvignies, G., Bernadó, P., Meier, S., Cho, K., Grzesiek, S., Brüschweiler, R., Blackledge, M.** (2005) Identification of slow correlated motions in proteins using residual dipolar and hydrogen-bond dipolar couplings. *Proc. Natl. Acad. Sci. USA.* **19**, 13885-13890.

- Bradford, M.** (1976) A rapid and sensitive method for the quantification of microgram quantities of protein utilizing the principle of protein-dye binding. *Anal. Biochem.* **72**, 248-254.
- Burgering, B., Bos, J.** (1995) Regulation of Ras-mediated signalling: more than one way to skin a cat. *Trends Biochem. Sci.* **20**, 18-22.
- Burmer, G.C., Loeb, L.A.** (1989) Mutations in the K-ras 2 oncogene during progressive stages of human colon carcinoma. *Proc. Natl. Acad. Sci. USA.* **86**, 2403-2407.
- Chen, A., Shapiro, M.J.** (1999) NOE pumping: a novel NMR technique for identification of compounds with binding affinity to macromolecules. *J. Am. Chem. Soc.* **120**, 10258-10259.
- Chen, A., Shapiro, M.J.** (2000) NOE pumping as high-throughput method to determine compounds with binding affinity to macromolecules. *J. Am. Chem. Soc.* **122**, 414-415.
- Clore, G.M., Gronenborn, A.M.** (1982) Theory and applications of the transferred nuclear Overhauser effect to the study of the conformations of small ligands bound to proteins. *J. Magn. Reson.* **48**, 402-417.
- Clore, G.M., Gronenborn, A.M.** (1983) Theory of the time dependent transferred nuclear Overhauser effect: applications to structural analysis of ligand-protein complexes in solution. *J. Magn. Reson.* **53**, 423-442.
- Colombo, S., Peri, F., Tisi, R., Nicotra, F., Martegani, E.** (2004) Design and synthesis of a new class of inhibitors of Ras activation. *Ann. N.Y. Acad. Sci.* **1030**, 52-61.
- Cortes, J., Faderl, S., Estey, E., Kurzrock, R., Thomas, D., Beran, M., Garcia-Manero, G., Ferrajoli, A., Giles, F., Koller, C., O'Brien, S., Wright, J., Bai, S.A., Kantarjian, H.** (2005) Phase I study of BMS-214662, a farnesyl transferase inhibitor in patients with acute leukemias and high-risk myelodysplastic syndromes. *J. Clin. Onc.* **23**, 2805-2812.
- Dalvit, C., Pevarello, P., Tatò, M., Veronesi, M., Vulpetti, A., Sundström, M.** (2000) Identification of compounds with binding affinity to proteins via magnetization from bulk water. *J. Biomol. NMR.* **18**, 65-68.
- Dalvit, C., Fogliatto, G., Stewart, A., Veronesi, M., Stockman, B.** (2001) WaterLOGSY as a method for primary NMR screening: practical aspects and range of applicability. *J. Biomol. NMR* **21**, 349-359.
- Dalvit, C., Fasolino, M., Flocco, M., Knapp, S., Pevarello, P., Veronesi, M.** (2002) NMR-based screening with competition water-ligand observed via gradient spectroscopy experiments: detection of high-affinity ligands. *J. Med. Chem.* **45**, 2610-2614.
- Dias, S.M.G., Cerione, R.A.** X-ray crystal structures reveal two activated states for RhoC. *Biochemistry* **46**, 6547-6558.
- Downward, J.** (1996) Control of Ras activation. *Cancer Surveys* **27**, 87-100.
- Downward, J.** (2003) Targeting Ras signalling pathways in cancer therapy. *Nat. Rev. Cancer* **3**, 11-22.

- Drugan, J.K., Koshravi-Far, R., White, M.A., Der, C.J., Sung, Y.-J., Hwang, Y.-W., Campbell, S.L. (1996) Ras interaction with two distinct binding domains in Raf-1 may be required for Ras transformation. *J. Biol. Chem.* **271**, 233-237.
- Dyson, H.J., Kostic, M., Liu, J., Martinez-Yamout, M.A. (2008) Hydrogen-deuterium exchange strategy for delineation of contact sites on protein complexes. *FEBS Lett.* **582**, 1495-1500.
- Emerson, S.D., Madison, V.S., Palermo, R.E., Waugh, D.S., Scheffler, J.E., Tsao, K.-L., Kiefer, S.E., Liu, S.P., Fry, D.C. (1995) Solution structure of the Ras-binding domain of c-Raf-1 and identification of its interaction surface. *Biochemistry* **34**, 6911-6918.
- Enomoto, T., Inoue, M., Perantoni, A.O., Terakawa, N., Tanizawa, O., Rice, J.M. (1990) K-ras activation in neoplasms of the female reproductive tract. *Cancer Res.* **50**, 6139-6145.
- Fam, N.P., Fan, W.T., Wang, Z., Zhang, L.J. Chen, H., Moran, M.F. (1997) Cloning and characterization of Ras-GRF2, a novel guanine nucleotide exchange factor for Ras. *Mol. Cell. Biol.* **17**, 1396-1406.
- Farrar, C.T., Halkides, C.J., Singel, D.J. (1997) The frozen structure of p21 ras determined by ESEEM spectroscopy reveals weak coordination of Thr35 to the active site metal ion. *Structure* **5**, 1055-1066.
- Ford, B., Skowronek, K., Boykewisch, S., Bar-Sagi, D., Nassar, N. (2005) Structure of the G60A mutant of Ras: implications for the dominant negative effect. *J. Biol. Chem.* **280**, 25697-25705.
- Ganguly, A.K., Pramanik, B.N., Huang, E.C., Liberles, S., Heimark, L., Liu, Y.H., Tsarbopoulos, A., Doll, R.J., Taveras, A.G., Remiszewski, S., Snow, M.E., Wang, Y.S., Vibulbhan, B., Cesarz, D., Brown, J.E., del Rosario, J., James, L., Kirschmeier, P., Girijavallabhan, V. (1997) Detection and structural characterization of Ras oncoprotein-inhibitor complexes by electrospray mass spectrometry. *Bioorg. Med. Chem.* **5**, 817-820.
- Ganguly, A.K., Wang, Y.-S., Pramanik, B.N., Doll, R.J., Snow, M.E., Taveras, A.G., Remiszewski, S., Cesarz, D., del Rosario, J., Vibulbhan, B., Brown, J.E., Kirschmeier, P., Huang, E.C., Heimark, L., Tsarbopoulos, A., Girijavallabhan, C.M. (1998) Interaction of a novel GDP exchange inhibitor with the Ras protein. *Biochemistry* **37**, 15631-15637.
- Gelb, M.H., Brunsfeld, L., Hrycyna, C.A., Michaelis, S., Tamanoi, F., Van Voorhis, W.C., Waldmann, H. (2006) Therapeutic intervention based on protein prenylation and associated modifications. *Nat. Chem. Biol.* **2**, 518-528.
- Gemmecker, G., Jahnke, W., Kessler, H. (1993) Measurements of fast proton exchange rates in isotopically labelled compounds. *J. Am. Chem. Soc.* **115**, 11620-11621.
- Geyer, M., Schweins, T., Herrmann, C., Prisner, T., Wittinghofer, A., Kalbitzer, H.R. (1996) Conformational transitions in p21^{ras} and its complexes with the effector protein Raf-RBD and the GTPase activating protein GAP. *Biochemistry* **35**, 10308-10320.
- Geyer, M., Herrmann, C., Wohlgemuth, S., Wittinghofer, A., Kalbitzer, H.R. (1997) Structure of the Ras-binding domain of RalGEF and implications for Ras binding and signaling. *Nat. Struct. Biol.* **4**, 694-699.

- Geyer, M., Assheuer, R., Klebe, C., Kuhlmann, J., Becker, J., Wittinghofer, A., Kalbitzer, H.R.** (1999) Conformational states of the nuclear GTP-binding protein Ran and its complexes with the exchange factor RCC1 and the effector protein RanBP1. *Biochemistry* **38**, 11250-11260.
- Goldfinger, L.E.** (2008) Choose your own path: specificity in Ras GTPase signaling. *Mol. Biosyst.* **4**, 293-299.
- Gorman, C., Skinner, R.H., Skelly, J.V., Neidle, S., Lowe, P.N.** (1996) Equilibrium and kinetic measurements reveal rapidly reversible binding to Raf. *J. Biol. Chem.* **271**, 6713-6719.
- Gosh, S., Xie, W.Q., Quest, A.F.G., Mabrouk, G.M., Strum, J.C., Bell, R.M.** (1994) The cysteine-rich region of Raf-1 kinase contains zinc, translocates to liposomes, and is adjacent to a segment that binds GTP-Ras. *J. Biol. Chem.* **269**, 10000-10007.
- Gosh, S., Bell, R.M.** (1994) Identification of discrete segments of human Raf-1 kinase critical for high affinity binding to Ha-Ras. *J. Biol. Chem.* **269**, 30785-30788.
- Graf, T.** (2006) Entwicklung neuer Inhibitoren für das Ras-Protein und dessen onkogene Mutanten auf Basis von Cyclenderivaten. Doctoral thesis, University of Regensburg
- Gronwald, W., Huber, F., Grünewald, P., Spörner, M., Wohlgemuth, S., Herrmann, C., Wittinghofer, A., Kalbitzer, H.R.** (2001) Solution structure of the Ras binding domain of the protein kinase Byr2 from *Schizosaccharomyces pombe*. *Structure* **9**, 1029-1041.
- Güntert, P.** (2009) Automated structure determination from NMR spectra. *Eur. Biophys. J.* **38**, 129-143.
- Hajduk, P.J.** (2006) SAR by NMR: putting the pieces together. *Mol. Interv.* **6**, 266-272.
- Halkides, C.J., Bellew, B.F., Gerfen, G.J., Farrar, C.T., Carter, P.H., Ruo, B., Evans, D.A., Griffin, R.G., Single, D.J.** (1996) High frequency (139.5 GHz) electron paramagnetic resonance spectroscopy of the GTP form of p21 *ras* with selective ¹⁷O labeling of threonine. *Biochemistry* **35**, 12194-12200.
- Herrmann, C., Block, C., Geisen, C., Haas, K., Weber, C., Winde, G., Möröy, T., Müller, O.** (1998) Sulindac sulfide inhibits Ras signaling. *Oncogene* **17**, 1769-1776.
- Herrmann, C.** (2003) Ras-effector interactions: after one decade. *Curr. Opin. Struct. Biol.* **13**, 122-129.
- Huang, S.L., Tsai, M.-D.** (1982) Does the magnesium(II) ion interact with the α -phosphate of adenosine triphosphate? An investigation by oxygen-17 nuclear magnetic resonance. *Biochemistry* **21**, 951-959.
- Huang, L., Weng, X.W., Hofer, F., Martin, G.S., Kim, S.H.** (1997) Three-dimensional structure of the Ras-interacting domain of RalGDS. *Nat. Struct. Biol.* **4**, 609-615.
- Huang, L., Hofer, F., Martin, G.S., Kim, S.-H.** (1998) Structural basis for the interaction of Ras with RalGDS. *Nat. Struct. Biol.* **5**, 422-426.

- Hunt, J.T., Ding, C.Z., Batorsky, R., Bednarz, M., Bhide, R., Cho, Y., Chong, S., Chao, S., Gullo-Brown, J., Guo, P., Kim, S.H., Lee, F.Y.F., Leftheris, K., Miller, A., Mitt, T., Patel, M., Penhallow, B.A., Ricca, C., Rose, W.C., Schmidt, R., Slusarchyk, W.A., Vite, G., Manne, V. (2000) Discovery of (R)-7-cyano-2,3,4,5-tetrahydro-1-(1*H*-imidazol-4-ylmethyl)-3-(phenylmethyl)-4-(2-thienylsulfonyl)-1*H*-1,4-benzodiazepine (BMS-214662), a farnesyltransferase inhibitor with potent preclinical antitumor activity. *J. Med. Chem.* **43**, 3587-3595.
- Inoue, K., Yamada, H., Akasaka, K., Herrmann, C., Kremer, W., Maurer, T., Döker, R., Kalbitzer, H.R. (2000) Pressure-induced local unfolding of the Ras binding domain of RalGDS. *Nat. Struct. Biol.* **7**, 547-550.
- Ito, Y., Yamasaki, K., Iwahara, J., Terada, T., Kamiya, A., Shirouzu, M., Muto, Y., Kawai, G., Yokoyama, S., Laue, E.D., Wlchli, M., Shibata, T., Nishimura, S., Miyazawa, T. (1997) Regional polysterism in the GTP-bound form of human c-Ha-Ras protein. *Biochemistry* **36**, 9109-9119.
- Iuga, A., Spoerner, M., Kalbitzer, H.R., Brunner, E. (2004) Solid-state ³¹P NMR spectroscopy of microcrystals of the Ras protein and its effector loop mutants: comparison between crystalline and solid state. *J. Mol. Biol.* **342**, 1033-1040.
- Jahnke, W., Floersheim, P., Ostermeier, C., Zhang, X., Hemming, R., Hurth, K., Uzonov, D.P. (2002) NMR reporter screening for the detection of high-affinity ligands. *Angew. Chem. Int. Ed.* **41**, 3420-3423.
- Jiang, L., Mao, X. (2001) NMR evidence for Mg(II) binding to N1 of ATP. *Spectrochim. Acta A* **57**, 1711-1716.
- John, J., Schlichting, I., Schiltz, E., Rösch, P., Wittinghofer, A. (1989) C-terminal truncation of p21^H preserves crucial kinetic and structural properties. *J. Biol. Chem.* **264**, 13086-13092.
- John, J., Sohmen, R., Feuerstein, J., Linke, R., Wittinghofer, A., Goody, R.S. (1990) Kinetics of the Interaction of nucleotides with nucleotide-free H-Ras p21. *Biochemistry* **29**, 6058-6065.
- Joneson, T., White, M.A., Wigler, M.H., Bar-Sagi, D. (1996) Stimulation of membrane ruffling and MAP kinase activation by distinct effectors of Ras. *Science* **271**, 810-812.
- Kachel, N., Kremer, W., Zahn, R., Kalbitzer, H.R. (2006) Observation of Intermediate States of the Human Prion Protein by High Pressure NMR Spectroscopy. *BMC Struct. Biol.* **6**, 16.
- Kalbitzer, H.R., Spoerner, M., Ganser, P., Hosza, C., Kremer, W. (2009) A fundamental link between Folding States and Functional States of Proteins. *J. Am. Chem. Soc.* **131**, 16714-16719.
- Kalk, A., Berendsen, H.J.C. (1976) Proton magnetic relaxation and spin diffusion in proteins. *J. Magn. Reson.* **24**, 343-366.
- Karaguni, I.-M., Herter, P., Debruyne, P., Chtarbova, S., Kasprzyński, A., Herbrand, U., Ahmadian, M.-R., Glüsenkamp, K.-H., Winde, G., Mareel, M., Möröy, T., Müller, O. (2002) The new sulindac derivative Ind 12 reverses Ras-induced cell transformation. *Cancer. Res.* **62**, 1718-1723.

- Karnoub, A.E., Weinberg, R.A.** (2008) Ras oncogenes: split personalities. *Mol. Cell. Biol.* **9**, 517-531.
- Kay, L.** (1998) Protein dynamics from NMR. *Biochem. Cell Biol.* **76**, 145-152.
- Khosravi-Far, R., Solski, P.A., Clark, G.J., Kinch, M.S., Der, C.J.** (1995) Activation of Rac1, RhoA, and mitogen-activated protein kinases is required for Ras transformation. *Mol. Cell. Biol.* **15**, 6443-6453.
- Khosravi-Far, R., White, M.A., Westwick, J.K., Solski, P.A., Chrzanowska, W., Van Aelst, L., Wigler, M.H., Der, C.J.** (1996) Oncogenic Ras activation of Raf/mitogen-activated protein kinase-independent pathways is sufficient to cause tumorigenic transformation. *Mol. Cell. Biol.* **16**, 3923-3933.
- Kiel, C., Aydin, D., Serrano, L.** (2004) Association rate constants of Ras-effector interactions are evolutionary conserved. *PLoS Comput. Biol.* **4**, 1-9.
- Kiel, C., Wohlgemuth, S., Rousseau, F., Schymkowitz, J., Ferkinghoff-Borg, J., Wittinghofer, F., Serrano, L.** (2005) Recognizing and defining true Ras binding domains II: *in silico* prediction based on homology modelling and energy calculations. *J. Mol. Biol.* **348**, 759-775.
- Kiel, C., Serrano, L.** (2006) The ubiquitin domain superfold: structure-based sequence alignments and characterization of binding epitopes. *J. Mol. Biol.* **355**, 821-844.
- Kigawa, T., Endo, M., Ito, Y., Shirouzu, M., Kikuchi, A., Yokoyama, S.** (1998) Solution structure of the Ras-binding domain of RGL. *FEBS Lett.* **441**, 413-418.
- Klein, J., Meinecke, R., Mayer, M., Meyer, B.** (1999) Detecting binding affinity to immobilized receptor proteins in compound libraries by HR-MAS STD NMR. *J. Am. Chem. Soc.* **121**, 5336-5337.
- Kremer, W., Steiner, G., Béraud-Dufour, S., Klabilitzer, H.R.** (2004) Conformational states of the small G protein Arf-1 in complex with the guanine nucleotide exchange factor ARNO-Sec-7. *J. Biol. Chem.* **279**, 17004-17012.
- Kremer, W.** (2006) High-Pressure NMR Studies on Proteins. *Annu. Rep. NMR Spectrosc.* **57**, 177-203.
- Krengel, U., Schlichting, I., Scherer, A., Schumann, R., Frech, M., John, J., Kabsch, W., Pai, E.F., Wittinghofer, A.** (1990) Three-dimensional structures of H-ras p21 mutants: molecular basis for their inability to function as signal switch molecules. *Cell* **62**, 539-548.
- Lämmli, U. K.** (1970). Cleavage of structural proteins during the assembly of the head of bacteriophage T4. *Nature* **227**, 680-685.
- Laurents, D.V., Gorman, P.M., Guo, M., Rico, M., Chakrabarty, A., Bruix, M.** (2005) Alzheimer's A β 40 studied by NMR at low pH reveals that DSS binds and promotes β -ball oligomerizations. *J. Biol. Chem.* **280**, 3675-3685.
- Le Bris, N., Bernard, H., Tripier, R., Handel, H.** (2007) A potentiometric and NMR investigation of triphosphate recognition by linear and bismacrocylic octaamines possessing a 1,4-xylene linker. *Inorg. Chim. Acta* **360**, 3026-3032.

- Lenzen, C., Cool, R.H., Prinz, H., Kuhlmann, J., Wittinghofer, A. (1998) Kinetic analysis by fluorescence of the interaction between Ras and the catalytic Domain of the guanine nucleotide exchange factor Cdc25^{Mm}. *Biochemistry* **37**, 7420-7430.
- Levitzi, A. (1994) Signal-transduction therapy. A novel approach to disease management. *Eur. J. Biochem.* **226**, 1-13.
- Li, N., Batzer, A., Daly, R., Yajnik, V., Skolnik, E., Chardin, P., Bar-Sagi, D., Margolis, B., Schlessinger, J. (1993) Guanine-nucleotide-releasing factor hSos1 binds to Grb2 and links receptor tyrosine kinases to Ras signalling. *Nature* **363**, 85-88.
- Lindfors, H.E., de Koning, P.E., Drijfhout, J.W., Venezia, B., Ubbink, M. (2008) Mobility of TOAC spin-labelled peptides binding to the Src SH3 domain studied by paramagnetic NMR. *J. Biomol. NMR* **41**, 157-167.
- Linnemann, T., Geyer, M., Jaitner, B.K., Block, C., Kalbitzer, H.R., Wittinghofer, A., Herrmann, C. (1999) Thermodynamic and kinetic characterization of the interaction between the Ras binding domain of AF6 and members of the Ras subfamily. *J. Biol. Chem.* **274**, 13556-13562.
- Lu, Q., Longo, F.M., Zhou, H., Massa, S.M., Chen, Y.-H. (2009) Signaling through Rho GTPase pathway as a viable drug target. *Curr. Med. Chem.* **16**, 1355-1365.
- Mayer, M., Meyer, B. (1999) Characterization of ligand binding by saturation transfer difference spectroscopy. *Angew. Chem. Int. Ed.* **38**, 1784-1788.
- Mayer, M., Meyer, B. (2001) Group epitope mapping by saturation transfer difference NMR to identify segments of a ligand in direct contact with a protein receptor. *J. Am. Chem. Soc.* **123**, 6108-6117.
- Margarit, M., Sondermann, H., Hall, B., Nagar, B., Hoelzl, A., Pirucello, M., Barsagi, D., Kuriyan, J. (2003) Structural evidence for feedback activation by Ras-GTP of the Ras-specific nucleotide exchange factor SOS. *Cell* **112**, 685-695.
- Martegani, E., Vanoni, M., Zippel, R., Coccetti, P., Brambilla, R., Ferrari, C., Sturani, E., Alberghina, L. (1992) Cloning by functional complementation of a mouse cDNA encoding a homologue of CDC25, a *Saccharomyces cerevisiae* RAS activator. *EMBO J.* **11**, 2151-2157.
- Matheu, A., Maraver, A., Serrano, M. (2008) The Arf/p53 pathway in cancer and aging. *Canc. Res.* **68**, 6031-6034.
- Maurer, T., Kalbitzer, H.R. (1996) Indirect referencing of ³¹P and ¹⁹F NMR spectra. *J. Magn. Reson.* **B113**, 177-178.
- Meinecke, R., Meyer, B. (2001) Determination of the binding specificity of an integral membrane protein by saturation transfer difference NMR: RGD peptide ligands binding to Integrin $\alpha_{IIb}\beta_3$. *J. Med. Chem.* **44**, 3059-3065.
- Meyer, B., Weimar, T., Peters, T. (1997) Screening mixtures for biological activity by NMR. *Eur. J. Biochem.* **246**, 705-709.
- Meyer, B., Peters, T. (2003) NMR spectroscopy techniques for screening and identifying ligand binding to protein receptors. *Angew. Chem. Int. Ed.* **42**, 864-890.

- Milburn, M., Tong, L., DeVos, M., Brunger, A., Yamaizumi, Z., Nishimura, S., Kim, S.** (1990) Molecular switch for signal transduction: structural differences between active and inactive forms of protooncogenic Ras proteins. *Science* **247**, 939-945.
- Minato, N., Hattori, M.** (2009) Spa-1 (Sipal) and Rap signaling in leukemia and cancer metastasis. *Cancer Sci.* **100**, 17-23.
- Müller, O., Gourzoulidou, E., Carpintero, M., Karaguni, I.-M., Langerak, A., Herrmann, C., Möröy, T., Klein-Hitpaß, L., Waldmann, H.** (2004) Identification of potent Ras signaling inhibitors by pathway-selective phenotype-based screening. *Angew. Chem. Int. Ed.* **116**, 456-460.
- Nagaraja, C.S.** (2006) Heteronuclear saturation transfer difference (HSTD) experiment for detection of ligand binding to proteins. *Chem. Phys. Lett.* **420**, 340-346.
- Nassar, N., Horn, G., Herrmann, C., Scherer, A., McCormick, F., Wittinghofer, A.** (1995) The 2.2 Å crystal structure of the Ras-binding domain of the serine/threonine kinase c-Raf1 in complex with Rap1A and a GTP analogue. *Nature* **375**, 554-560.
- Nassar, N., Horn, G., Herrmann, C., Block, C., Janknecht, R., Wittinghofer, A.** (1996) Ras/Rap effector specificity determined by charge reversal. *Nat. Struct. Biol.* **3**, 723-729.
- Neal, S.E., Eccleston, J.F., Webb, M.R.** (1990) Hydrolysis of GTP by p21 NRAS, the NRAS protooncogene, is accompanied by a conformational change in the wild-type protein: use of a single fluorescent probe at the catalytic site. *Proc. Natl. Acad. Sci. USA.* **87**, 3562-3565.
- Neidhardt, F.C., Bloch, P.L., Smith, D.F.** (1974) Culture medium for Enterobacteria. *J. Bacteriol.* **119**, 736-747.
- O'Connor, C., Kovrigin, E.L.** (2008) Global conformational dynamics in Ras. *Biochemistry* **47**, 10244-10246.
- Pacold, M.E., Suire, S., Perisic, O., Lara-Gonzalez, S., Davis, C.T., Walker, E.H., Hawkins, P.T., Stephens, L., Eccleston, J.F., Williams, R.L.** (2000) Crystal structure and functional analysis of Ras binding to its effector phosphoinositide 3-kinase γ . *Cell* **103**, 931-943.
- Pai, E.F., Krengel, U., Petsko, G.A., Goody, R.S., Kabsch, W., Wittinghofer, A.** (1990) Refined crystal structure of the triphosphate conformation of H-ras p21 at 1.35 Å resolution: implications for the mechanism of GTP hydrolysis. *EMBO J.* **9**, 2351-2359.
- Palmer, A.G., Cavanagh, J., Wright, P.E., Rance, M.** (1969) Sensitivity improvement in proton-detected two-dimensional heteronuclear correlation NMR spectroscopy. *J. Magn. Reson.* **93**, 151-170.
- Peikert, C., Seeger, K., Bhat, R.K., Berger, S.** (2004) Determination of the binding specificity of the 12S subunit of the transcarboxylase by saturation transfer difference spectroscopy. *Org. Biomol. Chem.* **2**, 1777-1781.
- Pellecchia, M., Bertini, I., Cowburn, D., Dalvit, C., Giralt, E., Jahnke, W., James, T.L., Homans, S.W., Kessler, H., Luchinat, C., Meyer, B., Oschkinat, H., Peng, J., Schwalbe, H., Gregg, S.** (2008) Perspectives of NMR in drug discovery: a technique becomes of age. *Nat. Rev. Drug Discov.* **7**, 738-743.

- Pearson, R. G.** (1963) Hard and soft acids and bases. *J. Am. Chem. Soc.* **85**, 3533-3539.
- Peng, J.W., Moore, J., Abdul-Manan, N.** (2004) NMR experiments for lead generation in drug discovery. *Prog. Nucl. Magn. Reson. Spect.* **44**, 225-256.
- Peri, F., Airoidi, C., Colombo, S., Martegani, E., van Neuren, S., Stein, M., Marizini, C., Nicotra, F.** (2005) Design, synthesis and biological evaluation of sugar-derived Ras-inhibitors. *ChemBioChem* **6**, 1839-1848.
- Ponting, C.P., Benjamin, D.R.** (1996) A novel family of Ras-binding domains. *Trends Biochem. Sci.* **21**, 422-425.
- Qiu, R.-G., Chen, J., McCormick, F., Symons, M.** (1995) A role for Rho in Ras transformation. *Proc. Natl. Acad. Sci. USA.* **92**, 11781-11785.
- Qiu, R.-G., Abo, A., McCormick, F., Symons, M.** (1997) Cdc42 regulates anchorage-independent growth and is necessary for Ras transformation. *Mol. Cell. Biol.* **17**, 3449-3458.
- Raiford, D.S., Fisk, C.L., Becker, E.D.** (1979) Calibration of methanol and ethylene glycol nuclear magnetic resonance thermometers. *Anal. Chem.* **51**, 2050-2051.
- Rensland, H., Lautwein, A., Wittinghofer, A., Goody, R.S.** (1991) Is there a rate-limiting step before GTP-cleavage by H-ras p21? *Biochemistry* **30**, 11181-11185.
- Rensland, H., John, J., Linke, R., Simon, I., Schlichting, I., Wittinghofer, A., Goody, R.S.** (1995) Substrate and product structural requirements for binding of nucleotides to H-ras p21: the mechanism of discrimination between guanosine and adenosine nucleotides. *Biochemistry* **34**, 593-599.
- Reif, B., Hennig, M., Griesinger, C.** (1997) Direct measurement of angles between bond vectors in high-resolution NMR. *Science* **276**, 1230-1233.
- Reiss, Y., Goldstein, J.L., Seabra, M.C., Casey, P.J., Brown, M.S.** (1990) Inhibition of purified p21^{ras} farnesyl:protein transferase by Cys-AAX tetrapeptides. *Cell* **62**, 81-88.
- Rodriguez-Viciana, P., Warn, P.J., Vanhaesebroeck, B., Waterfield, M.D., Downward, J.** (1996) Activation of phosphoinositide 3-kinase by interaction with Ras and by point mutation. *EMBO J.* **15**, 2442-2451.
- Rodriguez-Viciana, P., Warne, P.H., Khwaja, A., Marte, B.N.M., Pappin, D., Das, P., Waterfield, M.D., Ridley, A., Downward, J.** (1997) Role of phosphoinositide 3-OH kinase in cell transformation and control of the actin cytoskeleton by Ras. *Cell* **89**, 457-467.
- Rohrer, M., Prisner, T.F., Brüggmann, O., Käß, H., Spoerner, M., Wittinghofer, A., Kalbitzer, H.R.** (2001) Structure of the metal-water complex in Ras-GDP studied by high-field EPR spectroscopy and ³¹P NMR spectroscopy. *Biochemistry* **40**, 1884-1889.
- Rösch, P., Wittinghofer, A., Tucker, J., Sczakiel, G., Lebermann, R., Schlichting, I.** (1986) ³¹P NMR spectra of the Ha-ras p21 nucleotide complexes. *Biochem. Biophys. Res. Commun.* **135**, 549-555.

- Rose, W.C., Lee, F.Y.F., Fairchild, C.R., Lynch, M., Monticello, T., Kramer, R.A., Manne, V. (2001) Preclinical antitumor activity of BMS-214662, a highly apoptotic and novel farnesyltransferase inhibitor. *Canc. Res.* **61**, 7507-7517.
- Rosnizeck, I.C., Graf, T., Spoerner, M., Tränkle, J., Filchtinski, D., Herrmann, C., Gremer, L., Vetter, I.R., Wittinghofer, A., König, B., Kalbitzer, H.R. Stabilizing a weak binding state for effectors in the human Ras-protein by small compounds. *Angew. Chem. Int. Ed.* Accepted for publication.
- Sakamoto, T., Ojida, A., Hamachi, I. (2009) Molecular recognition, fluorescence sensing, and biological assay of phosphate anion derivatives using artificial Zn(II)-Dpa complexes. *Chem. Commun.*, Issue 2, 141-152.
- Sánchez-Pedregal, V.M., Reese, M., Meiler, J., Blommers, M.J.J., Griesinger, C., Carlomagno, T. (2005) The INPHARMA method: protein-mediated interligand NOEs for pharmacophore mapping. *Angew. Chem. Int. Ed.* **44**, 4172-4175.
- Saraste, M., Sibbald, P.R., Wittinghofer, A. (1990) The P-loop – a common motif in ATP- and GTP-binding proteins. *Trends Biochem. Sci.* **15**, 130-134.
- Schägger, H., von Jagow, G. (1987) Tricine-sodium dodecyl sulfate-polyacrylamide gel electrophoresis for the separation of proteins in the range from 1 to 100 kDa. *Anal. Biochem.* **166**, 368-379.
- Scheffzek, K., Lautwein, A., Kabsch, W., Ahmadian, M.R., Wittinghofer, A. (1996) Crystal structure of the GTPase-activating domain of human p120GAP and implications for the interaction with Ras. *Nature* **384**, 591-596.
- Scheffzek, K., Ahmadian, M.R., Kabsch, W., Wiesmüller, L., Lautwein, A., Schmitz, F., Wittinghofer, A. (1997) The Ras-RasGAP complex: structural basis for GTPase activation and its loss in oncogenic mutants. *Science* **277**, 333-338.
- Scheffzek, K., Grünwald, P., Wohlgemuth, S., Kabsch, W., Tu, H., Wigler, M., Wittinghofer, A. (2001) The Ras-Byr2 complex: structural basis for Ras effector interaction in yeast. *Structure* **9**, 1043-1050.
- Scherf, T., Anglister, J. (1993) A T1 rho-filtered two-dimensional transferred NOE spectrum for studying antibody interactions with peptide antigens. *Biophys. J.* **64**, 754-761.
- Schmidt, G., Lenzen, C., Simon, I., Deuter, R., Cool, R.H., Goody, R.S., Wittinghofer, A. (1996) Biochemical and biological consequences of changing the specificity of p21ras from guanosine to xanthosine nucleotides. *Oncogene* **12**, 87-96.
- Schubbert, S., Shannon, K., Bollag, G. (2007) Hyperactive Ras in developmental disorders and cancer. *Nature* **7**, 295-308.
- Schumann, F.H., Riepl, H., Maurer, T., Gronwald, W., Neidig, K.-P., Kalbitzer, H.R. (2007) Combined chemical shift changes and amino acid specific chemical shift mapping of protein-protein interactions. *J. Biomol. NMR* **39**, 275-289.

- Schweins, T., Geyer, M., Scheffzek, K., Warshel, A., Kalbitzer, H.R., Wittinghofer, A. (1995) Substrate-assisted catalysis as a mechanism for GTP hydrolysis of p21^{ras} and other GTP-binding proteins. *Nature* **2**, 36-44.
- Scrima, A., Thomas, C., Daeconescu, D., Wittinghofer, A. (2008) The Ras-RasGAP complex: GTP hydrolysis without catalytic glutamine and arginine residues. *EMBO J.* **27**, 1145-1153.
- Seeburg, P.H., Colby, W.W., Capon, D.J., Goeddel, D.V., Levinson, A.D. (1984) Biological properties of human c-Ha-ras1 genes mutated at codon 12. *Nature* **312**, 71-75.
- Seeger, K., Lein, S., Reuter, G., Berger, S. (2005) Saturation difference measurements with SU(VAR)3-9 and S-adenosyl-L-methionine. *Biochemistry* **44**, 6208-6213.
- Seewald, M.J., Körner, C., Wittinghofer, A., Vetter, I. (2002) RanGAP mediates GTP hydrolysis without an arginine finger. *Nature* **415**, 662-666.
- Shaka, A.J., Barker, P.B., Freeman, R. (1985) Computer-optimized decoupling scheme for wideband applications and low-level operation. *J. Magn. Reson.* **64**, 547-522.
- Shimotakahara, S., Furihata, K., Tashiro, M. (2005) Application of NMR screening techniques for observing ligand binding with a protein receptor. *Magn. Reson. Chem.* **43**, 69-72.
- Shirouzu, M., Koide, H., Fuita-Yoshigaki, J., Oshio, H., Toyama, Y., Yamasaki, K., Fuhrmann, S.A., Villafranca, E., Kaziro, Y., Yokoyama, S. (1994) Mutations that abolish the ability of Ha-Ras to associate with Raf-1. *Oncogene* **9**, 2153-2157.
- Shou, C., Farnsworth, C.L., Neel, B.G., Feig, L.A. (1992) Molecular cloning of cDNAs encoding a guanine-nucleotide-releasing factor. *Nature* **358**, 351-354.
- Shuker, S.B., Hajduk, P.J., Meadows, R.P., Fesik, S.W. (1996) Discovering high-affinity ligands for proteins: SAR by NMR. *Science* **274**, 1531-1534.
- Sigel, H., Griesser, R. (2005) Nucleoside 5' triphosphates: self-association, acid-base, and metal-ion binding properties in solution. *Chem. Soc. Rev.* **34**, 875-900.
- Smith, S.C., Theodorescu, D. (2008) The Ral GTPase pathway in metastatic bladder cancer: key mediator and therapeutic target. *Urol. Onc.* **27**, 42-47.
- Solomon, I. (1955) Relaxation processes in a system of two spins. *Phys. Rev.* **99**, 555-565.
- Spoerner, M., Herrmann, C., Vetter, I.R., Kalbitzer, H.R., Wittinghofer, A. (2001) Dynamic properties of the Ras switch I region and its importance for binding to effectors. *Proc. Natl. Acad. Sci. USA.* **98**, 4944-4949.
- Spoerner, M., Wittinghofer, A., Kalbitzer, H.R. (2004) Perturbation of the conformational equilibria in Ras by selective mutations as studied by ³¹P NMR spectroscopy. *FEBS Lett.* **578**, 305-310.
- Spoerner, M., Nuehs, A., Ganser, P., Herrmann, C., Wittinghofer, A., Kalbitzer, H.R. (2005a) Conformational states of Ras complexed with the GTP analogue GppNHp or GppCH₂p: implications for the interaction with effector proteins. *Biochemistry* **44**, 2225-2236.

- Spoerner, M., Prisner, T.F., Bennati, M., Hertel, M.M., Weiden, N., Schweins, T., Kalbitzer, H.R. (2005b) Conformational states of human H-Ras detected by high-field EPR, ENDOR, and ^{31}P NMR spectroscopy. *Magn. Reson. Chem.* **43**, 74-83.
- Spoerner, M., Graf, T., König, B., Kalbitzer, H.R. (2005c) A novel mechanism for the modulation of the Ras-effector interaction by small molecules. *Biochem. Biophys. Res. Commun.* **334**, 709-713.
- Spoerner, M., Nuehs, A., Herrmann, C., Steiner, G., Kalbitzer, H.R. (2007) Slow conformational dynamics of the guanine nucleotide-binding protein Ras complexed with the GTP analogue GTP γ S. *FEBS J.* **274**, 1419-1433.
- Steiner, G., Kremer, W., Linnemann, T., Herrmann, C., Geyer, M., Kalbitzer, H.R. (2000) Sequence-specific resonance assignment of the Ras-binding domain of AF6. *J. Biomol. NMR* **18**, 73-74.
- Stieglitz, B., Bee, C., Schwarz, D., Yildiz, Ö., Moshnikova, A., Khokhlatchev, A., Herrmann, C. (2008) Novel type of Ras effector interaction established between tumor suppressor NORE1A and Ras switch II. *EMBO J.* **27**, 1995-2005.
- Stumber, M., Geyer, M., Graf, R., Kalbitzer, H.R., Scheffzek, K., Haeblerlein, U. (2002) Observation of slow dynamic exchange processes in Ras protein crystals by ^{31}P solid state NMR spectroscopy. *J. Mol. Biol.* **323**, 899-907.
- Sydor, J.R., Engelhard, M., Wittinghofer, A., Goody, R.S., Herrmann, C. (1998) Transient kinetic studies on the interaction between Ras and the Ras-binding domain of c-Raf-1 reveal rapid equilibrium of the complex. *Biochemistry* **37**, 14292-14299.
- Szabó, Z. (2008) Multinuclear NMR studies of the interaction of metal ions with adenine-nucleotides. *Coord. Chem. Rev.* **252**, 2362-2380.
- Taveras, A.G., Remiszewski, S.W., Doll, R.J., Cesarz, D., Huang, E.C., Kirschmeier, P., Pranamik, B.N., Snow, M.E., Wang, Y.-S., del Rosario, J.D., Vibulbhan, B., Bauer, B.B., Brwon, J.E., Carr, D., Catino, J., Evans, C.A., Girijavallabhan, V., Heimark, L., James, L., Liberles, S., Nash, C., Perkins, L., Senior, M.M., Tsarbopoulos, A., Ganguly, A.K., Aust, R., Brown, E., Delisle, D., Fuhrmann, S., Hendrickson, T., Kissinger, C., Love, R., Siison, W., Villafranca, E., Webber, S.E. (1997) Ras oncoprotein inhibitors: the discovery of potent Ras nucleotide exchange inhibitors and the structural determination of a drug-protein complex. *Bioorg. Med. Chem.* **5**, 125-133.
- Thompson, H.J., Jiang, C., Lu, J., Mehta, R.G., Piazza, G.A., Paranka, N.S., Pamukcu, R., Ahnen, D.J. (1997) Sulfone metabolite of sulindac inhibits mammary carcinogenesis. *Cancer Res.* **57**, 267-271.
- Tominaga, M., Barbosa, S.R., Poletti, E.F., Zukerman-Schpector, J., Marchetto, R., Schreier, S., Paiva, A.C.M.M., Nakaie, C.R. (2001) Fmoc-POAC: [(9-Fluorenylmethyloxycarbonyl)-2,2,5,5-tetramethylpyrrolidine-*N*-oxyl-3-carboxylic acid]: a novel protected spin labelled β -amino acid for peptide and protein chemistry. *Chem. Pharm. Bull.* **49**, 1027-1029.

- Toniolo, C., Crisma, M., Formaggio, F.** (1998) TOAC, a nitroxide spin-labeled, achiral C $^{\alpha}$ -tetrasubstituted α -amino acid, is an excellent tool in material science and biochemistry. *Biopolymers* **47**, 153-158.
- Tucker, J., Sczakiel, G., Feuerstein, J., John, J., Goody, R.S., Wittinghofer, A.** (1986) Expression of p21 proteins in *Escherichia coli* and stereochemistry of the nucleotide-binding site. *EMBO J.* **5**, 1351-1358.
- Ubbink, M., Lain, L.Y., Modi, S., Evans, P.A., Bendall, D.S.** (1996) Analysis of the ^1H -NMR chemical shifts of Cu(I)-, Cu(II)- and Cd-substituted pea plastocyanin. Metal-dependent differences in the hydrogen-bond network around the copper site. *Eur. J. Biochem.* **242**, 132-147.
- Vasavada, K.V., Ray, B.D., Nageswara Rao, B.D.** (1984) ^{31}P NMR lineshape of β -P (ATP) in the presence of Mg^{2+} and Ca^{2+} : estimate of exchange processes. *J. Inorg. Biochem.* **21**, 323-335.
- Vavvas, D., Li, X., Avruch, J., Zhang, X.-F.** (1998) Identification of Nore1 as a potential Ras effector. *J. Biol. Chem.* **273**, 5439-5442.
- Vetter, I., Linnemann, T., Wohlgemuth, S., Geyer, M., Kalbitzer, H.R., Herrmann, C., Wittinghofer, A.** (1999) Structural and biochemical analysis of Ras-effector signaling via RalGDS. *FEBS Lett.* **451**, 175-180.
- Vetter, I.R., Wittinghofer, A.** (2001) The guanine nucleotide-binding switch in three dimensions. *Science* **294**, 1299-1304.
- Visvanathan, K.V., Pocock, R.D., Summerhayes, I.C.** (1988) Preferential and novel activation of Ha-ras in human bladder carcinomas. *Oncogene Res.* **3**, 77-86.
- Vogtherr, M., Peters, T.** (2000) Application of NMR based assays to identify key hydroxyl groups for intermolecular recognition. *J. Am. Chem. Soc.* **122**, 6093-6099.
- Waldmann, H., Karaguni, I.-M., Carpintero, M., Gourzoulidou, E., Herrmann, C., Brockmann, C., Oschkinat, H., Müller, O.** (2004) Sulindac-derived Ras pathway inhibitors target the Ras-Raf interaction and downstream effectors in the Ras pathway. *Angew. Chem. Int. Ed.* **116**, 460-464.
- Walker, E.H., Perisic, O., Ried, C., Stephens, L., Willams, R.L.** (1999) Structural insights into phosphoinositide 3-kinase catalysis and signalling. *Nature* **402**, 313-320.
- Wennerberg, K., Rossmann, K.L., Der, C.J.** (2005) The Ras superfamily at a glance. *Science* **118**, 843-846.
- White, M.A., Nicolette, C., Minden, A., Polverino, A., van Aelst, L., Karin, M., Wigler, M.H.** (1995) Multiple Ras functions can contribute to mammalian cell transformation. *Cell* **80**, 533-541.
- Wishart, D.S., Bigam, C.G., Yao, J., Abildgaard, F., Dyson, H.J., Oldfield, E., Markley, J.L., Sykes, B.D.** (1995) ^1H , ^{13}C and ^{15}N chemical shift references in biomolecular NMR. *J. Biomol. NMR* **6**, 135-140.
- Willumsen, B.M., Christensen, A.** (1984) The p21 Ras C-terminus is required for transformation and membrane association. *Nature* **310**, 583-586.

- Wittinghofer, F.** (1999) Caught in the act of the switch-on. *Nature* **394**, 317-320.
- Wittinghofer, A., Waldmann, H.** (2000) Ras- A molecular Switch involved in tumor formation. *Angew. Chem. Int. Ed.* **39**, 4192-4214.
- Wittinghofer, A.** (2006) Phosphoryl transfer in Ras proteins, conclusive or elusive? *Trends Biochem. Sci.* **31**, 20-23.
- Wohlgemuth, S., Kiel, C., Krämer, A., Serrano, L., Wittinghofer, F., Herrmann, C.** (2005) Recognizing and defining true Ras binding domains I: biochemical analysis. *J. Mol. Biol.* **348**, 741-758.
- Wolthuis, R.M., Bauer, B., van't Veer, L.J., Vries-Smits, A.M., Cool, R.H., Spaargaren, M., Wittinghofer, A., Burgering, B.M., Bos, J.L.** (1996) RalGDS-like factor (Rlf) is a novel Ras and Rap 1A-associating protein. *Oncogene* **13**, 353-362.
- Yamada, H.** (1974) Pressure-resisting glass cell for high pressure, high-resolution NMR measurements. *Rev. Sci. Instr.* **45**, 540-542.
- Ye, M., Shima, F., Muraoka, S., Liao, J., Okamoto, H., Yamamoto, M., Tamura, A., Yagi, N., Ueki, T., Kataoka, T.** (2005) Crystal structure of M-Ras reveals a GTP-bound "off" state conformation of Ras family small GTPases. *J. Biol. Chem.* **280**, 31267-31275.
- Zeng, J., Treutlein, H., Simonson, T.** (1999) Molecular dynamics simulation of the Ras:Raf and Rap:Raf complexes. *Proteins: Struct. Funct. Genet.* **35**, 89-100.
- Zeng, J., Treutlein, H.R.** (1999) A method for the combinatorial peptide design of inhibitors of the Ras protein. *Prot. Eng.* **12**, 457-468.
- Zeng, J., Nheu, T., Zorzet, A., Catimel, B., Nice, E., Maruta, H., Burgess, A.W., Treutlein, H.R.** (2001) Design of inhibitors of Ras-Raf interaction using a computational combinatorial algorithm. *Prot. Eng.* **14**, 39-45.
- Zhu, G., Yao, X.** (2008) TROSY-based NMR experiments for NMR studies of large biomolecules. *Prog. Nucl. Magn. Reson. Spec.* **52**, 49-68.
- Zor, T., Bar-Yaacov, M., Elgavish, S., Shaanan, B., Selinger, Z.** (1997) Rescue of a mutant G-protein by substrate-assisted catalysis. *Eur. J. Biochem.* **249**, 330-336.

8 APPENDIX

8.1 List of Abbreviations

aa	amino acid: alanine (Ala, A), arginine (Arg, R), aspartate (Asp, D), asparagine (Asn, N), cysteine (Cys, C), glutamic acid (Glu, E), glutamine (Gln, Q), glycine (Gly, G), histidine (His, H), isoleucine (Ile, I), leucine (Leu, L), lysine (Lys, K), methionine (Met, M), phenylalanine (Phe, F), proline (Pro, P), serine (Ser, S), threonine (Thr, T), tryptophane (Trp, W), tyrosine (Tyr, Y), valine (Val, V)
BSA	bovine serum albumine
c'	C-terminal truncated
CSP	chemical shift perturbation
DNase	desoxyribonuclease
DSS	3-(trimethylsilyl)-1-propanesulfonic acid
DTE	1,4-Dithioerythritol
EDTA	ethylenediaminetetraacetic acid
fl	full length
GAP	GTPase activating protein
GDP	guanosine 5'-diphosphate
GEF	guanine nucleotide exchange factor
GppCH₂p	guanosin-5'-(β,γ -methyleno)triphosphat
GppNHp	guanosine-5'-(β,γ -imido)triphosphate
GST	glutathion-S-transferase
GTP	guanosine-5'-triphosphate
GTPγS	guanosine-5'-O-(3-thiotriphosphate)
HEPES	4-(2-hydroxyethyl)piperazine-1-ethanesulfonic acid
HPLC	high performance liquid chromatography
HQSC	heteronuclear single quantum coherence
ITC	isothermal titration calorimetry
IPTG	isopropyl β -D-1-thiogalactopyranoside
K	Kelvin
kDa	kilo Dalton
Tris	2-amino-2-(hydroxymethyl)-1,3-propanediol
NMR	nuclear magnetic resonance
OD₆₀₀	optical density at 600 nm
PAGE	polyacrylamide gel electrophoresis
P_i	inorganic phosphate
PI(3)K	phosphoinositol(3)kinase
PMSF	phenylmethanesulfonyl fluoride
ppm	parts per million

PRE	paramagnetic relation enhancement
RBD	Ras binding domain
rpm	rounds per minute
SDS	sodium dodecyl sulfate
STD	saturation transfer difference
TROSY	transverse relaxation optimized spectroscopy
U	Unit
wt	wild type
δ	chemical shift
ϵ	extinction coefficient
λ	wave length

8.2 Experimental Data

Chemical Shifts of the Cross Peaks Assignable in the [^1H , ^{15}N]-TROSY HSQC Spectrum of c'Ras(T35A)·Mg $^{2+}$ ·GppNHp at pH 7.4 and 293 K.

residue number	amino acid	$\delta^1\text{H}$ [ppm]	$\delta^{15}\text{N}$ [ppm]	residue number	amino acid	$\delta^1\text{H}$ [ppm]	$\delta^{15}\text{N}$ [ppm]
2	THR	125.368	8.804	85	ASN	117.75	7.759
3	GLU	127.438	8.278	86	ASN	119.899	7.807
4	TYR	122.555	8.633	87	THR	125.172	9.152
5	LYS	124.274	8.933	88	LYS	124.938	8.353
6	LEU	126.813	9.063	89	SER	115.015	7.848
7	VAL	122.672	7.985	90	PHE	125.407	7.288
8	VAL	129.548	8.599	91	GLU	122.438	8.333
9	VAL	121.11	8.988	92	ASP	118.141	8.367
10	GLY	108.687	7.282	93	ILE	121.422	7.432
11	ALA	122.477	8.913	94	HIS	118.062	7.671
12	GLY	107.046	8.653	95	GLN	116.89	7.377
13	GLY	114.078	8.742	96	TYR	120.094	7.479
14	VAL	112.984	7.309	97	ARG	119.625	8.285
15	GLY	108.765	8.237	98	GLU	117.945	7.93
16	LYS	124.43	8.974	99	GLN	120.953	7.752
17	SER	120.602	9.404	100	ILE	120.953	7.752
18	ALA	125.993	8.974	101	LYS	118.023	7.691
19	LEU	121.305	8.708	102	ARG	118.766	7.643
20	THR	117.672	7.377	103	VAL	119.156	8.183
21	ILE	121.5	8.783	104	LYS	116.812	8.005
22	GLN	121.539	7.971	105	ASP	121.696	7.8
23	LEU	120.875	7.609	106	SER	109.859	7.432
24	ILE	114.859	8.012	107	ASP	122.907	8.258
25	GLN	116.812	8.783	108	ASP	121.852	8.285
26	ASN	117.32	7.855	109	VAL	123.532	7.602
27	HIS	113.101	6.681	111	MET	123.61	8.162
28	PHE	123.063	8.155	112	VAL	118.609	8.005
29	VAL	126.462	7.582	113	LEU	129.509	8.804
31	GLU	119.039	7.862	114	VAL	128.923	9.049
32	CYS	122.555	8.019	115	GLY	115.289	7.896
33	ASP	126.383	7.964	116	ASN	121.852	8.64
35	ALA	119.547	7.78	117	LYS	112.867	7.227
36	ILE	124.704	8.155	118	SER	114.859	8.647
37	GLU	122.75	8.06	119	ASP	118.141	8.469
38	ASP	121.422	7.971	120	LEU	121.656	7.677
39	SER	114.117	7.684	121	ALA	123.454	8.046

40	TYR	123.375	8.892	122	ALA	122.555	7.616
41	ARG	121.461	8.21	123	ARG	121.031	7.889
42	LYS	123.454	8.585	124	THR	115.172	9.043
43	GLN	129.821	8.81	125	VAL	125.29	7.5
44	VAL	121.735	8.981	126	GLU	127.79	8.626
45	VAL	121.852	7.998	127	SER	122.516	9.322
46	ILE	126.735	8.066	128	ARG	118.648	8.578
47	ASP	131.775	9.527	129	GLN	117.515	6.66
48	GLY	103.842	8.244	130	ALA	124.352	6.886
49	GLU	123.18	7.575	131	GLN	118.844	8.496
50	THR	127.126	8.838	132	ASP	120.875	8.101
51	CYS	124.821	9.363	133	LEU	124.391	7.363
52	LEU	122.711	8.626	134	ALA	122.555	8.312
53	LEU	124.743	9.049	135	ARG	119.117	8.326
54	ASP	126.423	8.626	136	SER	118.609	7.814
55	ILE	124.743	9.084	137	TYR	120.836	7.486
56	LEU	130.681	8.865	138	GLY	111.734	8.196
57	ASP	126.423	8.626	139	ILE	114.078	7.964
58	THR	114.156	7.22	141	TYR	120.719	8.176
59	ALA	123.141	8.326	142	ILE	130.87601	8.367
60	GLY	111.929	9.254	143	GLU	125.485	7.732
61	GLN	120.485	8.162	144	THR	113.257	8.694
62	GLU	122.516	8.681	145	SER	113.179	8.674
63	GLU	121.539	8.319	146	ALA	133.064	8.988
64	TYR	121.93	8.237	147	LYS	116.5	6.858
65	SER	120.133	7.766	148	THR	106.929	7.596
66	ALA	128.063	8.647	149	ARG	118.844	7.698
67	MET	117.633	7.896	150	GLN	125.016	7.698
68	ARG	121.031	7.534	151	GLY	115.914	8.831
69	ASP	119.352	7.971	152	VAL	121.422	6.974
70	GLN	118.727	7.677	153	GLU	117.633	8.155
71	TYR	119.195	7.985	154	ASP	117.281	8.08
72	MET	119.82	8.203	155	ALA	124.821	8.51
73	ARG	117.633	7.896	156	PHE	113.335	7.131
74	THR	109.312	7.602	157	TYR	120.133	9.466
75	GLY	108.999	7.712	158	THR	117.75	8.435
76	GLU	122.086	8.77	159	LEU	122.438	7.131
77	GLY	101.967	7.07	160	VAL	119.859	7.391
78	PHE	122.164	8.087	161	ARG	119.859	7.93
79	LEU	126.813	9.063	162	GLU	118.805	8.08
80	CYS	125.133	8.599	163	ILE	122.789	8.039
81	VAL	126.813	8.906	164	ARG	119.508	8.305
82	PHE	124.665	9.179	165	GLN	116.265	7.527
83	ALA	121.813	8.572	166	HIS	126.266	7.561
84	ILE	113.96	8.353				

pK_a-values Obtained for Single Residues in c'Ras(T35A)·Mg²⁺·GppNHp from a Titration in the pH Range of 5.5 to 7.5 Determined from the Chemical Shifts of ¹H and ¹⁵N, respectively.

residue number	amino acid	pK _a ¹ H	error	pK _a ¹⁵ N	error
2	Thr	7.33	0.28	6.59	0.18
3	Glu	--	--	5.97	0.11
4	Tyr	--	--	6.03	0.24
7	Val	6.82	0.71	4.66	1.29
8	Val	--	--	5.69	0.14
9	Val	--	--	5.24	0.1
10	Gly	--	--	5.1	0.48
12	Gly	4.92	1.26	5.4	0.17
13	Gly	--	--	5.74	0.08
14	Val	--	--	6.36	0.24
17	Ser	--	--	6.43	0.16
18	Ala	6.75	0.13	5.92	0.1
22	Gln	6.46	0.54	--	--
25	Gln	5.72	0.25	6.81	0.09
27	His	5.67	0.36	6.76	0.08
28	Phe	6.88	0.16	6.48	0.11
29	Val	6.72	0.1	6.72	0.1
32	Tyr	6.21	0.03	7.05	0.25
35	Ala	--	--	6.72	0.07
38	Asp	6.5	0.02	6.2	0.17
39	Ser	--	--	5.98	0.13
40	Tyr	5.54	0.14	6.23	0.06
46	Ile	6.47	0.19	6.69	0.07
52	Leu	7.09	1.66	5.23	0.09
55	Ile	5.91	0.33	6.3	0.22
70	Gln	6.65	0.13	5	0.16
72	--	6.32	0.08	5.55	--
74	Thr	--	--	5.29	0.02
76	Gly	--	--	5.21	0.09
77	Gly	--	--	6.16	0.21
78	Phe	6.88	0.16	--	--
92	Asp	4.97	0.1	5.72	0.03
93	Ile	6.51	0.16	5.94	0.04
94	His	6.05	0.03	6.05	0.05
95	Gln	5.67	0.09	6.03	0.04
106	Ser	5.48	0.15	6.28	0.08
108	Asp	7.19	0.39	7.47	0.49
116	Asn	--	--	7.11	0.37
117	Lys	--	--	7.07	0.23
162	Glu	4.31	1.1	--	--
166	His	--	--	6.93	0.12

Combined Chemical Shift Changes Observed in the [^1H , ^{15}N]-TROSY-HSQC Spectrum of c'Ras(T35A)·Mg $^{2+}$ ·GppNHp between pH 5.5 and 7.5 at 293 K.

residue number	amino acid	$\Delta\delta_{\text{comb}}$ [ppm]	residue number	amino acid	$\Delta\delta_{\text{comb}}$ [ppm]	residue number	amino acid	$\Delta\delta_{\text{comb}}$ [ppm]
1	MET	-	57	ASP	-	112	VAL	0.051
2	THR	0.118	58	THR	0.037	113	LEU	0.018
3	GLU	0.121	59	ALA	0.063	114	VAL	0.03
4	TYR	0.034	60	GLY	0.067	115	GLY	0.022
5	LYS	0.012	61	GLN	0.037	116	ASN	0.018
6	LEU	-	62	GLU	0.041	117	LYS	0.036
7	VAL	0.01	63	GLU	0.03	118	SER	0.017
8	VAL	0.061	64	TYR	0.025	119	ASP	0.021
9	VAL	0.044	65	SER	0.047	120	LEU	0.018
10	GLY	0.022	66	ALA	0.072	121	ALA	0.013
11	ALA	0.048	67	MET	0.008	122	ALA	0.024
12	GLY	0.026	68	ARG	0.019	123	ARG	0.031
13	GLY	0.052	69	ASP	0.014	124	THR	0.013
14	VAL	0.025	70	GLN	0.062	125	VAL	0.017
15	GLY	0.012	71	TYR	0.088	126	GLU	0.042
16	LYS	0.035	72	MET	0.085	127	SER	0.025
17	SER	0.03	73	ARG	-	128	ARG	0.024
18	ALA	0.081	74	THR	0.035	129	GLN	0.019
19	LEU	0.017	75	GLY	0.016	130	ALA	0.037
20	THR	0.012	76	GLU	0.102	131	GLN	0.019
21	ILE	0.012	77	GLY	0.027	132	ASP	0.049
22	GLN	0.026	78	PHE	0.035	133	LEU	0.043
23	LEU	0.007	79	LEU	0.047	134	ALA	0.03
24	ILE	0.04	80	CYS	0.044	135	ARG	0.002
25	GLN	0.102	81	VAL	0.011	136	SER	0.036
26	ASN	0.043	82	PHE	0.017	137	TYR	0.048
27	HIS	0.283	83	ALA	0.025	138	GLY	0.046
28	PHE	0.31	84	ILE	0.017	139	ILE	0.045
29	VAL	0.107	85	ASN	0.091	140	PRO	-
30	ASP	-	86	ASN	0.018	141	TYR	0.016
31	GLU	0.036	87	THR	0.178	142	ILE	0.021
32	CYS	0.06	88	LYS	0.008	143	GLU	0.019
33	ASP	0.03	89	SER	0.003	144	THR	0.043
34	PRO	-	90	PHE	0.048	145	SER	0.014
35	ALA	0.057	91	GLU	0.042	146	ALA	0.003
36	ILE	0.027	92	ASP	0.156	147	LYS	0.056
37	GLU	0.035	93	ILE	0.117	148	THR	0.017
38	ASP	0.1	94	HIS	0.491	149	ARG	0.019
39	SER	0.145	95	GLN	0.334	150	GLN	0.02
40	TYR	0.084	96	TYR	0.043	151	GLY	0.022
41	ARG	0.082	97	ARG	0.237	152	VAL	0.025
42	LYS	0.04	98	GLU	-	153	GLU	0.025
43	GLN	0.02	99	GLN	0.009	154	ASP	0.02
44	VAL	0.04	100	ILE	-	155	ALA	0.063
45	VAL	0.019	101	LYS	0.102	156	PHE	0.044
46	ILE	0.116	102	ARG	0.013	157	TYR	0.016
47	ASP	0.036	103	VAL	0.06	158	THR	0.054
48	GLY	0.018	104	LYS	0.019	159	LEU	0.1
49	GLU	0.003	105	ASP	0.039	160	VAL	0.116
50	THR	0.017	106	SER	0.087	161	ARG	0.023
51	CYS	0.017	107	ASP	0.072	162	GLU	0.115
52	LEU	0.146	108	ASP	0.042	163	ILE	0.035
53	LEU	-	109	VAL	0.039	164	ARG	0.03
54	ASP	0.223	110	PRO	-	165	GLN	0.031
55	ILE	0.064	111	MET	0.082	166	HIS	0.124
56	LEU	0.022						

Combined Chemical Shift Differences Observed between the [^1H , ^{15}N]-TROSY-HSQC Spectra of c'Ras(T35A) and c'Ras(T35S) Complexed to Mg^{2+} -GppNHp.

residue number	amino acid	$\Delta\delta_{\text{comb}}$ [ppm]	residue number	amino acid	$\Delta\delta_{\text{comb}}$ [ppm]	residue number	amino acid	$\Delta\delta_{\text{comb}}$ [ppm]
1	MET	-	57	ASP	0.081	112	VAL	0.051
2	THR	0.017	58	THR	0.029	113	LEU	0.004
3	GLU	0.034	59	ALA	0.062	114	VAL	0.011
4	TYR	0.008	60	GLY	0.051	115	GLY	0.011
5	LYS	0.056	61	GLN	0.005	116	ASN	0.001
6	LEU	0.012	62	GLU	0.064	117	LYS	0.002
7	VAL	0.007	63	GLU	0.038	118	SER	0.005
8	VAL	0.053	64	TYR	0.036	119	ASP	0.008
9	VAL	0.014	65	SER	0.02	120	LEU	0.004
10	GLY	0.006	66	ALA	0.056	121	ALA	0.002
11	ALA	0.009	67	MET	0.027	122	ALA	0.001
12	GLY	0.033	68	ARG	0.029	123	ARG	0.001
13	GLY	0.031	69	ASP	0.029	124	THR	0.002
14	VAL	0.004	70	GLN	0.043	125	VAL	0.002
15	GLY	0.006	71	TYR	0.048	126	GLU	0.01
16	LYS	0.029	72	MET	0.062	127	SER	0.002
17	SER	0.005	73	ARG	0.017	128	ARG	0.003
18	ALA	0.013	74	THR	0.022	129	GLN	0.003
19	LEU	0.015	75	GLY	0.004	130	ALA	0.004
20	THR	0.01	76	GLU	0.027	131	GLN	0.003
21	ILE	0.029	77	GLY	0.004	132	ASP	0.009
22	GLN	0.018	78	PHE	0.024	133	LEU	0.005
23	LEU	0.013	79	LEU	0.036	134	ALA	0.007
24	ILE	0.01	80	CYS	0.019	135	ARG	0.002
25	GLN	0.009	81	VAL	0.004	136	SER	0.011
26	ASN	0.009	82	PHE	0.005	137	TYR	0.011
27	HIS	0.012	83	ALA	0.002	138	GLY	0.006
28	PHE	0.023	84	ILE	0.003	139	ILE	0.004
29	VAL	0.031	85	ASN	0.002	140	PRO	-
30	ASP	-	86	ASN	0.002	141	TYR	0.011
31	GLU	0.07	87	THR	0.003	142	ILE	0.011
32	CYS	0.08	88	LYS	0.003	143	GLU	0.011
33	ASP	0.231	89	SER	0.006	144	THR	0.011
34	PRO	-	90	PHE	0.012	145	SER	0.013
35	ALA/SER	0.772	91	GLU	0.017	146	ALA	0.007
36	ILE	0.504	92	ASP	0.053	147	LYS	0.01
37	GLU	0.016	93	ILE	0.028	148	THR	0.003
38	ASP	0.09	94	HIS	0.107	149	ARG	0.02
39	SER	0.114	95	GLN	0.059	150	GLN	0.009
40	TYR	0.031	96	TYR	0.016	151	GLY	0.008
41	ARG	0.051	97	ARG	0.04	152	VAL	0.006
42	LYS	0.015	98	GLU	0.022	153	GLU	0.012
43	GLN	0.005	99	GLN	0.006	154	ASP	0.014
44	VAL	0.011	100	ILE	0.008	155	ALA	0.024
45	VAL	0.012	101	LYS	0.02	156	PHE	0.024
46	ILE	0.042	102	ARG	0.006	157	TYR	0.013
47	ASP	0.002	103	VAL	0.024	158	THR	0.022
48	GLY	0.002	104	LYS	0.005	159	LEU	0.049
49	GLU	0.009	105	ASP	0.029	160	VAL	0.019
50	THR	0.003	106	SER	0.017	161	ARG	0.028
51	CYS	0.002	107	ASP	0.025	162	GLU	0.059
52	LEU	0.074	108	ASP	0.013	163	ILE	0.011
53	LEU	0.038	109	VAL	0.01	164	ARG	0.022
54	ASP	0.081	110	PRO	-	165	GLN	0.02
55	ILE	0.005	111	MET	0.036	166	HIS	0.023
56	LEU	0.024						

Combined Chemical Shift Changes Observed in the [^1H , ^{15}N]-TROSY-HSQC Spectrum of c'Ras(T35A)·Mg $^{2+}$ ·GppNHp upon Addition of a 15-fold Excess of Zn $^{2+}$ -Cyclen.

residue number	amino acid	$\Delta\delta_{\text{comb}}$ [ppm]	residue number	amino acid	$\Delta\delta_{\text{comb}}$ [ppm]	residue number	amino acid	$\Delta\delta_{\text{comb}}$ [ppm]
1	MET	-	57	ASP	0.015	112	VAL	0.038
2	THR	0.011	58	THR	0.049	113	LEU	0.015
3	GLU	0.017	59	ALA	0.108	114	VAL	0.009
4	TYR	0.009	60	GLY	0.098	115	GLY	0.02
5	LYS	0.006	61	GLN	0.05	116	ASN	0.034
6	LEU	0.021	62	GLU	0.038	117	LYS	0.01
7	VAL	0.041	63	GLU	0.063	118	SER	0.01
8	VAL	0.029	64	TYR	0.072	119	ASP	0.005
9	VAL	0.026	65	SER	-	120	LEU	0.005
10	GLY	0.01	66	ALA	-	121	ALA	0.01
11	ALA	0.033	67	MET	0.011	122	ALA	0.016
12	GLY	0.01	68	ARG	0.05	123	ARG	0.032
13	GLY	0.103	69	ASP	0.043	124	THR	0.011
14	VAL	0.014	70	GLN	0.016	125	VAL	-
15	GLY	0.02	71	TYR	0.041	126	GLU	0.005
16	LYS	0.054	72	MET	-	127	SER	0.016
17	SER	0.044	73	ARG	0.016	128	ARG	0.011
18	ALA	0.016	74	THR	0.031	129	GLN	-
19	LEU	0.03	75	GLY	0.019	130	ALA	0.011
20	THR	0.01	76	GLU	0.012	131	GLN	0.005
21	ILE	0.044	77	GLY	0.01	132	ASP	0.011
22	GLN	0.016	78	PHE	0.005	133	LEU	0.01
23	LEU	0.041	79	LEU	0.021	134	ALA	0.006
24	ILE	0.039	80	CYS	0.01	135	ARG	0.011
25	GLN	0.07	81	VAL	0.004	136	SER	0.011
26	ASN	0.097	82	PHE	-	137	TYR	0.027
27	HIS	-	83	ALA	0.011	138	GLY	0.014
28	PHE	-	84	ILE	0.01	139	ILE	0.083
29	VAL	-	85	ASN	-	140	PRO	-
30	ASP	-	86	ASN	0.005	141	TYR	0.018
31	GLU	0.078	87	THR	-	142	ILE	0.009
32	CYS	-	88	LYS	0.017	143	GLU	0.023
33	ASP	0.01	89	SER	0.05	144	THR	0.015
34	PRO	-	90	PHE	0.028	145	SER	0.016
35	ALA	0.108	91	GLU	0.05	146	ALA	0.028
36	ILE	0.159	92	ASP	0.068	147	LYS	0.071
37	GLU	0.021	93	ILE	0.065	148	THR	0.019
38	ASP	0.119	94	HIS	0.019	149	ARG	0.011
39	SER	0.091	95	GLN	0.18	150	GLN	0.012
40	TYR	0.067	96	TYR	0.027	151	GLY	-
41	ARG	0.044	97	ARG	-	152	VAL	0.009
42	LYS	0.005	98	GLU	0.045	153	GLU	0.005
43	GLN	0.006	99	GLN	0.027	154	ASP	0.011
44	VAL	0.004	100	ILE	0.034	155	ALA	0.011
45	VAL	0.013	101	LYS	0.005	156	PHE	0.005
46	ILE	0.143	102	ARG	0.031	157	TYR	0.014
47	ASP	0.038	103	VAL	0.013	158	THR	0.01
48	GLY	0.005	104	LYS	0.042	159	LEU	0.02
49	GLU	0.012	105	ASP	0.081	160	VAL	0.008
50	THR	-	106	SER	0.027	161	ARG	0.022
51	CYS	0.014	107	ASP	-	162	GLU	0.06
52	LEU	0.015	108	ASP	0.106	163	ILE	0.157
53	LEU	0.016	109	VAL	0.032	164	ARG	-
54	ASP	0.015	110	PRO	-	165	GLN	0.028
55	ILE	0.029	111	MET	0.093	166	HIS	0.113
56	LEU	0.029						

Combined Chemical Shift Changes Observed in the [^1H , ^{15}N]-TROSY-HSQC Spectrum of c'Ras(T35A)·Mg $^{2+}$ ·GppNHp upon Addition of a 8-fold Excess of Zn $^{2+}$ -BPA.

residue number	amino acid	$\Delta\delta_{\text{comb}}$ [ppm]	residue number	amino acid	$\Delta\delta_{\text{comb}}$ [ppm]	residue number	amino acid	$\Delta\delta_{\text{comb}}$ [ppm]
1	MET	-	57	ASP	-	112	VAL	0.047
2	THR	-	58	THR	0.044	113	LEU	0.009
3	GLU	0.079	59	ALA	0.049	114	VAL	0.005
4	TYR	-	60	GLY	0.03	115	GLY	0.022
5	LYS	0.051	61	GLN	0.029	116	ASN	0.005
6	LEU	0.022	62	GLU	0.042	117	LYS	0.006
7	VAL	-	63	GLU	0.04	118	SER	0.003
8	VAL	0.035	64	TYR	0.011	119	ASP	0.01
9	VAL	0.016	65	SER	-	120	LEU	0.005
10	GLY	0.018	66	ALA	0.002	121	ALA	-
11	ALA	0.012	67	MET	-	122	ALA	0.012
12	GLY	0.022	68	ARG	0.017	123	ARG	0.007
13	GLY	0.001	69	ASP	0.027	124	THR	0.007
14	VAL	0.009	70	GLN	-	125	VAL	0.006
15	GLY	0.022	71	TYR	0.014	126	GLU	-
16	LYS	0.009	72	MET	-	127	SER	0.011
17	SER	0.045	73	ARG	0.056	128	ARG	0.01
18	ALA	0.071	74	THR	0.022	129	GLN	0.005
19	LEU	0.032	75	GLY	0.067	130	ALA	0.021
20	THR	0.047	76	GLU	0.038	131	GLN	0.007
21	ILE	0.027	77	GLY	0.029	132	ASP	0.004
22	GLN	0.04	78	PHE	0.027	133	LEU	0.028
23	LEU	0.027	79	LEU	-	134	ALA	-
24	ILE	0.022	80	CYS	0.017	135	ARG	0.007
25	GLN	0.115	81	VAL	0.01	136	SER	0.011
26	ASN	0.034	82	PHE	0.012	137	TYR	0.014
27	HIS	0.035	83	ALA	0.003	138	GLY	0.012
28	PHE	0.122	84	ILE	0.007	139	ILE	0.116
29	VAL	-	85	ASN	0.01	140	PRO	-
30	ASP	-	86	ASN	0.005	141	TYR	0.006
31	GLU	0.128	87	THR	-	142	ILE	0.002
32	CYS	0.026	88	LYS	0.014	143	GLU	0.014
33	ASP	0.017	89	SER	0.034	144	THR	0.014
34	PRO	-	90	PHE	-	145	SER	-
35	ALA	0.044	91	GLU	0.054	146	ALA	0.03
36	ILE	0.041	92	ASP	0.031	147	LYS	0.082
37	GLU	-	93	ILE	0.039	148	THR	0.009
38	ASP	0.134	94	HIS	0.03	149	ARG	-
39	SER	0.099	95	GLN	0.069	150	GLN	0.02
40	TYR	0.195	96	TYR	0.11	151	GLY	0.01
41	ARG	0.046	97	ARG	-	152	VAL	0.012
42	LYS	0.02	98	GLU	0.059	153	GLU	0.017
43	GLN	0.034	99	GLN	0.02	154	ASP	0.005
44	VAL	0.01	100	ILE	-	155	ALA	0.006
45	VAL	0.004	101	LYS	0.037	156	PHE	0.014
46	ILE	-	102	ARG	0.029	157	TYR	0.022
47	ASP	-	103	VAL	0.008	158	THR	0.006
48	GLY	0.008	104	LYS	0.009	159	LEU	0.038
49	GLU	0.142	105	ASP	0.02	160	VAL	0.073
50	THR	-	106	SER	0.069	161	ARG	0.067
51	CYS	0.03	107	ASP	0.045	162	GLU	0.113
52	LEU	0.111	108	ASP	0.194	163	ILE	-
53	LEU	-	109	VAL	0.036	164	ARG	-
54	ASP	0.074	110	PRO	-	165	GLN	0.072
55	ILE	0.023	111	MET	0.085	166	HIS	0.131
56	LEU	-						

Combined Chemical Shift Changes Observed in the [¹H, ¹⁵N]-TROSY-HSQC Spectrum of c'Ras(wt)·Mg²⁺·GppNHp upon Addition of a 4-fold Excess of CCAVFRL.

residue number	amino acid	Δδ _{comb} [ppm]	residue number	amino acid	Δδ _{comb} [ppm]	residue number	amino acid	Δδ _{comb} [ppm]
1	MET	-	57	ASP	-	112	VAL	0.102
2	THR	0.017	58	THR	-	113	LEU	0.01
3	GLU	0.034	59	ALA	-	114	VAL	0.023
4	TYR	0.022	60	GLY	-	115	GLY	0.023
5	LYS	0.133	61	GLN	-	116	ASN	0.002
6	LEU	0.005	62	GLU	-	117	LYS	0.008
7	VAL	0.018	63	GLU	-	118	SER	0.003
8	VAL	0.034	64	TYR	-	119	ASP	0.013
9	VAL	0.012	65	SER	0.09	120	LEU	0.003
10	GLY	-	66	ALA	0.03	121	ALA	0.007
11	ALA	0.022	67	MET	-	122	ALA	0.008
12	GLY	-	68	ARG	0.084	123	ARG	0.009
13	GLY	-	69	ASP	0.088	124	THR	0.001
14	VAL	0.009	70	GLN	-	125	VAL	0.004
15	GLY	0.028	71	TYR	-	126	GLU	0.031
16	LYS	-	72	MET	0.144	127	SER	0.013
17	SER	0.018	73	ARG	-	128	ARG	0.011
18	ALA	-	74	THR	0.008	129	GLN	0.006
19	LEU	0.025	75	GLY	0.021	130	ALA	0.011
20	THR	-	76	GLU	-	131	GLN	0.007
21	ILE	-	77	GLY	0.004	132	ASP	0.024
22	GLN	0.038	78	PHE	0.038	133	LEU	0.002
23	LEU	0.004	79	LEU	0.021	134	ALA	0.018
24	ILE	0.015	80	CYS	0.039	135	ARG	0.008
25	GLN	0.017	81	VAL	0.024	136	SER	0.016
26	ASN	0.007	82	PHE	0.009	137	TYR	0.024
27	HIS	0.02	83	ALA	0.011	138	GLY	0.004
28	PHE	0.009	84	ILE	0.013	139	ILE	0.01
29	VAL	-	85	ASN	0.004	140	PRO	-
30	ASP	-	86	ASN	0.002	141	TYR	0.016
31	GLU	-	87	THR	0.019	142	ILE	0.019
32	CYS	-	88	LYS	0.023	143	GLU	0.024
33	ASP	-	89	SER	0.026	144	THR	0.005
34	PRO	-	90	PHE	0.008	145	SER	0.021
35	THR	-	91	GLU	0.053	146	ALA	0.004
36	ILE	-	92	ASP	-	147	LYS	0.015
37	GLU	-	93	ILE	0.029	148	THR	0.009
38	ASP	-	94	HIS	0.031	149	ARG	0.019
39	SER	-	95	GLN	0.056	150	GLN	0.014
40	TYR	0.015	96	TYR	0.022	151	GLY	0.011
41	ARG	-	97	ARG	0.009	152	VAL	0.008
42	LYS	0.016	98	GLU	-	153	GLU	0.026
43	GLN	0.016	99	GLN	0.009	154	ASP	0.021
44	VAL	0.019	100	ILE	0.045	155	ALA	0.03
45	VAL	0.02	101	LYS	0.034	156	PHE	0.029
46	ILE	0.012	102	ARG	0.019	157	TYR	0.017
47	ASP	0.008	103	VAL	-	158	THR	0.024
48	GLY	0.005	104	LYS	0.012	159	LEU	0.077
49	GLU	0.016	105	ASP	-	160	VAL	0.023
50	THR	0.008	106	SER	0.016	161	ARG	0.056
51	CYS	0.003	107	ASP	0.029	162	GLU	0.112
52	LEU	0.133	108	ASP	0.04	163	ILE	0.025
53	LEU	0.161	109	VAL	0.014	164	ARG	0.036
54	ASP	0.03	110	PRO	-	165	GLN	0.037
55	ILE	0.026	111	MET	0.045	166	HIS	0.054
56	LEU	0.038						

Combined Chemical Shift Changes Observed in the [¹H, ¹⁵N]-TROSY-HSQC Spectrum of c'Ras(wt)·Mg²⁺·GppNHp upon Addition of a 3.2-fold Excess of CCFFFRRL.

residue number	amino acid	Δδ _{comb} [ppm]	residue number	amino acid	Δδ _{comb} [ppm]	residue number	amino acid	Δδ _{comb} [ppm]
1	MET	-	57	ASP	-	112	VAL	0.059
2	THR	0.011	58	THR	-	113	LEU	0.002
3	GLU	0.02	59	ALA	-	114	VAL	0.011
4	TYR	0.013	60	GLY	-	115	GLY	0.012
5	LYS	0.147	61	GLN	-	116	ASN	0.001
6	LEU	0.011	62	GLU	-	117	LYS	0.006
7	VAL	0.012	63	GLU	-	118	SER	0.011
8	VAL	0.022	64	TYR	-	119	ASP	0.01
9	VAL	0.002	65	SER	0.049	120	LEU	0.001
10	GLY	-	66	ALA	0.017	121	ALA	0.008
11	ALA	0.021	67	MET	-	122	ALA	0.005
12	GLY	-	68	ARG	0.038	123	ARG	-
13	GLY	-	69	ASP	0.077	124	THR	0.007
14	VAL	0.008	70	GLN	-	125	VAL	0.001
15	GLY	0.026	71	TYR	-	126	GLU	0.018
16	LYS	-	72	MET	0.039	127	SER	0.015
17	SER	0.01	73	ARG	-	128	ARG	0.01
18	ALA	-	74	THR	0.022	129	GLN	0.007
19	LEU	0.01	75	GLY	0.019	130	ALA	0.013
20	THR	-	76	GLU	0.048	131	GLN	0.016
21	ILE	-	77	GLY	0.004	132	ASP	0.038
22	GLN	0.06	78	PHE	0.019	133	LEU	0.013
23	LEU	0.012	79	LEU	0.022	134	ALA	0.019
24	ILE	0.003	80	CYS	0.027	135	ARG	0.006
25	GLN	0.018	81	VAL	0.02	136	SER	0.027
26	ASN	0.001	82	PHE	0.003	137	TYR	0.011
27	HIS	0.025	83	ALA	-	138	GLY	0.006
28	PHE	0.009	84	ILE	0.004	139	ILE	0.018
29	VAL	-	85	ASN	0.004	140	PRO	-
30	ASP	-	86	ASN	0.005	141	TYR	0.014
31	GLU	-	87	THR	0.004	142	ILE	0.028
32	CYS	-	88	LYS	0.007	143	GLU	0.023
33	ASP	-	89	SER	0.013	144	THR	0.002
34	PRO	-	90	PHE	0.004	145	SER	0.022
35	THR	-	91	GLU	0.036	146	ALA	0.001
36	ILE	-	92	ASP	-	147	LYS	0.006
37	GLU	-	93	ILE	0.017	148	THR	0.012
38	ASP	-	94	HIS	0.018	149	ARG	0.013
39	SER	-	95	GLN	0.04	150	GLN	0.004
40	TYR	0.014	96	TYR	0.014	151	GLY	0.021
41	ARG	-	97	ARG	0.012	152	VAL	0.003
42	LYS	0.023	98	GLU	-	153	GLU	0.021
43	GLN	0.001	99	GLN	-	154	ASP	0.021
44	VAL	0.017	100	ILE	0.021	155	ALA	0.024
45	VAL	0.006	101	LYS	0.02	156	PHE	0.019
46	ILE	0.016	102	ARG	0.013	157	TYR	0.012
47	ASP	0.015	103	VAL	-	158	THR	0.019
48	GLY	0.012	104	LYS	0.005	159	LEU	0.058
49	GLU	0.011	105	ASP	0.021	160	VAL	-
50	THR	0.006	106	SER	0.02	161	ARG	0.039
51	CYS	0.004	107	ASP	0.031	162	GLU	0.084
52	LEU	0.09	108	ASP	0.029	163	ILE	0.026
53	LEU	0.133	109	VAL	0.015	164	ARG	0.038
54	ASP	0.02	110	PRO	-	165	GLN	0.019
55	ILE	0.024	111	MET	0.049	166	HIS	0.042
56	LEU	0.023						

Combined Chemical Shift Changes Observed in the [¹H, ¹⁵N]-TROSY-HSQC Spectrum of c'Ras(T35A)·Mg²⁺·GppNHp upon Addition of a 4.8-fold Excess of CCAVFRL.

residue number	amino acid	$\Delta\delta_{\text{comb}}$ [ppm]	residue number	amino acid	$\Delta\delta_{\text{comb}}$ [ppm]	residue number	amino acid	$\Delta\delta_{\text{comb}}$ [ppm]
1	MET	-	57	ASP	0.125	112	VAL	0.108
2	THR	0.02	58	THR	0.029	113	LEU	0.003
3	GLU	0.044	59	ALA	0.004	114	VAL	0.018
4	TYR	0.017	60	GLY	0.095	115	GLY	0.01
5	LYS	0.017	61	GLN	0.022	116	ASN	0.01
6	LEU	0.017	62	GLU	0.077	117	LYS	0.011
7	VAL	0.016	63	GLU	0.044	118	SER	0.01
8	VAL	0.053	64	TYR	0.003	119	ASP	0.015
9	VAL	0.012	65	SER	0.006	120	LEU	0.004
10	GLY	0.007	66	ALA	0.031	121	ALA	0.005
11	ALA	0.016	67	MET	0.03	122	ALA	0.007
12	GLY	0.036	68	ARG	0.007	123	ARG	0.016
13	GLY	0.075	69	ASP	0.037	124	THR	0.01
14	VAL	0.003	70	GLN	0.059	125	VAL	0.002
15	GLY	0.034	71	TYR	0.035	126	GLU	0.032
16	LYS	0.016	72	MET	0.031	127	SER	0.012
17	SER	0.026	73	ARG	0.019	128	ARG	0.005
18	ALA	0.031	74	THR	0.02	129	GLN	0.005
19	LEU	0.021	75	GLY	0.011	130	ALA	0.005
20	THR	0.013	76	GLU	0.023	131	GLN	0.006
21	ILE	0.02	77	GLY	0.003	132	ASP	0.023
22	GLN	0.025	78	PHE	0.041	133	LEU	0.007
23	LEU	0.008	79	LEU	0.04	134	ALA	0.01
24	ILE	0.011	80	CYS	0.032	135	ARG	0.004
25	GLN	0.006	81	VAL	0.009	136	SER	0.017
26	ASN	0.012	82	PHE	0.008	137	TYR	0.011
27	HIS	0.015	83	ALA	0.003	138	GLY	0.007
28	PHE	0.015	84	ILE	0.005	139	ILE	0.007
29	VAL	0.032	85	ASN	0.003	140	PRO	-
30	ASP	-	86	ASN	0.006	141	TYR	0.014
31	GLU	0.068	87	THR	0.014	142	ILE	0.018
32	CYS	0.097	88	LYS	0.018	143	GLU	0.022
33	ASP	0.009	89	SER	0.032	144	THR	0.036
34	PRO	-	90	PHE	0.011	145	SER	0.014
35	ALA	0.05	91	GLU	0.025	146	ALA	0.008
36	ILE	0.023	92	ASP	0.089	147	LYS	0.02
37	GLU	-	93	ILE	0.023	148	THR	0.011
38	ASP	0.051	94	HIS	0.116	149	ARG	0.044
39	SER	0.011	95	GLN	0.07	150	GLN	0.011
40	TYR	0.013	96	TYR	0.04	151	GLY	0.016
41	ARG	0.096	97	ARG	0.038	152	VAL	0.003
42	LYS	0.009	98	GLU	0.044	153	GLU	0.022
43	GLN	0.014	99	GLN	0.004	154	ASP	0.024
44	VAL	0.022	100	ILE	0.013	155	ALA	0.038
45	VAL	0.021	101	LYS	0.031	156	PHE	0.037
46	ILE	0.02	102	ARG	0.006	157	TYR	0.024
47	ASP	0.006	103	VAL	0.026	158	THR	0.032
48	GLY	0.002	104	LYS	0.015	159	LEU	0.082
49	GLU	0.015	105	ASP	0.062	160	VAL	0.026
50	THR	0.01	106	SER	0.018	161	ARG	0.052
51	CYS	0.003	107	ASP	0.036	162	GLU	0.109
52	LEU	0.134	108	ASP	0.038	163	ILE	0.037
53	LEU	0.202	109	VAL	0.008	164	ARG	0.033
54	ASP	0.125	110	PRO	-	165	GLN	0.038
55	ILE	0.019	111	MET	0.052	166	HIS	0.055
56	LEU	0.027						

Combined Chemical Shift Changes Observed in the [¹H, ¹⁵N]-TROSY-HSQC Spectrum of c'Ras(T35A)·Mg²⁺·GppNHp upon Addition of a 4-fold Excess of CCFFFRRL.

residue number	amino acid	$\Delta\delta_{\text{comb}}$ [ppm]	residue number	amino acid	$\Delta\delta_{\text{comb}}$ [ppm]	residue number	amino acid	$\Delta\delta_{\text{comb}}$ [ppm]
1	MET	-	57	ASP	0.095	112	VAL	0.122
2	THR	0.009	58	THR	0.021	113	LEU	0.017
3	GLU	0.045	59	ALA	0.017	114	VAL	0.02
4	TYR	0.024	60	GLY	0.1	115	GLY	0.01
5	LYS	0.022	61	GLN	0.014	116	ASN	0.007
6	LEU	0.006	62	GLU	0.048	117	LYS	0.005
7	VAL	0.039	63	GLU	0.055	118	SER	0.008
8	VAL	0.049	64	TYR	0.008	119	ASP	0.012
9	VAL	0.012	65	SER	0.035	120	LEU	0.001
10	GLY	0.013	66	ALA	0.015	121	ALA	0.006
11	ALA	0.027	67	MET	0.02	122	ALA	0.004
12	GLY	0.019	68	ARG	0.008	123	ARG	0.015
13	GLY	0.099	69	ASP	0.026	124	THR	0.016
14	VAL	0.003	70	GLN	0.049	125	VAL	0.004
15	GLY	0.034	71	TYR	0.012	126	GLU	0.03
16	LYS	0.037	72	MET	0.02	127	SER	0.02
17	SER	0.03	73	ARG	0.008	128	ARG	0.005
18	ALA	0.026	74	THR	0.019	129	GLN	0.01
19	LEU	0.065	75	GLY	0.013	130	ALA	0.001
20	THR	0.019	76	GLU	0.014	131	GLN	0.006
21	ILE	0.022	77	GLY	0.002	132	ASP	0.04
22	GLN	0.025	78	PHE	0.035	133	LEU	0.013
23	LEU	0.011	79	LEU	0.037	134	ALA	0.022
24	ILE	0.01	80	CYS	0.033	135	ARG	0.008
25	GLN	0.014	81	VAL	0.007	136	SER	0.027
26	ASN	0.016	82	PHE	0.012	137	TYR	0.004
27	HIS	0.021	83	ALA	0.01	138	GLY	0.009
28	PHE	0.018	84	ILE	0.014	139	ILE	0.012
29	VAL	0.035	85	ASN	0.002	140	PRO	-
30	ASP	-	86	ASN	0.005	141	TYR	0.014
31	GLU	0.087	87	THR	0.019	142	ILE	0.021
32	CYS	0.101	88	LYS	0.023	143	GLU	0.023
33	ASP	0.008	89	SER	0.05	144	THR	0.012
34	PRO	-	90	PHE	0.009	145	SER	0.044
35	ALA	0.051	91	GLU	0.041	146	ALA	0.012
36	ILE	0.039	92	ASP	0.09	147	LYS	0.03
37	GLU	0.028	93	ILE	0.014	148	THR	0.017
38	ASP	0.052	94	HIS	0.096	149	ARG	0.037
39	SER	0.014	95	GLN	0.061	150	GLN	0.006
40	TYR	0.013	96	TYR	0.038	151	GLY	0.023
41	ARG	0.078	97	ARG	0.022	152	VAL	0.007
42	LYS	0.013	98	GLU	0.039	153	GLU	0.024
43	GLN	0.016	99	GLN	0.01	154	ASP	0.026
44	VAL	0.022	100	ILE	0.017	155	ALA	0.039
45	VAL	0.017	101	LYS	0.027	156	PHE	0.039
46	ILE	0.033	102	ARG	0.006	157	TYR	0.025
47	ASP	0.005	103	VAL	0.027	158	THR	0.037
48	GLY	0.005	104	LYS	0.022	159	LEU	0.101
49	GLU	0.015	105	ASP	0.072	160	VAL	0.024
50	THR	0.012	106	SER	0.02	161	ARG	0.05
51	CYS	0.004	107	ASP	0.039	162	GLU	0.115
52	LEU	0.141	108	ASP	0.05	163	ILE	0.026
53	LEU	0.246	109	VAL	0.007	164	ARG	0.041
54	ASP	0.095	110	PRO	-	165	GLN	0.038
55	ILE	0.03	111	MET	0.063	166	HIS	0.07
56	LEU	0.026						

Corrected First and Second Order Pressure Coefficients for ^1H Derived for c'Ras(wt)·Mg $^{2+}$ ·GppNHp at 278 K.

residue number	amino acid	B_1^* (H^N) [ppm/GPa]	error	B_2^* (H^N) [ppm/GPa 2]	error
3	Glu	9.7E-4	2.15E-4	-8.83E-7	1.03E-7
7	Val	5.56E-4	4.8E-5	-8.58E-8	2.3E-7
9	Val	-3.97E-4	8.32E-5	1.06E-6	3.98E-7
14	Val	-2.42E-4	2.32E-5	-5.95E-7	1.11E-7
26	Asn	-4.91E-4	3.46E-5	1.05E-7	1.65E-7
42	Lys	-5.53E-4	1.21E-4	-4.6E-7	5.79E-7
45	Val	-3.02E-4	3.57E-5	1.07E-6	1.71E-7
48	Gly	7.2E-4	5.48E-5	1.08E-7	2.62E-7
49	Glu	-3.66E-4	2.3E-5	8.25E-7	1.1E-7
50	Thr	7.57E-4	4.13E-5	-1.3E-6	1.97E-7
75	Gly	4.52E-4	5.75E-5	2.48E-7	2.75E-7
77	Gly	6.32E-4	4.93E-5	-2.04E-6	2.36E-7
82	Phe	-2.36E-4	4.72E-5	1.5E-7	2.25E-7
83	Ala	-9.32E-5	2.88E-5	1.92E-8	1.53E-7
84	Ile	5.21E-4	6.43E-5	-5.91E-7	3.07E-7
85	Asn	-1.45E-4	1.47E-5	-4.02E-7	7.01E-8
86	Asn	2.56E-4	1.15E-5	-4.62E-7	5.5E-8
88	Lys	6.09E-4	3.48E-5	-1.16E-7	1.66E-7
89	Ser	-2.72E-4	2.38E-5	8.92E-7	1.14E-7
96	Tyr	-6.87E-4	4.43E-7	8.97E-7	2.12E-7
105	Asp	-6.28E-4	3.64E-5	8.81E-7	1.74E-7
106	Ser	3.31E-4	2.18E-5	-5.44E-7	1.04E-7
107	Asp	6.57E-4	8.35E-5	-9.63E-7	6.58E-7
108	Asp	-2.48E-4	2.8E-5	3.56E-7	1.34E-7
109	Val	-7.96E-4	1.94E-5	8.14E-7	9.29E-8
111	Met	5.9E-4	2.75E-5	2.37E-7	1.31E-7
115	Gly	-6.01E-4	1.11E-4	5.73E-7	5.07E-7
117	Lys	1.51E-4	1.04E-5	-9.17E-7	4.98E-8
119	Asp	-6.74E-4	3.58E-5	6.88E-7	1.9E-7
120	Leu	-3.59E-4	1.63E-5	-1.5E-7	7.8E-8
122	Ala	4.02E-4	2.76E-5	-3.07E-7	1.32E-7
123	Arg	-2.85E-4	2.96E-5	-5.64E-8	1.41E-7
124	Thr	-1.16E-4	4.24E-5	-5.33E-7	2.03E-7
125	Val	7.63E-5	8.41E-6	-7.68E-7	4.02E-8
126	Glu	5.62E-5	2.27E-5	2.2E-7	1.08E-7
127	Ser	2.57E-4	5.96E-5	-1.23E-7	2.85E-7
129	Gln	-6.84E-4	4.57E-5	3.9E-8	2.18E-7
130	Ala	2.67E-4	2.67E-5	-1.06E-6	1.28E-7
132	Asp	-1.33E-4	3.12E-5	-4.93E-7	1.49E-7
136	Ser	1.17E-4	2.54E-5	-3.98E-7	1.22E-7
138	Gly	-2.79E-4	3.61E-5	4.2E-8	1.73E-7
139	Ile	-3.57E-4	2.55E-5	1.48E-8	1.22E-7
141	Tyr	7.53E-4	5.57E-5	9.58E-8	2.66E-7
142	Ile	5.92E-4	4.71E-5	-5.75E-7	2.25E-7
143	Glu	8.65E-4	1.44E-5	-6.85E-7	6.86E-8
146	Ala	-9.87E-4	7.32E-5	1.21E-6	3.49E-7
147	Lys	-0.00102	8.3E-5	1.28E-7	3.98E-7
150	Gln	-2.86E-4	1.23E-7	2.88E-7	5.87E-8
153	Glu	3.84E-4	2.91E-5	-2.01E-7	1.39E-7
155	Ala	-5.81E-4	7.11E-5	6.9E-8	3.4E-7
156	Phe	-3.68E-4	4.4E-5	-2.75E-9	2.1E-7
158	Thr	-1.85E-4	6.16E-5	-2.92E-8	2.94E-7
159	Leu	-4.19E-4	3.42E-5	-4.32E-7	1.63E-7
160	Val	-6.72E-4	2.79E-5	1.18E-6	1.33E-7
161	Arg	-7.66E-4	5.12E-5	3.06E-7	2.45E-7
162	Glu	-1.68E-4	3.59E-5	-4.07E-7	1.72E-7
165	Gln	-3.12E-4	2.88E-5	-3.24E-7	1.38E-7
166	His	-2.3E-4	2.54E-5	-6.81E-7	1.21E-7

First and Second Order Pressure Coefficients for ^{15}N Derived for c'Ras(wt)·Mg $^{2+}$ ·GppNHp at 278 K.

residue number	amino acid	B ₁ (N) [ppm/GPa]	error	B ₂ (N) [ppm/GPa ²]	error
3	Glu	1.90544	0.16119	-1.9049	0.77969
4	Tyr	5.64042	0.37934	-10.05164	1.80505
7	Val	5.69335	0.27623	-3.28227	1.32067
9	Val	5.38397	0.50615	4.889	2.40842
14	Val	7.5519	0.19574	-7.70219	0.93585
19	Leu	4.73599	0.68228	0.92628	3.26204
26	Asn	3.39208	0.22247	-1.88544	1.06363
42	Lys	0.29332	0.56869	-9.35359	2.75083
45	Val	-1.03154	0.2567	3.2336	1.22728
48	Gly	4.20029	0.64215	-2.97965	3.07015
50	Thr	3.69398	0.41221	-3.77134	1.97081
75	Gly	6.25371	0.14857	-9.33667	0.71031
77	Gly	3.63529	0.39717	-2.92653	1.8989
78	Phe	6.4699	0.42032	-10.75531	2.00956
82	Phe	2.00251	0.23697	-1.10501	1.13297
83	Ala	1.94297	0.14544	-0.74256	0.69538
84	Ile	4.9846	0.17759	0.3414	0.84907
85	Asn	0.75352	0.12133	-0.87713	0.58006
86	Asn	4.62946	0.18623	-0.52625	0.89038
88	Lys	3.77585	0.21126	-1.57668	1.01006
89	Ser	1.91327	0.45472	1.07895	2.17406
96	Tyr	4.55986	0.18628	-7.30364	0.89063
105	Asp	2.42688	0.21342	-1.22225	1.02038
106	Ser	4.53064	0.20895	-3.55661	0.99899
107	Asp	5.64834	0.60056	-5.29784	2.87132
108	Asp	1.42056	0.24031	4.39741	1.14893
109	Val	0.90498	0.17159	2.69552	0.8204
111	Met	1.85488	0.34883	0.85354	1.6678
115	Gly	1.43542	0.25617	4.68091	1.22479
116	Asn	1.44928	0.17824	-2.95077	0.85216
117	Lys	9.73091	0.13899	-7.17092	0.66454
120	Leu	1.47764	0.18804	-1.84045	0.89903
122	Ala	2.22503	0.15616	-1.45938	0.74663
123	Arg	3.75434	0.11083	-5.73707	0.52989
124	Thr	6.66887	0.40819	-8.41673	1.95159
125	Val	2.71192	0.16713	-3.69909	0.79907
126	Glu	-2.32381	0.25857	4.18494	1.23625
127	Ser	3.55924	0.21144	0.91485	1.01093
128	Arg	3.0459	0.15239	-0.3738	0.7286
129	Gln	5.35085	0.50714	-6.31485	2.42467
130	Ala	5.09046	0.18557	-3.80719	0.88723
131	Gln	3.63528	0.17509	-1.53879	0.83713
132	Asp	2.01767	0.14188	-2.41384	0.67832
133	Leu	3.9879	0.20219	-3.34398	0.9667
136	Ser	4.62878	0.19078	-3.00082	0.91213
138	Gly	2.04566	0.26705	0.69375	1.27679
139	Ile	1.38043	0.22422	0.21602	1.07199
141	Tyr	1.25834	0.1815	-1.06405	0.86778
142	Ile	4.03971	0.29203	-4.4678	1.39619
143	Glu	4.23264	0.21652	-1.23799	1.03519
144	Thr	8.54537	0.30139	-7.85139	1.44095
145	Ser	2.39653	0.62858	-0.69678	3.00528
146	Ala	2.51605	0.30442	-3.79123	1.45543
147	Lys	-2.53959	0.23103	2.30555	1.10939
148	Thr	6.77998	0.52649	-7.82484	2.51717
150	Gln	2.82753	0.18573	-0.11904	0.888
151	Gly	3.44022	0.24417	-2.98066	1.16739
153	Glu	3.38834	0.17847	-2.97131	0.85327
155	Ala	-2.21166	0.22856	5.37271	1.09277
158	Thr	4.36428	0.20648	-4.42782	0.98718

159	Leu	2.64885	0.20113	-2.34257	0.96163
160	Val	2.61603	0.14853	2.68062	0.71014
162	Glu	1.90315	0.31775	-2.76617	1.51917
165	Gln	1.50392	0.13679	-0.8498	0.65401
166	His	2.46999	0.1938	-1.39099	0.92656

Corrected First and Second Order Pressure Coefficients for ^1H Derived for c'Ras(wt)·Mg $^{2+}$ ·GppNHp at 303 K.

residue number	amino acid	$B_1^* (\text{H}^N)$ [ppm/GPa]	error	$B_2^* (\text{H}^N)$ [ppm/GPa 2]	error
3	Glu	0.00101	2.59466E-5	-1.06475E-6	1.37787E-7
4	Tyr	-4.54145E-4	2.22226E-5	3.82581E-7	1.18011E-7
9	Val	-2.91338E-4	2.92867E-5	-1.181E-8	1.53844E-7
11	Ala	-2.94833E-4	2.3798E-5	1.83577E-7	1.25011E-7
14	Val	-6.17124E-4	7.99577E-5	-6.16583E-8	4.20019E-7
15	Gly	-2.42724E-4	2.96305E-5	-1.30374E-7	1.5735E-7
17	Ser	-1.16408E-4	3.56342E-5	1.20712E-7	1.89232E-7
18	Ala	-0.0014	3.47809E-5	-7.41133E-7	1.847E-7
23	Leu	3.35241E-5	5.0651E-5	-3.04413E-6	3.01972E-7
24	Ile	1.06431E-4	4.39057E-5	-1.70081E-6	2.61758E-7
25	Gln	-8.14175E-4	8.21622E-5	4.96774E-8	4.36313E-7
27	His	-4.18356E-5	4.31254E-5	-5.06198E-7	2.29013E-7
28	Phe	1.58311E-4	2.59697E-5	-1.22917E-6	1.37909E-7
29	Val	4.51047E-4	4.5074E-5	-9.32895E-7	2.39361E-7
39	Ser	-1.38291E-4	3.20558E-5	-2.01029E-7	1.70229E-7
42	Lys	-2.99645E-4	3.78326E-5	-6.75343E-7	2.00906E-7
44	Val	-3.21115E-4	5.59029E-5	-8.05108E-8	3.33283E-7
45	Val	-3.44598E-4	2.15759E-5	5.10253E-7	1.14576E-7
46	Ile	-0.00162	9.15864E-5	9.54859E-7	4.86359E-7
49	Glu	-4.19456E-4	3.17021E-5	8.26574E-7	1.68351E-7
51	Cys	1.81104E-4	2.1091E-5	-1.13914E-6	1.10791E-7
52	Leu	4.31337E-4	3.20358E-5	-5.70986E-7	1.70122E-7
53	Leu	-5.86749E-4	2.58298E-5	5.91159E-7	1.37166E-7
56	Asp	1.29674E-4	3.93977E-5	1.21223E-6	2.09217E-7
65	Ser	-0.00119	3.64032E-5	1.25366E-6	2.4721E-7
66	Ala	-4.94914E-4	3.31801E-5	8.57099E-8	1.76199E-7
67	Met	-3.1237E-4	4.2015E-5	-5.01901E-7	2.23116E-7
73	Arg	-0.00116	2.24802E-5	8.13417E-7	1.19379E-7
75	Gly	4.83609E-4	3.75786E-5	-4.31512E-7	1.99557E-7
77	Gly	5.11692E-4	3.76394E-5	-8.47383E-7	1.9988E-7
78	Phe	1.95344E-4	1.67539E-5	-5.76426E-7	9.05162E-8
80	Cys	2.26882E-4	3.04393E-5	-4.31726E-7	1.59898E-7
82	Phe	-2.53853E-4	2.93231E-5	1.32531E-10	1.54035E-7
83	Ala	-1.43151E-4	2.30401E-5	-2.26856E-8	1.2103E-7
84	Ile	6.68167E-4	3.17498E-5	-1.17252E-6	1.68604E-7
85	Asn	-1.81581E-4	3.00775E-5	-1.95509E-7	1.59723E-7
86	Asn	2.02169E-4	1.50754E-5	-5.22996E-7	8.98768E-8
88	Lys	6.24296E-4	4.35596E-5	-4.49797E-7	2.31318E-7
90	Phe	-2.31374E-4	3.04046E-5	-5.05008E-7	1.6146E-7
94	His	-7.49374E-4	3.68313E-5	2.53431E-7	1.95588E-7
97	Arg	0.00114	5.97623E-5	-2.24658E-6	3.18429E-7
98	Glu	-1.12256E-4	1.82538E-5	-4.0645E-7	9.69347E-8
100	Ile	-3.27282E-4	4.18489E-5	-6.43501E-7	2.22234E-7
102	Arg	-3.57357E-4	3.49096E-5	7.59906E-7	1.85384E-7
105	Asp	-6.89862E-4	2.17933E-5	5.45291E-7	1.15731E-7
106	Ser	4.39137E-4	3.99457E-5	-1.1517E-6	2.12127E-7
107	Asp	7.69427E-4	7.82298E-5	-3.86531E-6	6.15817E-7
108	Asp	-1.56373E-4	2.30223E-5	-5.72975E-8	1.37255E-7
109	Val	6.38478E-4	4.47348E-5	-7.52209E-7	2.37559E-7
111	Met	5.73134E-4	3.56924E-5	1.61241E-7	1.8954E-7
112	Val	-3.83767E-4	3.46486E-5	2.0874E-7	1.80038E-7
113	Leu	7.53785E-4	3.67006E-5	-5.23082E-7	1.94895E-7

114	Val	-4.33437E-4	3.25512E-5	-4.63106E-7	1.72859E-7
115	Gly	-7.1211E-4	3.02256E-5	1.16628E-6	1.6051E-7
116	Asn	-5.04298E-5	1.1386E-5	-3.65579E-7	6.04643E-8
117	Lys	-2.59476E-6	1.17068E-5	-6.57929E-7	6.21676E-8
118	Ser	-3.98014E-4	2.89954E-5	7.20001E-7	1.53977E-7
119	Asp	-6.28315E-4	5.65226E-5	3.71509E-7	3.10126E-7
120	Leu	-3.57923E-4	2.46677E-5	-2.52114E-7	1.30995E-7
121	Ala	5.21894E-4	3.1902E-5	-3.10909E-7	1.69412E-7
122	Ala	5.25996E-4	4.66017E-5	-7.62192E-7	2.47473E-7
123	Arg	-3.64416E-4	3.35856E-5	6.08313E-7	1.78353E-7
124	Thr	-1.71186E-4	2.2308E-5	-3.8351E-7	1.17185E-7
125	Val	1.78541E-4	3.19079E-5	-1.17399E-6	1.90229E-7
127	Ser	4.8738E-4	2.6188E-5	-1.59084E-6	1.56128E-7
129	Gln	-7.96184E-4	2.34113E-5	3.96817E-7	1.24323E-7
132	Asp	-1.08585E-4	2.56064E-5	-4.89291E-7	1.3598E-7
133	Leu	1.22536E-4	1.47565E-5	-6.57387E-7	7.83626E-8
134	Ala	-6.75294E-4	3.31862E-5	6.67005E-7	1.76232E-7
135	Arg	-3.41568E-4	2.47851E-5	2.98273E-7	1.30197E-7
136	Ser	1.02547E-4	2.61577E-5	-3.77262E-7	1.38908E-7
137	Tyr	-7.35652E-4	3.5616E-5	8.44947E-7	1.89135E-7
138	Gly	-1.67295E-4	1.73593E-5	-3.96442E-7	9.21849E-8
139	Ile	-3.08797E-4	3.05661E-5	-2.91367E-7	1.62318E-7
141	Tyr	9.19663E-4	4.98517E-5	-9.31499E-7	2.64732E-7
142	Ile	5.81281E-4	3.26712E-5	-1.01723E-6	1.73497E-7
143	Glu	8.81904E-4	3.98348E-5	-8.99209E-7	2.11538E-7
144	Thr	9.30092E-5	2.74942E-5	-3.42165E-7	1.44428E-7
145	Ser	7.09581E-4	5.0765E-5	-3.50644E-7	2.69582E-7
146	Ala	-8.87784E-4	1.99716E-5	5.266E-7	1.06057E-7
147	Lys	-0.00119	2.85183E-5	8.00097E-7	1.51443E-7
149	Arg	1.60493E-4	4.39073E-5	3.68754E-7	1.96386E-7
150	Gln	-2.54646E-4	2.61681E-5	-2.33257E-7	1.38963E-7
151	Gly	2.45394E-4	2.04679E-5	-8.16364E-7	1.22026E-7
152	Val	-7.35617E-4	3.30619E-5	7.30336E-7	1.75572E-7
153	Glu	-3.25452E-4	3.5853E-5	1.94664E-6	2.13749E-7
155	Ala	-3.84399E-4	2.16814E-5	-4.73054E-7	1.15136E-7
156	Phe	-5.01262E-4	3.65247E-5	7.35255E-8	1.9396E-7
157	Tyr	4.99101E-4	4.91752E-5	5.68544E-7	2.6114E-7
158	Thr	-3.10387E-5	3.47885E-5	-7.4629E-7	1.87415E-7
159	Leu	-5.01105E-4	3.08026E-5	1.43349E-7	1.63574E-7
161	Arg	-9.26749E-4	1.80564E-5	5.7095E-7	9.58865E-8
162	Glu	-1.56495E-4	1.27137E-5	1.88603E-7	6.67853E-8
164	Arg	-6.97667E-4	4.8587E-5	4.65418E-7	2.61752E-7
165	Gln	5.50902E-4	4.68242E-5	2.06558E-7	2.48655E-7
166	His	-2.21767E-4	3.88918E-5	-6.16789E-7	2.06531E-7

First and Second Order Pressure Coefficients for ^{15}N Derived for c'Ras(wt)·Mg $^{2+}$ ·GppNHp at 303 K.

residue number	amino acid	B_1 (N) [ppm/GPa]	error	B_2^* (N) [ppm/GPa 2]	error
3	Glu	0.00148	8.48466E-5	9.35116E-7	4.50569E-7
4	Tyr	-0.00348	1.18143E-4	6.33261E-6	6.27387E-7
5	Lys	0.00282	1.08469E-4	-2.22404E-6	5.76015E-7
9	Val	0.00216	8.24846E-5	6.56089E-6	4.38025E-7
11	Ala	0.00348	1.13449E-4	2.95951E-7	6.0246E-7
14	Val	0.00132	5.77778E-4	6.4944E-6	3.03508E-6
15	Gly	-0.00129	9.15206E-5	-8.21609E-7	4.8601E-7
17	Ser	0.0021	1.18129E-4	-6.40225E-6	6.27312E-7
18	Ala	-6.99372E-6	1.02009E-4	4.55928E-6	5.4171E-7
19	Leu	0.00441	1.14054E-4	-1.4843E-7	6.05669E-7
23	Leu	0.00606	1.3978E-4	-9.51708E-6	8.33342E-7
24	Ile	0.00172	5.99262E-5	-4.24587E-6	3.18232E-7
25	Gln	0.00149	1.22512E-4	-1.79092E-6	6.50585E-7
27	His	0.00615	1.74759E-4	3.69086E-6	9.2804E-7
28	Phe	-2.92092E-4	1.88665E-4	-2.83542E-6	1.00189E-6
29	Val	0.00403	1.673E-4	-4.66884E-6	8.88428E-7
39	Ser	0.00957	1.57707E-4	-6.35269E-6	8.37484E-7
42	Lys	-1.81702E-4	8.11001E-5	-3.55174E-6	4.30673E-7
44	Val	0.00404	2.07707E-4	7.95808E-7	1.103E-6
45	Val	-0.00186	1.37877E-4	7.86781E-6	7.32183E-7
46	Ile	-3.68836E-4	1.34703E-4	4.47469E-6	7.15324E-7
49	Glu	7.77514E-4	5.74613E-5	1.68181E-6	3.05142E-7
51	Cys	0.00121	1.01878E-4	-2.48728E-6	5.41011E-7
52	Leu	0.00536	1.52948E-4	-5.74905E-6	8.12216E-7
53	Leu	0.00359	1.41388E-4	-2.95794E-6	7.50824E-7
56	Asp	0.00288	2.08605E-4	4.507E-6	1.10778E-6
65	Ser	8.19594E-4	1.31276E-4	2.07063E-7	8.91482E-7
66	Ala	-0.00195	8.61805E-5	3.41839E-6	4.57652E-7
67	Met	9.0301E-4	6.54908E-5	-5.63455E-8	3.47782E-7
73	Arg	-0.00271	7.06022E-5	1.16505E-5	3.74926E-7
75	Gly	0.00583	1.3296E-4	-7.324E-6	7.06071E-7
77	Gly	0.00329	9.12068E-5	-8.60204E-7	4.84344E-7
78	Phe	0.00507	1.43872E-4	-4.7617E-6	7.64016E-7
80	Cys	1.08567E-4	8.23706E-5	-2.54713E-6	4.3742E-7
82	Phe	0.00165	6.78501E-5	2.28781E-7	3.60311E-7
83	Ala	0.00173	7.70435E-5	-4.17911E-7	4.09131E-7
84	Ile	0.00486	1.3969E-4	-1.03122E-7	7.41811E-7
85	Asn	9.61122E-4	5.59271E-5	-8.39043E-7	2.96995E-7
86	Asn	0.00456	1.48429E-4	-1.96425E-6	7.88215E-7
88	Lys	0.00316	1.28445E-4	6.60725E-7	6.82095E-7
90	Phe	0.00733	2.08697E-4	-1.22574E-5	1.10826E-6
94	His	0.00176	1.37634E-4	3.17674E-7	7.3089E-7
97	Arg	0.00408	1.19982E-4	-5.41288E-6	6.39297E-7
98	Glu	0.00279	1.111E-4	-8.69203E-7	5.89987E-7
100	Ile	0.00439	1.57037E-4	-5.81811E-6	8.33926E-7
102	Arg	0.00225	8.95088E-5	-4.75459E-6	4.75327E-7
105	Asp	0.0031	1.39851E-4	-3.52421E-6	7.42662E-7
106	Ser	0.0046	1.13504E-4	-4.36285E-6	6.0275E-7
107	Asp	0.00624	4.124E-4	-6.86355E-6	2.19001E-6
108	Asp	0.00125	8.22474E-5	3.70996E-6	4.36766E-7
109	Val	0.00708	2.34618E-4	-1.0465E-5	1.24592E-6
111	Met	0.00133	1.145E-4	2.58245E-6	6.08042E-7
112	Val	-0.01116	2.44631E-4	-1.02363E-5	1.27113E-6
113	Leu	-0.00207	9.95469E-5	-6.0674E-6	5.28633E-7
114	Val	0.00371	1.34985E-4	-7.37816E-6	7.16821E-7
115	Gly	0.00223	1.7371E-4	7.10182E-7	9.22466E-7
116	Asn	8.47467E-4	6.95981E-5	-3.225E-7	3.69593E-7
117	Lys	0.008	2.11735E-4	-8.92478E-6	1.1244E-6
118	Ser	0.00137	6.27916E-5	1.34593E-6	3.33448E-7
120	Leu	0.00158	7.998E-5	-1.70075E-6	4.24725E-7

121	Ala	0.00563	9.86528E-5	-2.8641E-6	5.23885E-7
122	Ala	0.00258	2.34224E-4	-2.88375E-6	1.24382E-6
123	Arg	0.00416	1.44258E-4	-7.55837E-6	7.66066E-7
124	Thr	0.00682	1.51417E-4	-6.82088E-6	8.04084E-7
125	Val	0.00359	1.20591E-4	-4.3134E-6	6.40386E-7
127	Ser	0.00383	2.39111E-4	-1.35622E-6	1.26977E-6
129	Gln	0.00455	1.34564E-4	-2.90296E-6	7.14585E-7
132	Asp	0.00261	2.91023E-4	-4.74678E-6	1.54545E-6
133	Leu	0.00429	1.03771E-4	-4.04356E-6	5.51062E-7
134	Ala	0.00106	7.37455E-5	3.17264E-6	3.91618E-7
135	Arg	0.00244	1.0294E-4	-1.52472E-6	5.46653E-7
136	Ser	0.00508	1.5056E-4	-4.2837E-6	7.99534E-7
137	Tyr	-3.1046E-4	7.81129E-5	4.39868E-6	4.1481E-7
138	Gly	0.00147	7.07661E-5	1.26664E-6	3.75796E-7
139	Ile	0.00101	8.13817E-5	1.49331E-6	4.32169E-7
141	Tyr	4.04108E-4	1.37365E-4	2.44707E-6	7.29464E-7
142	Ile	0.00429	1.65789E-4	-5.0656E-6	8.80407E-7
143	Glu	0.00376	1.18338E-4	-9.04618E-7	6.2842E-7
144	Thr	0.00793	1.74722E-4	-6.46863E-6	9.27844E-7
145	Ser	0.00264	1.10335E-4	-1.58355E-6	5.85921E-7
146	Ala	0.00201	1.35697E-4	-1.70979E-6	7.20606E-7
147	Lys	-6.98673E-4	7.28955E-5	-7.03423E-7	3.87104E-7
149	Arg	0.00413	2.52915E-4	-6.24095E-6	1.13122E-6
150	Gln	0.00306	1.21108E-4	-1.21538E-6	6.43129E-7
151	Gly	0.00339	1.24464E-4	-1.66344E-6	6.6095E-7
152	Val	0.00277	1.34186E-4	-4.89026E-7	7.1258E-7
153	Glu	9.08523E-4	7.8958E-5	4.83561E-7	4.19298E-7
155	Ala	-0.00112	9.81958E-5	2.92069E-6	5.21458E-7
157	Tyr	0.00331	1.17515E-4	1.29934E-6	6.2405E-7
158	Thr	0.00442	3.48562E-4	-2.79346E-6	1.8778E-6
159	Leu	0.00248	1.07485E-4	-7.57719E-7	5.70787E-7
161	Arg	0.00116	9.41192E-5	-3.5832E-7	4.9981E-7
162	Glu	5.45723E-4	8.17093E-5	2.69854E-6	4.33908E-7
164	Arg	0.00152	3.25711E-4	3.38451E-6	1.75469E-6
165	Gln	6.49932E-4	2.51019E-4	9.82248E-6	1.33301E-6
166	His	0.00237	1.6449E-4	-1.99048E-6	8.73507E-7

8.3 Contributions to Conferences and Publications

Talks

- **24th Colloquium of Rabenstein**, Pottenstein, Germany, June 2006
Inhibition of the Interaction between Oncogenic Ras and Its Effectors by Small Organic Molecules
- **25th Colloquium of Rabenstein**, Pottenstein, Germany, June 2007
BPAs as Potential Inhibitors of the Ras-Effector Interaction
- **3rd Symposium of the Planned Center for Biochemistry and Biophysics Regensburg**, Kostenz, Germany, September 2007
NMR-Aided Development of Inhibitors of the Ras-Effector Interaction
- **2nd EuChems European Chemistry Congress**, Torino, Italy, September 2008
NMR-Assisted Design of a New Type of Ras Inhibitors

Poster Contributions

- **3rd Summer School Medicinal Chemistry**, University of Regensburg, Germany, September 2006
Inhibition of the Interaction between Oncogenic Ras and Its effectors by Small Organic Molecules
- **Intensive Course Medicinal Chemistry**, University of Ho Chi Minh City, Vietnam, October/November 2006
Inhibition of the Interaction between Oncogenic Ras and Its effectors by Small Organic Molecules
- **29th Annual Discussion Meeting Magnetic Resonance in Biophysical Chemistry**, University of Göttingen, Germany, September 2007
NMR-Aided Development of Inhibitors of the Ras-Effector Interaction
- **Joint Meeting of the Graduate Colleges GRK677 Bonn and GRK760 Regensburg**, Nürnberg, Germany, October 2007
NMR-Aided Development of Inhibitors of the Ras-Effector Interaction
- **Annual Meeting on Frontiers of Medicinal Chemistry**, University of Regensburg, March 2008
Modulation of the Ras-Effector Interaction by Stabilization of Low Populated Conformational States

Publications

- **Rosnizeck, I.C.**, Graf, T., Spoerner, M., Tränkle, J., Filchtinski, D., Herrmann, C., Gremer, L., Vetter, I.R., Wittinghofer, A., König, B., Kalbitzer, H.R.: Stabilizing a weak binding state for effectors in the human Ras-protein by small compounds. *Angew. Chem. Int. Ed.*, accepted for publication.
- Schmidt, F., **Rosnizeck, I.C.**, Spoerner, M., Kalbitzer, H.R., König, B.: Zinc(II)cyclen Peptide Conjugates as Potential Inhibitors of the Ras mediated signal transduction. submitted.

8.4 Curriculum Vitae

Personal

Name	Ina C. Rosnizeck
Date of Birth	September 23 rd , 1981
Place of Birth	Burglengenfeld, Germany

Education

12/05 – present	Doctoral Thesis with Prof. Dr. Dr. H. R. Kalbitzer, Institute of Physical Biochemistry and Biophysics, University of Regensburg, Germany: <i>Modulation of Conformational Equilibria of Human H-Ras Protein by Metal-Chelate Derivatives and High Pressure Studied by NMR Spectroscopy</i>
03/05 – 11/05	Diploma Thesis with Prof. Dr. O. S. Wolfbeis, Institute of Analytical Chemistry, Chemo- and Biosensors, University of Regensburg, Germany: <i>Luminescence-Based Inhibition Assay of Alkaline Phosphatase</i>
09/03 – 02/04	Erasmus Student Exchange , University of Dublin, Ireland
10/02 – 12/04	Graduate in Chemistry, University of Regensburg, Germany Advanced Studies: Medicinal Chemistry
10/00 – 09/02	Undergraduate in Chemistry, University of Regensburg, Germany
09/91 – 06/00	J-M-F-Gymnasium (High School), Burglengenfeld, Germany
09/87 – 08/91	Geschwister-Scholl-Grundschule (Elementary School), Burglengenfeld, Germany

Fellows, Scholarships and Awards

- **Erasmus** Scholarship for Student Exchange, Dublin, Ireland (09/03 – 02/04)
- PhD Scholarship, **Graduate College GRK760** “Medicinal Chemistry: Molecular Recognition - Ligand-Receptor Interaction” (12/05 – 11/08)

- **Asia Link** Travel Fellowship for the Summer School Medicinal Chemistry in Ho Chi Minh City, Vietnam (11/06)
- Travel Fellowship by the **German Chemical Society** for the 2nd EuChems Congress, Torino, Italy (09/08)
- **Poster Award** at the 4th Summer School “Medicinal Chemistry” in Regensburg (09/08)

Publications

- 1) Schrenkhammer, P., **Rosnizeck, I.C.**, Duerkop, A., Wolfbeis, O.S., Schäferling, M. (2008) Time-Resolved Fluorescence-Based Assay for the Determination of Alkaline Phosphatase Activity and its Application to the Screening of its Inhibitors. *J. Biomol. Screen.* **13**, 9-16.
- 2) **Rosnizeck, I.C.**, Graf, T., Spoerner, M., Tränkle, J., Filchtinski, D., Herrmann, C., Gremer, L., Vetter, I.R., Wittinghofer, A., König, B., Kalbitzer, H.R.: Stabilizing a weak binding state for effectors in the human Ras-protein by small compounds. *Angew. Chem. Int. Ed.*, accepted for publication.
- 3) Schmidt, F., **Rosnizeck, I.C.**, Spoerner, M., Kalbitzer, H.R., König, B.: Zinc(II)cyclen Peptide Conjugates as Potential Inhibitors of the Ras-mediated signal transduction. submitted.

8.5 Acknowledgement

For the aid and support during the years of my PhD work I would like to express my gratitude to the following people at this point.

- First of all I want to thank **Prof. Dr. Dr. Hans Robert Kalbitzer** for giving me the possibility to work in an interdisciplinary team and in a technically highly equipped laboratory. I had the opportunity to learn a lot of methods within molecular biology and NMR spectroscopy. Especially I would like to thank him for his help and advice during the evaluation of the high pressure NMR data.
- Special thanks go to **Dr. Michael Spörner (Spö)** for sharing all his experience in the field of Ras and ^{31}P NMR spectroscopy with me and for his never ending patience! I am very grateful for all his support.
- **Prof. König** from the University of Regensburg and especially his former and actual Ph.D. students **Dr. Daniel Vomasta**, **Dr. Georg Dirscherl** and **Florian Schmidt (Schmidl)** I want to thank for the pleasant cooperation and of course the synthesis of the metal(II)-chelate complexes and the bivalent ligands.
- Thanks a lot to **Prof. Dr. Herrmann** and **Daniel Filchtinski** from the University of Bochum for the interesting and pleasant cooperation especially concerning the investigations on the Ras-effector interaction. Daniel I want to thank for really helpful and constructive discussions in Bad Kissingen and on the phone.
- I very much appreciate all the help and advice from **Prof. Dr. Claudia Munte** for the performance and processing of 2D NMR spectra and the practical assistance with the high pressure series.
- Thanks to **Dr. Jochen Trenner** and **Dr. Konrad Brunner** from the Auremol team for listening to any suggestion concerning the program Auremol and their will to realize it, when possible.
- I am very grateful for the assistance I achieved from **Emmi Fuchs** and **Sabine Ruppel** in the “eastern” and “western” labs.
- For the excellent atmosphere in the office (or Auremol User Club?) I want to thank my colleague **Christoph Liebold**. Thanks to all the people from the group, especially **Maren Schmidt**, **Sandra Kreitner**, **Tanja Meierhofer**, **Kathrin Stroka**, **Dr. Katharina Lutz**, **Dr. Christian Gröger “Groggy”** and **Dörte** for the enjoyable daily tea and lunch breaks, the barbecues, after work events and company, when needed.
- At the end I grant the aid, support and understanding of my **parents**, my sister **Karin** and my brother **Frank** and very good friends (**Bianca and Julia**) in any stage of my studies or PhD in any way.

Erklärung

Hiermit erkläre ich, dass ich die vorliegende Arbeit selbständig angefertigt und keine anderen Hilfsmittel außer den angegebenen verwendet habe.

Regensburg, den 19.06.2010 _____